Evolution of Preconsolidation Pressure of Normally Consolidated Clays Over Full Temperature Range

Suzanna Gevorgyan

Thesis submitted to the faculty of the Virginia Polytechnic Institute and State University
in partial fulfillment of the requirements for the degree of

Master of Science
In
Civil Engineering

Sherif L. Abdelaziz, Chair
Joseph E. Dove
Reihaneh Hosseini

December 17, 2024
Blacksburg, VA

Keywords: Preconsolidation, temperature, clays, freeze, heat

Evolution of Preconsolidation Pressure of Normally Consolidated Clays over Full Temperature Range

Suzanna Gevorgyan

ACADEMIC ABSTRACT

While it has been established that temperature can change the preconsolidation pressure of clays, the current understanding is limited to specific ranges of temperatures, with temperatures above freezing being studied entirely independently of temperatures below freezing. However, as temperature is a continuous domain and clays may be subjected to both above- and below- freezing temperatures over the course of an engineering application, a unified view is necessary. The first goal of this thesis is to develop a single model which can be used to predict the preconsolidation pressure of a normally consolidated clay at any temperature over a wide range which includes both frozen and elevated temperatures.

To do so, consolidation tests were run at various temperatures between -7 °C and 50 °C, and the yield stress at each consolidation temperature was determined. As previous studies have established that the temperature response of clays is dependent upon their mechanical stress history, the specimens were consolidated initially at a reference temperature until they reached the normally consolidated state. Subsequently, the temperature of the specimens was changed and the volume changes during the temperature change stage were recorded. Once the specimens stabilized at the new temperature, they were consolidated once again and the preconsolidation pressure determined at the new consolidation temperature.

The volumetric strains and changes in preconsolidation pressure for each temperature used in this study align generally with the previous data published for each

temperature domain. Heating led to a decrease in the volume of the specimens, cooling to minimal strain, and freezing to an increase in the specimen volume. Changing the consolidation temperature by either heating, cooling, or freezing the specimen led to various degrees of increase in the preconsolidation pressure. A mathematical model was developed to fit the observed preconsolidation pressures at each consolidation temperature. This model can be used to predict the yield stress of NC kaolinite at any temperature within the tested range, and captures the smaller magnitude increases in yield stress which occur upon heating and cooling as well as the large increases which occur upon freezing the clay.

With the effects of unidirectional thermal paths having been treated in the previous portion, a second investigation was also undertaken to assess how much of the temperature history of the soil might influence the behavior at its final consolidation temperature. In particular, the impacts of previous freezing on the preconsolidation pressure at elevated temperatures were investigated. The same clay material was first consolidated to the NC state and then frozen to -15 °C. Subsequently, the material was thawed or heated to various final temperatures and consolidated further to determine the preconsolidation pressure. The results of these tests indicate that the preconsolidation pressure was independent of the consolidation temperature for previously-frozen soil. While increasing contractive axial strains were recorded with increasing temperature, there was no accompanying increase in the preconsolidation pressure. These results indicate the thermal history of the clay can alter its behavior at the current temperature, overriding the effects of the most recent thermal path.

Evolution of Preconsolidation Pressure of Normally Consolidated Clays over Full Temperature Range

Suzanna Gevorgyan

GENERAL AUDIENCE ABSTRACT

Temperatures around the globe are becoming more extreme every year due to global warming. The warming climate has destabilized permafrost. Additionally, new energy applications, such as heat exchange piles, and existing energy infrastructure, such as oil and gas pipelines, also constitute extreme thermal environments. The settlement of soils in these conditions must be well understood so that engineers can predict and mitigate potentially damaging conditions. One engineering parameter which is necessary to predicting the amount of consolidation settlement in clays is the overconsolidation ratio (OCR), and the preconsolidation pressure of clays is required in order to compute OCR. Previous studies have established that preconsolidation pressure is a function of temperature. However, in addition to changing soil temperatures due to climate, soil temperatures between in situ and laboratory settings where preconsolidation pressure is determined are often different as well. Therefore, in order to develop resilient foundations and structures in areas with thermal variations, a thorough understanding of how the preconsolidation pressure changes with temperature is necessary.

The goal of this study is firstly to develop a mathematical model which can be used to predict the preconsolidation pressure of a clay over a wide temperature range which includes both frozen (<0 °C) and heated (>20 °C) temperatures. Consolidation tests were run on kaolinite clay specimens to determine the preconsolidation pressure at various temperatures within the chosen range. Then, a single expression was developed to allow the user to predict the preconsolidation pressure at any temperature within this range. While

the mineralogy and stress state of the clay impact the parameters of this equation, the general form models the expected change in yield stress for a given change in temperature. The second goal is to assess whether the thermal history of the clay, in particular a prior frozen state, affects the preconsolidation pressure determined following subsequent thawing and heating.

ACKNOWLEDGMENTS

Firstly, I'd like to acknowledge the Dr. Sherif L. Abdelaziz and the Cold Regions Research and Engineering Laboratory (CRREL) for funding my research. Thank you also to my professors in the geotechnical engineering program at Virginia Tech for the knowledge and instruction I received in my time as a student.

My research and the preparation of this thesis were a labor of love, and not just mine: I am grateful to so many people for the love and support they gave me throughout this time. I can't name them all, but I'll try anyway.

To Dr. Abdelaziz: Thank you for your guidance and support throughout this last year. Through all kinds of obstacles, you were generous and patient with me, and I'll always remember the lessons you taught me – about research, academic writing, and life.

To Dr. Seyed Morteza Zeinali: You were the best post-doc a grad student could ask for. I wouldn't have been able to do this without your emotional and intellectual support and encouragement. You were there for me whenever I needed you, regardless of what time of day or night it was. You're more than just my post-doc: you're a mentor, a boss, and an inspiration.

To Sepehr Akhtarshenas: I've said it before and I'll say it again and always – thank you. You made time for me no matter how busy you were, and you made the greatest efforts to help me however you could. I am so grateful to have been able to call you my labmate, and so privileged to be able to call you my friend. I admire you – your character and your heart – so much.

To my English Lab buddies, my fellow Abdelaziz Lab buddies, and my Hokies: I probably made it seem like I was the first person in the history of the world to do a thesis for the amount that I complained about it. Thank you for the constant words of encouragement, for checking on me, for distracting me when I needed it and giving me space to work when I needed it, and, most of all, for keeping me smiling through this long and difficult process.

To Jasleen, Rakshitha, Carole, and Saad: Through months of back and forth between New York and Virginia, you put roofs over my head, kept my belly full, and got me wherever I needed to be whenever I needed it. I'll never forget your generosity. Thank you, my friends.

To my bestie, Vanessa: Thank you for being there from the very first day to the very last, and for being a rock at my side through it all. I count my lucky stars that we became friends through this program. The fun starts now.

To my parents and my sister: Thank you for your endless, truly endless, support in everything I do. Even though you only listen to about 50% of what I say (my sister) or you only understand 50% of what I'm doing (my parents), you are always giving me 300% of your time and care. I wouldn't be who I am today without you. I get my persistence (although you call it stubbornness) from you. Thank you.

TABLE OF CONTENTS

LIST OF FIGURES

LIST OF TABLES

CHAPTER 1. INTRODUCTION

1.1 Research Motivation

Temperature impacts on soil behavior became critical in recent years due to several reasons including: the well-recognized vital impacts of climate change, the increasing interests in strategically critical arctic regions, and the desired use of thermo-active geostructures (e.g., energy foundations and retaining walls). Climate change, for example, is subjecting geostructures to unprecedented extreme temperatures, which were argued to threaten most of civil infrastructures (Palin et al., 2021; Salimi and Al-Ghamdi, 2020; Schweikert et al., 2014) and increase the frequency of natural disasters (Berlemann and Steinhardt, 2017; Javadinejad et al., 2019; Mbaye, 2017). Also, construction and drilling in the Arctic region are increasing nowadays as this region was identified as a rich source of the world's remaining undiscovered oil and gas (Bird et al., 2008). These activities demand a more robust understanding of the response of soils under extremely low temperatures and under temperature cycles. Additionally, there are continuous requests to increase the use of energy foundations in U.S. markets, which subjected foundation elements and their surrounding soils to temperature cycles (Brandl, 2006).

The behavior of frozen and frozen-thawed soils has been considered in several studies in the literature (Morgenstern and Nixon, 1971; Chamberlain, 1981; Graham and Au, 1984; Eigenbrod, 1996; Qi et al., 2008; Qi et al., 2010; Ozgan et al., 2015; Shastri et al., 2021; Cai et al., 2024). The main triggering motive for these studies was centered around engineering applications in cold regions. However, the use of artificial ground freezing for underground construction in rural areas has recently emerged as another motive for understanding the behavior of frozen and frozen-thawed soils (Chang and Lacy, 2008; Zheng et al., 2021). Generally, most of these studies have focused on understanding the impact of freezing and freezing-thawing cycles on compression

indices (Graham and Au, 1984; Cai et al., 2024), preconsolidation pressure (Chamberlain 1981; Qi et al., 2008; Qi et al., 2010; Shastri et al., 2021; Cai et al., 2024), and the permeability of thawed clays (Chamberlain 1981; Ozgan et al., 2015; Ghazavi et al., 2023). As freezing-thawing repeats seasonally, the impact of the number of freeze-thaw cycles on the observed soil properties were also investigated (Ozgan et al., 2015; Ghazavi et al., 2023). For both freezing and freezing-thawing, it has been shown that the freezing process produces significant axial strains depending on the temperature and amount of water in the clay (Eigenbrod et al., 1996; Qi et al., 2008), and the fabric undergoes fundamental changes due to pore water migration (Chamberlain 1981; Graham and Au, 1984; Eigenbrod et al., 1996). While these studies elucidated the expected behavior for soils subjected to freezing temperatures, they all assumed a thawing temperature around ambient or room temperature and ignored the possibility of elevated temperatures prior to or following freezing.

On the other hand, studies on the effects of heating and heating-cooling only considered test temperatures at and above room temperature (Campanella and Mitchell, 1968; Plum and Esrig, 1969; Demars and Charles, 1981; Baldi et al., 1988; Erikkson, 1989; Tidfors and Sallfors, 1989; Burghighnoli, 1992; Towhata et al, 1993; Boudali et al., 1994; Delage et al., 2000; Cekerevac et al., 2002; Sultan et al., 2002; Abuel-Naga et al., 2005; Coccia and McCartney, 2016; Samarkoon and McCartney, 2020). The purpose of most of these studies was to understand how clays and clay-rich soils in thermo-active applications, such as oil and gas pipelines, heat storage or nuclear waste disposal, would behave upon heating. Some authors also pointed out the change in temperature which occurs between sampling and testing in the laboratory, particularly in areas with lower in situ temperatures, which may influence engineering properties obtained through laboratory testing (Plum and Esrig, 1969; Demars and Charles, 1981). The focus of these studies

were the volumetric strains produced by heating and heating-cooling in drained tests and the excess porewater pressure induced in undrained tests (Campanella and Mitchell, 1968; Plum and Esrig, 1969; Demars and Charles, 1981; Baldi et al., 1988; Abuel-Naga et al., 2005). The volume response was shown experimentally to depend on the stress history of the material, with OCR playing an important role in axial strains produced upon heating and heating-cooling (Baldi et al., 1988; Abuel-Naga et al., 2005). Other studies have focused on the impact of elevated temperatures on recompression index, compression index, and preconsolidation pressure after heating or heating-cooling (Erikkson, 1989; Tidfors and Sallfors, 1989; Burghighnoli, 1992; Towhata et al, 1993; Boudali et al., 1994; Delage et al., 2000; Cekerevac et al., 2002; Sultan et al., 2002; Abuel-Naga et al., 2005; Coccia and McCartney, 2016; Samarkoon and McCartney, 2020). Thus, the compressibility of clay under thermal stress was shown to be a function of mineralogy and pressure (Cekerevac et al., 2002). While these studies yielded critical results on the behavior of clays at elevated temperatures, but they did not consider the impacts of frozen history on heating and heating-cooling behavior.

It appears that, to date, temperature has been treated as a discontinuous domain when the thermo-mechanical behavior of soils is considered; two temperature ranges were considered: above ambient temperatures (i.e., heating) and below freezing temperatures. A robust understanding of the temperature impacts on soil behavior mandates a treatment of temperature as a single domain that applies to soils, mimicking real in situ conditions. Such treatment will facilitate the development of more representative simplified analytical relations or complex constitutive models to predict desired properties of soils subjected to any temperature. This thesis represents a step towards addressing this overarching goal.

1.2 Literature Review

Studies considering the effect of temperature on soil compressibility behavior were first reported in the beginning in the 1960s. This body of work is divided based on the temperature range of focus into studies that focused on the effects of heating and heating-cooling and others that focused on the effects of freezing and freezing-thawing. The following sections briefly summarize the main findings of the literature for these studies.

1.2.1 Effects of heating and heating-cooling on soil behavior

Campanella and Mitchell (1968) were among the first to publish data on the volume changes caused by heating and heating-cooling of remolded illite clay. Prior to their study, others had studied the effect of temperature on interparticle forces, porewater pressures, and swelling behavior (Lambe, 1953, 1960a, 1961); Ladd, 1961; Scott, 1963; Mitchell, 1964; Duncan and Campanella, 1965). Campanella and Mitchell (1968) extended the previous work by focusing on the axial strains associated with these temperature changes and by developing an explanation for the physical mechanisms behind the observed volume changes. There experimental results indicated that heating normally consolidated (NC) clay specimens under drained conditions and constant stress led to volumetric contractions, and subsequent cooling caused some volume recovery. They also found that consecutive heating-cooling cycles within the established range did not yield the same amount of volume contractions as the first cycle. This observation was furthered by the high secondary compression rate following the first heating stage, while following stages had lower rates of creep (Campanella and Mitchell, 1968). By analyzing the time versus deformation graphs for the various temperature changes (heating and cooling), Campanella and Mitchell (1968) suggested that thermal stress produces similar curves as mechanical stress, and consolidation due to temperature changes is similar to consolidation due to mechanical stress.

Campanella and Mitchell (1968) also developed a relation to predict the amount of volume change expected for a given change in temperature. Two mechanisms were identified as causing the observed heating-induced contraction of clayey soils. The first was the difference in the expansion coefficients of the soil particles and the porewater; as the pore water has a much higher thermal expansion coefficient compared to the soil, positive pore pressures were expected upon heating which then led to drainage of pore water from specimens. The second mechanism was the decrease in the interparticle forces as temperatures rose, which caused the soil structure itself to densify until it reached equilibrium under the constant applied effective stress. While these two mechanisms allowed them to develop their relation, they do not address the role of the diffused double layer (DDL) on clay behavior under thermal loads. Other researchers such as Yong et al. (1962) and Lambe (1960b) provided contrasting views on the effect of temperature on the thickness of the DDL and thus on the volume change expected upon heating. While the former suggested that the DDL should expand upon heating, the latter found that it should decrease in thickness. Others still, Mitchell (1969) among them, argue that the thickness of the DDL is not affected by temperature as it is counterbalanced by the change in dielectric constant. It stands to reason that the thickness of the DDL would impact the interparticle forces of the soil. However, despite this potential shortcoming, the model presented by Mitchell and Campanella (1968) agreed generally with the observed heating-induced volumetric strains, which suggests that their analysis of the physical changes induced by temperature variations is generally accurate.

Additionally, Plum and Esrig (1969) tested both remolded illite and remolded glacial clay whose primary clay mineral was hydrous mica chlorite. Their specimens were consolidated in slurries at very low pressures of about 12 kPa (as opposed to Campanella and Mitchell's (1968) 200 kPa), and they found that heating of the glacial clay at 200 kPa had no impact on volume,

while heating of the illite at the same pressure led to contraction of the specimen. This suggests that mineralogy, which impacts the activity of the clay, plays an important role in the effect of temperature on volume changes. For consolidation tests run at different constant temperatures, they found for both soils that the compressibility of these clays were different at low pressures (below 200 kPa), while the slopes were the same at high pressures (above 200 kPa). Mitchell and Campanella (1968) also performed consolidation tests under various constant temperatures, and found that while higher temperatures resulted in lower void ratios, the recompression and compression indices were not affected by temperature. It should be noted that the pressure range considered by Campanella and Mitchell (1968) started at 200 kPa, and as such their results agree with those of Plum and Esrig (1969). However, while Campanella and Mitchell (1968) only ran constant temperature consolidation tests, Plum and Esrig (1969) also applied heating-cooling cycles during consolidation tests, and observed that the tested clay exhibited overconsolidated behavior following heating-cooling at both 100 kPa and 200 kPa. From this, they suggested that temperature changes can lead to a change in the preconsolidation pressure of the specimen.

Further studies expanded upon these findings by considering the impact of heating and heating-cooling on volume changes and compressibility for various clay mineralogies and stress ranges. Demars and Charles (1981) applied successive heating-cooling cycles from 25 to 50 °C to marine clays at several different pressures (3.5, 7, 14, 28, and 55 kPa) during their consolidation tests, and showed, in agreement with the previous studies, that there was unrecovered thermal plastic strain following each temperature cycle. This first confirmed the observation of Campanella and Mitchell (1968) that the strain after the first temperature cycle at a given constant pressure induces the largest amount of strain. It further adds that changing the mechanical pressure applied to the specimens causes additional irreversible thermal strains with temperature cycles (Demars

and Charles 1981). Demars and Charles (1981) showed that specimens that were heated and cooled prior to consolidation testing had steeper recompression slopes and, thus, lower preconsolidation pressures, than specimens that did not undergo the temperature cycle prior to loading. Demars and Charles (1981) also considered the effect of the preconsolidation pressure on volume change of the clay specimens and found that specimens with higher overconsolidation ratios (OCR) experienced smaller magnitudes of thermal strains when subjected to heating-cooling cycles than specimens with lower OCR. Finally, Demars and Charles (1981) tested natural marine specimens of various mineralogies and reported that silt specimens developed half the volume change that clay specimens experienced.

Baldi et al. (1988) were the first to explicitly investigate the difference in the response of overconsolidated (OC) and normally consolidated (NC) clays to thermal loadings. OC clays experienced reversible volume changes upon heating-cooling, while irreversible volume changes were observed in NC clays at any effective stress level (Baldi et al., 1988). Baldi et al. (1988) also found that clays in the OC range experienced dilation upon heating, while NC clays experienced contraction upon heating. Based on their observed axial strains, Baldi et al. (1988) presented an analysis of the microstructure of low-porosity clays which accounted for the lower magnitude strains observed in their testing. They highlighted the importance of mechanical stress history on the thermal response of clays, and laid the groundwork for understanding the behavior observed in subsequent studies on the effect of temperature in consolidation testing.

Erikkson (1989) and Tidfors and Sallfors (1989) reported a decrease in the preconsolidation pressure of OC clays as the consolidation temperature increased. This decrease in preconsolidation pressure was accompanied by an increase in the recompression slope at higher temperatures; no changes in the compression slope with temperature were reported. Erikkson (1989) compared

heating to long-term creep, in that it induced higher strains at higher temperatures in the same way that longer load increments lead to lower void ratios for a given effective stress. The decrease in preconsolidation pressure associated with an increase in temperature for OC clays was further reported by several studies (Boudali et al. 1994, Akagi and Komiya 1995, and Cekerevac et al. 2002). Zeinali and Abdelaziz (2023a) showed also that heating OC clay specimens from 20 to 40 °C and further consolidation at 40 °C led to a decrease in preconsolidation pressure. We can conclude that, for OC clays, higher temperatures in the thermal history of the clay, either in heating-cooling or in heating, lead to a decrease in the preconsolidation pressure.

Similar investigations showed the opposite effect arising in NC clays. Burghignoli et al. (1992) confirmed the observations of Baldi et al. (1988) regarding the dilatant strains produced by OC specimens and contractive strains produced by NC specimens, and also showed that heating-cooling cycles increased the preconsolidation pressure of NC remolded specimens. Abuel-Naga et al. (2005) and Samarkoon and McCartney (2020) also showed an increase in yield stress following heating-cooling cycles on NC clays. Some studies also compared the effect of heating-cooling on the preconsolidation pressure to that of heating only. Towhata et al. (1993) confirmed that heating (i.e., initial consolidation at 20 °C followed by a heating stage to 90 °C and subsequent consolidation at 90 °C) led to an increase in the preconsolidation pressure. Additionally, they found that a comparable specimen which was heated to 90 °C at the same stress level and then cooled to 20 °C before continuing consolidation had a preconsolidation pressure slightly higher than that of the specimen which experienced heating only. Sultan et al. (2002) showed similar results in which the preconsolidation pressure of an NC Boom clay was higher after heating-cooling than after heating. Figure 1.1 summarizes the increase in preoconsolidation pressure observed in several studies on heating and heating cooling of NC clays. From all these studies, we can state that

elevated temperatures in the thermal history of NC clays leads to an increase in the preconsolidation pressure, with the magnitude of the impact depending on the final consolidation temperature.

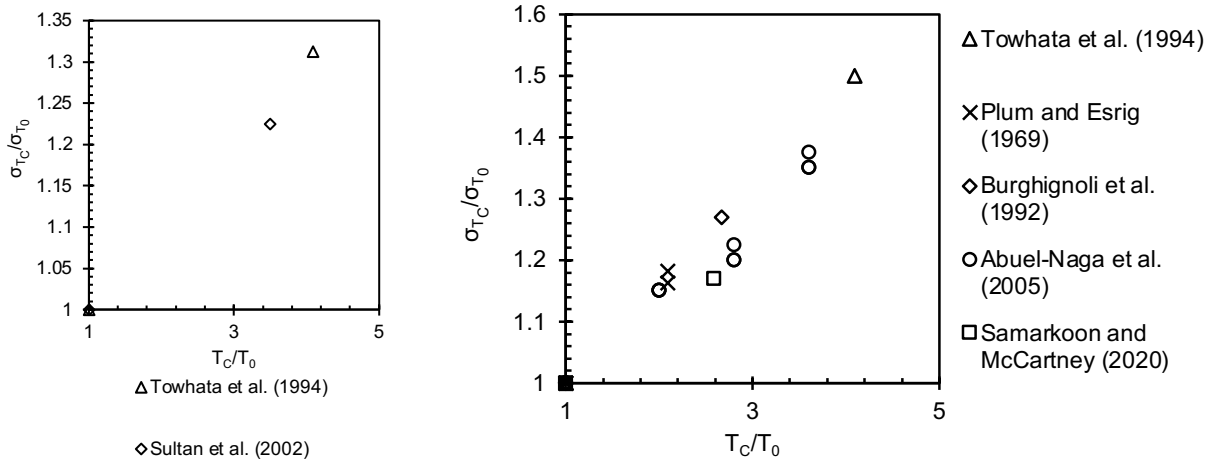

(a) (b)

Figure 1.1 Change in preconsolidation pressure with temperature for (a) heating and (b) heating-cooling thermal paths.

Other studies have also considered the impact of thermal changes on compressibility, coefficient of consolidation, and permeability. As far as the compressibility of OC and NC clays, the findings of the aforementioned studies have generally shown that while the recompression slope is affected by temperature, whether as a result of temperature cycles or constant temperature increase during consolidation tests, the compression slope remains unchanged. As for the coefficient of consolidation, Delage et al. (2000) reported that there was an increase in the rate of drainage from specimens and an increase in the permeability upon heating. Similarly, Towhata et al. (1993), Akagi and Komiya (1995), and Cui et al. (2009) reported increases in the coefficient of consolidation of both NC and OC clays following heating.

1.2.2 Effect of freezing and freezing-thawing on soil behavior

Studies focusing on the consolidation of frozen soils are largely centered around the problem of thaw-induced consolidation settlement. Chamberlain (1981) approached this topic by first providing an explanation for the processes which occur within a soil mass during freezing, and then by applying this framework to the results of consolidation tests on a frozen-thawed clay. While freezing causes an increase in the volume of soil due to the expansion of pore water upon phase change to ice, the negative pore water pressures associated with the migration of pore water toward the freezing front (i.e., cryo-suction) increase the effective stress, which leads to an overconsolidated state in the portion of soil which water migrates from. Consolidation tests on a thawed dredged soil showed lower void ratios for a given effective stress than the pre-frozen material, and a decrease in the compression slope (Chamberlain and Blouin, 1978). The coefficient of consolidation of the thawed soil was also reported to be two orders of magnitude greater than that of the pre-frozen material (Chamberlain, 1981). This increase was linked to the increase in permeability of the frozen-thawed soil. Although Chamberlain (1981) pointed this process out theoretically, the change in soil fabric caused by freeze-thaw cycles was actually recorded by Graham and Au (1984), who noted the fissured microfabric which develops as a consequence of ice lens formation and soil lens densification after the application of six freeze-thaw cycles to 76-mm diameters specimens of a natural plastic clay. Additionally, for pressures below the in-situ preconsolidation pressure, Graham and Au (1984) reported higher rates of drainage from frozen-thawed specimens than unfrozen specimens during anisotropic triaxial consolidation tests. Eigenbrod et al. (1996), in freezing tests which captured the change in pore pressure during the freezing process, recorded initial positive spikes in the pore water pressure followed by the development of negative porewater pressures. The positive maximums were roughly equal to the

overburden pressure, while the negative maximums were correlated to the volume changes of the specimens following freeze-thaw. Eigenbrod et al. (1996) also noted that no volume changes were observed within the specimens during the initial stages of freezing, as ice formation was counterbalanced by the compression of the soil fabric. This time-dependent analysis reveals the role of pore pressure in the densification of the soil. In an analysis of the effects of freeze-thaw on the microstructure of a kaolinite clay, Zeinali and Abdelaziz (2020) performed nitrogen gas adsorption on frozen-thawed specimens with both single- and double-drainage boundaries. They found that while the specific surface area (SSA) decreased after thawing over the entire length of the specimen, the SSA during freezing increased near the drainage boundaries and decreased away from drainage boundaries. On the macro-scale, Ozgan et al. (2015) reported that after thirty freeze-thaw cycles particle diameters of fine-grained soils decreased, as particles disaggregated and disintegrated due to ice formation. It's clear from these results that freezing-thawing induces important micro- and macro-structural changes in the soil fabric which result in the changes observed in consolidation behavior of soils after thawing.

Because freeze-thaw processes in nature are typically cyclic, researchers have also reported the changes in soil behavior after various numbers of freeze-thaw cycles. Chamberlain (1981) showed that the first in a series of three or four freeze-thaw cycles caused the greatest volumetric contractions of a soil. Ghazavi et al. (2023) reported that permeability increased with number of freeze-thaw cycles until either the second or third cycles (depending on the mineralogy of the soil), after which it became constant. The compressibility index experienced similar increases until the third freeze-thaw cycle and plateaued after subsequent cycles (Ghazavi et al., 2023). Ozgan et al. (2015) also showed that the amount of consolidation expected from fine-grained soils increased after thirty freeze-thaw cycles as compared to the unfrozen soil. The compressibility of clays was

thus shown to be affected most by the initial freeze-thaw cycles, after which the changes stabilize.

Another important parameter which is affected by freeze-thaw cycles is the preconsolidation pressure. Chamberlain (1981) found that the negative pore pressures generated during freezing led to a higher apparent preconsolidation pressure upon thawing, as demonstrated by consolidation tests in which either three or four freeze-thaw cycles were applied to the specimen. Following three freeze-thaw cycles applied at a pressure of 16 kPa, the yield stress increase to 240 kPa, while for four freeze-thaw cycles applied at a pressure of 128 kPa, the yield stress increased to 660 kPa. Chamberlain (1981) claimed that the difference between the initial preconsolidation pressure and the post-thaw one was equivalent to the amount of negative effective stress which was generated during the cyclic freezing processes. Qi et al. (2008) found that the impact of freeze-thaw on the preconsolidation pressure depended on the dry unit weight of the specimen. Specimens with low initial dry unit weights (<16.25 kN/m^3) had higher yield stresses following freeze-thaw cycles, while specimens with initial dry unit weights above 16.25 kN/m^3 had lower preconsolidation pressures after freeze-thaw cycles. They also found that the lower the applied temperature, the greater the change in the preconsolidation pressure. In a similar vein, Dumais and Konrad (2023) found that whether a soil was ice-rich or ice-poor, which is a function of the initial water content of the specimen, determined whether the plastic strains recorded during freezing were significant or not. When juxtaposed, these two results indicate that the change in preconsolidation pressure with freezing-thawing may be linked to the amount of water in the specimen. However, as suggested by the results of Qi et al. (2008), the reported experimental results do not provide a conclusive determination of whether freeze-thaw cycles increase or decrease the preconsolidation pressure of fine-grained soils. More generally, while experimental data on freeze-thaw cycles are important to understanding the impact of a frozen history on the

current behavior of clays, they are limited in that they cannot be used to explain the behavior of soils that still contains some portion of ice.

Unlike for frozen-thawed soil, modeling the consolidation behavior of thawing or still-frozen soils requires an understanding of the behavior of both ice and water in the soil pores. In their study on consolidation of thawing soils, Morgenstern and Nixon (1971) presented a closed-form solution to predict the pore pressures that arise during consolidation of a thawing soil both under its self-weight and during the loading stage. In developing their solution, they state that below the freeze-thaw isotherm, under which soil is entirely frozen, no significant pore pressures or deformations are expected. The implication of this statement on the compressive behavior of frozen soil is two-fold: first, that the compressive behavior of frozen soil is dominated by the pore ice, and second, that this pore ice is relatively incompressible. However, this is a simplification of soil behavior, and it has since been shown experimentally that frozen soil does, in fact, deform.

Qi et al. (2010), Shastri et al. (2021), and Cai et al. (2024) demonstrated that frozen soils exhibited extremely high preconsolidation pressures upon consolidation testing. Qi et al. (2010) introduced the term pseudo-preconsolidation pressure (PPC) to describe the pressure after which frozen soils will begin to deform. In these studies, frozen soils subjected to consolidation testing yielded at high pressures (>1 MPa), with the PPC increasing as the test temperature decreased (i.e., more freezing). Figure 1.2 summarizes the results of two such studies (Qi et al., 2010; Shastri et al., 2021). These results suggest that even in soils which are frozen, deformation can occur due to loading. However, the mechanisms by which frozen soils deform are not well understood.

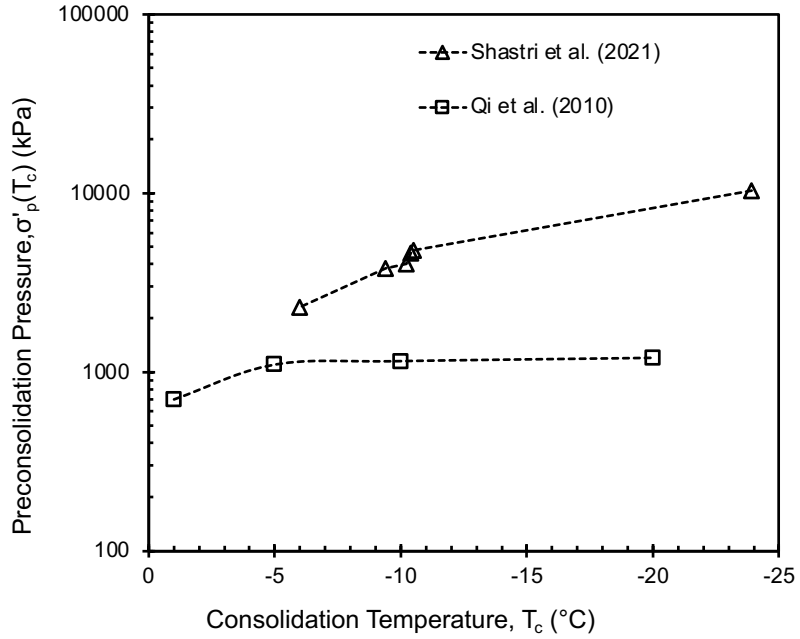

Figure 1.2 Changes in preconsolidation pressure with temperature for frozen soil specimens.

Establishing a concept of volume deformation of frozen soil is complicated by the presence of bound water. Researchers have long understood that not all water in soils freezes even below the freezing point of bulk water (Taber, 1929; Eigenbrod et al., 1996). In fact, the freezing point of pore water in soils has been reported to be between -3 and -4 °C, primarily due to the chemical interactions between soil particles and water (Cai et al., 2024; Kozlowski, 2009; Zhou et al., 2018). Furthermore, even at extremely low temperatures, a portion of the pore water does not freeze; this super-cooled fluid is referred to as the bound water (Tian et al., 2014; Sotthewes et al., 2017; Jin et al., 2020). Others have pointed out that the freezing point of pore water, and by extension the melting point of pore ice, may be linked to pressure; for example, an increase in the applied pressure during loading for consolidation testing can lead to pressure melting of the ice in soils (Black, 1995; Zhou et al., 2018; Shastri et al., 2021). The presence of bound water and the possibility of pressure melting complicate efforts to model the behavior of the pore ice in frozen

soils. However, as reported by Williams and Burt (1974), Bishop and Henkel (1962) and Yao et al. (2018), the unfrozen water in frozen soils does migrate, albeit slowly, and therefore consolidation of frozen soils is possible. Given the complex mechanisms which can occur in frozen soils, further investigation is necessary to develop a simplified, yet robust relations to capture the consolidation response of frozen soils.

Finally, Zeinali and Abdelaziz (2023) considered the impact of a frozen stage on the consolidation behavior of a heated OC clay. In their study, they compared the change in preconsolidation pressure of a heated OC kaolinite specimen to that of a frozen-thawed-heated specimen. They concluded that the previous frozen state impacted the preconsolidation pressure determined at the final consolidation temperature. This study suggests that soils may have a thermal stress history similar to that of a mechanical stress history, and that, in order to determine the behavior at the current temperature, it is necessary to take into account what temperatures the soil has previously been subjected to. However, the impact of the thermal stress history on NC soils has not been confirmed yet and thus required assessment.

1.3 Research Objectives

While the division in focus of previous research seems natural in the context of their proposed applications and differing physical explanations, expanding geothermal applications and worsening temperature extremes across the globe have revealed the limits of these findings. Now more than ever, as permafrost melts at higher rates and historic global temperatures are being recorded each year, it is clear that the range of temperatures that soil is subjected to is ever-widening. More importantly, it is becoming more and more likely for a soil to subjected to more than one temperature extreme. As engineers consider the problems of sustainability, reliability, and resilience of geotechnical systems, understanding the behavior of soil over the entire temperature

domain is more important than ever.

This research is motivated by the growing need for a holistic model for soil behavior over the continuous temperature domain. As can be seen from the literature review section, the behavior of soil under different temperatures is influenced not only by the temperature itself, but also by mechanical stress history, mineralogy, and pore fluid characteristics, to name a few confounding factors. As such, the focus of this thesis has been narrowed down to a single soil type to allow us to identify specifically the effect of temperature on the parameters of interest. Furthermore, several soil properties are expected to change with temperature. However, a single parameter, the preconsolidation pressure, was identified upon which to focus our efforts due to the time limitation. The overconsolidation ratio (OCR) of clays is useful in both compressibility and strength analyses, and the determination of preconsolidation pressure is critical to establishing the OCR of a soil. The two tasks which are the focus of this thesis are:

1. Determining how preconsolidation pressure of an NC clay evolves over a continuous temperature domain ranging from freezing to elevated temperature. The ultimate output of this task is a simple, yet robust relation to predict the preconsolidation pressure over full temperature domain.
2. Assessing how temperature history affects preconsolidation pressure of NC clays, which will highlight the importance of temperature history (as compared to mechanical stress history) on the behavior of NC clays.

1.4 Thesis Organization

The main body of this thesis consists of two draft manuscripts presented in Chapters 2 and 3, which will be submitted to recognized peer-review publishers in geotechnical engineering. The

conclusion and the recommendations for future research of this thesis are presented in Chapter 4.

- Chapter 2 discusses how the preconsolidation pressure of normally consolidated clays evolves over a continuous temperature domain extending from freezing to elevated temperatures.
- Chapter 3 discusses how thermal history impacts the preconsolidation pressure of normally consolidated clay. Since this chapter represents the first attempt to highlight the importance of thermal history of soil behavior, it explicitly focuses on the impact of past freezing on the preconsolidation pressure at elevated temperatures.
- Chapter 4 presents conclusions derived from the experiments performed in this thesis and provides recommendations for future research.

References

Abdelaziz, S.L., Olgun, C.G., and Martin, J.R. II (2011). "Design and operational considerations of geothermal energy piles." Geo-Frontiers 2011: Advances in geotechnical engineering, 450-59.

Abuel-Naga, H.M., Bergado, D.T., Soralump, S., and Rujivipat, P. "Thermal consolidation of soft Bangkok clay." Lowland Technology International, 7(1): 13-21.

Akagi, H. and Komiya, K. (1995). "Constant rate of strain consolidation properties of clayey soil at high temperature." International Symposium on Compression and Consolidation of Clayey Soils - IS Hiroshima's 95, Hiroshima, 1, 3-8.

Baldi, G., Hueckel, T., and Pellegrini, R. (1988). "Thermal volume changes of the mineral-water system in low porosity clay soils." Canadian Geotechnical Journal, 25: 807-825.

Berlemann, M., & Steinhardt, M. F. (2017). Climate change, natural disasters, and migration—a survey of the empirical evidence. *CESifo Economic Studies*, *63*(4), 353-385.

Bird, K.J., Charpentier, R.R., Gautier, D.L., Houseknecht, D.W., Klett, T.R., Pitman, J.K., Moore, T.E., Schenk, C.J., Tennyson, M.E., and Wandrey, C.J. (2008). "Circum-Arctic Resource Appraisal: Estimates of Undiscovered Oil and GAS North of the Arctic Circle." USGS Fact Sheet 2008-3049.

Bishop, A.W. and Henkel, D.J. (1962). "The Measurement of Soil Properties in the Triaxial Test." Edward Arnold, London.

Black, P.B. (1995). "Applications of the Clapeyron equation to water and ice in porous media." Cold Regions Research & Engineering Laboratory Report 95-6.

Boudali, M., Leroueil, S., and Srinivasa Murthy, B.R. (1994). "Viscous behavior of natural clays." XIII ICSMFE, New Delhi, India.

Brandl, H. (2006). "Energy foundations and other thermoactive ground structures."Geotechnique, 56(2): 81-122.

Burghignoli, A., Desideri, A., and Miliziano, S. (1992). "Deformability of clays under non isothermal conditions." Revista Italiana Di Geotecnica, 4: 227-235

Cai, W., Zhu, C., and Lein, W. (2024). "Measurement and modeling of thermo-hydro-mechanical behaviors of frozen clays: frost susceptibility and compressibility." Transportation Research Record, 00(0): 1-12.

Campanella, R.G. and Mitchell, J.K. (1968). "Influence of temperature variations on soil behavior." ASCE Journal of the Soil Mechanics and Foundations Division, 94(3): 709-734.

Cekerevac, C., Laloui, L., and Vulliet, L. (2002). “Dependency law for thermal evolution of preconsolidation pressure.” Numerical Models in Geomechanics VIII: 687-692.

Chamberlain, E.J. and Blouin, S.E. (1978). “Densification by freezing and thawing of fine material dredged from waterways.” Third International Conference on Permafrost: 623-628.

Chamberlain, E.J. (1981). “Overconsolidation effects of ground freezing.” Engineering Geology, 18: 97-110.

Chang, D.K. and Lacy, H.S. (2008). “Artificial Ground Freezing in Geotechnical Engineering.” Sixth International Conference on Case Histories in Geotechnical Engineering, Arlington, VA, USA: Paper No. 7.56a.

Cui, Y.J., Le, T.T., Tang, A.M., Delage, P., and Li, X.X. (2009). “Investigating the time-dependent behaviour of Boom clay under thermos-mechanical loading.”

Delage, P., Sultan, N., and Cui, Y.J. “On the thermal consolidation of Boom clay.” Canadian Geotechnical Journal, 37: 343-354.

Demars, K.R. and Charles, R.D. (1981). “Soil volume changes induced by temperature cycling.” Canadian Geotechnical Journal, 19: 188-194.

Dumais, S. and Konrad, J.-M. (2023). “Framework for thaw consolidation of fine-grained soils.” Canadian Geotechnical Journal, 61: 931-944.

Duncan, J.M. and Campanella, R.G. (1965). “The Effect of Temperature Changes During Undrained Tests.” U.s. Army Engineers Waterways Experiment Station, Soil Mechanics and Bituminous Materials Research Lab, Report TE-65-10.

Eigenbrod, K.D., Knutsson, S., and Sheng, D. (1996). “Pore-water pressures in freezing and thawing fine-grained soils.” Journal of Cold Regions Engineering, 10(2): 77-92.

Eriksson, L.G. (1989). “Temperature effects on consolidation properties of sulphide clays.” 12th International Conference on Soil mechanics and Foundation Engineering, Rio de Janeiro, Brazil: 2087-2090.

Ghazavi, M., Roustaei, M., Safaei, V., and Kahlor, A. (2023). “Effect of freeze-thaw cycles on consolidation behavior of two plastic fine soils.” Geotechnical and Geological Engineering, 41: 1473-1483.

Graham, J. and Au, V.C.S. (1984). “Effects of freeze-thaw and softening on a natural clay at lows stresses.” Canadian Geotechnical Journal, 22: 69-78.

Javadinejad, S., Eslamian, S., Ostad-Ali-Askari, K., Nekooei, M., Azam, N., Talebmorad, H., Hasantabar-Amiri, A., & Mousavi, M. (2019). Relationship between climate change, natural disaster, and resilience in rural and urban societies. *Handbook of climate change resilience*, 1-25.

Jin, X., Yang, W., Gao, X., Zhao, J.-Q., Li, Z., and Jian, J. (2020). “Modeling the unfrozen water content of frozen soil based on the adsorption effects of clay surfaces.” Water Resources Research, 56, e2020WR027482.

Ladd, C.C. (1961). “Physico-Chemical Analysis of the Shear Strength of Saturated Clays.” Thesis, Massacusetts Institute of Technology.

Lambe, T.W. (1953). “The Structure of Inorganics Soil.” Proceedings, ASCE, 79: No. 315.

Lambe, T.W. (1960a). “The Structure of Compacted Clay.” Transactions, ASCE, 125: 682-706.

Lambe, T.W. (1960b). “A Mechanistic Picture of Shear Strength in Clay.” ASCE Research Conference on Shear Strenght of Cohesive Soils Proceedings: 555-580.

Lambe, T.W. (1961). “Residual Pore Pressures in Compacted Clay.” Fifth International Conference on Soil Mechanics and Foundation Engineering Proceedings, 1: 207.

Mbaye, L. M. (2017). Climate change, natural disasters, and migration. *IZA World of Labor*.

Ozgan, E., Serin, S., Erturk, S., and Vural, I. (2015). “Effects of freezing and thawing on the consolidation settlement of soils.” Soil Mechanics and Foundation Engineering, 52(5): 247-253.

Palin, E. J., Stipanovic Oslakovic, I., Gavin, K., & Quinn, A. (2021). Implications of climate change for railway infrastructure. *Wiley Interdisciplinary Reviews: Climate Change*, *12*(5), e728.

Plum, R.L. and Esrig, M.I. (1969). “Some temperature effects on soil compressibility and pore water pressure.” Highway Research Board Special Report 103: 231-242.

Qi, J., Ma, W., and Song, C. (2008). “Influence of freeze-thaw on engineering properties of a silty soil.” Cold Regions Science and Technology, 53: 397-404.

Qi, J., Hu, W., and Ma, W. (2010). “Experimental study of a pseudo-preconsolidation pressure in frozen soils.” Cold Regions Science and Technology, 60: 230-233.

Salimi, M., & Al-Ghamdi, S. G. (2020). Climate change impacts on critical urban infrastructure and urban resiliency strategies for the Middle East. *Sustainable Cities and Society*, *54*, 101948.

Samarkoon, R.A. and McCartney, J.S. (2020). “Effect of drained heating and cooling on the preconsolidation stress of saturated normally consolidated clays.” GSP Geo-Congress 315: 620-629.

Schuur, E.A., Bockheim, J., Canadell. J.G., Euskirchen, E., Field., C.B., Goryachkin, S.V., Hagemann, S., Kuhry, P., Lafleur, P.M., Lee, H., and Mazhitova, G. (2008). “Vulnerability of permafrost carbon to climate change; Implications for the global carbon cycle.” BioScience, 58(8): 701-714.

Schweikert, A., Chinowsky, P., Espinet, X., & Tarbert, M. (2014). Climate change and infrastructure impacts: Comparing the impact on roads in ten countries through 2100. *Procedia Engineering*, *78*, 306-316.

Scott, R.F. (1963). “Principles of Soil Mechanics.” Addison-Wesley Publishing Co., Inc., New York.

Shastri, A., Sanchez, M., Gai, X., Lee, M.Y., and Dewers, T. (2021). “Mechanical behavior of frozen soils: experimental investigation and numerical modeling.” Computers and Geotechnics, 138: 104361.

Sotthewes, K., Bampoulis, P., Zandvliet, H.J.W., Lohse, D., and Poelsema, B. (2017). “Pressure-induced melting of confined ice.” ACS Nano, 11: 12723-12731.

Sultan, N., Delage, P., and Cui, Y.J. (2002). “Temperature effects on the volume change behavior of Boom clay.” Engineering Geology, 64: 135-145.

Taber, S. (1929). “Frost Heaving.” The Journal of Geology, 37(5): 428-461.

Tian et al. (2014): Tian, H., Wei, C., Wei, H., and Zhou, J. (2014). “Freezing and thawing characteristics of frozen soils: bound water content and hysteresis phenomenon.” Cold Regions Science and Technology, 103: 74-81.

Tidfors, M. and Sallfors, G. (1989). “Temperature effect on preconsolidation pressure.” Geotechnical Testing Journal, 12(1): 93-97.

Towhata, I., Kuntiwattakanu, P., Seko, I., and Ohishi, K. (1993). “Volume change of clays by heating as observed in consolidation tests.” Soils and Foundations, 33(4): 170-183.

Williams, P.J. and Burt, T.P. (1974). “Measurement of hydraulic conductivity of frozen soils.” Canadian Geotechnical Journal, 11(4): 647-650.

Yao, X., Qi, J., Zhang, J., Yu, F. (2018). “A one-dimensional creep model for frozen soils taking temperature as an independent variable.” Soils and Foundations, 58: 627-640.

Yong, R.T., Taylor, L., and Wrkentin, B.P. (1962). “Swelling Pressures of Sodium Montmorillonite at Depressed Temperatures.” Eleventh National Conference on Clay and Clay Minerals Proceedings: 268-281.

Zeinali, S.M. and Abdelaziz, S.L. (2020). “Freezing-thawing effect on saturated clay microstructure.” GSP Geo-Congress 319: 40-48.

Zeinali, S.M. and Abdelaziz, S.L. (2023). “Effect of freezing-thawing on preconsolidation pressure.” GSP Geo-Congress 340: 505-513).

Zheng, L., Gao, Y., Zhou, Y., Liu, T., and Tian, S. (2021). “A practical method for predicting ground surface deformation induced by the artificial ground freezing method.” Computers and Geotechnics, 130: 103925.

Zhou, J., Wei, C., Lai, Y., Wei, H., and Tian, H. (2018). “Application of the generalized Clapeyron equation to freezing point depression and unfrozen water content.” Water Resources Research, 54: 9412-9431.

CHAPTER 2. EVOLUTION OF PRECONSOLIDATION PRESSURE OF NORMALLY CONSOLIDATED CLAYS WITH TEMPERATURE

The contributions of the authors to the composition of this manuscript are delineated as follows:

Suzanna Gevorgyan

- Performed literature review.
- Set up the equipment for laboratory tests.
- Performed all experiments.
- Performed analyses associated with laboratory data.
- Prepared the figures and tables.
- Wrote the draft manuscript.

Dr. Sherif L. Abdelaziz

- Developed the idea for this research investigation.
- Oversaw the analysis associated with laboratory data.
- Provided feedback throughout this study.
- Reviewed and edited the draft and final manuscripts.

Evolution of Preconsolidation Pressure of Normally Consolidated Clays with Temperature

Suzanna Gevorgyan[1] and Sherif L. Abdelaziz[2]

[1] Graduate Student, Department of Civil and Environmental Engineering, Virginia Tech, Blacksburg, 24061 VA.; e-mail: gevorgyansm@vt.edu

[2] Associate Professor, Department of Civil and Environmental Engineering, Virginia Tech, Blacksburg, 24061 VA; e-mail: saziz@vt.edu.

The authors of the following manuscript intend to submit it to the ASCE Journal of Geoenvironmental and Geotechnical Engineering.

2.1 Abstract

Normally consolidated (NC) clays which have undergone a temperature change, either in situ, in sampling, in testing, or in application (i.e. in energy infrastructure, around nuclear waste disposal, or geothermal infrastructure such as heat exchange piles), can have different design parameters than those determined in laboratory testing due to the temperature dependence of clay compressibility. To quantify the change in preconsolidation pressure due to temperature changes, a series of temperature-controlled consolidation tests were run on normally consolidated reconstituted kaolinite clay. Bulk samples were incrementally consolidated to a vertical stress of 100 kPa, after which specimens were trimmed and consolidated to 400 kPa to ensure an NC state. Subsequently, the specimens were subjected to a temperature change, including heating, cooling, and freezing, utilizing a thermally-modified, fixed-ring consolidation cell. Following the temperature cycles, the specimens were unloaded and reloaded, and the preconsolidation pressure was determined from the compression curves via the Butterfield method. The preconsolidation pressure was found to increase upon heating, cooling and freezing, with the magnitude of the preconsolidation pressure change varying based on the type of temperature change. The preconsolidation pressure was plotted across the entire temperature domain to determine its relationship with consolidation temperature. A unified mathematical model was proposed based on the experimental results to predict the preconsolidation pressure within the temperature range considered in this study, which included both frozen and elevated temperatures.

2.2 Introduction

Previous studies on the effect of temperature on the engineering properties of soils were spurred by a variety of potential applications. Where soils could be used as backfill or foundations of energy-related applications (e.g., pipelines, electric cables, and thermo-active foundations), the

effect of elevated temperatures was relevant to design (Erikkson, 1989; Tidfors and Sallfors, 1989; Baldi et al., 1988; Delage et al., 2000; Sultan et al., 2002; Abdelaziz et al., 2011). In latitudes where soils undergo seasonal freezing-thawing cycles, understanding the impacts of this thermal path was necessary to prevent damage to structures and roads due to thaw consolidation (Morgenstern and Nixon, 1971). In the use of ground freezing as a construction stabilization method, the behavior of the soil had to be understood both in its frozen and thawed states (Chang and Lacy, 2008; Zheng et al., 2021). Even in northern latitudes where the ground is frozen year-round, the compressibility and strength of frozen soils was relevant to foundation design (Loktionov et al, 2022). Current engineering developments, such as the spreading use of heat exchange piles or the growing interest in building infrastructure in the Arctic zone, increasingly require a thorough understanding of temperature effects on soils (Abdelaziz et al., 2015; Bird et al., 2008). Furthermore, as global temperature extremes widen year-to-year due to global warming (Maninder et al., 2021; Jungvist et al., 2014), the range of temperatures which a soil may be subjected widen as well. In some areas, increasingly cold weather applies freeze-thaw cycles to soils which were previously unfrozen, and in others permafrost which was stably frozen for centuries begins to melt. As engineers contend with these challenges, they require methods to estimate temperature-dependent properties of soil to design more resilient infrastructure.

Preconsolidation pressure is one such parameter which is particularly useful in both settlement and strength analyses (Ladd and Foott, 1974) and has been proven to vary with temperature (Chamberlain, 1981; Graham and Au, 1984; Eriksson, 1989; Tidfors and Sallfors, 1989; Towhata et al., 1994; Moritz, 1995; Sultan et al., 2002; Abuel-Naga et al., 2005). Extensive prior work has been undertaken to explore the effects of temperature on preconsolidation pressure, but this work is limited in its breadth. Since researchers were primarily focused on the thermal

paths which were relevant to their specific applications of interest, the current body of work can be used only for narrow ranges of temperature.

The first range of temperatures is the elevated temperature side, for which heating and heating-cooling thermal paths have been considered. Initially, researchers focused on identifying the volume changes induced by these thermal paths. Campanella and Mitchell (1968), for example, conducted heating-cooling tests on clays. They found that heating led to contraction of soil specimens, but the magnitude was dependent on the maximum cyclic temperature applied. For cycles where the applied temperature was less than the maximum past temperature, heating-cooling cycles resulted in elastic thermal contraction, i.e., recoverable strains upon cooling. However, for cycles in which the applied temperature exceeded the maximum past temperature, irrecoverable volumetric strains were reported upon heating. Later work clarified an important caveat: that the volumetric response of clays to heating and heating-cooling paths was dependent upon their stress history (Baldi et al., 1992). While NC clays exhibited irrecoverable contractive volumetric strains at elevated temperatures, OC clays underwent reversible dilation (Baldi et al., 1992). There was a similar opposing trend discovered for preconsolidation pressure: while heating and heating-cooling cycles decreased the preconsolidation pressure of OC clays (Erikkson 1989; Tidfors and Sallfors, 1989; Moritz, 1995), they increased the preconsolidation pressure of NC clays (Plum and Esrig, 1969; Burghignoli et al., 1992; Towhata et al., 1993; Sultan et al., 2002 Abuel-Naga et al., 2005; Samarkoon and McCartney, 2020). It should be noted that in some previous works there wasn't a clear distinction as to whether the tested clay was in the NC or OC state when temperature changes were initiated (Eriksson, 1989; Tidfors and Sallfors, 1989; Moritz, 1995). This led to some disagreement regarding the effect of heating on the preconsolidation pressure of NC clays. However, in some cases, it is clear that the temperature change was applied

when the clay was in an OC state after sampling (Tidfors and Sallfors, 1989) and, in other cases, there was likely thermal disturbance of natural samples which may have induced an altered stress state prior to testing (Erikkson, 1989). While there is a widespread agreement in that elevated temperatures decrease the preconsolidation pressure of OC clays, the results of these studies complicated establishing a clear effect for NC clays. More recently, several studies have published data which verifies that the preconsolidation pressure varies directly with temperature for NC clays (Towhata et al., 1994; Sultan et al., 2002; Abuel-Naga et al., 2005). Furthermore, it has also been found that the initial preconsolidation pressure does not impact the magnitude of the preconsolidation pressure change for a given temperature change. Abuel-Naga et al. (2005), for example, found that three specimens initially consolidated to 100, 200, and 300 kPa all produced similar OCR values after heating to the same temperature. It has been thus demonstrated that the heating and heating-cooling thermal paths induce an overconsolidated state in NC clays.

The second range of temperatures is the frozen temperatures side, which encompasses both frozen and frozen-thawed soils. As freezing-thawing cycles are more predominant in nature and as an engineering challenge, most of the work on frozen soils have focused on this thermal path. Despite this, it is not well established whether freeze-thaw cycles lead to an increase or decrease in preconsolidation pressure. While some studies have published data to suggest that the preconsolidation pressure decreases as cycles are applied (Graham and Au, 1984), others have found that it increases after thawing (Chamberlain, 1981). Qi et al. (2008) found that the preconsolidation pressure response to freeze-thaw cycles was dependent on the initial dry unit weight of the soil, with specimens below some critical initial condition demonstrating an increase in preconsolidation pressure and those above that limit demonstrating a decrease in their preconsolidation pressure. For frozen soils, the results have been more uniform: Qi et al. (2010),

Shastri et al. (2021), and Cai et al. (2024) all found that the preconsolidation pressure increased as the frozen specimen temperature decreased. Thus, it appears that freezing-thawing and freezing of soils alter the preconsolidation pressure of soils.

The separation between the elevated and frozen temperature domains is most apparent when the physical mechanisms acting in each temperature range are considered. Campanella and Mitchell (1968) purported that the contraction witnessed at elevated temperatures is caused in part by the differential expansion due to temperature of the soil grains and porewater and by the decrease in interparticle friction at higher temperatures. This explanation and the mathematical expressions they presented to predict the change in volume for a given change in temperature have been used and modified subsequently as the body of experimental data has grown. On the other side of the temperature spectrum, the effects of freezing and freezing-thawing on soil fabric and soil particles are totally different in nature. Chamberlain (1981), supported by later work by Eigenbrod et al. (1996) and Graham and Au (1984), put forward that migration of porewater towards the frozen front during freezing leads to densification of soil in between the migration channels. This may be responsible for the apparent overconsolidation reported by some studies (Chamberlain, 1981; Qi et al., 2008). Ozgan et al. (2015) noted that, aside from the soil fabric, the soil particles themselves experience deterioration as freeze-thaw cycles compound on each other. In combination, these changes in the soil structure may explain the variation in the change in preconsolidation pressure following thawing. For frozen soils, the source of the apparent overconsolidation may be easier to identify but not easy to model. The relative incompressibility of ice as a pore fluid likely drives the preconsolidation pressure of frozen soils higher. As more of the pore fluid freezes at lower temperatures (Shastri et al., 2021), the observed increase in yield stress with decreasing temperature aligns with this physical model. However, it is still unclear how

supercooled bound water, which does not freeze even at extremely low temperatures (Sotthewes et al., 2017), or potential pressure melting at high pressures (Shastri et al., 2021) would impact the preconsolidation pressure of frozen soils.

While the isolation of each temperature range makes sense in the historical context, the aforementioned climate change and developing engineering applications create scenarios in which both temperature extremes may be applied to soil in the lifetime of engineered structures. Since lab testing for preconsolidation pressure cannot be undertaken at every temperature of interest, a simple relationship which encompasses the expected soil behavior across frozen to elevated temperatures would allow for more resilient designs. As such, it is necessary to expand upon the results of previous work into an overarching framework which combines these two domains. The purpose of this study is, thus, to develop a simple yet robust relationship that captures clay behavior over the continuous temperature domain from freezing to elevated temperatures. To do so, NC clay specimens were subjected to various temperature changes and then consolidated at their final temperature. With the preconsolidation pressure determined at each final consolidation temperature, the relationship between preconsolidation pressure and consolidation temperature was modeled over a range from -15 °C to 50 °C, thus capturing both elevated and frozen temperatures.

2.3 Experimental Apparatus and Calibration

The testing system used in this study is the same as that used by Zeinali and Abdelaziz (2023) for their study on temperature effects on the preconsolidation pressure of OC clays. A diagram of the system can be found in Figure 2.1 below. The system has two components: a consolidation chamber within a mechanical load frame and a temperature control apparatus.

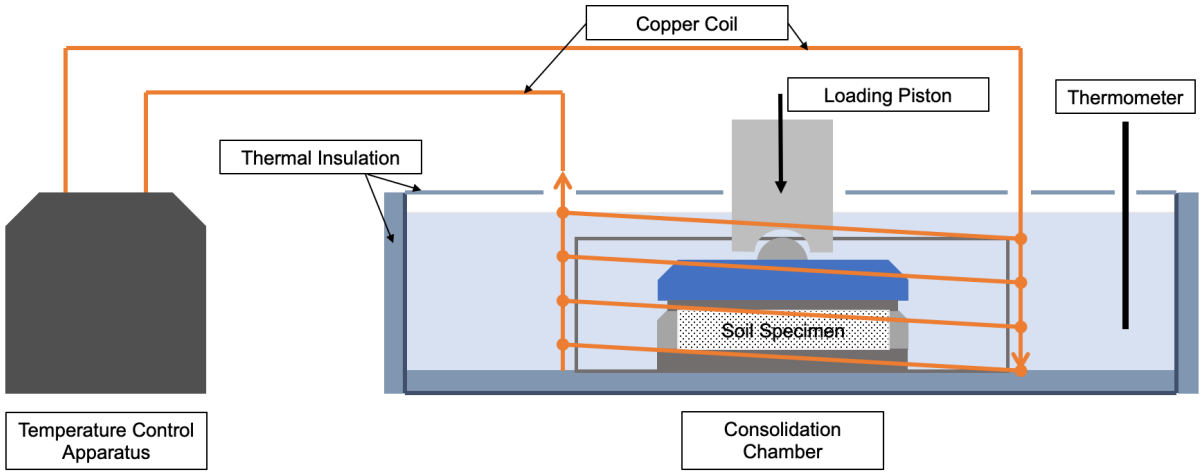

Figure 2.1 Diagram of the experimental testing apparatus used in this study.

A custom-built, thermally insulated consolidation chamber was placed onto the platen of the load frame, and specimens were placed inside the consolidation chamber for testing. The chamber was filled with Julabo Thermal C5 Oil, which is a stable liquid over a temperature range of -60 °C to 100 °C, exceeding the desired temperature for the testing program. This stability allowed the fluid to maintain the temperature inside the consolidation chamber throughout the test with minor variations (±0.1 °C). A copper coil was placed around the specimen inside the consolidation chamber, and this copper coil was connected to the temperature control apparatus. As the temperature unit changed the temperature of the oil circulating within the copper coil, the temperature of the chamber fluid subsequently changed as well. A thermometer was placed inside the consolidation chamber to monitor the chamber temperature; the temperature unit was programmed to adjust the temperature until the chamber fluid temperature matched the desired test temperature. The thermometer was also used to record the chamber temperature throughout the test. Previous calibrations by Zeinali and Abdelaziz (2023) showed that the temperature of the specimen equilibrated with the temperature of the consolidation chamber within 60 minutes.

To isolate the specimen deflections in the test data, calibration tests were run at every temperature of interest to measure the machine deflections at different testing temperatures. An aluminum dummy specimen conforming to ASTM D2345 was used in these calibration tests, with everything else set up to match actual testing conditions (ASTM D2435M-11, ASTM International, 2020). First, the specimen was loaded to 5 kPa (the seating load), and the temperature unit was turned on and set to the reference temperature of 20 °C. Once the chamber temperature stabilized at the reference temperature, the mechanical load was increased to 400 kPa and held for fifteen minutes to allow the machine deflection to stabilize. Then, the temperature was changed to one of the target temperatures, and the machine deflection throughout the temperature change stage were recorded for 6 hours, over which time the chamber temperature stabilized and ample time was given to ensure that the machine deflections stabilized as well. Then, with the target temperature held constant, the dummy specimen was unloaded to 100 kPa and reloaded to the maximum allowable pressure for the load frame. The loading schedules used were identical to those used during actual testing, except that the load duration was shortened to five minutes, staying in accordance with ASTM D2435 (ASTM D2435M-11, ASTM International, 2020). Each calibration test was run at least twice in order to ensure that the recorded machine deflections were consistent. As an example, the machine deflections recorded for three test temperatures can be found in Figure 2.2. The higher temperature (40 °C) caused the largest amount of machine deflection, followed by the reference temperature of 20 °C. The frozen temperature (-4 °C) caused the least amount of machine deflection to be recorded.

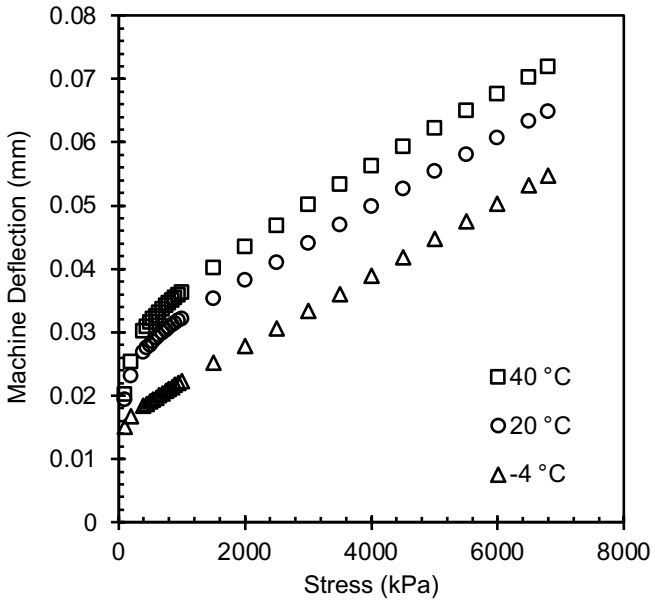

Figure 2.2 Comparison of the machine deflections recorded for three different test temperatures in the pressure range of 100 kPa to the maximum allowable pressure for the load frame.

A calibration test was also conducted at the reference temperature from 5 kPa to 400 kPa to be used in adjusting the test data during the initial consolidation stage of each test.

2.4 Materials and Preparation of Bulk Samples

The clay used in this study is EPK (Edgar Plastic Kaolinite), which is acquired from Edgar, Florida. At room temperature, this clay has a plastic limit (PL) of 29% and a liquid limit (LL) of 54%, resulting in a plasticity index (PI) of 25%. Thus, it classifies as a highly plastic clay (CH) according to the Unified Soil Classification System (USCS). This clay contains more than 97% Kaolinite clay minerals with Zeolite minerals forming the remaining percentage (Jaradat et al., 2017; Ung, 2023).

The bulk samples for this study were prepared by mixing a slurry of the EPK clay powder with de-ionized water at about 1.5 times the LL measured at room temperature. After mixing, the

slurry was poured into a 101.6 mm- (4 inch-) diameter Proctor mold, with the inner surface of the mold smeared with a thin layer of vacuum grease to minimize side friction during the consolidation of the sample preparation. Moreover, two fine sand layers (~ 10 mm each) were placed in the mold, one at the top and another at the bottom with filter papers between the clay slurry and the sand, to allow drainage from the two boundaries of the samples. Once the clay slurry was sandwiched between the sand layers, it was left to consolidate under the weight of a 50 mm (~2 inch) concrete loading cap for 24 hours to reduce piping. Then, the mold was placed in a loading frame and the bulk sample was further consolidated to 100 kPa at room temperature in five loading steps (5, 10, 25, 50, and 100 kPa). Once a vertical effective stress of 100 kPa was achieved, the sample was unloaded, extruded from the Proctor mold, wrapped in plastic wrap, stored in a humidity-controlled room until it was used to trim specimens for the testing program. No samples were stored for more than two weeks to avoid any potential changes in water content or any impact of thixotropy effects.

2.5 Testing Procedure and Program

In general, the specimen preparation follows ASTM D2435 (ASTM D2435M-11, ASTM International, 2020) requirements, with some modifications made to accommodate the thermal phase of the testing program. Specimens were trimmed from the bulk sample using a cutting consolidation ring of about 63.5 mm (2.5 inches) in diameter and 25.4 mm (1 inch) in height. The initial water content of each specimen was determined from the trimmings.

Once specimens were trimmed, they were placed in a thermally-insulated consolidation chamber (oedometer) and inundated. As mentioned previously, the cell fluid used in the consolidation chamber was Julabo Thermal C5 oil. The use of this oil, rather than water, for the testing program is not expected to impact the consolidation results since liquid paraffin used as a

cell fluid did not influence the behavior of specimens during isotropic consolidation testing (Iverson and Moum, 1975). Once the consolidation chamber was filled, a copper coil connected to an external temperature unit was placed around the specimen. The external temperature unit was used to regulate the temperature of the oil circulating within in the copper coil, which subsequently changed the temperature of the cell fluid and therefore the tested specimens. A thermometer was placed in the cell fluid and used to target the desired cell (and specimen) temperature.

For all tested specimens, a seating stage was initiated in which a vertical stress of 5 kPa and an initial set temperature of 20 °C were applied. This seating stage was considered completed upon the stabilization of both vertical stress and cell temperature readings at the desired initial values (i.e., 5 kPa and 20 °C). After that, an initial consolidation stage was initiated at 20 °C until the specimen reached a vertical effective stress of 400 kPa (Figure 2.3). This vertical stress is four times greater than the maximum past pressure used during the preparation of the bulk sample, ensuring the normally consolidated (NC) state of the tested specimens prior to inducing any temperature change (Head, 1992).

Then, while maintaining the vertical stress at 400 kPa, the desired temperature change for each specimen (Table 2.1) was applied. The desired temperature was applied for 24 hours, under 400 kPa, before proceeding with the loading schedule; this duration exceeds the 60 minutes that was identified to be sufficient for the specimen temperature to equilibrate with the set and cell temperatures (Zeinali et al. 2020). The volumetric strain and the temperature in the consolidation chamber were recorded during this temperature change and stabilization stage.

Table 2.1 Testing program for this study and the initial water content and void ratio for each of the tested specimens.

No.	Consolidation Temperature, Tc (°C)	Thermal Path	Initial Water Content	Initial Void Ratio
1	50.0	Heating	47.0%	1.34
2	40.0	Heating	47.4%	1.35
3	30.0	Heating	46.9%	1.35
4	20.0	Reference Temperature, T0	47.2%	1.36
5	10.0	Cooling	47.8%	1.37
6	4.0	Cooling	47.2%	1.32
7	0.0	Freezing	47.8%	1.34
8	-2.0	Freezing	47.3%	1.33
9	-4.0	Freezing	47.7%	1.36
10	-5.5	Freezing	46.9%	1.33
11	-7.0	Freezing	47.5%	1.34

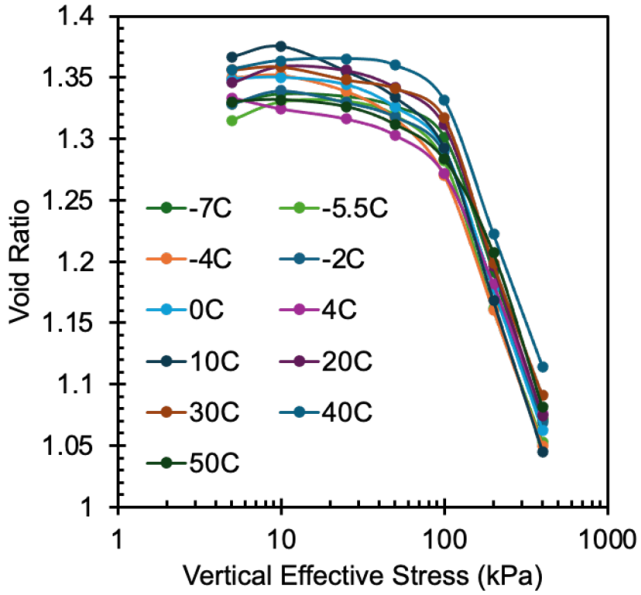

Figure 2.3 Compression curves for all tests during the initial consolidation stage to the NC state to 400 kPa (T = 20 °C).

After the completion of the temperature change/stabilization stage, a second consolidation stage was initiated at the desired test temperature (Table 2.1). The loading schedule used in this stage depended on the temperature, but in all cases, it featured an unloading-reloading loop and final

effective stress greater than 2000 kPa. For specimens subjected to temperatures above freezing (i.e., specimens 1 through 6 in Table 2.1), the loading schedule was 400, 200, 100, 200, 400, 450, 500, 550, 600, 650, 700, 800, 900, 1000, 1500, 2000, and 2500 kPa. While specimens subjected to temperatures less than freezing (i.e., specimens 7 through 12 in Table 2.1), the loading schedule was 400, 200, 100, 200, 400, 1000, 2000, 3000, 4000, 5000, 6000, 7000, 8000, 9000, 10000, 11000, 12000, 13000, and 14000 kPa. Each load duration for each stage was 24 hours. The volumetric deformation and temperature were recorded during each loading and unloading step.

Upon reaching the end of the final loading step, specimens were unloaded to the initial seating vertical stress of 5 kPa and held until the volume change stabilized in order to minimize variations in final measured heights and water contents during removal and extrusion. Specimens were then unloaded completely, removed from the consolidation chamber, and extruded intactly from the oedometer ring. The final specimen height was measured using a caliper, and then the final water content of the specimen was determined.

2.6 Results

2.6.1 Temperature-induced volume changes

The volumetric strains recorded during the temperature change stages for each are shown in Figure 2.2(a) along with the consolidation chamber temperature in Figure 2.4(b). Heating from the reference temperature induced positive axial strains, indicating contraction, in all three heated tests (30 °C, 40 °C, and 50 °C), with more heating-induced axial strains for higher heating temperatures. On the other hand, cooling (to 10 °C and 4 °C) led to negligible contractions, with the recorded strains being an order of magnitude less than those recorded during heating tests. For a 10 °C increase in temperature (i.e., specimen subjected to 30 °C), the specimen contracted 0.32%, while

for a 10 degree decrease in temperature (i.e., specimen subjected to 10 °C), the specimen contracted 0.03%. To better explain this, we need to look at the time versus axial strain graphs for cooling capture the change in volume of the specimen as the temperature changes. Figure 2.5, for example, shows that as the temperature cooled to 4 °C (which developed similarly to the specimen cooled to 10 °C but was selected for analysis because the response is clearer due to the larger temperature difference), the specimen initially experienced positive axial strains, but, ultimately, contracted as the temperature stabilized. In the framework suggested by Campanella and Mitchell (1968), this initial expansion can be attributed to the development of negative porewater pressures as the temperature began to decrease. As the volume expansion coefficient of water is an order of magnitude greater than that of soil, cooling initially leads to the development of suction pressures as the porewater shrinks.

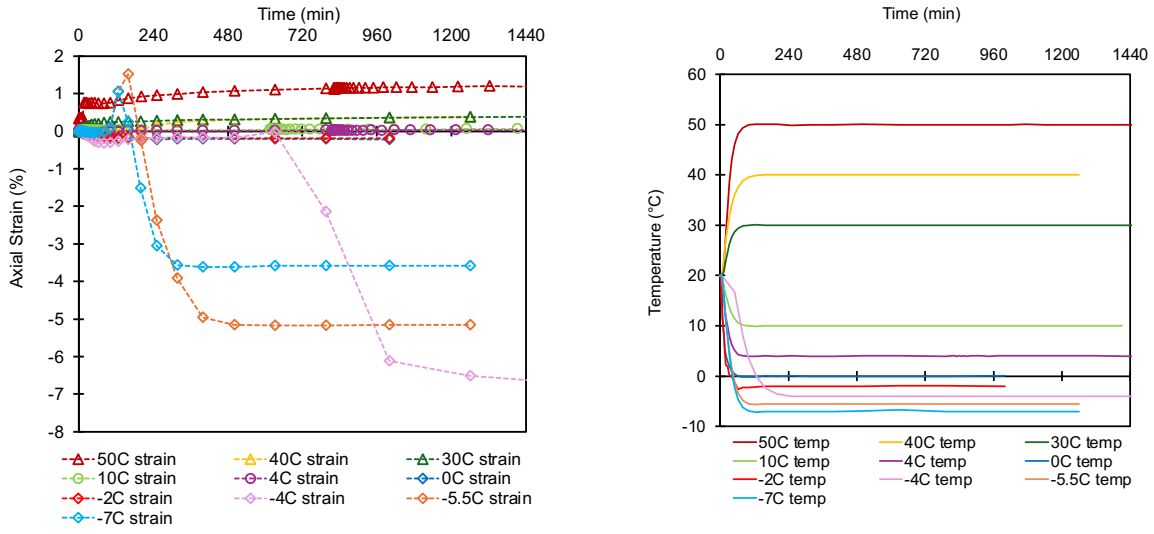

(a) (b)

Figure 2.4 Axial strains (a) and chamber temperature (b) vs time during the temperature change stage.

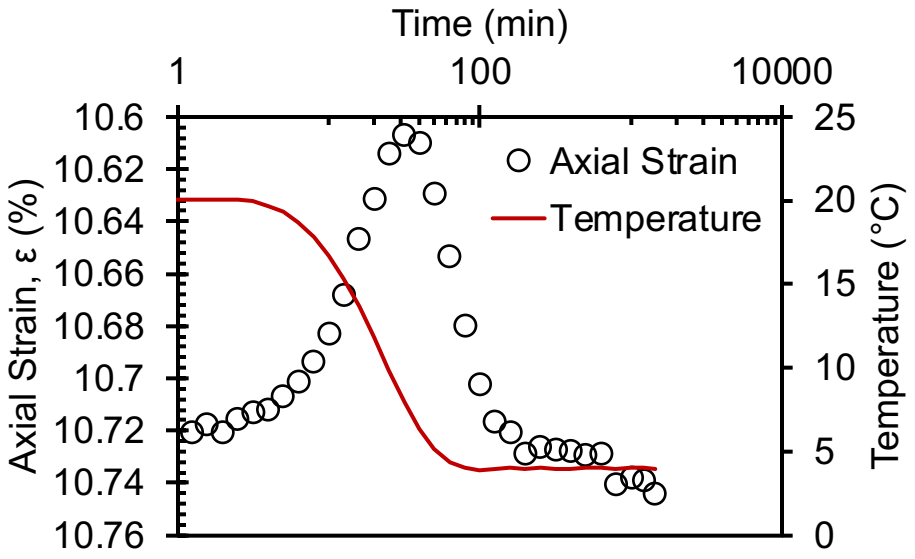

Figure 2.5 Axial strain and temperature vs time during the temperature change stage from 20 °C to 4 °C for 4 °C specimen.

For temperatures below freezing, the specimens expanded (i.e., recorded negative strains) due to ice formation. The strains in the two specimens at temperatures close to the freezing point of bulk water (0 °C and -2 °C) were lower than those at lower temperatures (-4 °C, -5.5 °C, and -7 °C). The higher strains recorded at and below -4 °C support the idea that the freezing point of pore water is lower than that of bulk water, which has been reported previously by others (Kozlowski, 2009; Cai et al., 2024). However, the specimens at temperatures at and below -4 °C did not seem to follow a trend of increasing volumetric strain with decreasing temperature. While the -4 °C specimen recorded an expansion corresponding to around -7% axial strain, the -5.5 °C specimen experienced only -5% axial strain, and -7 °C specimen only recorded around -4% strain. This behavior is counter to expectations from theory, which suggests that as the temperature decreases, more and more weakly bonded pore water would begin to freeze (Shastri et al., 2021). Finally, the low strains at temperatures above -4 °C suggest that there may be some ice crystal formation in the specimens at these temperatures, but the majority of the pore water does not freeze.

2.6.2 Evolution of preconsolidation pressure over temperature

Data collected during each consolidation stage after the completion of the temperature change stage were used to build compression curves for each consolidation temperature. These curves were used to determine the preconsolidation pressure of the specimen at the considered temperature. The initial portion of the total compression curve (<400 kPa, shown in Figure 2.3) indicates that all specimens were normally consolidated before the beginning of the thermal stage. As an example, Figure 2.6 shows the total compression curves for a heated (30 °C), cooled (4 °C), and near 0 °C frozen (-2 °C), and frozen (-4 °C) specimen. The Butterfield method (Butterfield, 1979), which is based on ln(1+*e*)-log(*p*') (Figure 2.7), was used on the loading steps following the temperature change to determine the preconsolidation pressure. Table 2.2 summarizes the preconsolidation pressure estimated for each of the considered temperatures.

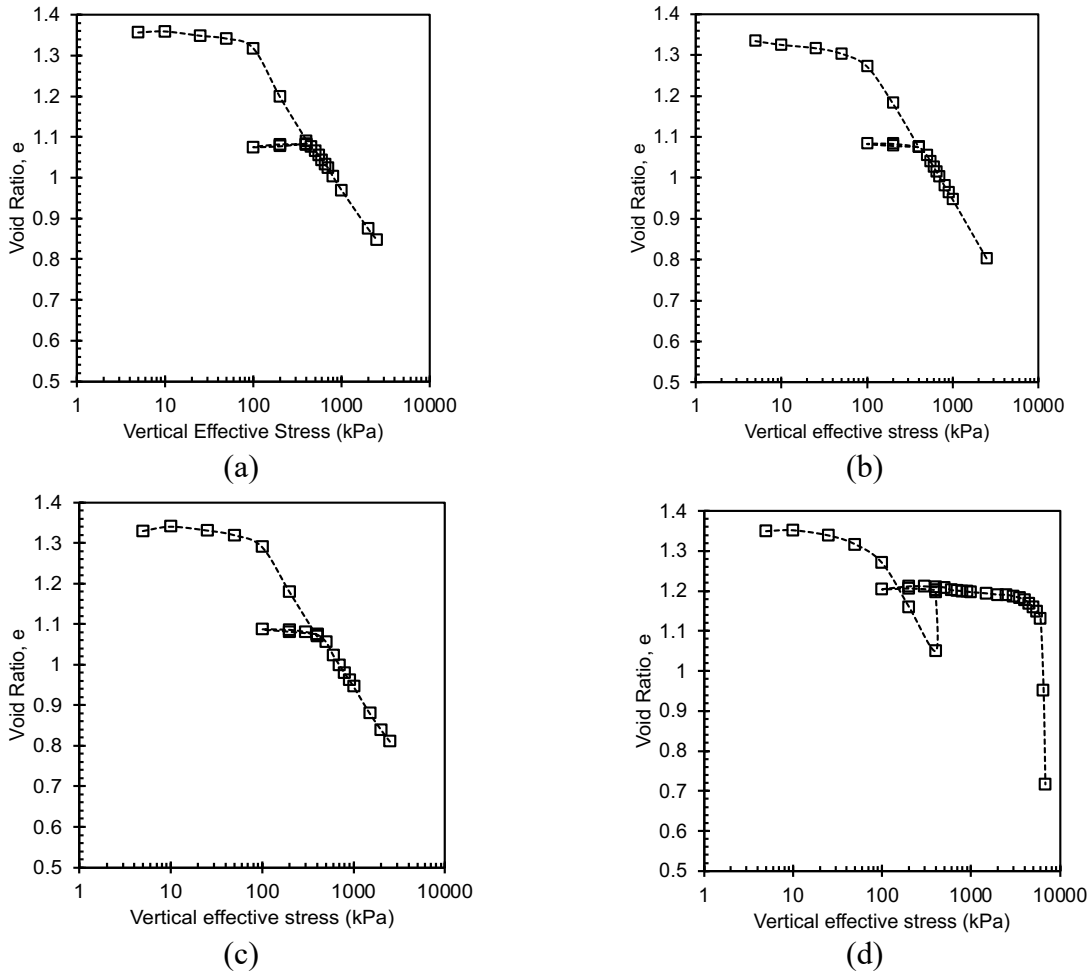

Figure 2.6 Compression curves for 30 °C (a), 4° C (b), -2° C (c), and -4 °C (d).

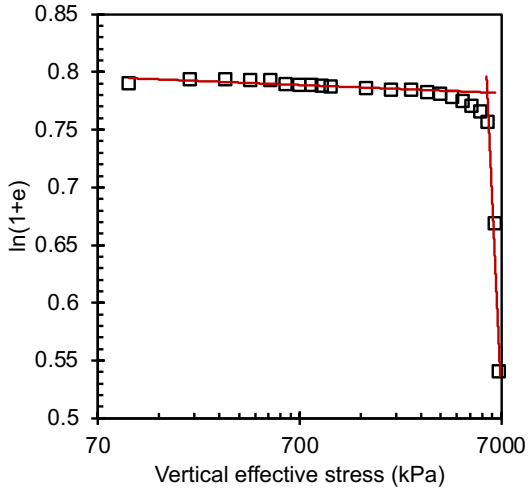

Figure 2.7 Determination of the preconsolidation pressure via the Butterfield ln(1+e) – log stress method for the -4°C specimen.

2.6.3 Evolution of compression and recompression indices versus temperatures

Additionally, the recompression and compression indices before and after the temperature change stage were determined from the compression curves and have been reported in Table 2.2 below for each test. The temperature impact is observed in the compression and recompression indices to different extents. The compression index (C_c) did not change for elevated temperatures, which agrees with the general observation in the literatures for heated soils (Towhata et al., 1994; Sultan et al., 2002). The compression index also did not experience any change for the two specimens consolidated at 0 and -2 °C; it did, however, increase significantly for specimens subjected to lower freezing temperatures. This observation supports the previous discussed hypothesis that no significant freezing of the pore water took place at lower freezing temperatures (0 and -2 °C), while significant phase change of the pore water into ice occurred at lower freezing temperatures. The recompression index (C_r), on the other hand, does not show significant changes over the considered temperature range except at very low freezing temperatures. At these temperatures, C_r appears to be close to zero due to the relative incompressibility of the pore ice in the specimens.

Table 2.2 Estimated preconsolidation pressure, thermally induced OCR, and change in compression and recompression indices.

Test No.	Consolidation Temperature, Tc (°C)	Estimated preconsolidation pressure, σ(TC) (kPa)	Thermally Induced OCR, σ(TC)/σ(T0)	Cr		Cc	
				Reference Temperature (20 °C)	Consolidation Temperature	Reference Temperature (20 °C)	Consolidation temp
1	50	480	1.20	0.034	-0.001	0.34	0.35
2	40	450	1.125	0.032	0.009	0.38	0.35
3	30	430	1.075	0.028	-0.012	0.38	0.32
4	20	400	1	0.029	0.001	0.28	0.34
5	10	420	1.05	0.035	0.001	0.41	0.36
6	4	440	1.1	0.030	0.014	0.33	0.36
7	0	430	1.075	0.033	0.021	0.38	0.36
8	-2	440	1.1	0.030	0.021	0.37	0.35
9	-4	6,000	15	0.033	0.015	0.37	7.34
10	-5.5	10,000	25	0.045	0.009	0.38	-
11	-7	-	-	0.033	0.001	0.38	-

2.7 Discussion

2.7.1 Behavior of heated specimens

The preconsolidation pressure increased with consolidation temperature for all three heated specimens (Table 2.2). Accordingly, the OCR increased to 1.075, 1.125, and 1.20 upon heating to 30 °C, 40 °C, and 50 °C, respectively. The magnitudes of these increases align with those of other studies in both heating and heating-cooling on NC clays (Figure 2.8).

Of note also is the change in the recompression index observed following heating. As can be seen in Table 2.2, the direction of the recompression slope reversed after the temperature change was applied, resulting in continued contraction even as the specimens were unloaded during the unload-reload curve. Coccia and McCartney (2016) previously explained a similar trend using the concept of accelerated thermal creep, the direction of which relied on the direction of the mechanical loading or unloading. The effects of the thermal path can thus be related to the mechanical stress path applied to the specimen.

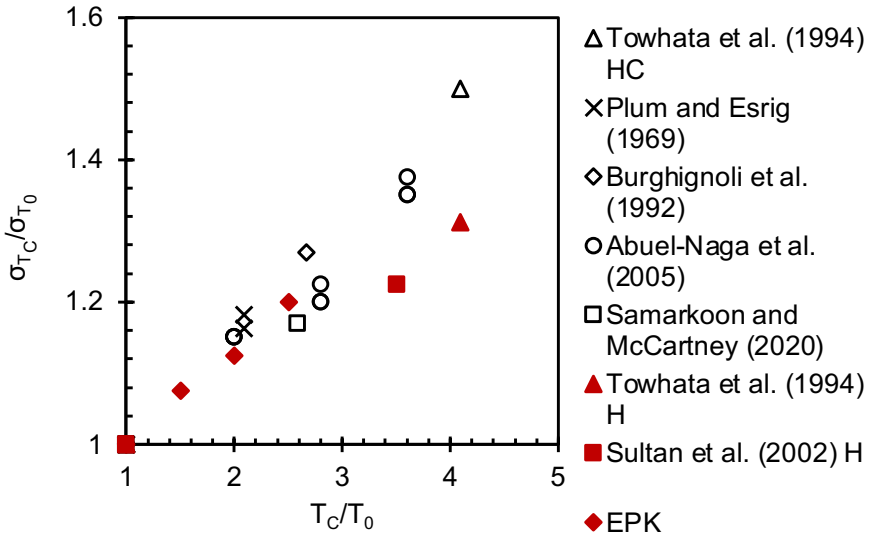

Figure 2.8 Variation of preconsolidation pressure (σ_{Tc}) with temperature (T_c) for NC clays for both heating and heating-cooling thermal paths including the results of this study included for the heated specimens. Note: σ_{T0} is the preconsolidation pressure for the different studies estimated at the reference temperature T_0.

2.7.2 Behavior of cooled specimens (less than reference temperature but above freezing)

There is no existing data for the effects of cooling thermal paths on NC clays. Erikkson (1989), among others (Tidfors and Sallfors, 1989; Moritz, 1995), did report the effect of cooling on OC clays, and showed that the preconsolidation pressure of their tested marine clay was higher at low temperatures (5 °C) than at elevated temperatures (50 °C). For NC clays, cooling has only been considered as part of heating-cooling cycles, and the volumetric behavior and changes in preconsolidation pressure noted after heating-cooling are heavily influenced by the initial heating stage. Because cooling has not been isolated previously, the results of this study cannot be compared for veracity. While more investigations on the cooling thermal path are necessary to better understand the impact of isolated cooling on the volume change behavior of NC clays, the observed volumetric and preconsolidation pressure changes of this study can generally be explained using the literature on the heating-cooling side as a basis. In the framework of Campanella and Mitchell (1968), cooling would cause differential contraction between the pore

water and soil particles which would lead to absorption of water into the specimen. The contractions of the pore water and soil skeleton probably happen much faster than the ability of the water to flow into the specimen, ultimately leading to the contraction upon cooling observed for specimens subjected to 10 and 4 °C in this study.

Similar to heating, cooling induced an overconsolidated state in the specimens. There was a small increase in OCR with decreasing temperature (Table 2.2); the specimen cooled to 10 °C had an OCR of 1.05, while the specimen cooled to 4 °C had an OCR of 1.10. While this apparent overconsolidation may be attributed to the volumetric contraction observed during the temperature change application, the relatively small strains in cooling (as compared to heating) suggest that the volume change may not be totally responsible for this effect. The increased stiffness may instead be attributed to the development of negative pore pressures during cooling, which correspond to increases in effective stress on the macro-scale.

2.7.3 Behavior of frozen specimens

Few studies have considered the preconsolidation pressure of frozen soils (Qi et al., 2010; Shastri et al., 2020; and Cai et al., 2024). All these studies have noted that the preconsolidation pressure increased as the temperature decreased, which is in line with the results of this study. More specifically, the specimens frozen to temperatures above -4 °C in this study exhibited significantly lower preconsolidation pressures than those frozen at and below -4 °C, indicating that there is a critical change in specimen behavior below this temperature (Figure 2.9). When considered in conjunction with the observed axial strains at each temperature, it can be deduced that until most of the pore water freezes at or around -4 °C, the stiffness of the specimen is still controlled by the compressibility of the soil skeleton and the unfrozen water. Once the bulk of the pore water freezes into ice, the stiffness is controlled by the compressibility of the pore ice. As ice is relatively

incompressible compared to soil, significant changes in the preconsolidation pressure are observed.

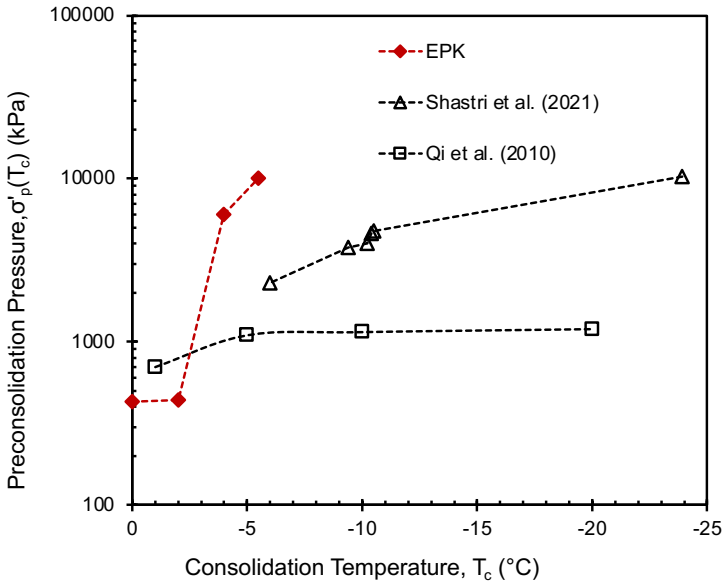

Figure 2.9 The variation of preconsolidation pressure with temperature for frozen thermal path, with the results of this study included.

Figure 2.10 shows the Butterfield method (Butterfield, 1979) determination of preconsolidation pressure for the -4 °C, -5.5 °C and -7 °C specimens. While the yield point for the specimen frozen to -4 °C is clear, the specimen frozen to -5.5 °C did not seem to reach the normally consolidated state even at the maximum equipment load limits. The best estimate for the yield stress at -5.5 °C is 10,000 kPa, which is likely an underestimation since the "virgin compression" portion of the data was much shallower than would be expected based on the results of the -4 °C specimen. The specimen frozen to -7 °C did not even begin to yield at the equipment limit of 15,000 kPa, making determination of the preconsolidation pressure at this temperature impossible using the current instrument. Suffice it to say that the preconsolidation pressure is higher than 15,000 kPa, which falls within the trend of increasing OCR with decreasing temperature.

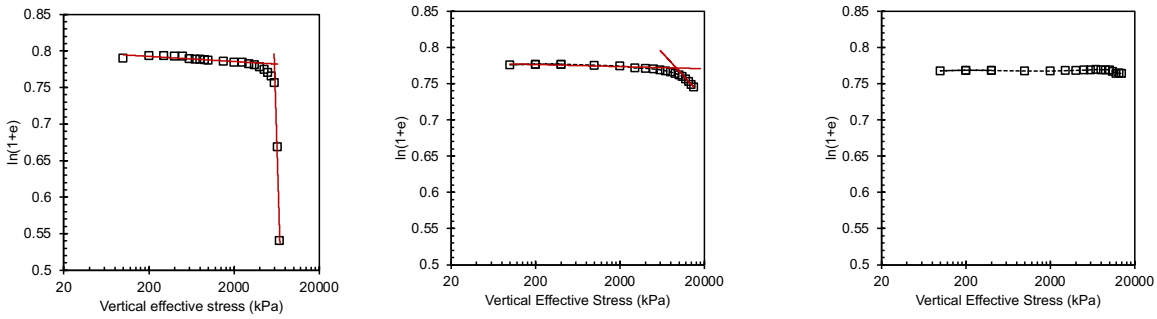

(a) (b) (c)

Figure 2.10 Comparison of the preconsolidation pressure for specimens frozen to -4 °C (a), -5.5 °C (b), and -7 °C (c).

2.7.4 Simplified preconsolidation pressure versus temperature relation

The preconsolidation pressure determined for each test temperature was combined into a single figure to illustrate how the preconsolidation pressure changes with temperature over the entire studied range (Figure 2.11). As can be seen in this figure, the increase in the preconsolidation pressure due to freezing is much more pronounced than that observed due to heating; the latter is better shown in Figure 2.8. This is potentially due to the impact of cryo-suction and the presence of ice in the frozen specimens.

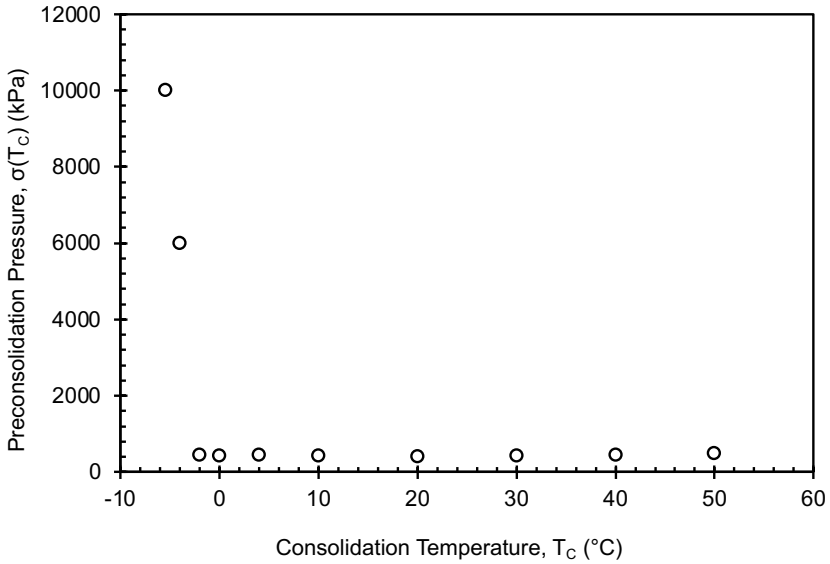

Figure 2.11 Variation of preconsolidation pressure with temperature over the entire studied temperature range (-7 °C to 50 °C).

2.7.4.1 Heating relations for normally consolidated clays

Moritz (1995) and Cekerevac et al. (2002) presented mathematical models to capture the relationship between consolidation temperature (T_c) and change in preconsolidation pressure for heated and heated-cooled clays (i.e. thermally-induced OCR). Moritz (1995) used an exponential fit to model the change in preconsolidation pressure with temperature in their study (Eq. 1), while Cekerevac et al. (2002) developed a fit using a logarithmic function (Eq. 2). Note that the exponential equation originally proposed by Mortiz (1995) has been modified in Eq. 1 by making the exponent negative so that the consolidation temperature may be normalized by the reference temperature in the independent variable, rather than the inverse. Both of the aforementioned studies were performed on OC clays, and the reported parameters reflected the decrease in preconsolidation pressure with increasing temperature. By changing the sign of the fitting parameter in each equation, the direct relationship between temperature and change in preconsolidation pressure could be captured for NC clays, i.e., an increase in the preconsolidation

pressure with temperature increase as shown in Figure 2.12 for the latter relation. As can be seen in Figure 2.13, the two relations were able to represent the increase in preconsolidation pressure as temperature increased for studies in which NC clays were heated, including this study. Table 2.3 summaries the fitting parameters for the two relations for all heated and heated-cooled NC clays reported in the literature and those tested in this study. As can be seen from the values in Table 2.3, the fitting parameters for all clays including the EPK clay used in this study are comparable.

$$\frac{\sigma'_p(T_C)}{\sigma'_p(T_0)} = \left(\frac{T_C}{T_0}\right)^{-\alpha} \quad \text{Eq. 1}$$

$$\frac{\sigma'_p(T_C)}{\sigma'_p(T_0)} = \lambda - \gamma * log\left(\frac{T_C}{T_0}\right) \quad \text{Eq. 2}$$

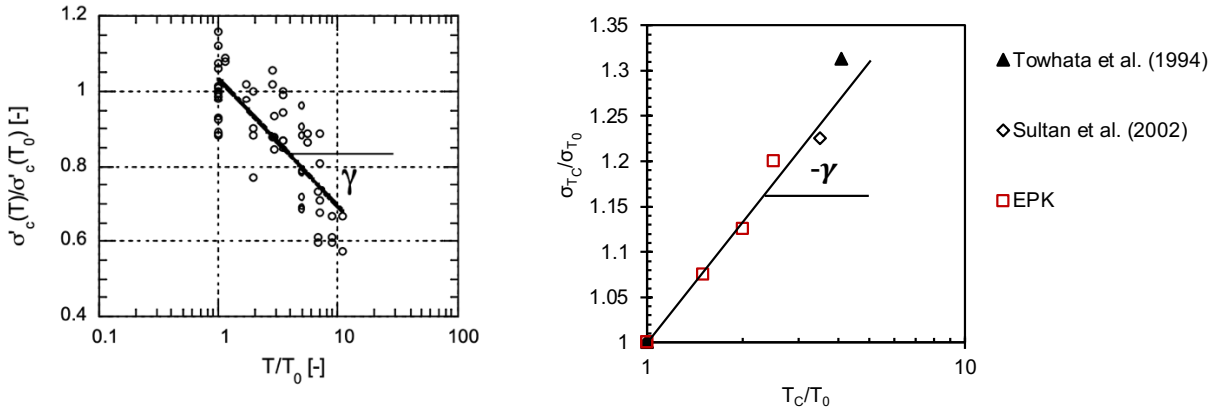

(a) (b)

Figure 2.2 The logarithmic fit from Cekerevac et al. 2002 (a) for OC clays (from Cekerevac et al., 2002) and (b) when used to fit NC heated clay data. Note the change in the sign of the slope in 2.10.b as compared to 2.10.a (from Cekerevac et al., 2002).

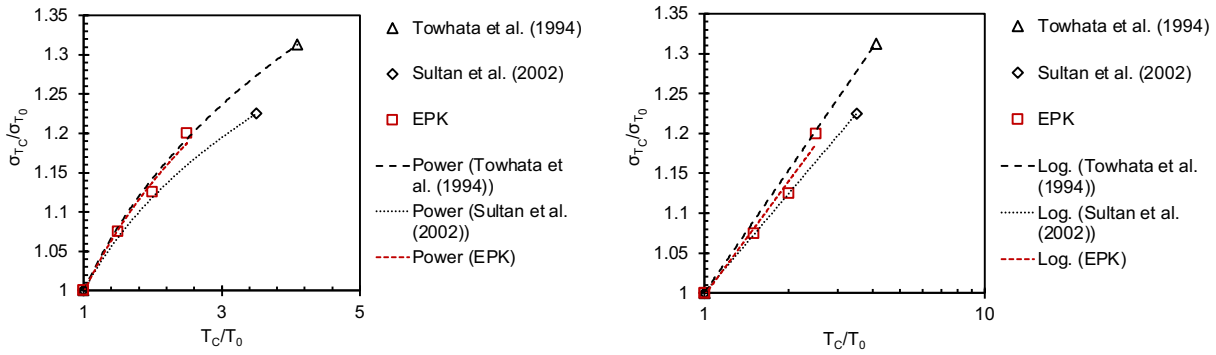

(a) (b)

Figure 2.13 a) exponential fit for heated data (via modified Moritz, 1995), and b) logarithmic fit for heated data (via Cekerevac et al., 2002).

Table 2.3 Fitting parameters for heated data for equations from Moritz (1995) and Cekerevac et al. (2002).

Type of temperature change applied	Reference	α (modified Moritz, 1995)	γ (Cekerevac et al., 2002)
Heating	Towhata et al. (1994)	-0.19	-0.51
	Sultan et al. (2005)	-0.16	-0.41
	EPK (this study)	*-0.19*	*-0.48*
Heating-Cooling	Towhata et al. (1994)	-0.29	-0.82
	Plum and Esrig (1969)	-0.22	-0.54
	Burghignoli et al. (2002)	-0.24	-0.63
	Abuel-Naga et al. (2005)	-0.22	-0.60
	Samarkoon and McCartney (2020)	-0.16	-0.41

2.7.4.2 Freezing relations for normally consolidated clays

While many researchers have developed correlations to capture the strength of frozen soils, no equation for the relationship between preconsolidation pressure and freezing temperature was developed. Shastri et al. (2020) presented a relation to predict the cryo-suction pressure at freezing temperatures, which, as put forward by Chamberlain (1981), is closely related to the preconsolidation pressure. However, to capture the change in preconsolidation pressure with temperature directly, a Boltzmann curve was fitted to Qi et al. (2010) data. This data was chosen

as opposed to data from Shastri et al. (2020) and Cai et al. (2024), or the data produced in this study, because it captured the plateau of the preconsolidation pressure at low freezing temperatures. Because there will always be some portion of super-cooled bonded pore water, a theoretical limiting preconsolidation pressure is reasonable, as there should be a temperature below which no additional ice formation is expected and the stiffness of the soil is controlled by the frozen pore fluid. The maximum preconsolidation pressure value reported by Qi et al. (2010) at -20°C was fixed as a fitting parameter as their data indicated that the expected limiting preconsolidation pressure was already reached.

From the results of this study, while the preconsolidation pressure at temperatures cooler than the reference temperature of 20°C is higher, there is a plateau between the reference temperature and the freezing point of porewater around -4°C (see Figure 2.11). As such, the data from Qi et al. (2010) was extrapolated back using the preconsolidation pressure determined at -1°C, which was the maximum temperature used by Qi et al. (2010). Figure 2.14 shows their published data (filled triangular symbols) and the extrapolated data (hollow symbols).

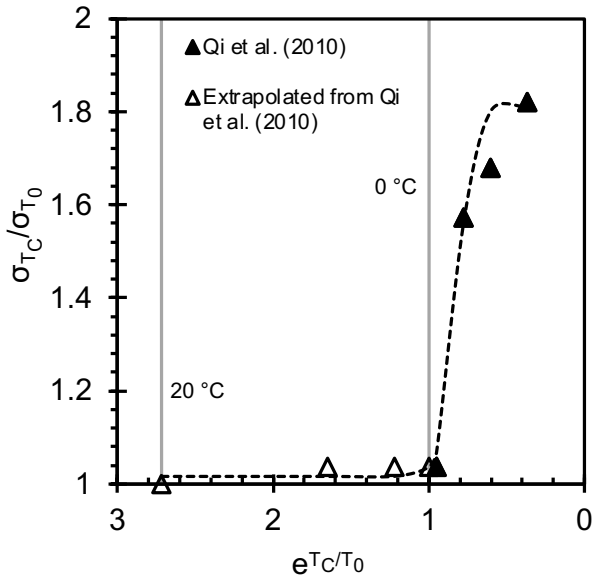

Figure 2.14 Curve fit for Qi et al. (2010) data capturing the plateau at low temperatures.

Then, a Boltzmann curve (Eq. 3) was fitted to this data as it was determined to give the best shape and fit to the data; the four calibration parameters for the equation, as well as the regression coefficient, are presented in Table 2.4. Despite the apparent overestimation at temperatures directly adjacent to the freezing point of pore water, this equation captures the increase in preconsolidation pressure and the plateau which occurs at low temperatures as shown in Figure 2.14.

$$\frac{\sigma(T_C)}{\sigma(T_0)} = A_2 + \frac{A_1 - A_2}{e^{\left[\frac{e^{\left(\frac{T_C}{T_0}\right)} - x_0}{dx}\right]}} \qquad \text{Eq. 3}$$

Table 2.4 Fitting parameters for Qi et al. (2010) data and NC EPK data (this study) for the proposed Boltzmann curve fit.

Parameter	Qi et al. (2010) (fixed *A1*)	NC EPK	NC EPK (fixed *dx*)
A1	1.81	33.023±0.410	78.920±21.703
A2	1.015±0.032	1.056±0.021	0.531±0.618
X0	0.816±0.020	0.815±9.084E-4	0.741±0.022
dx	0.050±0.019	0.0136±0.002	0.050
R^2 (COD)	0.98	0.99	0.99

This formulation was then used to model the data from this study (third and fourth columns of Table 2.4). First, the Boltzmann curve was fit to the data without fixing any parameters (third column of Table 2.4). While the R^2 value for this relation is high, the plateau value of preconsolidation pressure at low temperatures was estimated to be very close to the value determined in the -5.5°C test (Figure 2.15.a). However, because specimens which were subjected to -7°C (and even -10°C and -15°C, data not reported here) did not show any indication of yielding at pressures up to 15,000 kPa, this plateau value likely underestimates the yield stress at those temperatures. To get a better estimate of the plateau pressure, the spacing parameter *dx*, which controls the transition rate of the steep portion of the curve, was fixed to the value determined for the Qi et al. (2010) data (fourth column of Table 2.4). With the *dx* parameter set to match that of the experimental data from Qi et al. (2010), the plateau value increased significantly to around 31 MPa (Figure 2.15.b). Further experimental work is necessary to verify the veracity of these results. However, as indicated by Cai et al. (2024), the preconsolidation pressure can increase by as much as 66 times when the temperature is decreased to -20°C, making the 77 times increase to 31 MPa within the realm of possibility.

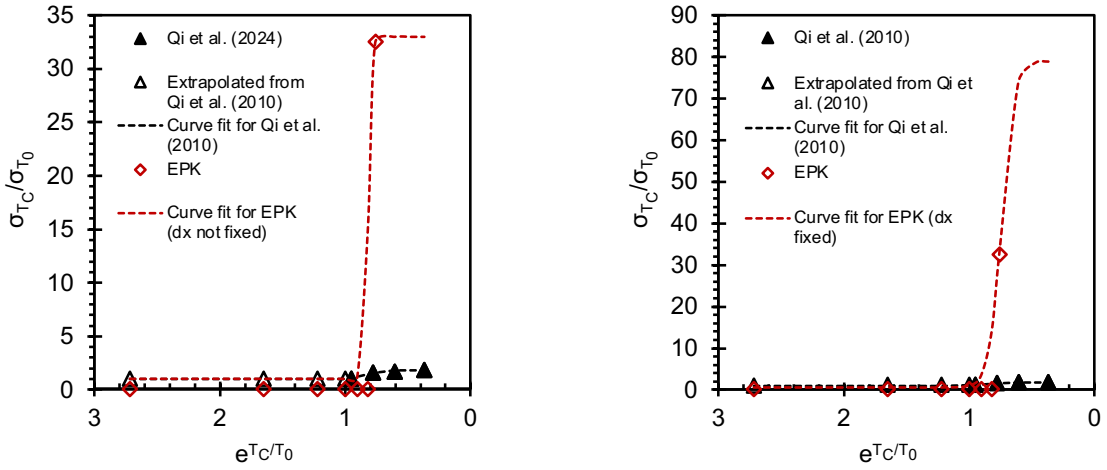

(a) (b)

Figure 2.15 Curve fit using general expression in Eq. 3 to EPK clay data (a) without fixing any parameters (third column in Table 2.4) and (b) with *dx* parameter used to fit Qi et al. (2010).

2.7.4.3 Unified relation for preconsolidation evolution over continuous temperature range

Based on the previously presented models for the elevated and frozen domains, a modified Boltzmann equation (Eq. 4) was used to develop a single equation over the entire temperature range. The first term in Eq. 4 is responsible for determining the preconsolidation pressure at frozen temperatures and captures the plateau in preconsolidation pressure at extremely low temperatures. The second term of Eq. 4, which is a modification from the traditional Boltzmann equation, corresponds to the heating portion of the curve and models the increase in yield stress at elevated temperatures. The fitting parameters used for the data from this study can be found in Table 2.5. It should be noted that the spacing parameter *dx* was fixed to 0.050, which is the value of *dx* determined previously for the frozen data from Qi et al. (2010). As this spacing parameter only appears in the first term corresponding to the frozen temperatures and the spacing parameter determined for Qi et al. (2010) fit the frozen NC EPK data reasonably well, it was also used in the modified Boltzmann equation while fitting the NC EPK data over the entire temperature domain.

$$\frac{\sigma(T_C)}{\sigma(T_0)} = \frac{A_1 - A_2}{e^{\left(\left({T_C}/{T_0 - x_0}\right)/{dx}\right)}} + A_2 * e^{k*(T_C - x_0)} \quad \text{Eq. 4}$$

Table 2.5. Fitting parameters used for the data from this study for the modified Boltzmann equation.

Calibration Parameters	A_1	A_2	X_0	dx (fixed)	K	R^2 (COD)
EPK (this study)	32.928	0.436	-0.216	0.050	0.428	0.989

Figure 2.16 shows the predicted values at each consolidation temperature juxtaposed with the experimental data. With a fitting coefficient of 0.989, this curve fit can be seen to predict the preconsolidation pressure at elevated and frozen temperatures relatively well. However, for temperatures around 0 °C, it does overestimate the values of yield stress. While further work is necessary to refine the fitting parameters, this model represents the behavior of the soil at various consolidation temperatures in a range which includes both frozen and elevated temperatures.

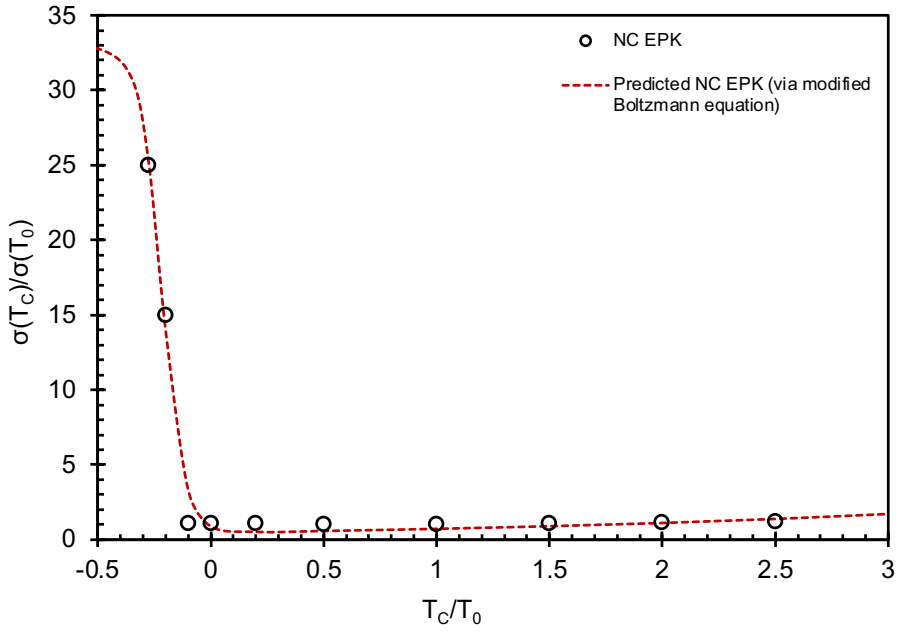

Figure 2.16 The values predicted by the modified Boltzmann model over the studied temperature range, with the experimental data at each tested temperatures included.

2.8 Conclusions

The thermal preconsolidation pressure of an NC Kaolinite clay was modeled over the range of -7 °C to 50 °C. This temperature range includes both heated and frozen domains, and the model presented herein is an attempt to link the behavior of the NC clay across both temperature domains. Different physical mechanisms cause the observed changes in preconsolidation pressure in each domain, and the magnitude of their impact is reflected in the shape of the curve. As freezing causes the most destruction to the clay fabric and increases the strength of the pore fluid, the largest increase in preconsolidation pressure occurs upon freezing. At the other temperature extreme, heating causes contraction of the soil and the subsequent densification results in more modest increases in the preconsolidation pressure. For the temperature range between the reference temperature and the freezing temperature, there was a small increase in the preconsolidation pressure. A modified Boltzmann equation was used to develop a mathematical model which captures the changes in the preconsolidation pressure of the tested NC clay due to various temperature changes.

References

Abdelaziz, S.L., Olgun, C.G., and Martin, J.R. II (2011). “Design and operational considerations of geothermal energy piles.” Geo-Frontiers 2011: Advances in geotechnical engineering, 450-59.

Abuel-Naga, H.M., Bergado, D.T., Soralump, S., and Rujivipat, P. “Thermal consolidation of soft Bangkok clay.” Lowland Technology International, 7(1): 13-21.

Baldi, G., Hueckel, T., and Pellegrini, R. (1988). “Thermal volume changes of the mineral-water system in low porosity clay soils.” Canadian Geotechnical Journal, 25: 807-825.

Burghignoli, A., Desideri, A., and Miliziano, S. (1992). “Deformability of clays under non isothermal conditions.” Revista Italiana Di Geotecnica, 4: 227-235.

Butterfield, R. (1979). “A natural compression law for soils (an advance on e-log p’).”

Cai, W., Zhu, C., and Lein, W. (2024). “Measurement and modeling of thermo-hydro-mechanical behaviors of frozen clays: frost susceptibility and compressibility.” Transportation Research Record, 00(0): 1-12.

Campanella, R.G. and Mitchell, J.K. (1968). “Influence of temperature variations on soil behavior.” ASCE Journal of the Soil Mechanics and Foundations Division, 94(3): 709-734.

Cekerevac, C., Laloui, L., and Vulliet, L. (2002). “Dependency law for thermal evolution of preconsolidation pressure.” Numerical Models in Geomechanics VIII: 687-692.

Chamberlain, E.J. (1981). “Overconsolidation effects of ground freezing.” Engineering Geology, 18: 97-110.

Chang, D.K. and Lacy, H.S. (2008). “Artificial Ground Freezing in Geotechnical Engineering.” Sixth International Conference on Case Histories in Geotechnical Engineering, Arlington, VA, USA: Paper No. 7.56a.

Coccia, C.J.R. and McCartney, J.S. (2016). “Thermal volume change of poorly draining soils I: Critical assessment of volume change mechanisms.” Computers and Geotechnics, 80: 26-40..

Delage, P., Sultan, N., and Cui, Y.J. “On the thermal consolidation of Boom clay.” Canadian Geotechnical Journal, 37: 343-354.

Demars, K.R. and Charles, R.D. (1981). “Soil volume changes induced by temperature cycling.” Canadian Geotechnical Journal, 19: 188-194.

Eigenbrod, K.D., Knutsson, S., and Sheng, D. (1996). “Pore-water pressures in freezing and thawing fine-grained soils.” Journal of Cold Regions Engineering, 10(2): 77-92.

Eriksson, L.G. (1989). “Temperature effects on consolidation properties of sulphide clays.” 12th International Conference on Soil mechanics and Foundation Engineering, Rio de Janeiro, Brazil: 2087-2090.

Ghazavi, M., Roustaei, M., Safaei, V., and Kahlor, A. (2023). “Effect of freeze-thaw cycles on consolidation behavior of two plastic fine soils.” Geotechnical and Geological Engineering, 41: 1473-1483.

Graham, J. and Au, V.C.S. (1984). “Effects of freeze-thaw and softening on a natural clay at lows stresses.” Canadian Geotechnical Journal, 22: 69-78.

Head, K.H. (1992). “Manual of Soil Laboratory Testing.” (2nd ed., 388 pp).

Iverson, K. and Moum, J. (1974). “The paraffin method – triaxial testing without a rubber membrane.” Geotechnique, 24(4): 665-670.

Jaradat, K.A., Darbari, Z., Elbakhshwan, M., Abdelaziz, S.L., Gill, S.K., Dooryhee, E., Ecker, L.E. (2017). “Heating-freezing effects on the orientation of kaolin clay particles.” Applied Clay Science, 150: 163-174.

Jungvist, G., Oni, S.K., Teutschbein, C., and Futter, M.N. (2014). “Effect of climate change on soil temperature in Swedish boreal forests.” PloS one, 9: e93957.

Kozlowski, T. (2009). “Some factors affecting supercooling and the equilibrium feezing point in soil-water systems.” Cold Regions Science and Technology, 59: 25-33

Ladd, C.C. and Foott, R. (1974). “New Design Procedure for Stability of Soft Clays.” Journal of Geotechnical Engineering Division, GT7: 763-786.

Loktionov, E.Y., Sharaborova, E.S., and Shepitko, T.V. (2022). “A sustainable concept for permafrost thermal stabilization.” Sustainable Energy Technologies and Assessments, 52: 102003.

Maninder, S.A., Omar, A., Malviya, A., and Shukla, J.B. (2021). “Effects of global warming temperature.” The International Journal of Climate Change: Impacts and Responses, 13(2): 1-19.

Morgenstern, N.R. and Nixon, J.F. (1971). “One-dimensional consolidation of thawing soils.” Canadian Geotechnical Journal, 8: 558-565.

Moritz, L. (1995). “Geotechnical properties of clay at elevated temperatures.” Swedish Geotechnical Institute Report 47.

Ozgan, E., Serin, S., Erturk, S., and Vural, I. (2015). “Effects of freezing and thawing on the consolidation settlement of soils.” Soil Mechanics and Foundation Engineering, 52(5): 247-253.

Plum, R.L. and Esrig, M.I. (1969). “Some temperature effects on soil compressibility and pore water pressure.” Highway Research Board Special Report 103: 231-242.

Qi, J., Ma, W., and Song, C. (2008). “Influence of freeze-thaw on engineering properties of a silty soil.” Cold Regions Science and Technology, 53: 397-404.

Qi, J., Hu, W., and Ma, W. (2010). “Experimental study of a pseudo-preconsolidation pressure in frozen soils.” Cold Regions Science and Technology, 60: 230-233.

Samarkoon, R.A. and McCartney, J.S. (2020). “Effect of drained heating and cooling on the preconsolidation stress of saturated normally consolidated clays.” GSP Geo-Congress 315: 620-629.

Shastri, A., Sanchez, M., Gai, X., Lee, M.Y., and Dewers, T. (2021). “Mechanical behavior of frozen soils: experimental investigation and numerical modeling.” Computers and Geotechnics, 138: 104361.

Sotthewes, K., Bampoulis, P., Zandvliet, H.J.W., Lohse, D., and Poelsema, B. (2017). “Pressure-induced melting of confined ice.” ACS Nano, 11: 12723-12731.

Sultan, N., Delage, P., and Cui, Y.J. (2002). “Temperature effects on the volume change behavior of Boom clay.” Engineering Geology, 64: 135-145.

Tidfors, M. and Sallfors, G. (1989). “Temperature effect on preconsolidation pressure.” Geotechnical Testing Journal, 12(1): 93-97.

Towhata, I., Kuntiwattakanu, P., Seko, I., and Ohishi, K. (1993). “Volume change of clays by heating as observed in consolidation tests.” Soils and Foundations, 33(4): 170-183.

Ung, A. (2023). “Effects of Temperature on Residual Shear Strength of Cohesive Soils.” Master’s Thesis. Virginia Tech. 33 pp.

Zeinali, S.M. and Abdelaziz, S.L. (2020). “Freezing-thawing effect on saturated clay microstructure.” GSP Geo-Congress 319: 40-48.

Zheng, L., Gao, Y., Zhou, Y., Liu, T., and Tian, S. (2021). “A practical method for predicting ground surface deformation induced by the artificial ground freezing method.” Computers and Geotechnics, 130: 103925.

CHAPTER 3. IMPACT OF THERMAL HISTORY ON PRECONSOLIDATION PRESSURE OF NORMALLY CONSOLDIATED CLAYS

The contributions of the authors to the composition of this manuscript are delineated as follows:

Suzanna Gevorgyan

- Performed literature review.
- Set up the equipment for laboratory tests.
- Performed all experiments.
- Performed analyses associated with laboratory data.
- Prepared the figures and tables.
- Wrote the draft manuscript.

Dr. Sherif L. Abdelaziz

- Developed the idea for this research investigation.
- Oversaw the analysis associated with laboratory data.
- Provided feedback throughout this study.
- Reviewed and edited the draft and final manuscripts.

Impact of Thermal History on Preconsolidation Pressure of Normally Consolidated Clays

Suzanna Gevorgyan[1] and Sherif L. Abdelaziz[2]

[1] Graduate Student, Department of Civil and Environmental Engineering, Virginia Tech, Blacksburg, 24061 VA.; e-mail: gevorgyansm@vt.edu

[2] Associate Professor, Department of Civil and Environmental Engineering, Virginia Tech, Blacksburg, 24061 VA; e-mail: saziz@vt.edu.

The authors of the following manuscript intend to submit it to ASCE Geo-Congress 2026 Conference.

3.1 Abstract

The variety of geotechnical applications in which soil is subjected to temperature cycles is increasing with climate change, which leads to phenomena such as melting permafrost, and also to the advancement of alternative geothermal energy exploration and infrastructure. As more foundations will start to bear on previously-frozen soils and complex geothermal systems and equipment will heat up the soils around them, it's important to understand the effect that temperature plays on engineering parameters of soils. Previous researchers have demonstrated that temperature changes, such as simple heating, and temperature cycles, such as heating-cooling and freezing-thawing, can have pronounced effects on the compressibility parameters of clays. It has also been established that the stress state and mineralogy/structure of a clay influence how the temperature will affect the compressibility. Given the potential interest in melting permafrost and in the context of previous research, the focus of this study is to understand the impact of a previously-frozen state on the preconsolidation pressure of normally consolidated clays. To that end, consolidation tests were performed on frozen-thawed specimens of normally consolidated kaolinite clay which were subjected to various heating paths following thawing. From these tests, the axial strains and preconsolidation pressure were determined, and, from them, the impacts of freezing on the preconsolidation pressure determined at the final consolidation temperatures.

3.2 Introduction

Thawing soils can be found in building foundations and around geothermal energy infrastructure. Particularly as global temperatures continue to rise year-to-year, the rates of permafrost thaw have been found to increase (Schuur et al., 2008) making the thaw consolidation of these soils a non-trivial issue in geotechnical designs. While it is possible to use the consolidation design parameters determined from ambient temperature tests, it's unclear if these parameters will be representative

for previously-frozen soils at the same temperatures. Previous researchers have pointed out that the sampling process subjects soils to both mechanical and thermal disturbance (Plum and Esrig, 1969; Demars and Charles, 1981) and, especially in energy infrastructure such as high-voltage cables (Delage et al., 2000), as heat storage (Erikkson, 1988; Tidfors and Sallfors, 1989; Moritz, 1995), or as a nuclear waste disposal host (Baldi et al., 1988; Sultan et al., 2002), soils may be subjected to extremely high temperatures even in-situ. As such, it is more relevant than ever to know how a frozen history might impact design parameters for clays.

It has previously been established that the freeze-thaw process leads to changes in the behavior of fine-grained soils. As described by Chamberlain (1981), freezing leads to destruction of the soil fabric due to migration of the porewater towards the freezing front and subsequent densification of the soil in areas adjacent to the freezing front. Early research on freeze-thaw cycles documented the fabric changes which occur on the macro-scale (Graham and Au, 1984; Eigenbrod et al., 1996). The manifestation of these macro-scale changes is thaw consolidation (Ozgan et al., 2015), increased vertical permeability (Ghazavi et al., 2023), decreased shear strength (Graham and Au, 1984), decreased compression slopes (Graham and Au, 1984), and variation in the preconsolidation pressure (Chamberlain, 1981; Graham and Au, 1984; Qi et al., 2008). While Chamberlain (1981) found that freezing-thawing increased the preconsolidation pressure of their tested clay, Qi et al. (2008) found that preconsolidation pressure varied differently depending on the initial dry unit weight of the pre-frozen soil. Soils with low initial dry unit weights experienced an increase in the preconsolidation pressure following thawing, while soils with high initial dry unit weights experienced a decrease in yield stress (Qi et al., 2008). Graham and Au (1984) showed yet another inconclusive result showing that the preconsolidation pressure decreased after freezing and thawing.

Additionally, of all the researchers who have considered the effect of freeze-thaw on preconsolidation pressure, none have tested the possibility of soils being subjected to subsequent heating above pre-frozen temperatures. However, heating and heating-cooling of soils have been demonstrated to cause changes in the compressibility and preconsolidation pressure of fine-grained soils. Elevated temperatures induce volume changes in soils which are dependent on the stress state of the soil: heating overconsolidated (OC) clays, for example, produces reversible dilative axial strains (Plum and Esrig, 1969; Demars and Charles, 1981; Baldi et al., 1988). Normally consolidated (NC) clays, on the other hand, manifest irreversible contractive strains upon heating (Campanella and Mitchell, 1968; Baldi et al., 1988; Towhata et al., 1994). Elevated temperatures have also been documented to have opposite effects on the preconsolidation pressure of OC and NC clays: while OC clays experience an increase in OCR upon heating, NC clays develop higher preconsolidation pressures (Erikkson, 1989; Tidfors and Sallfors, 1989; Burghignoli et al., 1992; Towhata et al., 1993; Boudali et al., 1994; Moritz, 1995; Cekerevac et al., 2002; Sultan et al., 2005; Abuel-Naga et al., 2005; Samarkoon and McCartney, 2020). More recently, Zeinali and Abdelaziz (2023) ran heating and freezing-heating tests on an OC clay and compared the preconsolidation pressure at the final test temperature. They found that the previous frozen state in a clay's thermal history led to a different preconsolidation pressure than simple heating. Thus, while it is clear that both freezing-thawing and heating are anticipated to impact the preconsolidation pressure of soils, the impact of having both of these temperature changes acting on a single soil has still not been investigated for NC clays.

The current work aims to bridge these two temperature extremes and investigate what effect a freeze-thaw cycle will have on the preconsolidation pressure of an NC soil at various post-thaw temperatures. By running thermally-controlled consolidation tests on NC clays after inducing

a freeze-thaw cycle, we can determine the preconsolidation pressure of the specimen at various final temperatures. Because we know the change in preconsolidation pressure we would expect to see given simple heating, we can then determine if the frozen state made some lasting impact on the soil fabric or if the final consolidation temperature dominates the soil response.

3.3 Testing Program

The material tested in this study is remolded EPK (Edgar Plastic Kaolinite) purchased in powdered form from Edgar, Florida. The clay classifies as a high plasticity clay (CH) according to the USCS, with a liquid limit of 54 and a plasticity index of 29 at room temperature.

Bulk samples were created by mixing EPK clay powder and deionized water at a 1 to 1.5 times the LL ratio. The slurry was then poured into a 4-inch diameter mold and consolidated under the weight of a concrete cap at room temperature (20 °C) for 24 hours to reduce piping. The bulk sample was then further consolidated to 100 kPa in five loading steps, with each step applied for 24 hours. Then, the bulk sample was extruded from the mold and preserved in plastic wrap in a humidity-controlled room until testing.

For this study, three specimens were trimmed from the bulk sample within two weeks of storage into a consolidation ring with a 63.7 mm (2.5-inch) diameter and 25.4 mm (1-inch) height. The trimmed specimens were then placed in a temperature-controlled consolidation chamber, which was subsequently filled with Julabo Thermal C5 oil, under a seating load of 5 kPa. Once the seating load stabilized, a copper coil placed around the specimen inside the chamber was used to set the temperature to the selected reference temperature (20 °C). It should be mentioned that all components for the used temperature-controlled consolidation apparatus were calibrated for temperature effects. To achieve a normally consolidated state at the reference temperature, the

specimens were first loaded to 400 kPa with the temperature in the chamber being held at the selected reference temperature (20 °C). Figure 3.1 show the initial compression curves for the three tested specimens at the selected reference temperature (20 °C), while the numeric values for the different physical properties are summarized in Table 3.1. While one specimen started with a lower initial void ratio and water content (specimen -15 > 30 °C) than the others, all specimens exhibited the same void upon consolidating to 400 kPa at 20 °C.

Table 3.1 Initial conditions of tested specimens.

Temperature Path	-15 > 20 °C	-15 > 30 °C	-15 > 50 °C
Water content	47.4%	47.4%	47.0%
Initial voids ratio (e_0)	1.36	1.35	1.32
Voids ratio after consolidation (e_{C1})	1.07	1.08	1.05

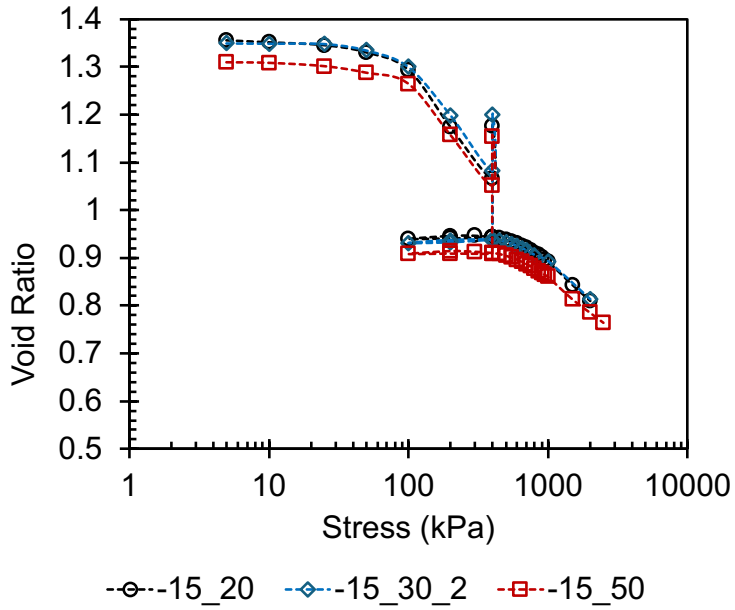

Figure 3.1 Consolidation curves at reference temperature (20 °C) for the tested specimens.

Once each of the tested specimens reached the end of primary consolidation under the 400 kPa at 20 °C, this stress was held constant while the desired temperature cycle for each specimen was applied. The temperature cycles considered were freezing-thawing (-15> 20 °C) and freezing-

heating (-15> 50 °C and -15>30 °C). Each temperature step was applied for 24 hours to ensure the temperature and volume of the specimens stabilized. The axial strains of the specimens and the chamber temperature were measured throughout the tests. After stabilizing the temperature and volume at the final temperature for each specimen, specimens were consolidated from 400 kPa to 2500 kPa at the final consolidation temperature.

3.4 Results and Discussions

The thermally-induced volumetric strains for the three specimens are presented in Figure 3.2. Upon freezing to -15 °C, all specimens generated similar negative axial strains of approximately -4.5±0.2% (Table 3.2). Upon thawing (to 20 °C) or heating (to 30 and 50 °C), all specimens exhibited positive axial strains; the higher the post-freezing temperature, the greater the contraction experienced by the specimen (Table 3.2).

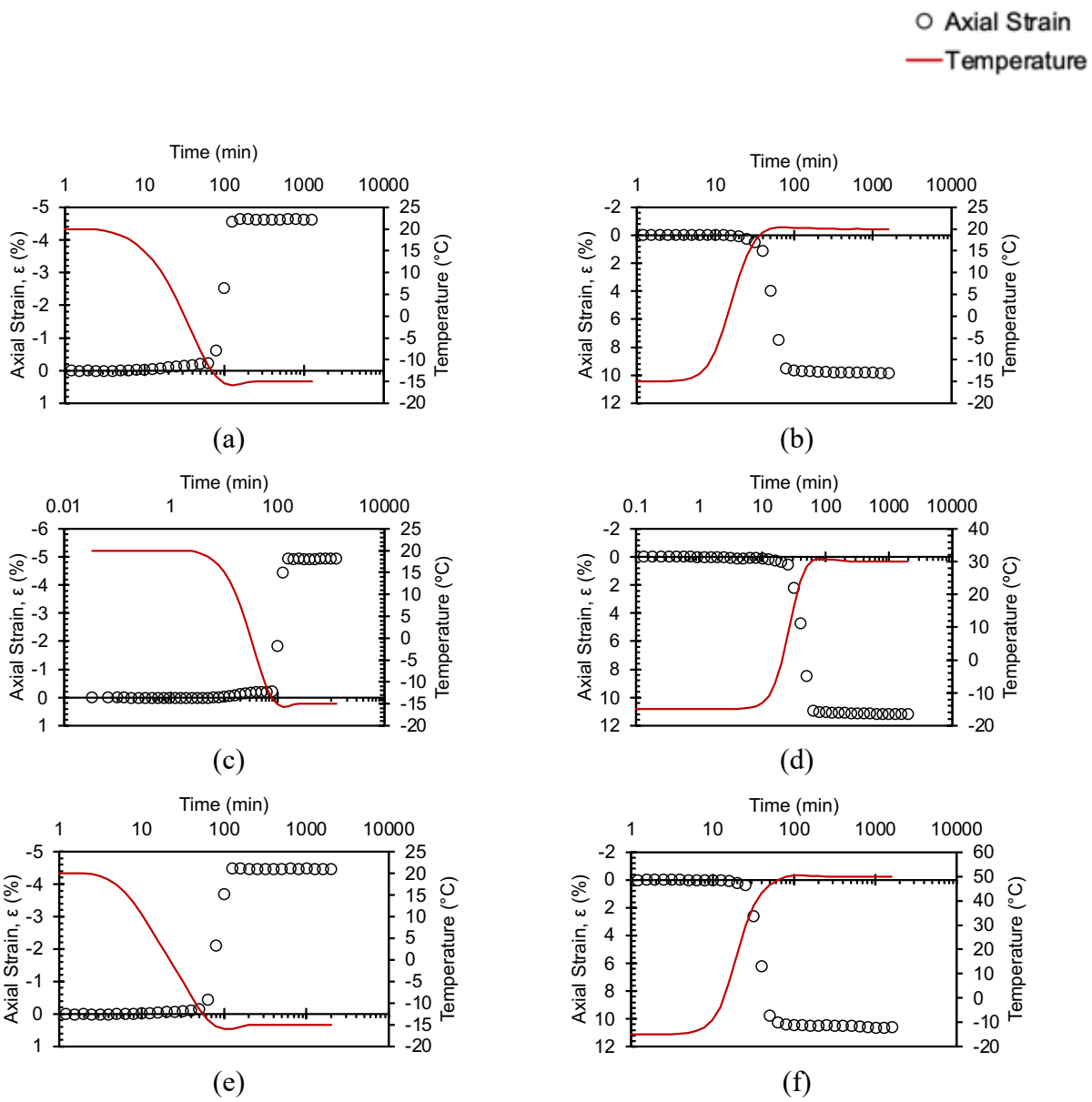

Figure 3.2 Axial strain versus time due to temperature change during freezing from 20 to -15 °C in -15 °C >20 °C test (a), thawing from -15 to 20 °C (b), freezing from 20 to -15 °C in -15 °C >30 °C test (c), thawing from -15 to 30 °C (d), freezing from 20 to -15 °C in -15 °C >50 °C test (e), and thawing from -15 to 50 °C (f).

Table 3.2 Axial strains at the end of temperature stages for each of the tested specimens.

Temperature Path	-15_20	-15_30	-15_50
Freezing (20 -> -15)	-4.62%	-4.94%	-4.47%
Thawing/Heating	9.84%	10.11%	10.60%

The compression curves after the temperature change stage are shown in Figure 3.3. Figure 3.3.a shows the compression curves with y-axis as void ratio, which demonstrates the permanent reduction in void ratio of the specimens consolidated at higher temperatures. Figure 3.3.b, on the other hand, shows the post-thermal change portion of the compression curves normalized against the void ratio at the start of the second consolidation stage. As can be seen in Figure 3.3.a, the axial strains observed for each specimen align with the expected volumetric changes for each type of temperature change. All three specimens exhibited heave upon freezing, which agrees with the literature (e.g., Eigenbrod et al., 1996). The contraction of the specimen after the thawing stage for the -15>20 °C test also demonstrates the thaw consolidation reported in the literature (e.g., Chamberlain, 1981; Ozgan et al., 2015; Ghazavi et al., 2023). For tests in which the final temperature was higher than the initial pre-frozen temperature (20 °C), the contractive axial strains in the thawing/heating stage are greater than those of the simple thawing test (Table 3.2). The greatest contractive strain was recorded in -15>50 °C test, followed by -15>30 °C test, with -15>20 °C test showing the least contraction. In the context of simple heating, Baldi et al. (1988), among others, found that OC clays expanded upon heating while NC clays contracted upon heating to the same temperatures. The behavior of the material in this study after the freezing-thawing cycle matches that of NC clay upon heating.

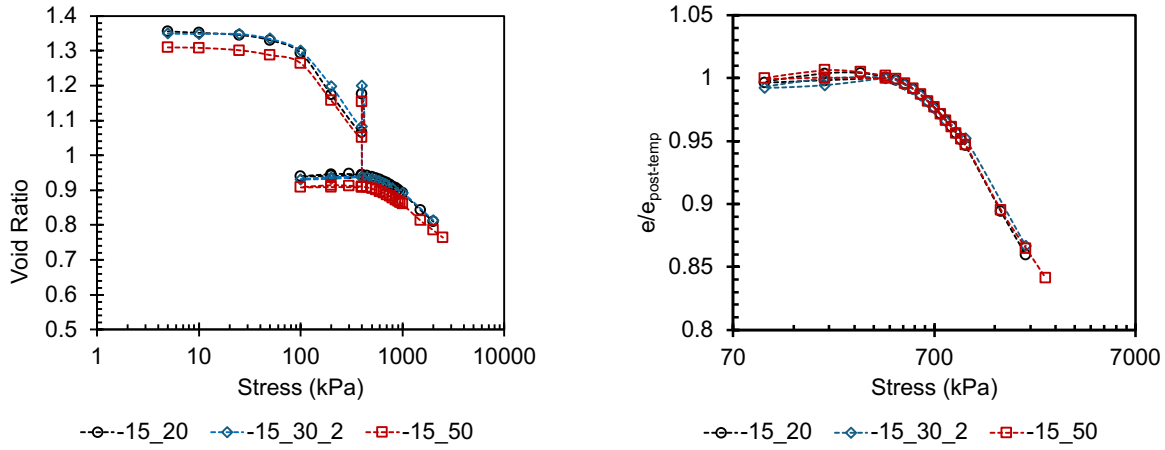

(a) (b)

Figure 3.3 (a) Compression curves for the three tested specimens over the entire tests, and (b) enlarged to the compression curves for the three specimens after temperature changes with the void ratio normalized against void ratio after final temperature change.

From the compression curves, the data can be modified to be used in the Butterfield method (Butterfield, 1979) of determining preconsolidation pressure post freeze-thawing or freeze-heating (Figure 3.4). The preconsolidation pressure was found to be the same for all three specimens despite the different final consolidation temperatures. Also, it appears that the recompression and compression indices of all three specimens are similar (Figure 3.3.b).

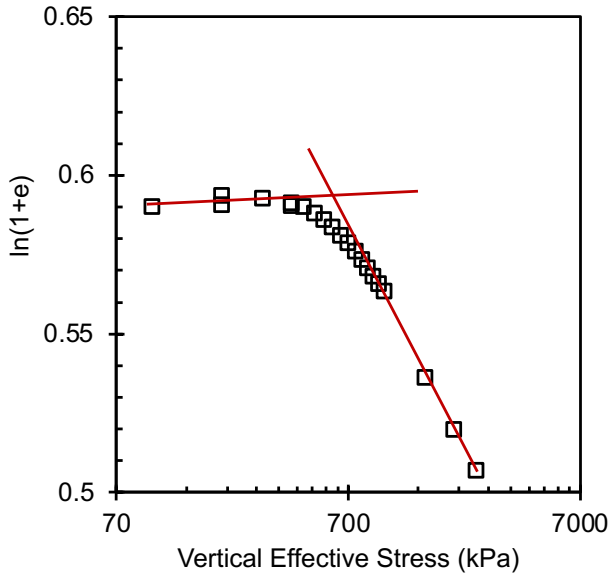

Figure 3.4 Butterfield method determination of preconsolidation pressure for -15>20 °C test.

While the initial yield stress for this material was 400 kPa, the preconsolidation pressure after the freezing-thawing or freezing-heating cycle was estimated to be around 610 kPa. The results of the -15>20 °C test indicate that the preconsolidation pressure of this NC clay increases after freezing-thawing, which is in agreement with the results of Chamberlain (1981). However, the apparent overconsolidation revealed through the higher preconsolidation pressure is contrary to the contractive behavior exhibited by the specimen upon heating to temperatures above 20 °C. While we would expect previously-unfrozen OC specimens to dilate upon heating to 30 and 50 °C, the contraction of the -15>50 °C specimen was roughly 0.8% greater than that of the simply thawed -15>20 °C specimen, and the contraction of the -15>30 °C specimen was roughly 0.3% greater. This additional contraction of the frozen-heated specimens while they are apparently overconsolidated suggests that the behavior of previously-frozen clay is highly influenced by the fabric changes which are induced in the specimen during the freezing stage.

Additionally, it's clear from the compression curves that the preconsolidation pressure of all three specimens (Figure 3.3.b) is extremely similar if not identical. While the final consolidation temperature did produce variation in the axial strains recorded at the end of the temperature change stage, it did not change the preconsolidation pressure in the way we might expect heating only to change it. Campanella and Mitchell (1968) delineated two primary mechanisms which govern the decrease in axial strain in heated specimens: the difference in the expansion coefficients of the pore water and soil and the decrease of friction at the particle-to-particle contacts. The first effect leads to drainage of the pore water to relieve the excess porewater pressure that builds up because of the expansion of the soil constituents, while the latter leads to reorientation of the soil fabric until the friction has sufficiently increased to carry the same effective stress. If both factors governed the increase in the effective stress, the expected result would be an increase in the

preconsolidation pressure at higher temperatures. However, our observed results suggest that freezing causes some change in the soil fabric which negates the effect of one or both of these mechanisms on the increase in the preconsolidation pressure.

Chamberlain (1981) and Graham and Au (1984) pointed out the fundamental changes which occur in the soil fabric due to freezing, as channels are formed between lenses of soil which induce a fissured microfabric with higher permeability. Eigenbrod et al. (1996) also noted that, in the beginning of the freezing process, negative effective stresses are generated in the soil, which further supports Chamberlain's (1981) claim that it's the freezing stage rather than the thawing stage which densifies the soils. These observations justify the higher preconsolidation pressure recorded from the specimens in this study. Ozgan et al. (2015) reported that they observed a decrease in the particle size of their tested fine-grained soil over repeated freeze-thaw cycles. One or a combination of these various changes in the soil fabric reported by previous studies may be responsible for the incongruent volumetric behavior of the specimens upon heating.

3.5 Summary and Conclusions

A series of freezing-thawing and freezing-heating tests were run on a normally consolidated Kaolinite clay to determine the impact of the temperature cycles on the preconsolidation pressure. The results of these tests showed that the final consolidation temperature following a freeze-thaw cycle has negligible effects on the preconsolidation pressure. While the axial strains for each temperature change were in line with expectations from prior studies, there was no change in preconsolidation pressure as might have been anticipated. This suggests that the change in preconsolidation pressure induced by temperature changes is not caused by the same mechanisms which lead to the observed axial strains. We can state from these results that the thermal history of the specimens has an irrevocable effect on the current behavior of the clay.

References

Abuel-Naga, H.M., Bergado, D.T., Soralump, S., and Rujivipat, P. “Thermal consolidation of soft Bangkok clay.” Lowland Technology International, 7(1): 13-21.

Baldi, G., Hueckel, T., and Pellegrini, R. (1988). “Thermal volume changes of the mineral-water system in low porosity clay soils.” Canadian Geotechnical Journal, 25: 807-825.

Burghignoli, A., Desideri, A., and Miliziano, S. (1992). “Deformability of clays under non isothermal conditions.” Revista Italiana Di Geotecnica, 4: 227-235.

Butterfield, R. (1979). “A natural compression law for soils (an advance on e-log p’).”

Campanella, R.G. and Mitchell, J.K. (1968). “Influence of temperature variations on soil behavior.” ASCE Journal of the Soil Mechanics and Foundations Division, 94(3): 709-734.

Cekerevac, C., Laloui, L., and Vulliet, L. (2002). “Dependency law for thermal evolution of preconsolidation pressure.” Numerical Models in Geomechanics VIII: 687-692.

Chamberlain, E.J. (1981). “Overconsolidation effects of ground freezing.” Engineering Geology, 18: 97-110.

Delage, P., Sultan, N., and Cui, Y.J. “On the thermal consolidation of Boom clay.” Canadian Geotechnical Journal, 37: 343-354.

Demars, K.R. and Charles, R.D. (1981). “Soil volume changes induced by temperature cycling.” Canadian Geotechnical Journal, 19: 188-194.

Eigenbrod, K.D., Knutsson, S., and Sheng, D. (1996). “Pore-water pressures in freezing and thawing fine-grained soils.” Journal of Cold Regions Engineering, 10(2): 77-92.

Eriksson, L.G. (1989). “Temperature effects on consolidation properties of sulphide clays.” 12th International Conference on Soil mechanics and Foundation Engineering, Rio de Janeiro, Brazil: 2087-2090.

Ghazavi, M., Roustaei, M., Safaei, V., and Kahlor, A. (2023). “Effect of freeze-thaw cycles on consolidation behavior of two plastic fine soils.” Geotechnical and Geological Engineering, 41: 1473-1483.

Graham, J. and Au, V.C.S. (1984). “Effects of freeze-thaw and softening on a natural clay at lows stresses.” Canadian Geotechnical Journal, 22: 69-78.

Moritz, L. (1995). “Geotechnical properties of clay at elevated temperatures.” Swedish Geotechnical Institute Report 47.

Ozgan, E., Serin, S., Erturk, S., and Vural, I. (2015). “Effects of freezing and thawing on the consolidation settlement of soils.” Soil Mechanics and Foundation Engineering, 52(5): 247-253.

Plum, R.L. and Esrig, M.I. (1969). “Some temperature effects on soil compressibility and pore water pressure.” Highway Research Board Special Report 103: 231-242.

Qi, J., Ma, W., and Song, C. (2008). “Influence of freeze-thaw on engineering properties of a silty soil.” Cold Regions Science and Technology, 53: 397-404.

Samarkoon, R.A. and McCartney, J.S. (2020). “Effect of drained heating and cooling on the preconsolidation stress of saturated normally consolidated clays.” GSP Geo-Congress 315: 620-629.

Schuur, E.A., Bockheim, J., Canadell. J.G., Euskirchen, E., Field., C.B., Goryachkin, S.V., Hagemann, S., Kuhry, P., Lafleur, P.M., Lee, H., and Mazhitova, G. (2008). "Vulnerability of permafrost carbon to climate change; Implications for the global carbon cycle." BioScience, 58(8): 701-714.

Sultan, N., Delage, P., and Cui, Y.J. (2002). "Temperature effects on the volume change behavior of Boom clay." Engineering Geology, 64: 135-145.

Tidfors, M. and Sallfors, G. (1989). "Temperature effect on preconsolidation pressure." Geotechnical Testing Journal, 12(1): 93-97.

Towhata, I., Kuntiwattakanu, P., Seko, I., and Ohishi, K. (1993). "Volume change of clays by heating as observed in consolidation tests." Soils and Foundations, 33(4): 170-183.

CHAPTER 4. GENERAL DISCUSSIONS, SUMMARY OF CONCLUSIONS, AND RECOMMENDATIONS FOR FUTURE RESEARCH

4.1 Thermally Induced Changes in the Preconsolidation Pressure of NC Clays

The experimental results from Chapter 2 of this thesis were used to develop a single mathematical expression which could be used to predict the preconsolidation pressure of the NC EPK material over a wide temperature range which included freezing and heating thermal paths. In agreement with other studies, the preconsolidation pressure was found to increase due to both heating and freezing of the material, and applying isolated cooling paths also led to apparent overconsolidation of the tested soil. Freezing of the soil induced relatively larger increases in stiffness than either heating or cooling did. The model which was developed was demonstrated to capture the change in preconsolidation pressure at either temperature extreme.

Chapter 3 of this thesis focused on understanding the impact of a frozen history on the current behavior of clay following the imposition of heating thermal paths after thawing. The results of this study indicated that the freezing process induced changes in the soil which negated the effects of subsequent thermal paths. A single preconsolidation pressure was identified for both frozen-thawed (to 20 °C) and frozen heated (to 30 °C and 50 °C) specimens, which suggests that the thermal history of a soil is relevant to determining its preconsolidation pressure at other temperatures.

4.2 Summary of Conclusions

The goals of this thesis were to develop a relation between the change in preconsolidation pressure of an NC clay for a given temperature change and to assess how far back the thermal memory of NC clays extends. A single equation based on experimental data was developed in Chapter 2 to capture the relationship described in the first goal, and thermally-controlled consolidation testing

was used to address the second aim.

The results of these experimental studies are summarized below:

- Thermal paths, whether they be heating, cooling, or freezing, were found to induce overconsolidated behavior in the tested NC material. The magnitude of the change in yield stress was larger for freezing thermal paths than heating or cooling.
- The recompression index of the soil was impacted by the applied thermal paths. Heating led to thermal creep which reversed the direction of the recompression slope during unloading; cooling led to stiffening and a decrease in the recompression slope; and freezing caused the soil to resist deformation and become flat once that bulk of the porewater transitioned to pore ice.
- The compression index was unaffected by heating or cooling thermal paths, and freezing to temperatures close to the freezing point of bulk water (0 °C) similarly did not lead to any discernable change. However, temperatures at or below -4 °C caused the compression slope to increase.
- The axial strains recorded during the freezing stage showed that the freezing point of porewater is lower than that of bulk water, as heaving was not observed until the test temperature was -4 °C or below.
- A modified Boltzmann curve can be used to model the change in preconsolidation pressure over a temperature range from -7 C to 50 °C. This equation can predict the large increases in OCR following freezing, as well as the more modest overconsolidation effect induced by heating and cooling paths.
- When clays were frozen prior to the application of heating paths, the effects of the

heating paths were negated, and a single preconsolidation pressure was determined irrespective of the final consolidation temperature.

4.3 Recommendations for Future Research

In order to make the current study tenable, a single type of clay was tested at a unique stress state. Furthermore, the range of pressures available from the testing equipment limited the investigation to some degree. To expand the applicability of the results of this thesis, the following can be done:

- The theoretical limiting yield stress of frozen soils can be determined by using more powerful equipment to consolidate to higher temperatures. Concurrently, the initial preconsolidation pressure of the material can be varied to determine whether it has an impact on the yield stress at extremely low temperatures.
- As the literature indicates that minerology plays a role in the change in OCR with temperature, clays of other mineralogies may be tested under similar unidirectional and bidirectional thermal paths to assess this role.
- The evolution of axial strain with cooling can be further investigated to better establish the physical mechanisms which lead to the observed increase in preconsolidation pressure at these lower temperatures.
- Conducting additional unidirectional thermal paths over frozen to elevated temperature ranges would allow for further refinement of the proposed modified Boltzmann equation. The parameters of this equation may be analyzed to understand if they may be related to physical properties of the soils.
- The application of more complex thermal paths, such as heating-freezing-thawing paths, can be used to assess the extent to which clays are influenced by their thermal

history.

- The tests conducted in the studies in Chapter 2 and 3, as well as those suggested in the previous points, can also be conducted on overconsolidated clays to establish a similar relationship for change in OCR with temperature.

Appendices

50 °C

Consolidation Test Data Sheet			
Test No.	50_NC_KAOL_EXT_2	Consolidometer No.	Geojac_2k_20
Date started	11/3/24	Date ended	11/24/24
Test method	B	Condition of test	Inundated
Interpretation Method	Both 1 and 2	Classification	Remolded EPK (CH)
	Before Test - 20°C		After Test - 50°C
	Specimen	Trimmings	Specimen
Tare No.	Ring	LUIGI	T81
Tare plus wet soil (g)	351.59	245.05	153.56
Tare plus dry soil (g)	-	173.69	123.84
Tare (g)	215.09	21.94	32.12
Water (g)	43.66	71.36	29.72
Dry Soil (g)	92.84	151.75	91.72
Water content (%)	47.0	47.0	32.4
Area of specimen, A (cm2)	31.67		
Specific Gravity of Solids, Gs	2.7		
Height of solids, Hs (cm)	1.086		
Initial - 20°C		Final - 50°C	
Height of specimen, H0 (cm)	2.540	Height of specimen, Hf (cm)	2.014
Height of water, Hw0 (cm)	1.379	Height of water, Hwf (cm)	0.938
Height of voids, Hv0 (cm)	1.454	Height of voids, Hvf (cm)	0.928
Void ratio, e0	1.34	Void ratio, ef	0.86
Degree of saturation, S0 (%)	94.8	Degree of saturation, Sf (%)	101.1

Dry density, γ0 (g/cm2)	1.15	Dry density, γf (g/cm2)	1.46
		Differential height, Hd (cm)	-0.0509
		Preconsolidation pressure, σp'(kPa)	480
		Load increments (kPa) - seating loads held for 60 min, all other loads 1440 min	
Initial temperature, 20°C		5 (seating), 10, 25, 50, 100, 200, 400	
Temperature change(s)	20°C to 50°C	400	
Final temperature (°C)	50°C	400 (seating), 200, 100, 200, 400, 450, 500, 550, 600, 650, 700, 800, 1000, 2500	
Notes			
Note that the final height of the specimen Hf is the height recorded at the end of the test after the specimen was rebounded to 5 kPa until strain stabilized - it does not correspond to the final height at the maximum applied stress. The differential height is the difference between the final recorded height Hf and final height measured with a caliper following specimen extraction from ring at the end of the test.			

Initial Consolidation C1 (20 °C)

5 kPa

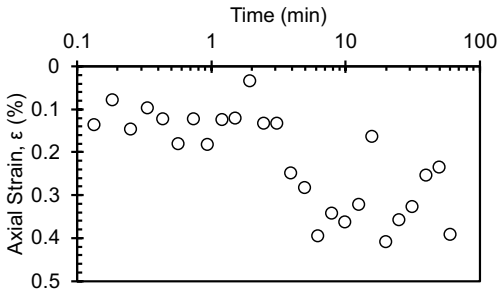

Seating load

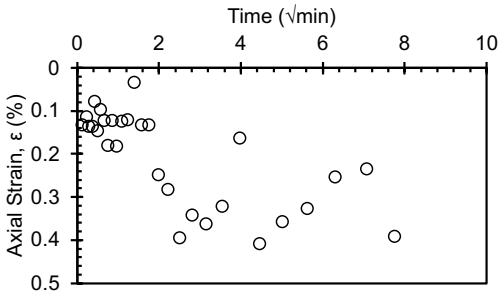

10 kPa

LIR = 1

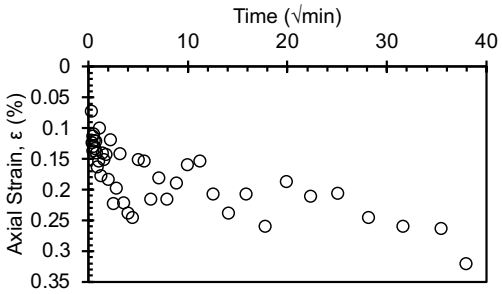

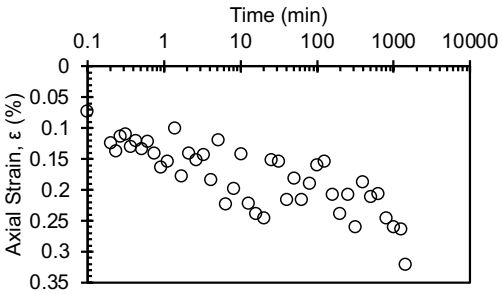

25 kPa

LIR = 1.5

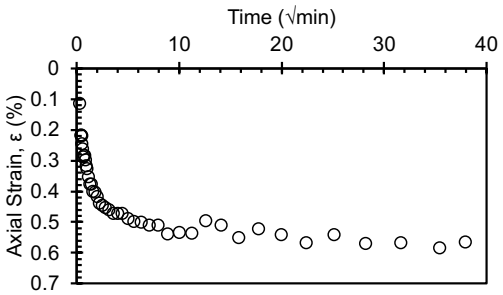

50 kPa

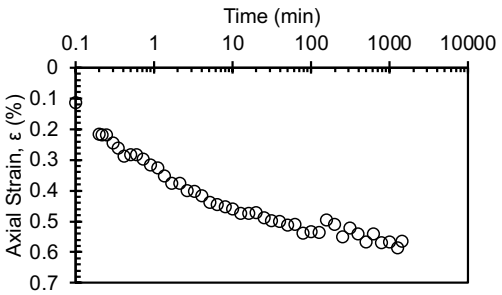

LIR = 1

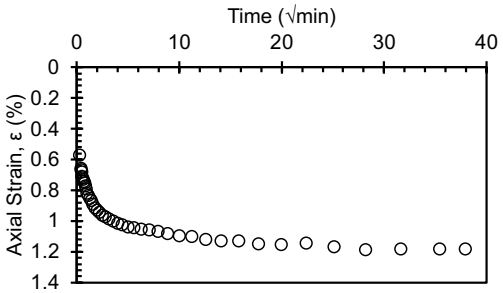

100 kPa

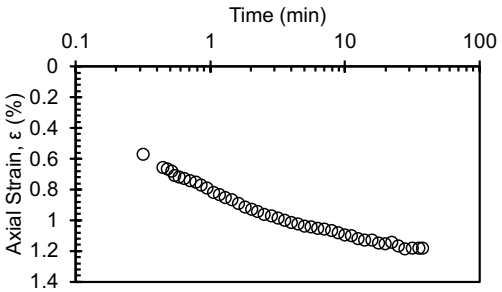

LIR = 1

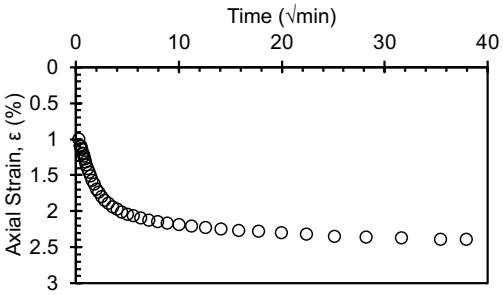

200 kPa

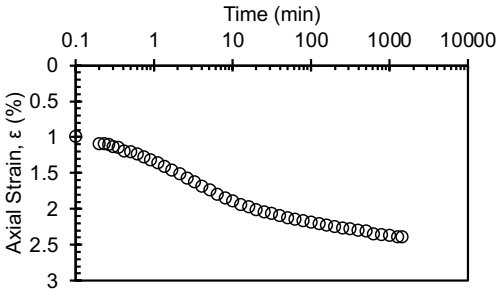

LIR = 1

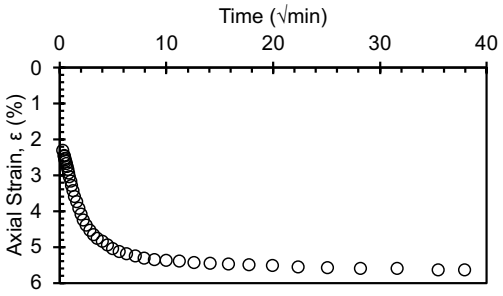

400 kPa

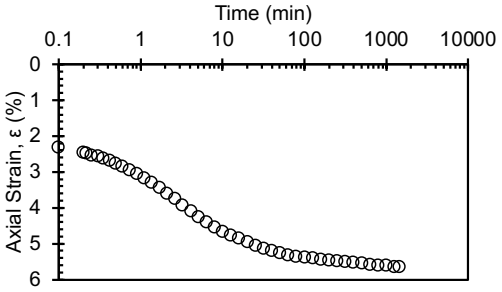

LIR = 1

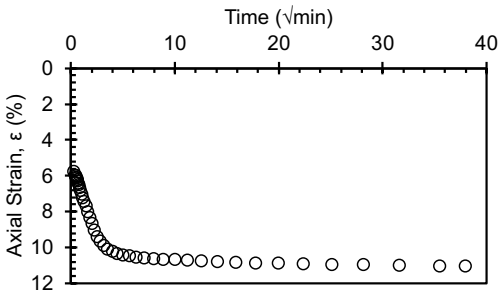

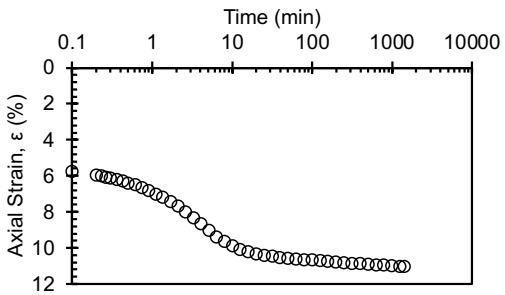

Temperature Change Stage: 20 °C>50 °C

400 kPa

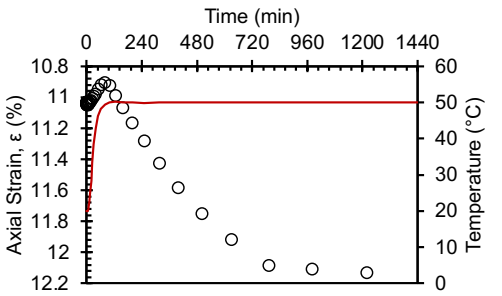

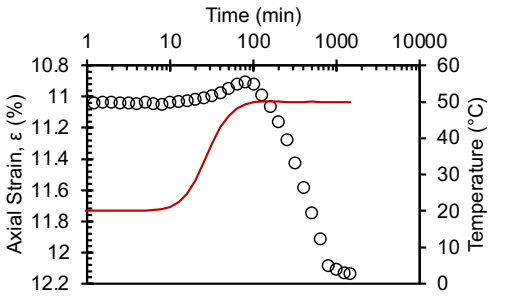

Second Consolidation C2 (50 °C)

200 kPa

LIR = -0.5

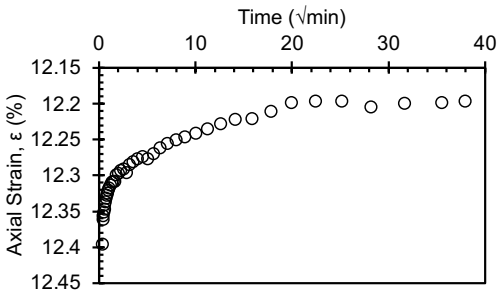

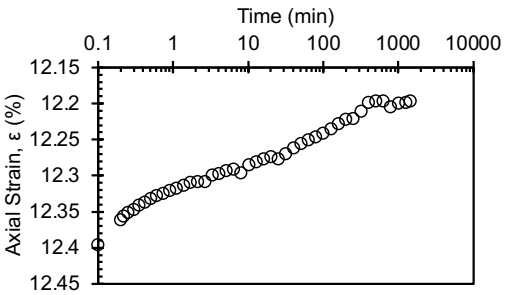

100 kPa

LIR =-0.5

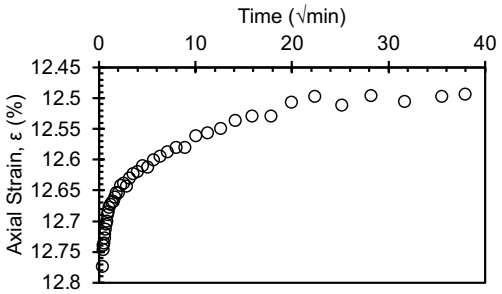

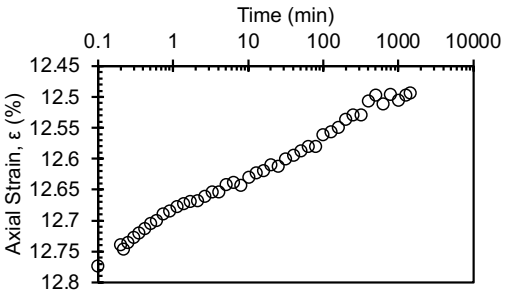

200 kPa

LIR = 1

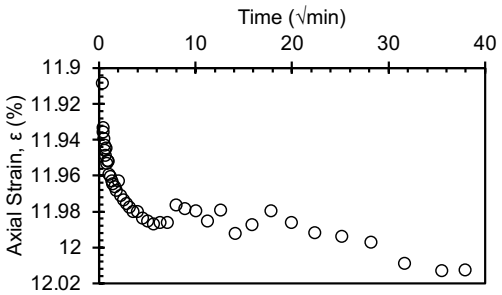

400 kPa

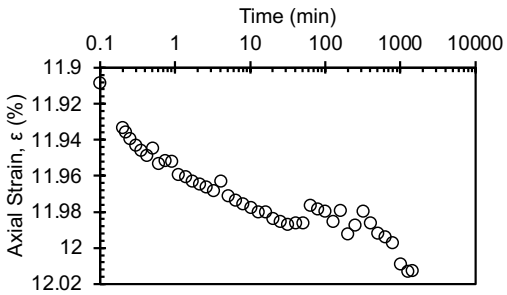

LIR = 1

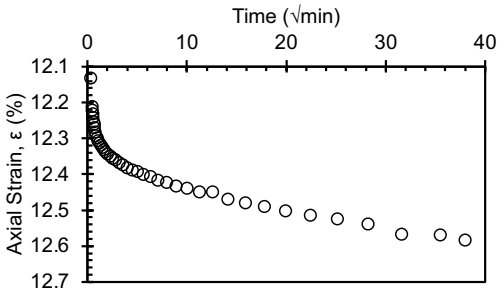

450 kPa

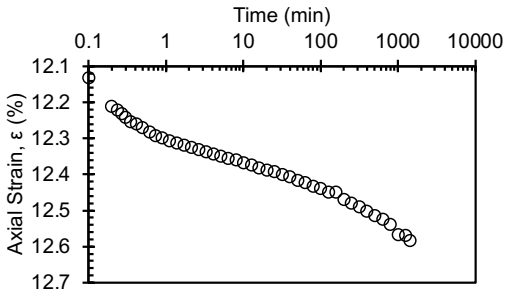

LIR = 0.125

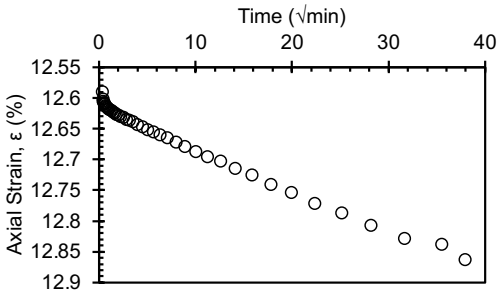

500 kPa

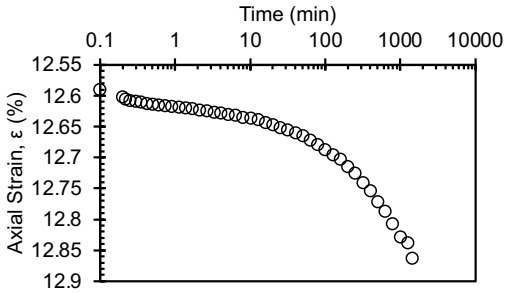

LIR = 0.11

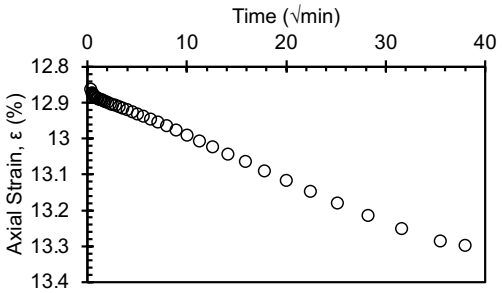

550 kPa

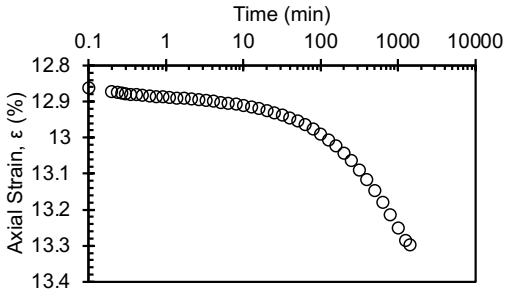

LIR = 0.1

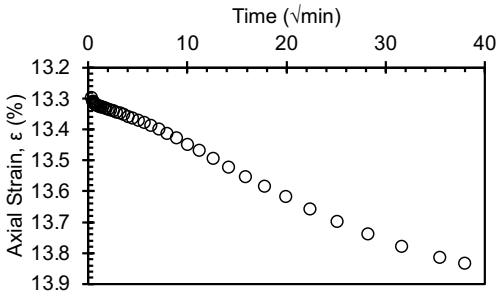

600 kPa

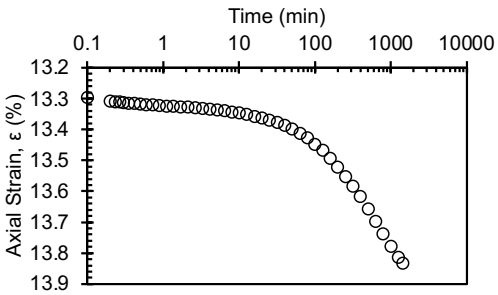

LIR = 0.091

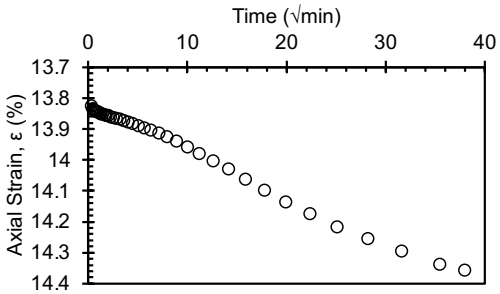

650 kPa

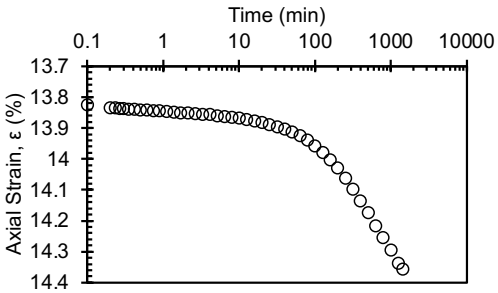

LIR = 0.83

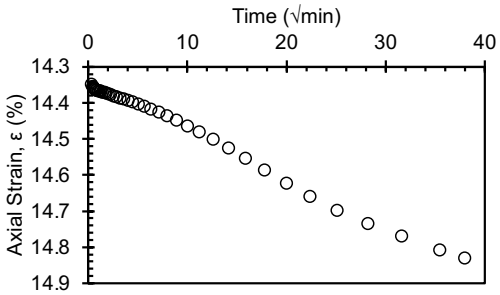

700 kPa

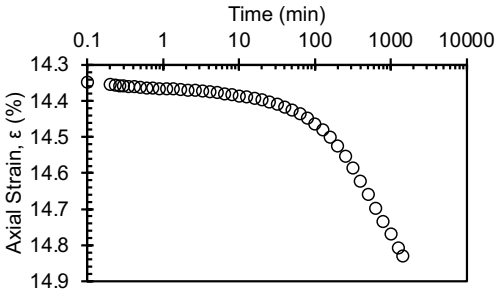

LIR = 0.077

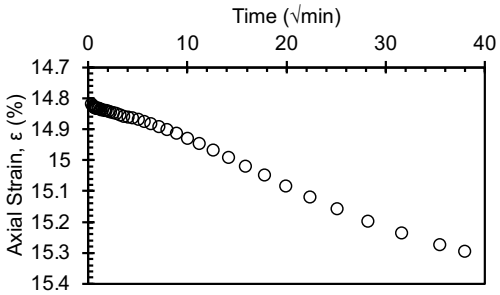

800 kPa

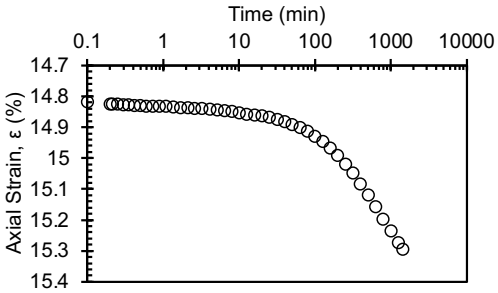

LIR = 0.143

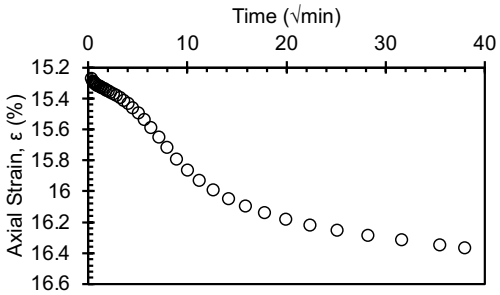

1000 kPa

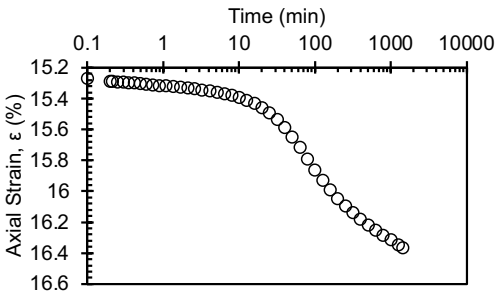

LIR = 0.2

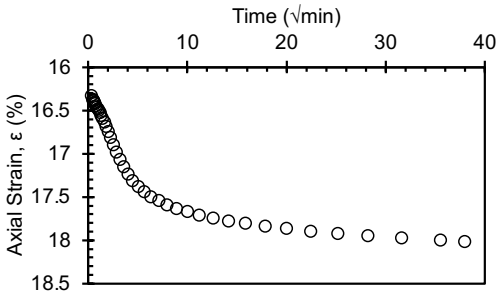

2500 kPa

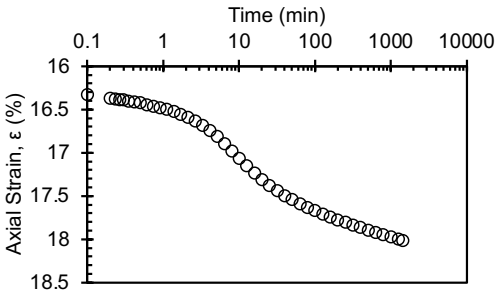

LIR = 1.5

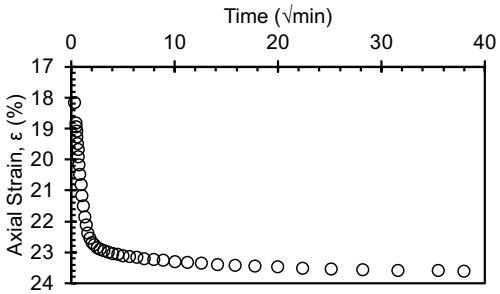

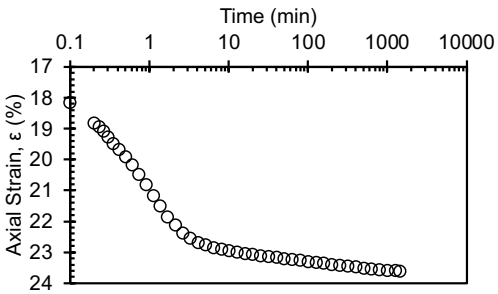

Final

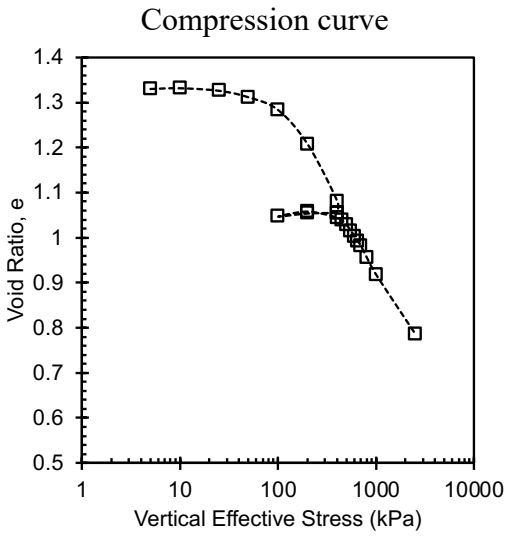
Compression curve
Void Ratio, e
1.4
1.3
1.2
1.1
1
0.9
0.8
0.7
0.6
0.5
1
10
100
1000
10000
Vertical Effective Stress (kPa)

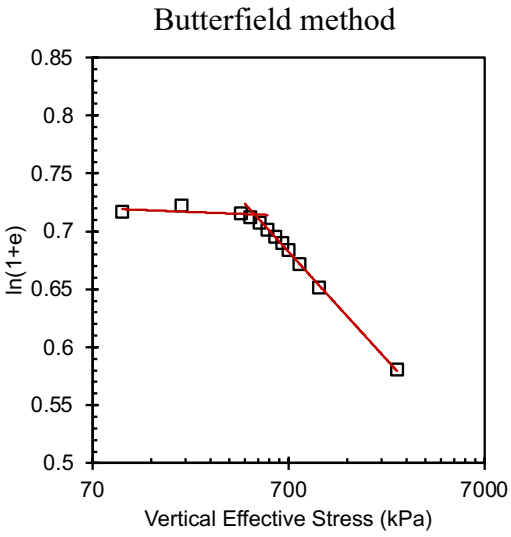
Butterfield method
ln(1+e)
0.85
0.8
0.75
0.7
0.65
0.6
0.55
0.5
70
700
7000
Vertical Effective Stress (kPa)

40 °C

Consolidation Test Data Sheet			
Test No.	40_NC_KAOL_EXT_2	Consolidometer No.	Geojac_2k_20
Date started	11/24/24	Date ended	12/14/204
Test method	B	Condition of test	Inundated
Interpretation Method	Both 1 and 2	Classification	Remolded EPK (CH)
	Before Test - 20°C		After Test - 40°C
	Specimen	Trimmings	Specimen
Tare No.	Ring	T-01	5C
Tare plus wet soil (g)	351.05	213.55	139.90
Tare plus dry soil (g)	-	150.70	109.90
Tare (g)	215.09	18.12	18.07
Water (g)	43.72	62.85	30.00
Dry Soil (g)	92.24	132.58	91.83
Water content (%)	47.4	47.4	32.7
Area of specimen, A (cm^2)	31.67		
Specific Gravity of Solids, G_s	2.7		
Height of solids, H_s (cm)	1.079		
Initial - 20°C		Final - 40°C	
Height of specimen, H_0 (cm)	2.540	Height of specimen, H_f (cm)	2.021
Height of water, H_{w0} (cm)	1.381	Height of water, H_{wf} (cm)	0.947
Height of voids, H_{v0} (cm)	1.461	Height of voids, H_{vf} (cm)	0.942
Void ratio, e_0	1.35	Void ratio, e_f	0.87
Degree of saturation, S0 (%)	94.5	Degree of saturation, S_f (%)	100.5
Dry density, γ_0 (g/cm^2)	1.15	Dry density, γ_f (g/cm^2)	1.44

		Differential height, H_d (cm)	0.050
		Preconsolidation pressure, σ_p'(kPa)	450
		Load increments (kPa) - seating loads held for 60 min, all other loads 1440 min	
Initial temperature, 20°C		5 (seating), 10, 25, 50, 100, 200, 400	
Temperature change(s)	20°C to 40°C	400	
Final temperature (°C)	40°C	400 (seating), 200, 100, 200, 400, 500, 600, 700, 800, 900, 1000, 2000, 2500	
Notes			
Note that the final height of the specimen H_f is the height recorded at the end of the test after the specimen was rebounded to 5 kPa until strain stabilized - it does not correspond to the final height at the maximum applied stress. The differential height is the difference between the final recorded height H_f and final height measured with a caliper following specimen extraction from ring at the end of the test.			

Initial Consolidation C1 (20 °C)

5 kPa

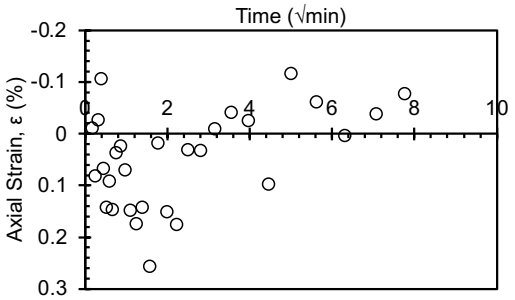

Seating load

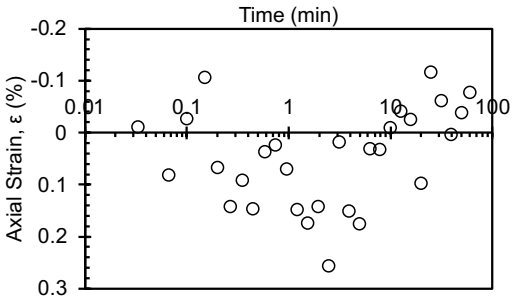

10 kPa

LIR = 1

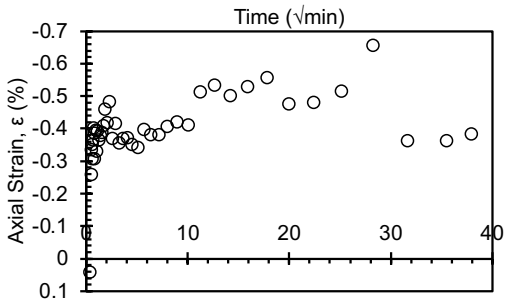

25 kPa

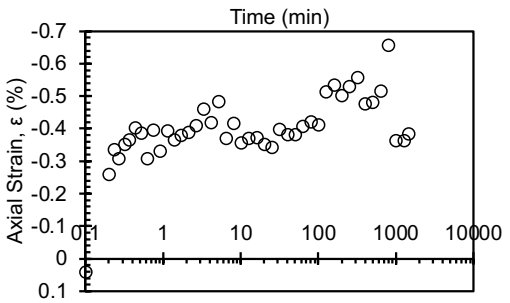

LIR = 1.5

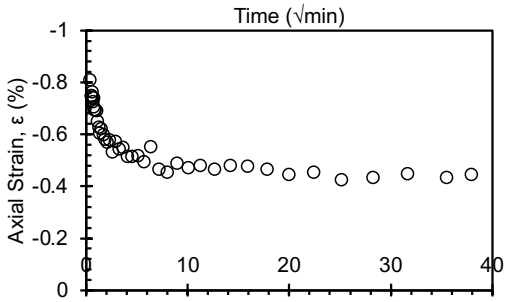

50 kPa

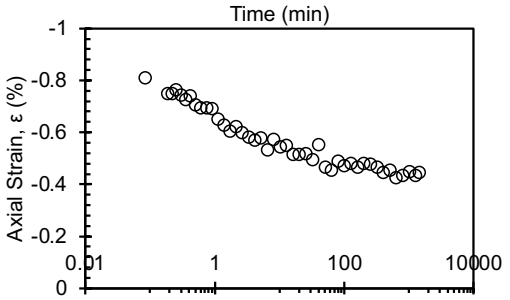

LIR = 1

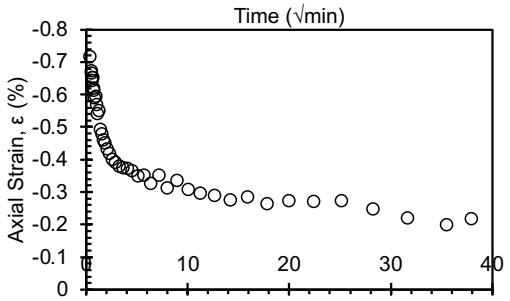

100 kPa

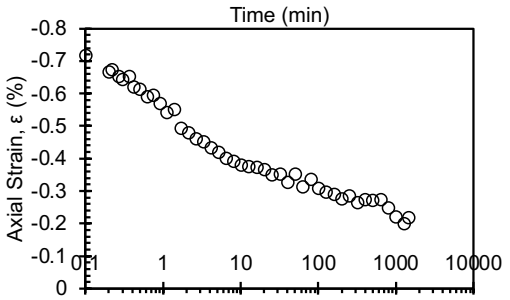

LIR = 1

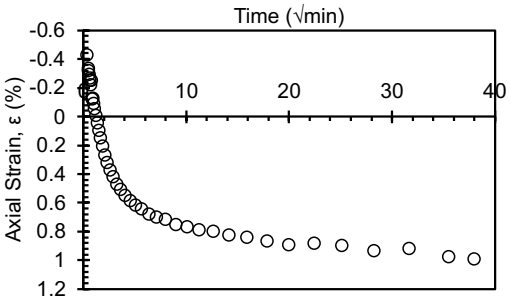

200 kPa

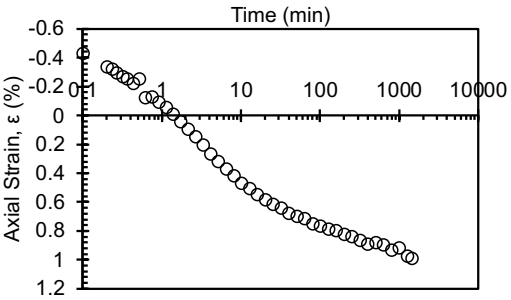

LIR = 1

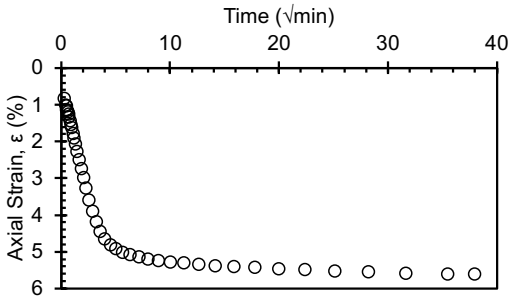

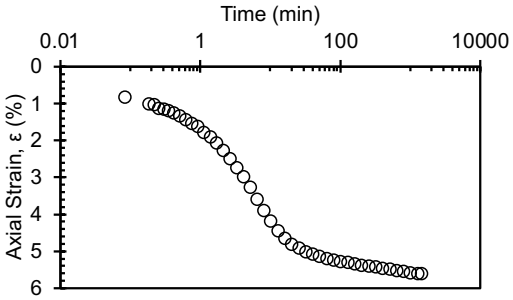

400 kPa

LIR = 1

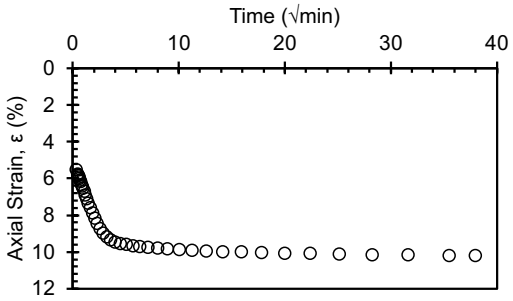

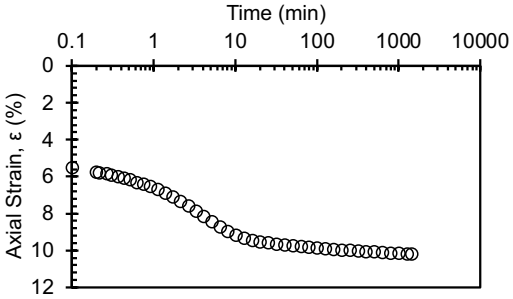

Temperature Change Stage: 20 °C>40 °C

400 kPa

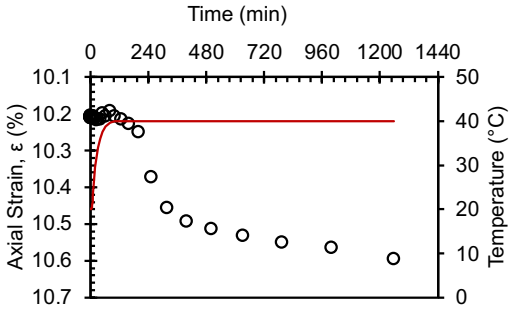

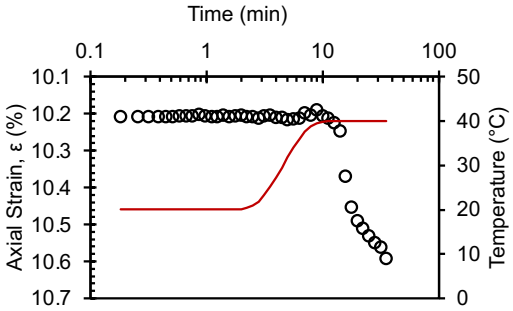

Second Consolidation C2 (40 °C)

400 kPa

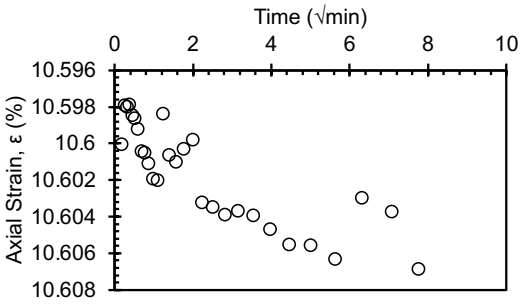

Seating load

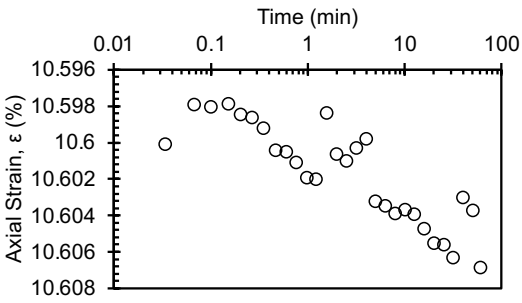

200 kPa

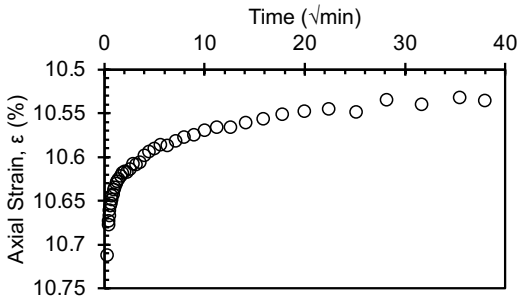

LIR = -0.5

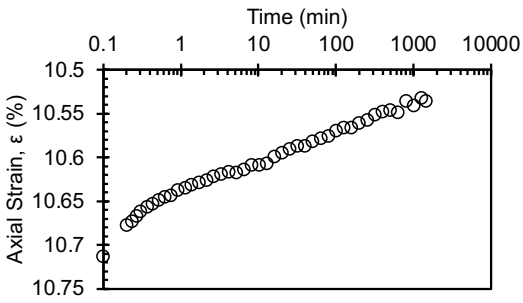

100 kPa

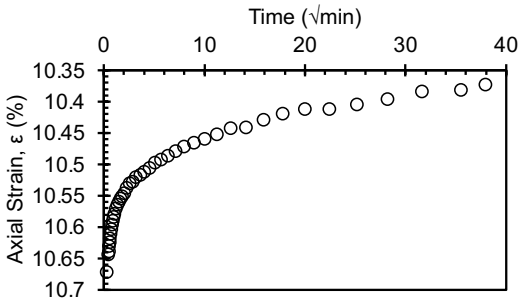

LIR =-0.5

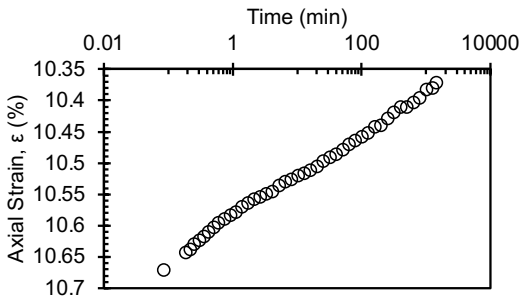

200 kPa

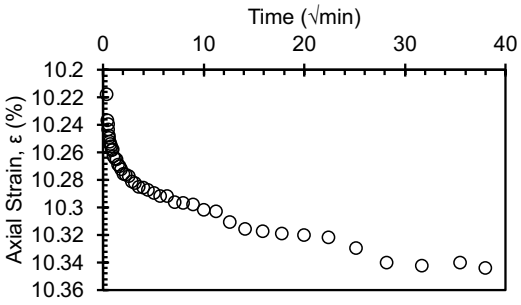

LIR = 1

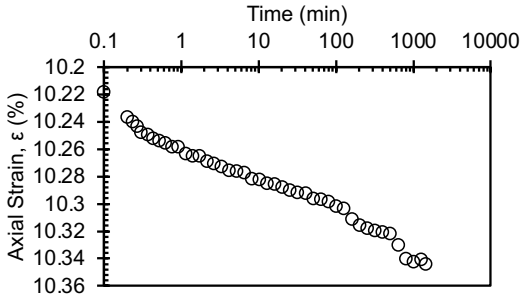

400 kPa

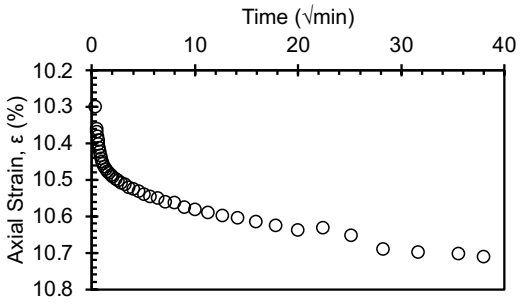

LIR = 1

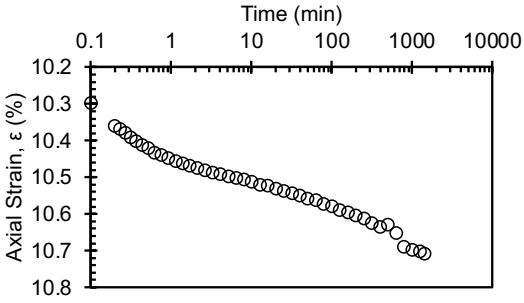

500 kPa

LIR = 0.25

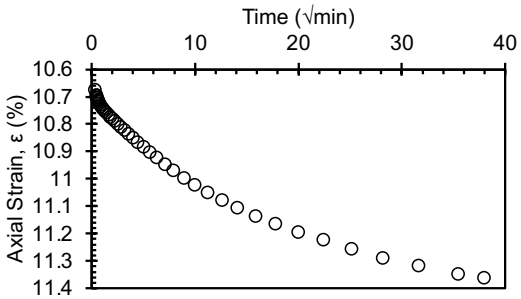

600 kPa

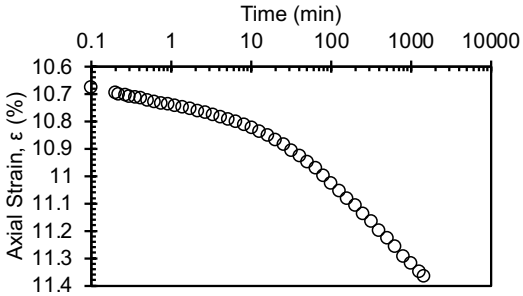

LIR = 0.2

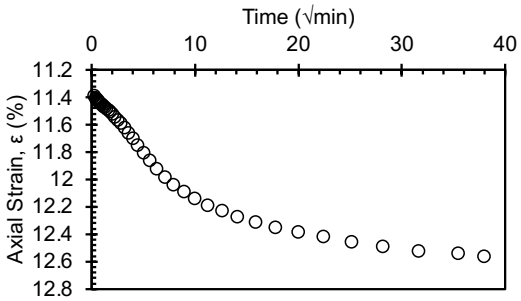

700 kPa

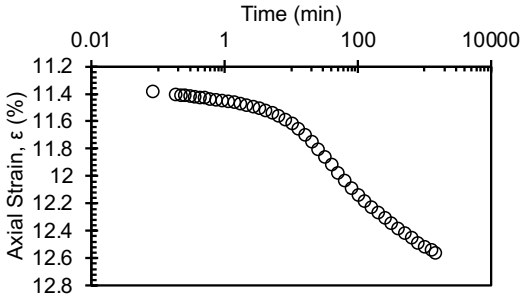

LIR = 0.167

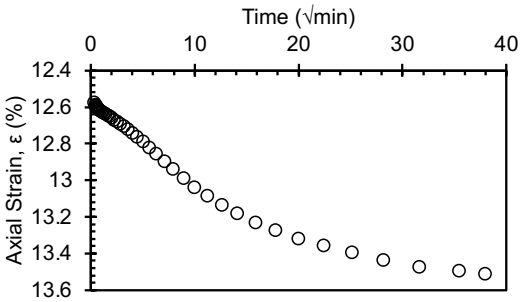

800 kPa

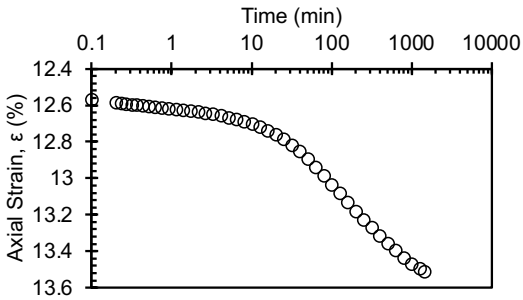

LIR = 0.143

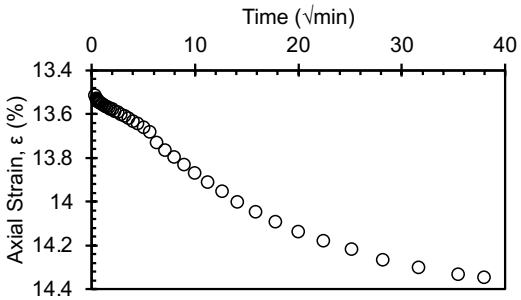

900 kPa

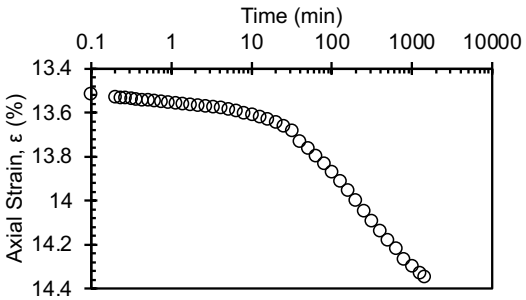

LIR = 0.125

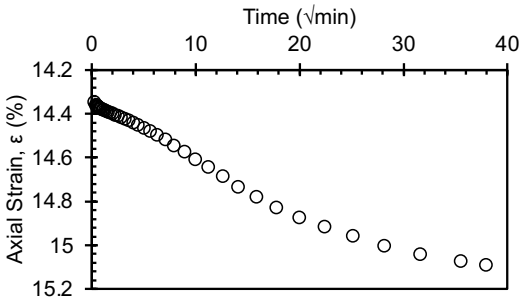

1000 kPa

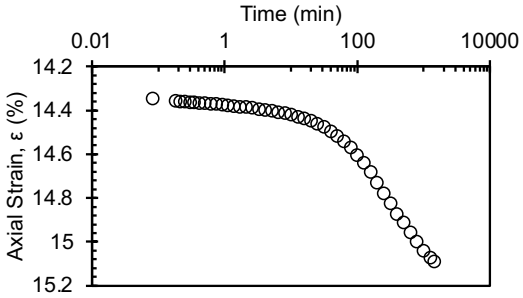

LIR = 0.111

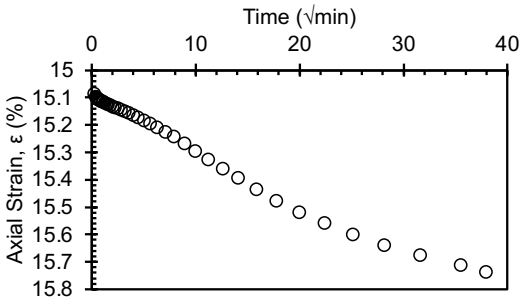

2000 kPa

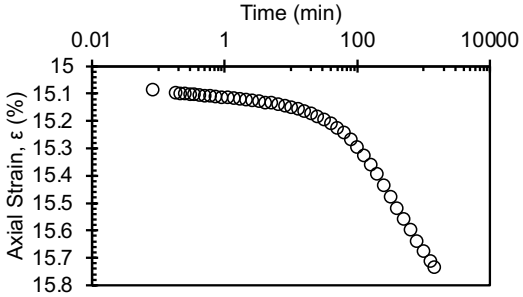

LIR = 1

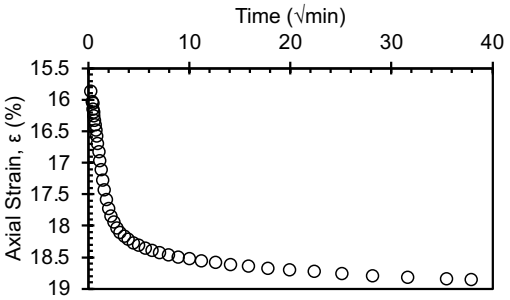

2500 kPa

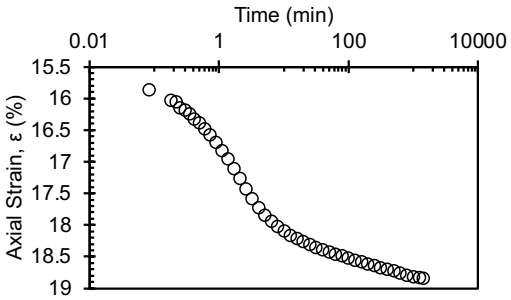

LIR = 0.25

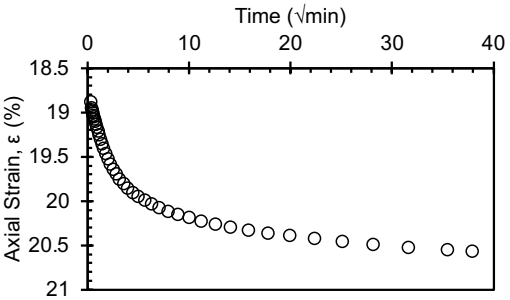

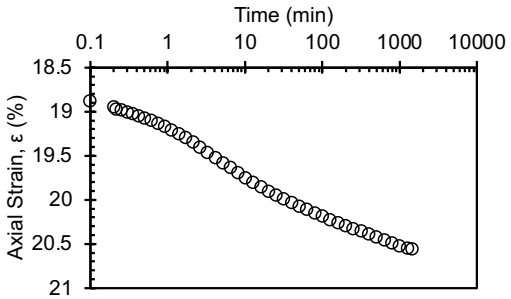

Final

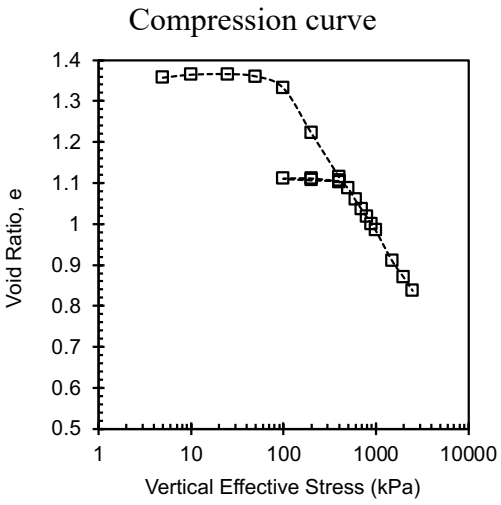
Compression curve
Void Ratio, e
1.4
1.3
1.2
1.1
1
0.9
0.8
0.7
0.6
0.5
1
10
100
1000
10000
Vertical Effective Stress (kPa)

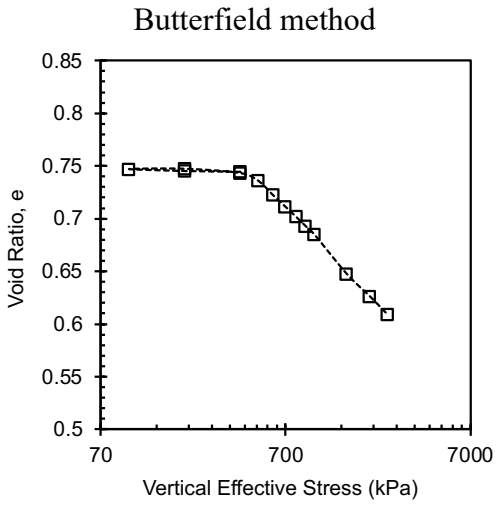
Butterfield method
Void Ratio, e
0.85
0.8
0.75
0.7
0.65
0.6
0.55
0.5
70
700
7000
Vertical Effective Stress (kPa)

30 °C

Consolidation Test Data Sheet			
Test No.	30_NC_KAOL_EXT_3	Consolidometer No.	Geojac_2k_20
Date started	10/13/24	Date ended	11/3/24
Test method	B	Condition of test	Inundated
Interpretation Method	Both 1 and 2	Classification	Remolded EPK (CH)
	Before Test - 20°C		After Test - 30°C
	Specimen	Trimmings	Specimen
Tare No.	Ring	T81	MARIO
Tare plus wet soil (g)	350.56	315.59	143.67
Tare plus dry soil (g)	-	225.12	113.57
Tare (g)	215.07	32.1	22.78
Water (g)	43.24	90.47	30.1
Dry Soil (g)	92.25	193.02	90.79
Water content (%)	46.9	46.9	33.2
Area of specimen, A (cm2)	31.67		
Specific Gravity of Solids, Gs	2.7		
Height of solids, Hs (cm)	1.079		
Initial - 20°C		Final - 30°C	
Height of specimen, H0 (cm)	2.540	Height of specimen, Hf (cm)	2.028
Height of water, Hw0 (cm)	1.365	Height of water, Hwf (cm)	0.950
Height of voids, Hv0 (cm)	1.461	Height of voids, Hvf (cm)	0.949
Void ratio, e0	1.35	Void ratio, ef	0.88
Degree of saturation, S0 (%)	93.4	Degree of saturation, Sf (%)	100.1

Dry density, γ0 (g/cm2)	1.15	Dry density, γf (g/cm2)	1.44
		Differential height, Hd (cm)	-0.041
		Preconsolidation pressure, σp'(kPa)	430
		Load increments (kPa) - seating loads held for 60 min, all other loads 1440 min	
Initial temperature, 20°C		5 (seating), 10, 25, 50, 100, 200, 400	
Temperature change(s)	20°C to 30°C	400	
Final temperature (°C)	30°C	400 (seating), 200, 100, 200, 400, 450, 500, 550, 600, 650, 700, 800, 1000, 2000, 2500	
Notes			
Note that the final height of the specimen Hf is the height recorded at the end of the test after the specimen was rebounded to 5 kPa until strain stabilized - it does not correspond to the final height at the maximum applied stress. The differential height is the difference between the final recorded height Hf and final height measured with a caliper following specimen extraction from ring at the end of the test.			

Initial Consolidation C1 (20 °C)

5 kPa

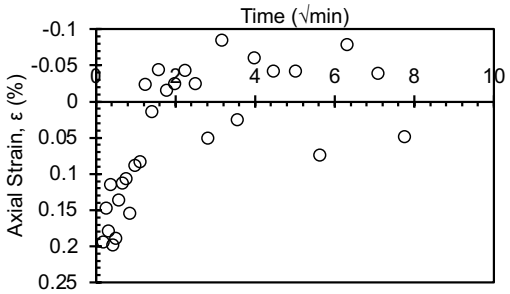

Seating load

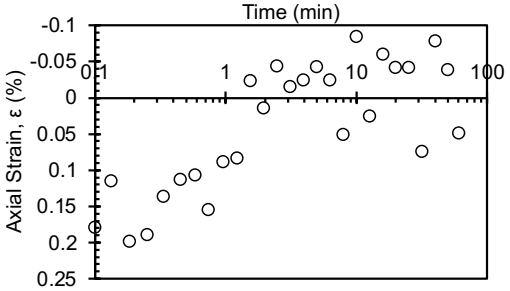

10 kPa

LIR = 1

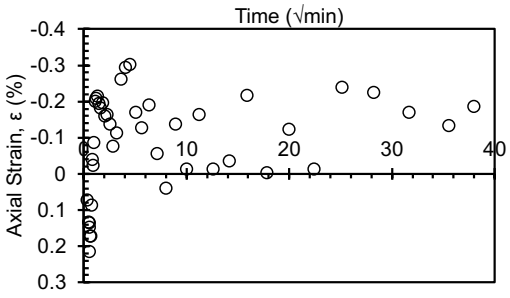

25 kPa

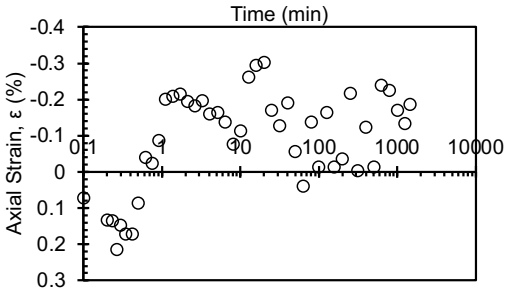

LIR = 1.5

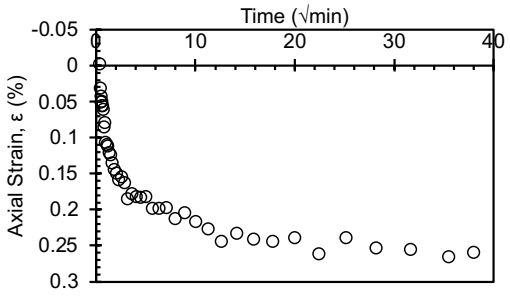

50 kPa

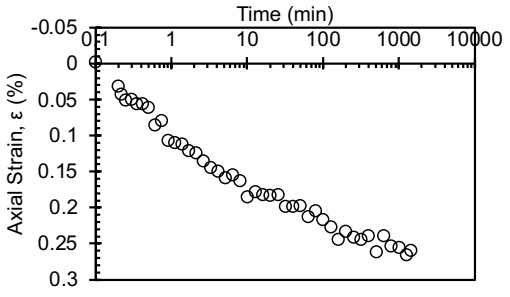

LIR = 1

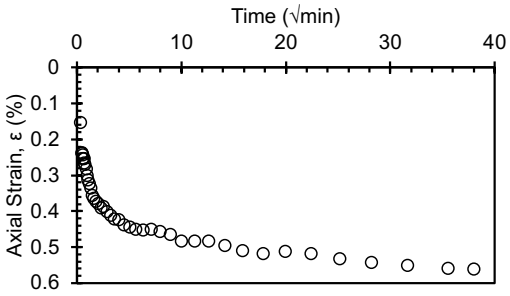

100 kPa

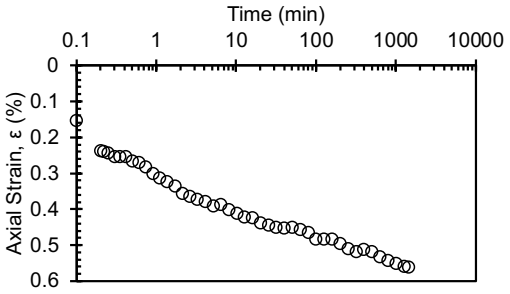

LIR = 1

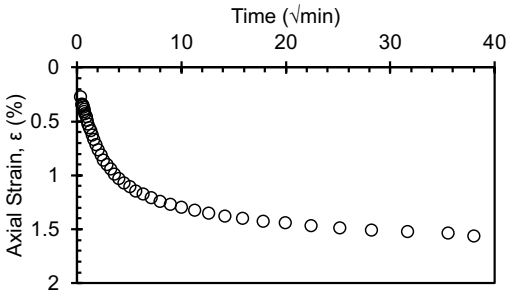

200 kPa

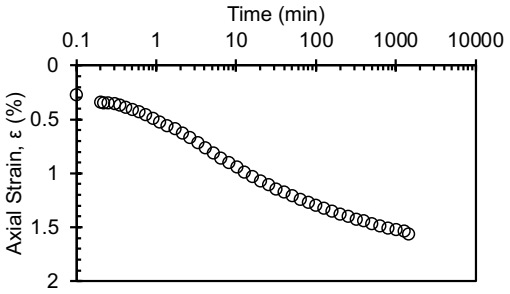

LIR = 1

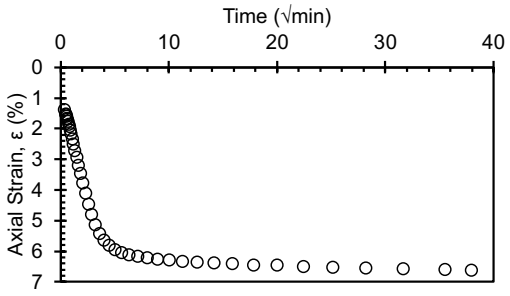

400 kPa

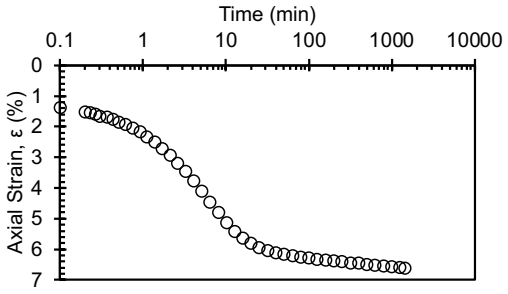

LIR = 1

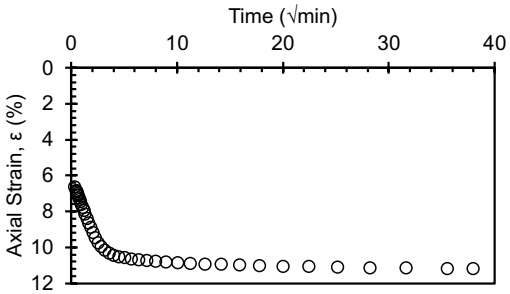

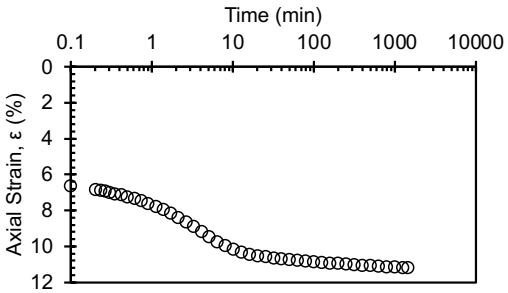

Temperature Change Stage: 20 °C>30 °C

400 kPa

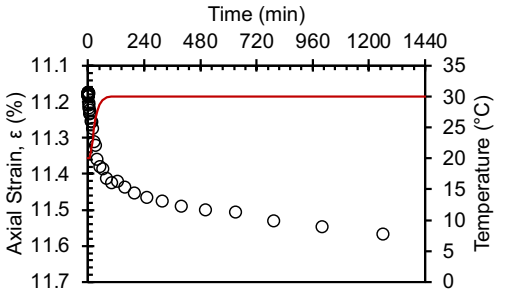

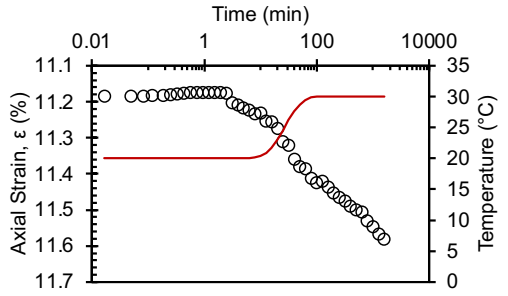

Second Consolidation C2 (30 °C)

400 kPa

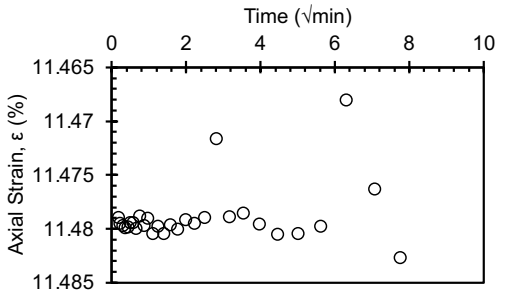

200 kPa

Seating load

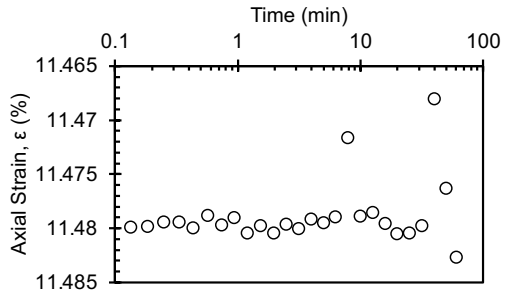

LIR = -0.5

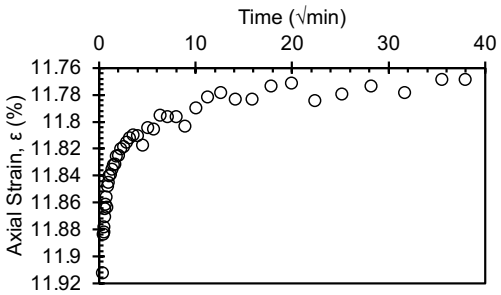

100 kPa

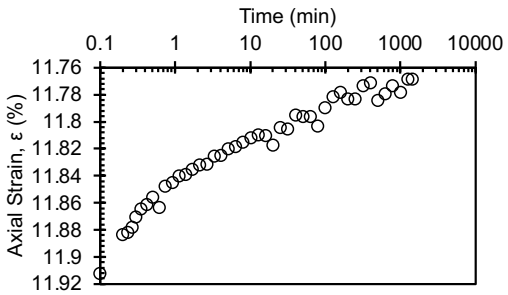

LIR =-0.5

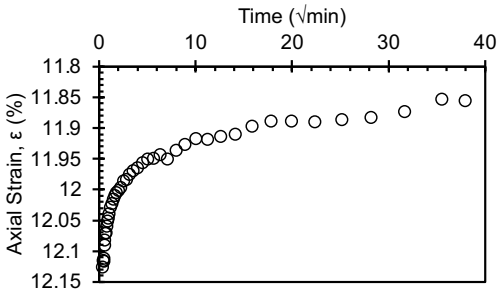

200 kPa

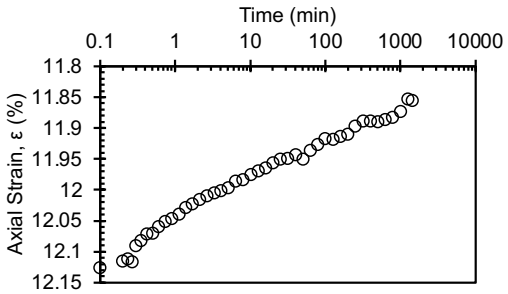

LIR = 1

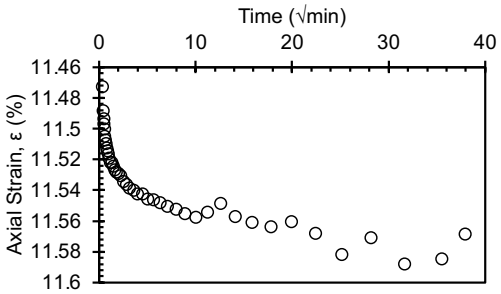

400 kPa

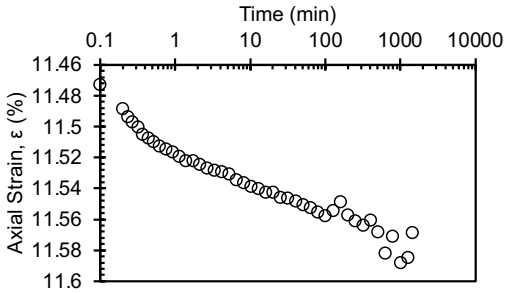

LIR = 1

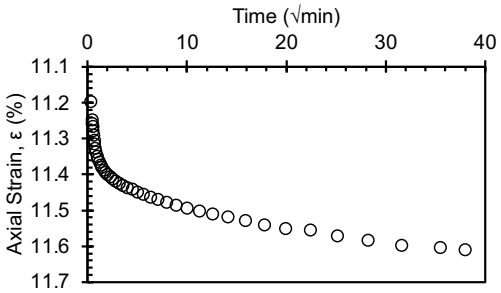

450 kPa

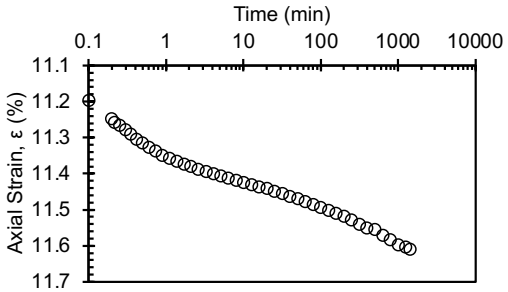

LIR = 0.125

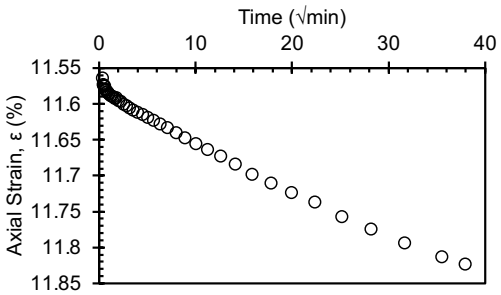

500 kPa

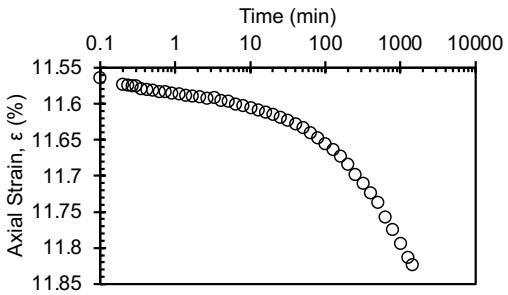

LIR = 0.11

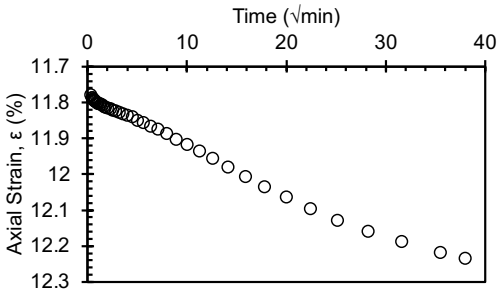

550 kPa

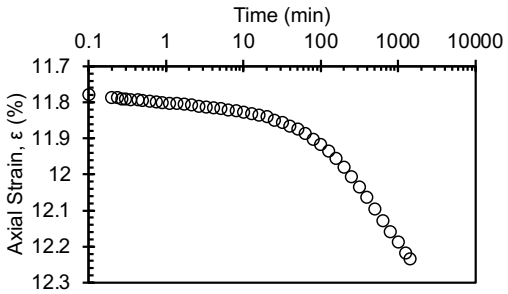

LIR = 0.1

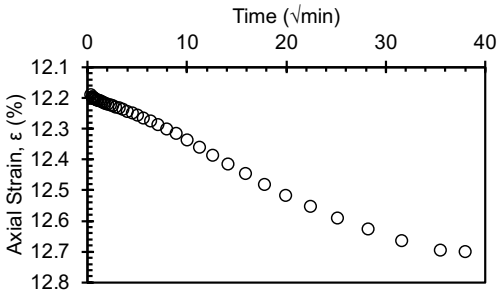

600 kPa

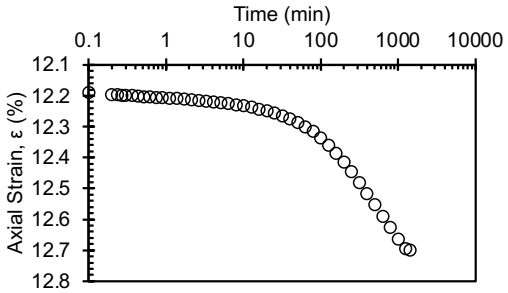

LIR = 0.091

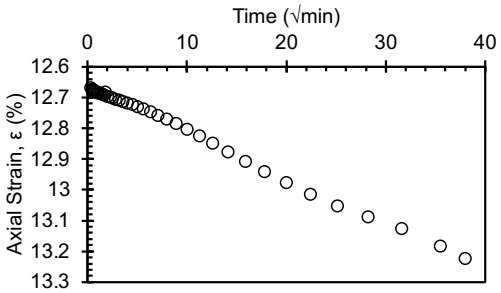

650 kPa

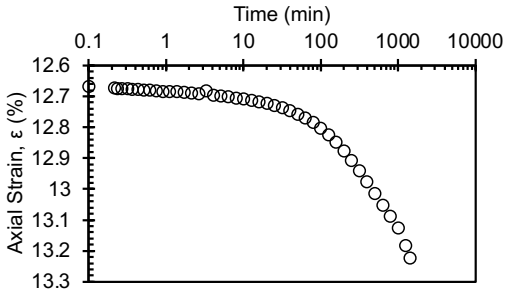

LIR = 0.83

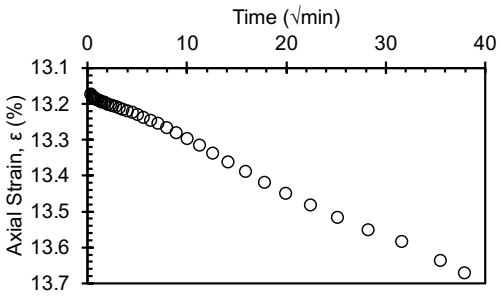

700 kPa

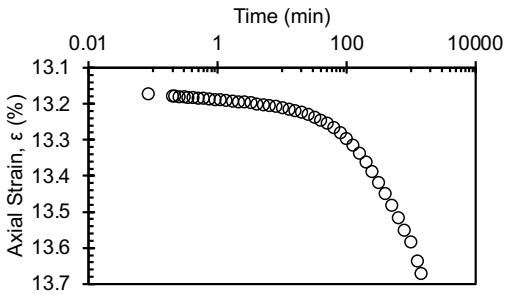

LIR = 0.077

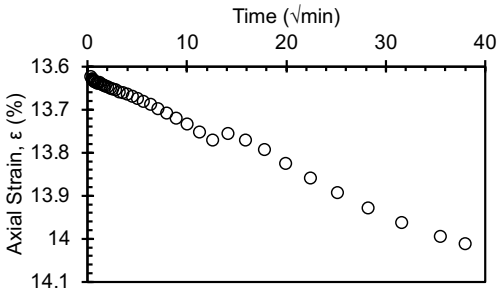

800 kPa

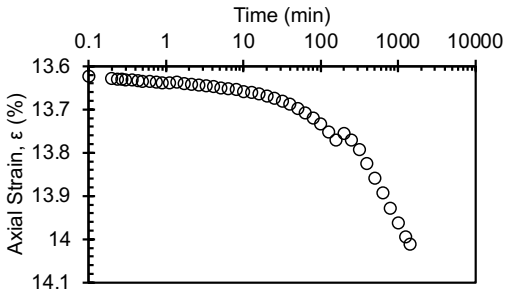

LIR = 0.143

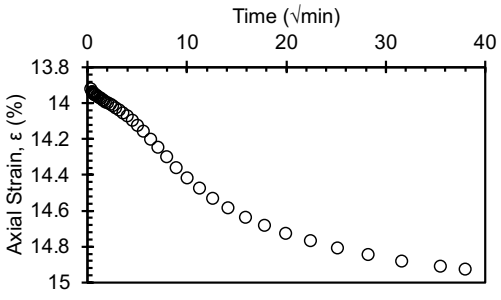

1000 kPa

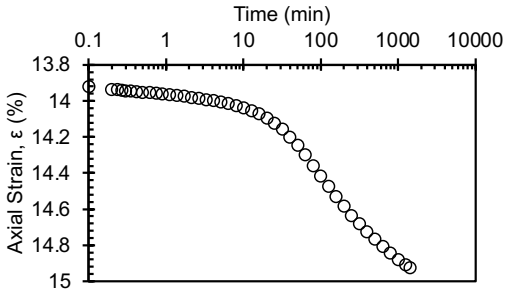

LIR = 0.2

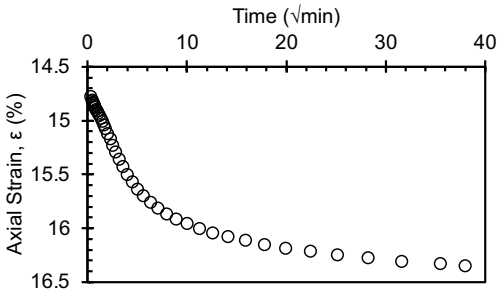

2000 kPa

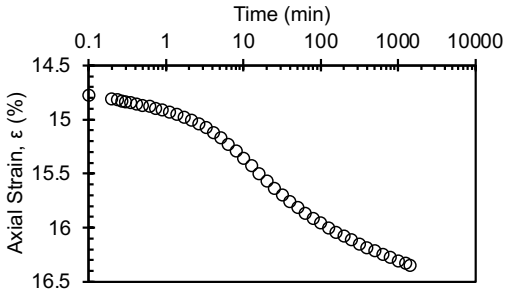

LIR = 1

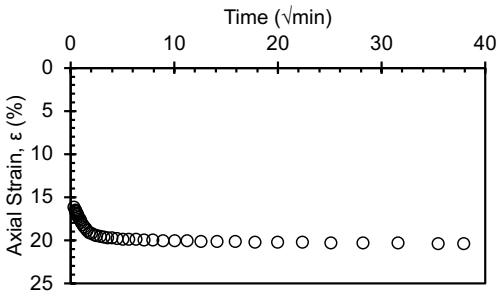

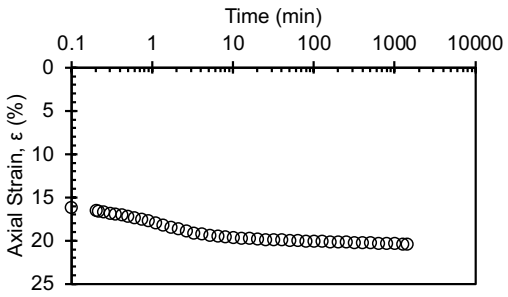

2500 kPa

LIR = 0.25

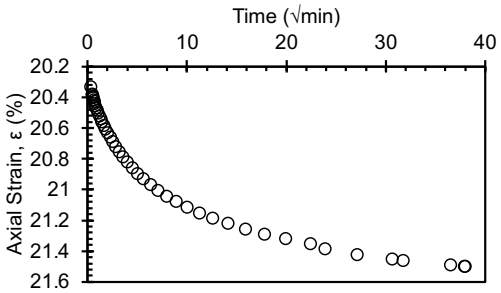

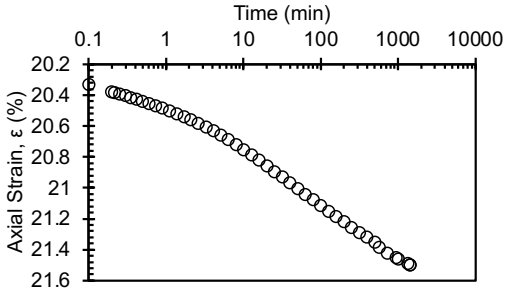

Final

Compression curve

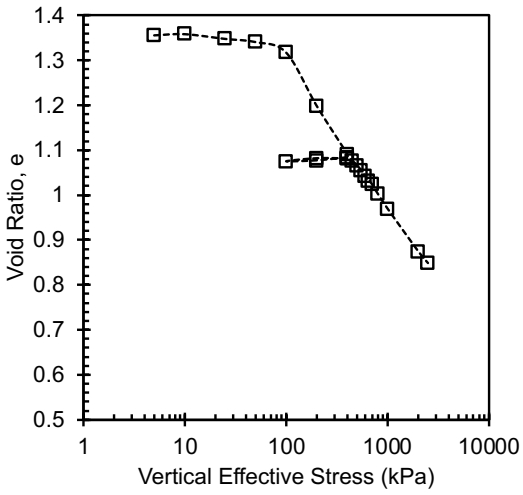

Butterfield method

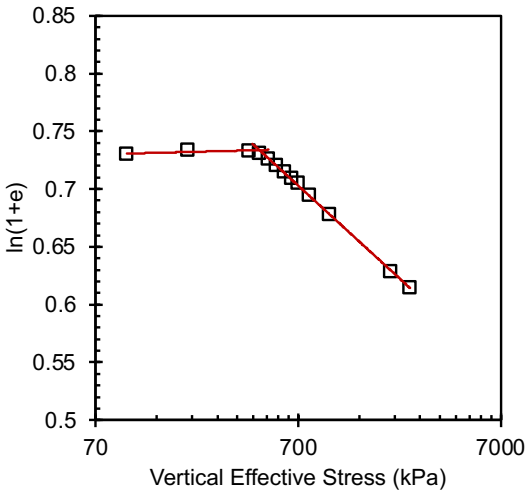

20 °C

Consolidation Test Data Sheet			
Test No.	20_NC_KAOL_EXT_2	Consolidometer No.	Sigma1_5k_20
Date started	8/16/24	Date ended	9/8/24
Test method	B	Condition of test	Inundated
Interpretation Method	Both 1 and 2	Classification	Remolded EPK (CH)
	Before Test - 20°C		After Test - 20°C
	Specimen	Trimmings	Specimen
Tare No.	Ring	LUIGI	MARIO
Tare plus wet soil (g)	356.93	233.44	153.77
Tare plus dry soil (g)	-	170.35	121.11
Tare (g)	215.72	22.1	22.71
Water (g)	42.2	63.09	32.66
Dry Soil (g)	99.1	148.25	98.4
Water content (%)	42.6	42.6	33.2
Area of specimen, A (cm^2)	31.67		
Specific Gravity of Solids, G_s	2.7		
Height of solids, H_s (cm)	1.158		
Initial - 20°C		Final - 20°C	
Height of specimen, H_0 (cm)	2.540	Height of specimen, H_f (cm)	2.189
Height of water, H_{w0} (cm)	1.331	Height of water, H_{wf} (cm)	1.031
Height of voids, H_{v0} (cm)	1.382	Height of voids, H_{vf} (cm)	1.031
Void ratio, e_0	1.19	Void ratio, e_f	0.89

Degree of saturation, S0 (%)	96.3	Degree of saturation, S_f (%)	100.1
Dry density, γ_0 (g/cm^2)	1.23	Dry density, γ_f (g/cm^2)	1.43
		Differential height, H_d (cm)	-0.087
		Preconsolidation pressure, σ_p'(kPa)	400
		Load increments (kPa) - seating loads held for 60 min, all other loads 1440 min	
Initial temperature, 20°C		5 (seating), 10, 25, 50, 100, 200, 400	
Temperature change(s)	none		
Final temperature (°C)	20°C	400 (seating), 200, 100, 200, 300, 400, 450, 500, 550, 800, 900, 1000, 1500, 2000, 2500	
Notes			
Note that the final height of the specimen H_f is the height recorded at the end of the test after the specimen was rebounded to 5 kPa until strain stabilized - it does not correspond to the final height at the maximum applied stress. The differential height is the difference between the final recorded height H_f and final height measured with a caliper following specimen extraction from ring at the end of the test.			

Initial Consolidation C1 (20 °C)

5 kPa

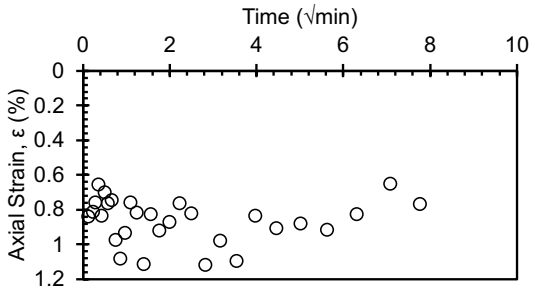

Seating load

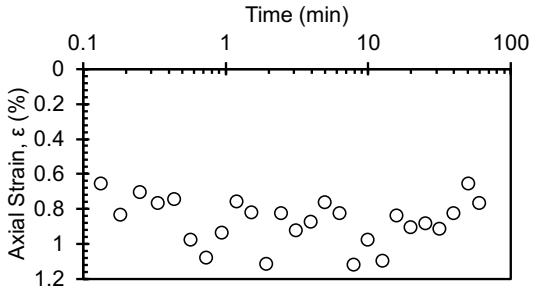

10 kPa

LIR = 1

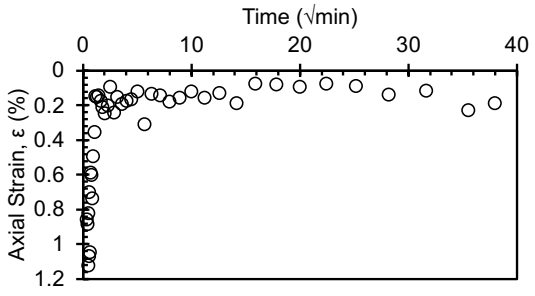

25 kPa

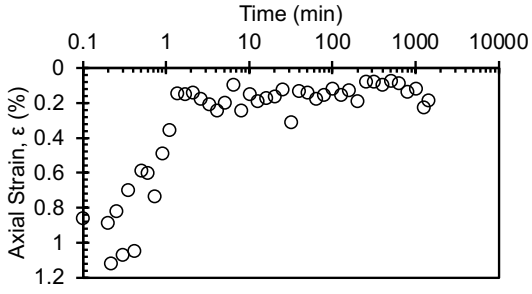

LIR = 1.5

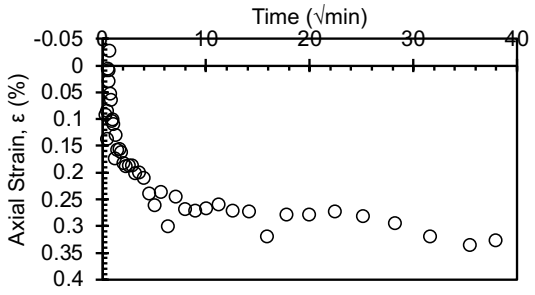

50 kPa

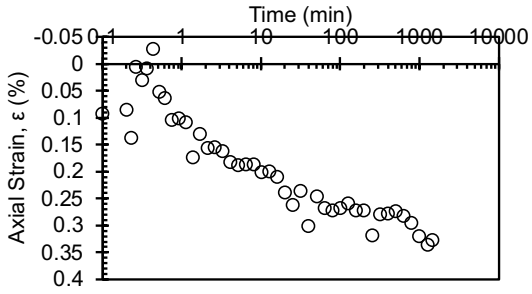

LIR = 1

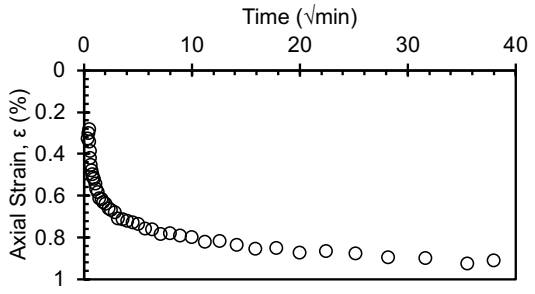

100 kPa

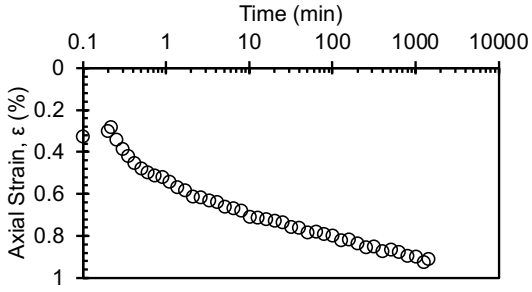

LIR = 1

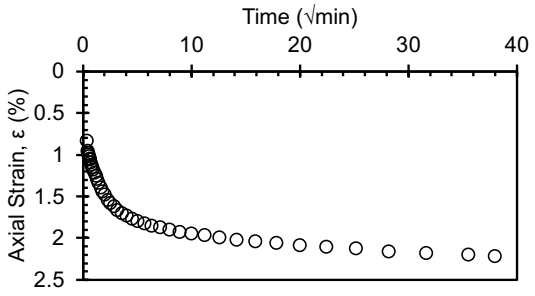

200 kPa

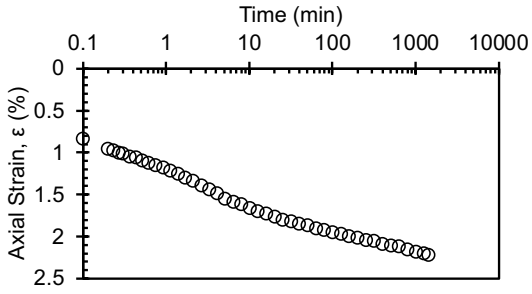

LIR = 1

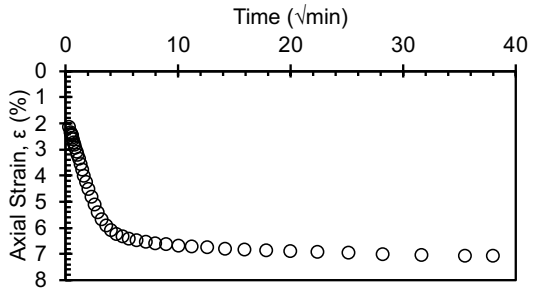

400 kPa

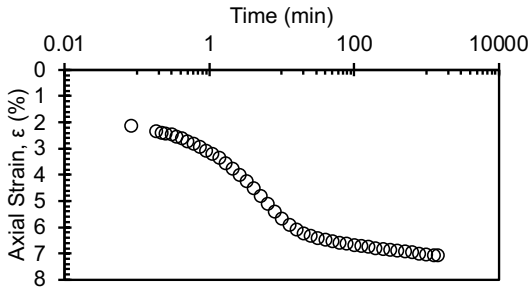

LIR = 1

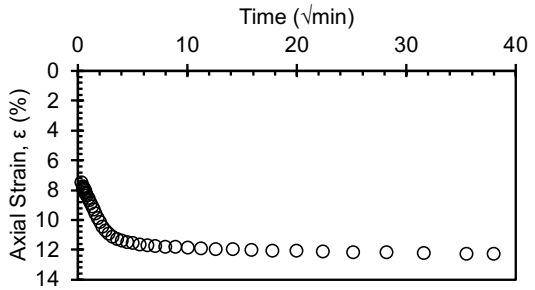

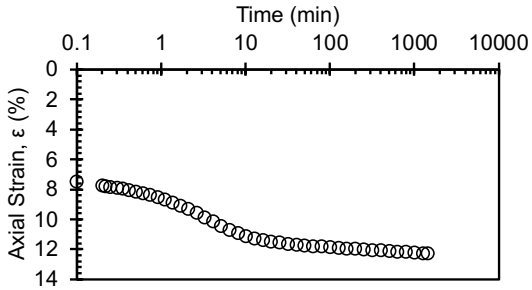

Second Consolidation C2 (20 °C)

400 kPa

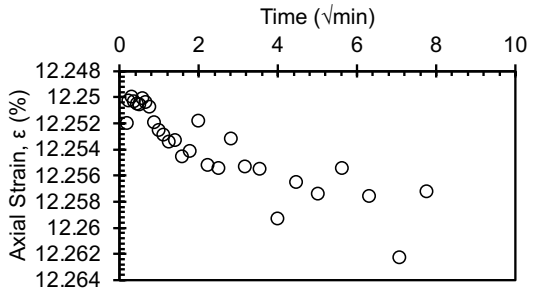

200 kPa

Seating load

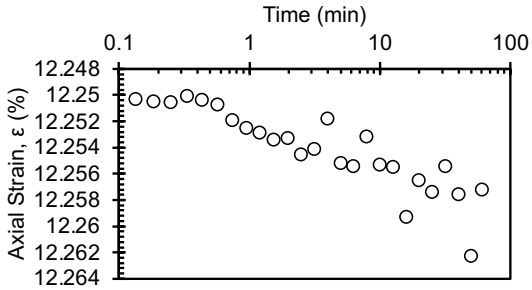

LIR = -0.5

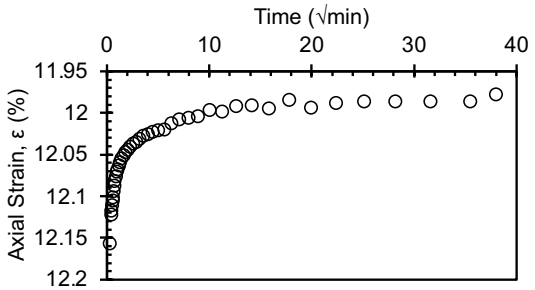

100 kPa

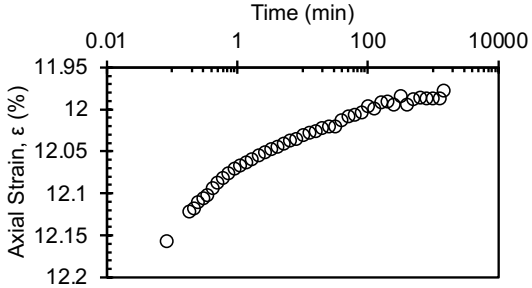

LIR =-0.5

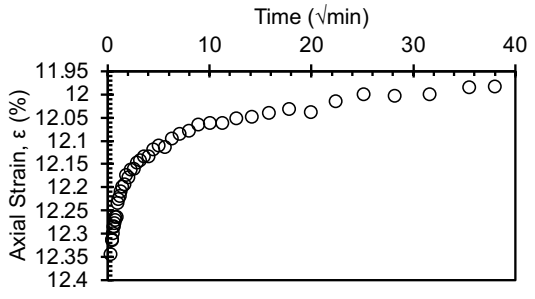

200 kPa

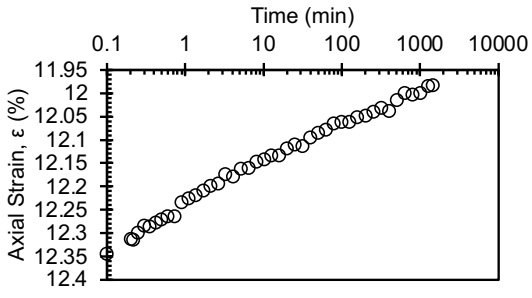

LIR = 1

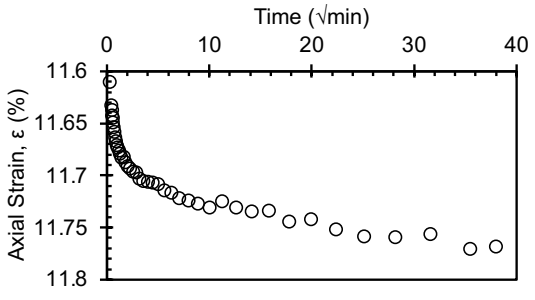

400 kPa

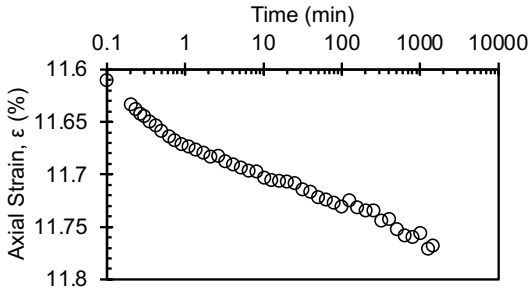

LIR = 1

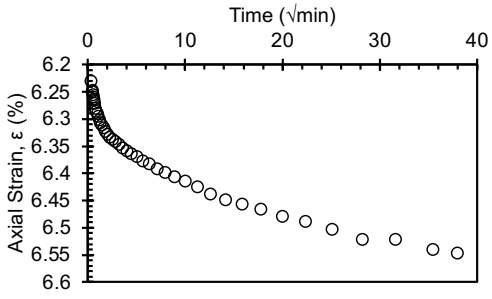

450 kPa

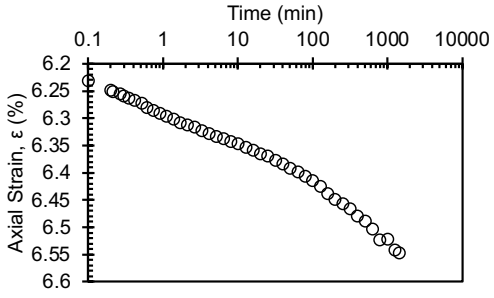

LIR = 0.125

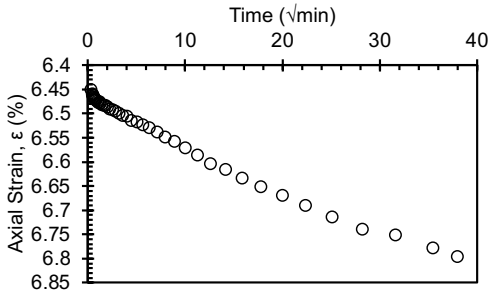

500 kPa

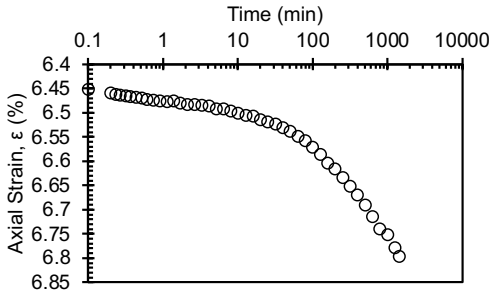

LIR = 0.11

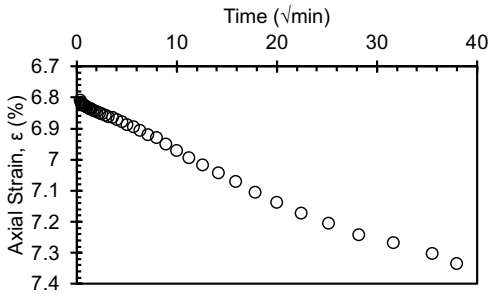

550 kPa

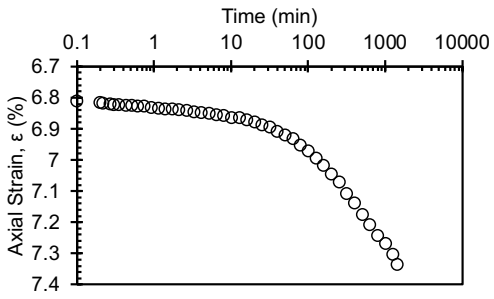

LIR = 0.1

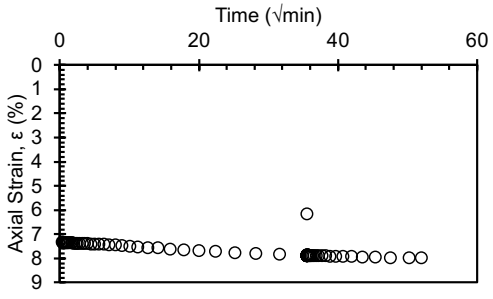

800 kPa

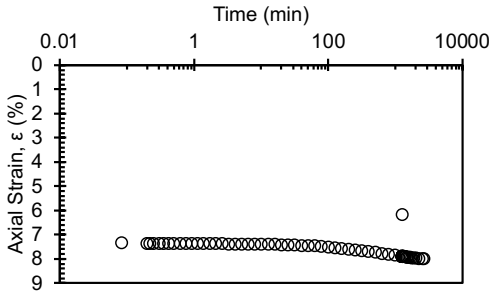

LIR = 0.455

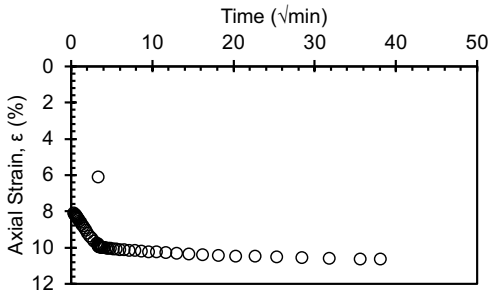

900 kPa

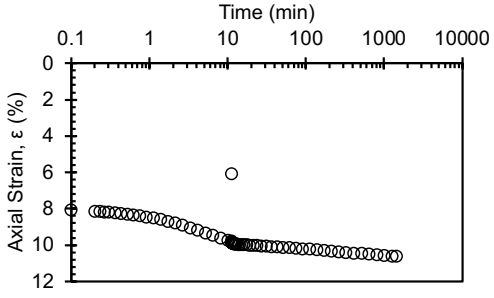

LIR = 0.125

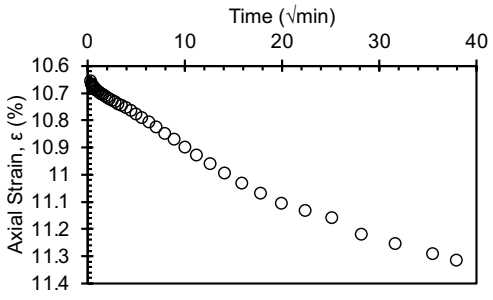

1000 kPa

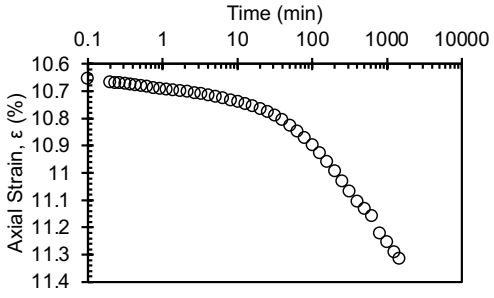

LIR = 0.1

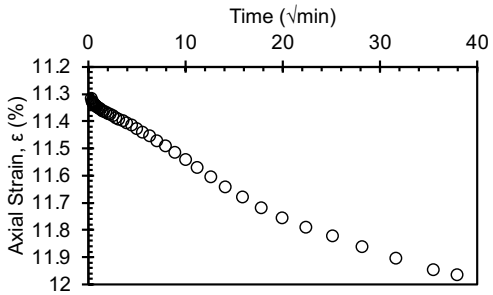

1500 kPa

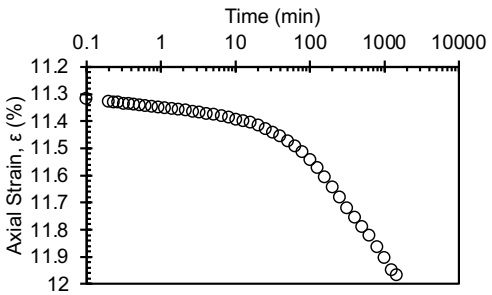

LIR = 0.5

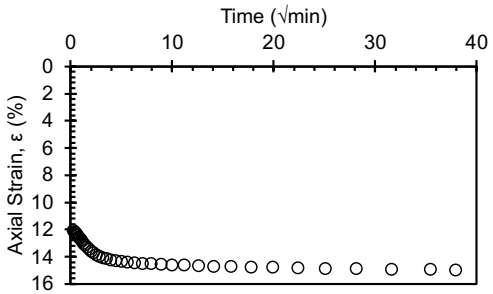

2000 kPa

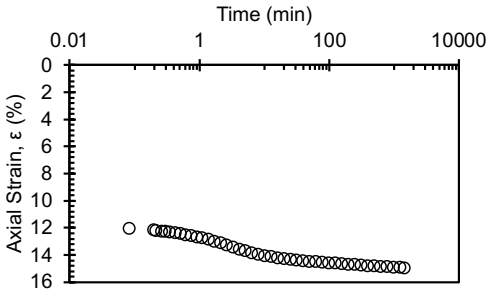

LIR = 0.333

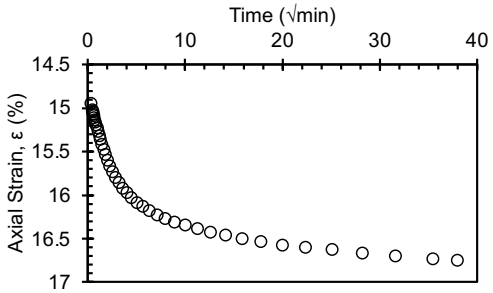

2500 kPa

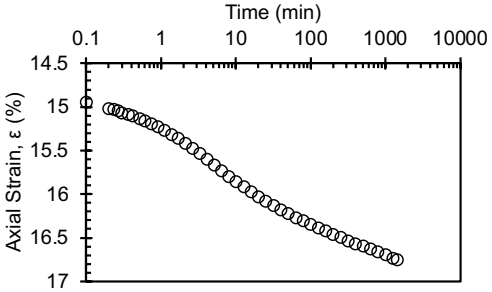

LIR = 0.25

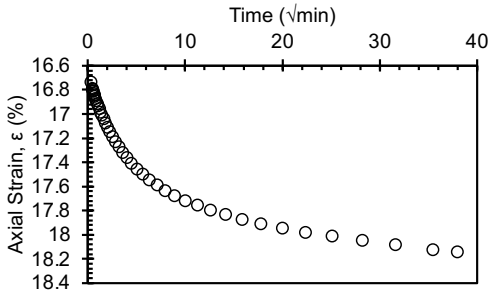

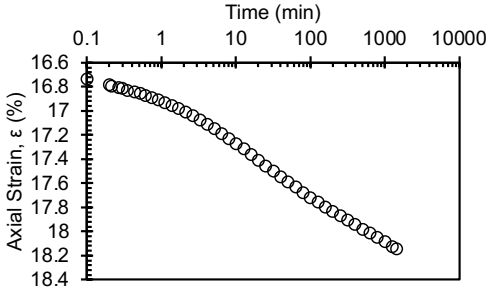

Final

Compression curve

Butterfield method

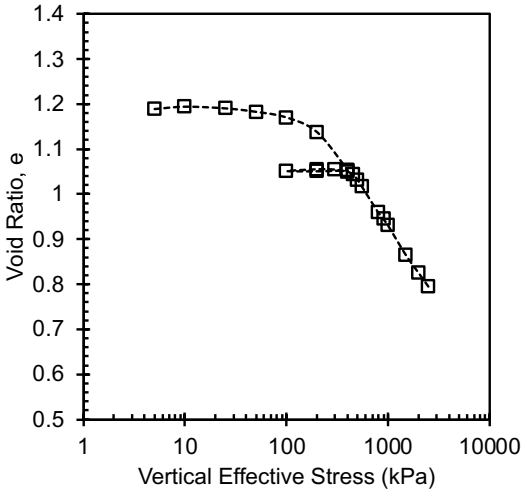
Void Ratio, e
1.4
1.3
1.2
1.1
1
0.9
0.8
0.7
0.6
0.5
1
10
100
1000
10000
Vertical Effective Stress (kPa)

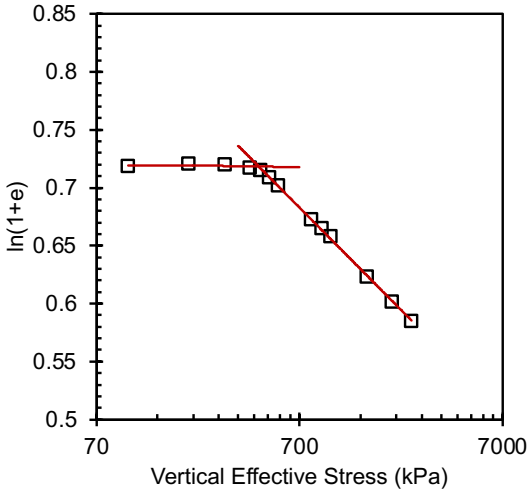
ln(1+e)
0.85
0.8
0.75
0.7
0.65
0.6
0.55
0.5
70
700
7000
Vertical Effective Stress (kPa)

10 °C

Consolidation Test Data Sheet			
Test No.	10_NC_KAOL_EXT_2	Consolidometer No.	Sigma1_5k_20
Date started	10/27/24	Date ended	11/17/24
Test method	B	Condition of test	Inundated
Interpretation Method	Both 1 and 2	Classification	Remolded EPK (CH)
	Before Test - 20°C		After Test - 10°C
	Specimen	Trimmings	Specimen
Tare No.	Ring	MARIO	T81
Tare plus wet soil (g)	348.80	253.46	153.21
Tare plus dry soil (g)	-	178.89	122.77
Tare (g)	213.49	22.76	32.10
Water (g)	43.74	74.57	30.44
Dry Soil (g)	91.57	156.13	90.67
Water content (%)	47.8	47.8	33.6
Area of specimen, A (cm^2)	31.67		
Specific Gravity of Solids, G_s	2.7		
Height of solids, H_s (cm)	1.071		
Initial - 20°C		Final - 10°C	
Height of specimen, H_0 (cm)	2.540	Height of specimen, H_f (cm)	2.030
Height of water, H_{w0} (cm)	1.381	Height of water, H_{wf} (cm)	0.961
Height of voids, H_{v0} (cm)	1.469	Height of voids, H_{vf} (cm)	0.959
Void ratio, e_0	1.37	Void ratio, e_f	0.90

Degree of saturation, S0 (%)	94.0	Degree of saturation, S_f (%)	100.2
Dry density, γ_0 (g/cm^2)	1.14	Dry density, γ_f (g/cm^2)	1.42
		Differential height, H_d (cm)	0.006
		Preconsolidation pressure, σ_p'(kPa)	420
		Load increments (kPa) - seating loads held for 60 min, all other loads 1440 min	
Initial temperature, 20°C		5 (seating), 10, 25, 50, 100, 200, 400	
Temperature change(s)	20°C to 10°C	400	
Final temperature (°C)	10°C	400 (seating), 200, 100, 200, 400, 450, 500, 550, 600, 650, 900, 1000, 2500	
Notes			
Note that the final height of the specimen H_f is the height recorded at the end of the test after the specimen was rebounded to 5 kPa until strain stabilized - it does not correspond to the final height at the maximum applied stress. The differential height is the difference between the final recorded height H_f and final height measured with a caliper following specimen extraction from ring at the end of the test.			

Initial Consolidation C1 (20 °C)

5 kPa

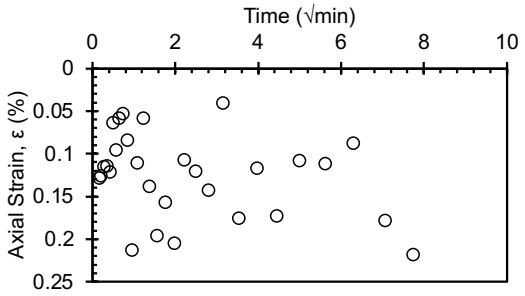

10 kPa

Seating Load

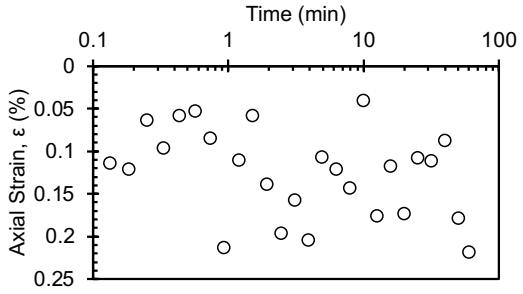

LIR = 1

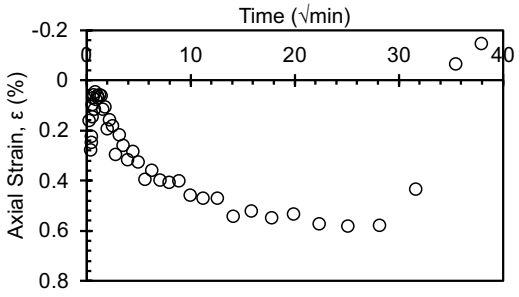

25 kPa

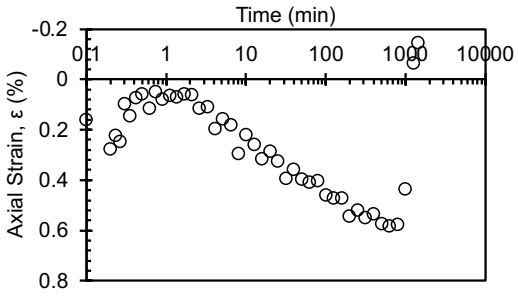

LIR = 1.5

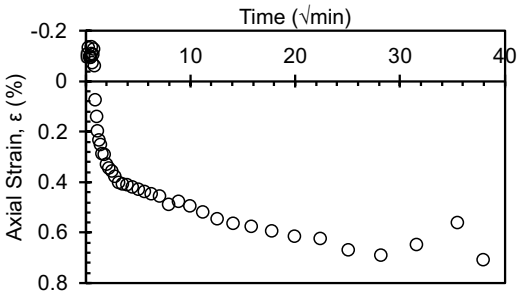

50 kPa

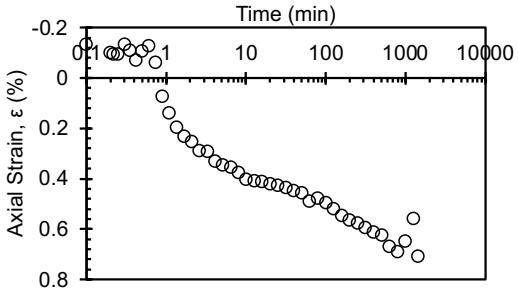

LIR = 2

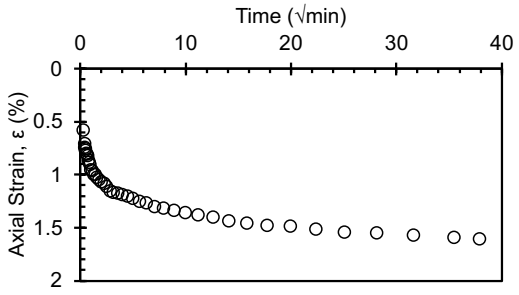

100 kPa

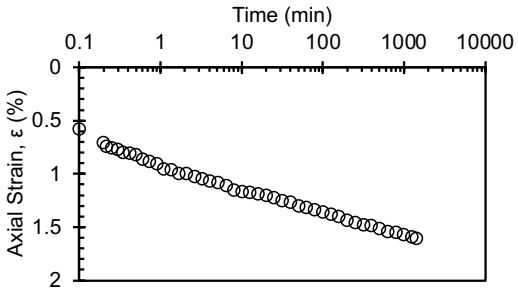

LIR = 1

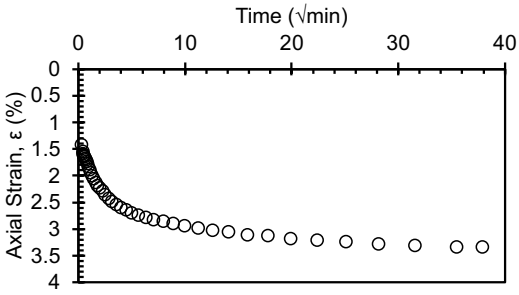

200 kPa

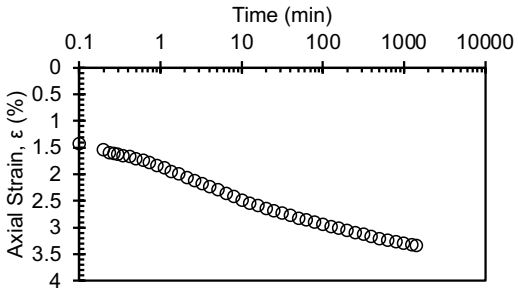

LIR = 1

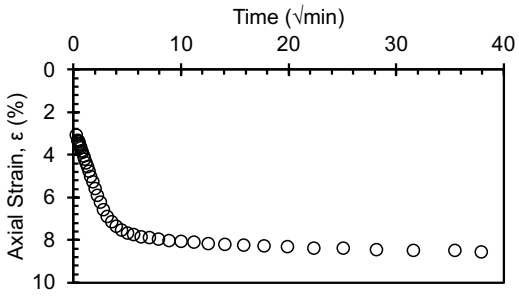

400 kPa

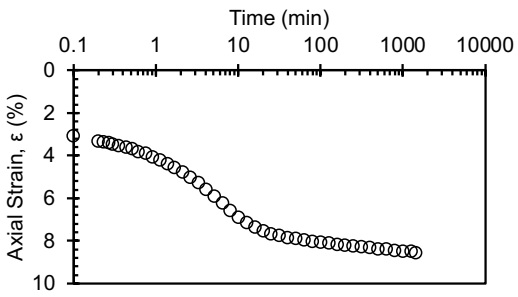

LIR = 1

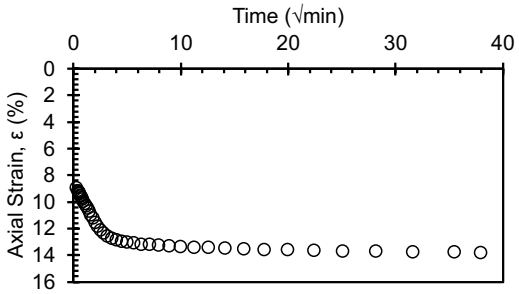

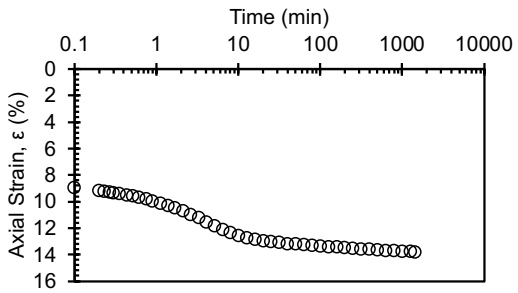

Temperature Change Stage: 20 °C>10 °C

400 kPa

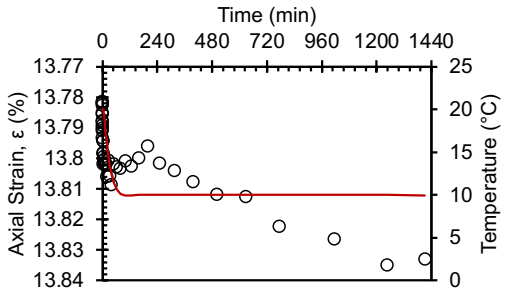

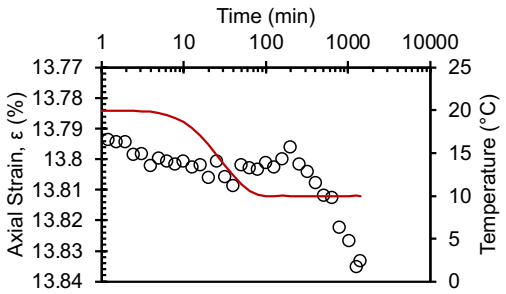

Second Consolidation C2 (10 °C)

400 kPa

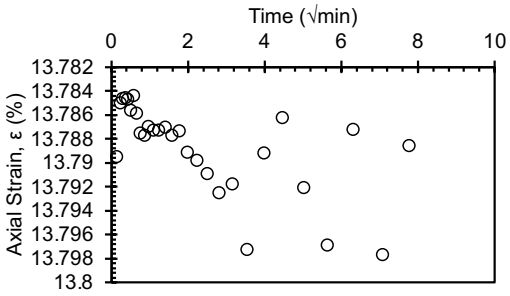

200 kPa

Seating load

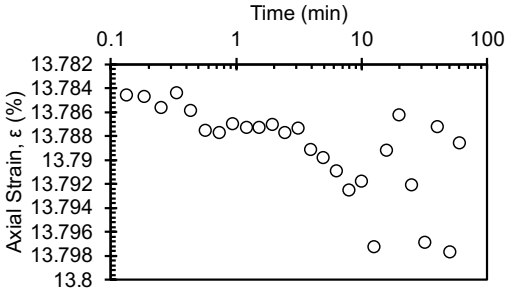

LIR = -0.5

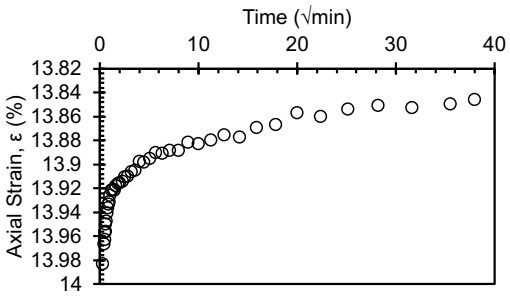

100 kPa

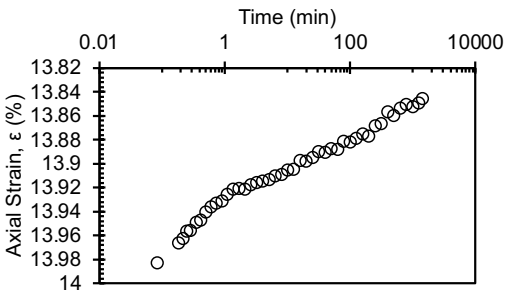

LIR =-0.5

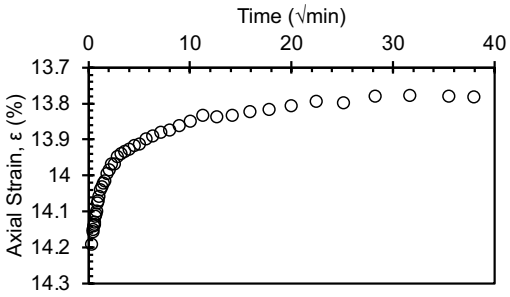

200 kPa

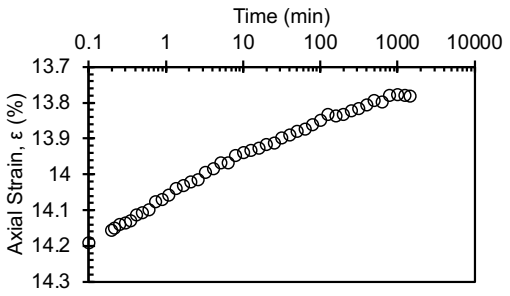

LIR = 1

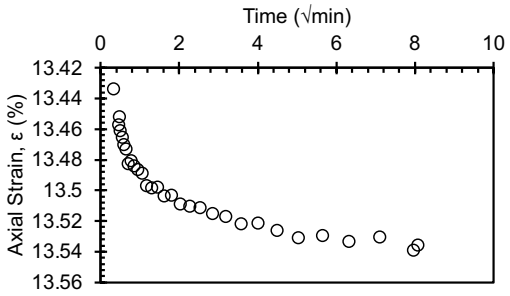

400 kPa

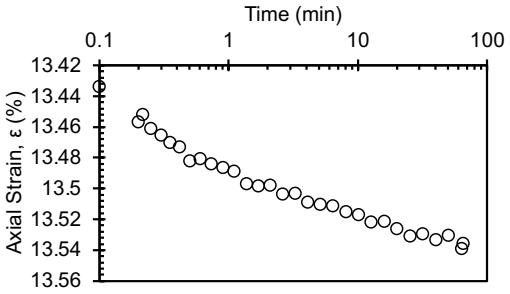

LIR = 1

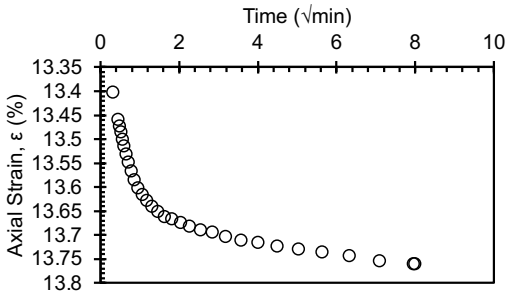

450 kPa

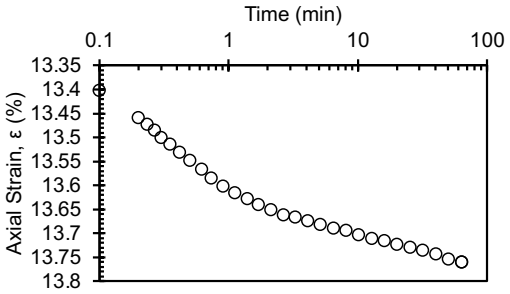

LIR = 0.125

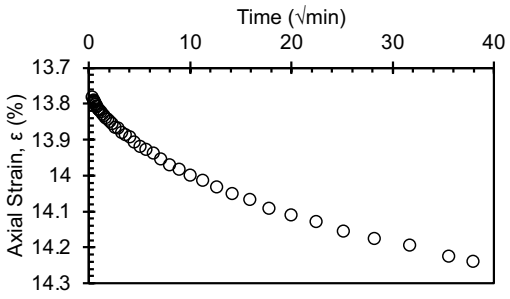

500 kPa

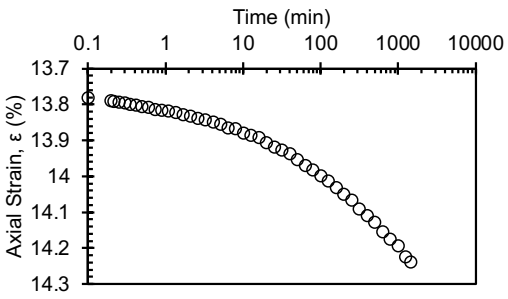

LIR = 0.11

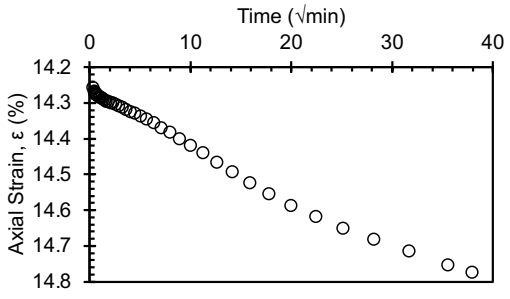

550 kPa

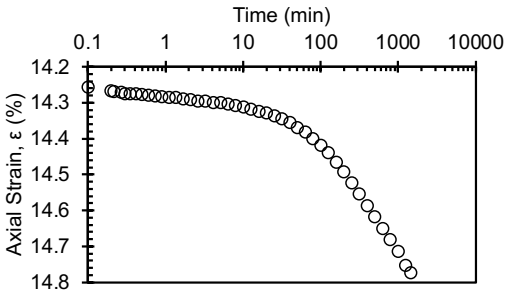

LIR = 0.1

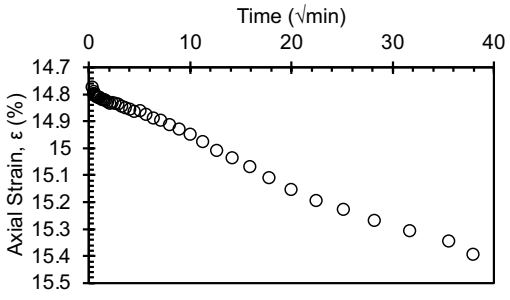

600 kPa

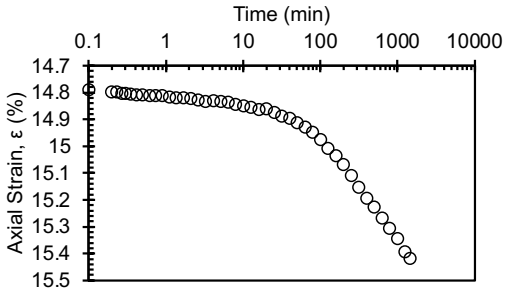

LIR = 0.091

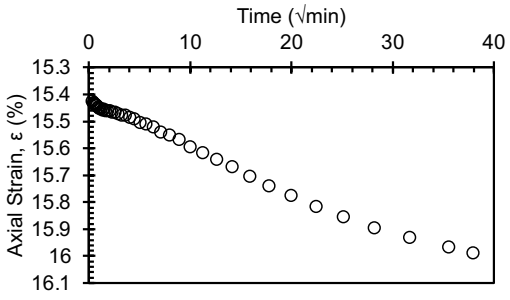

650 kPa

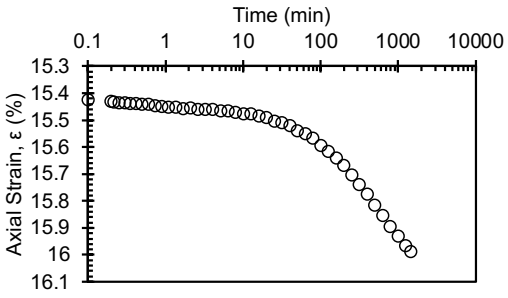

LIR = 0.83

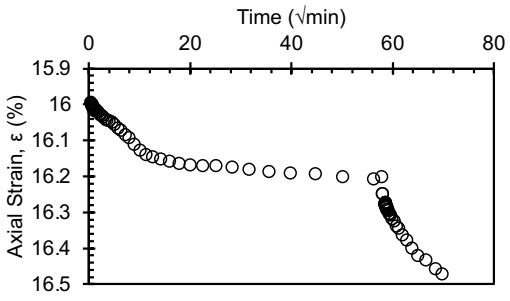

900 kPa

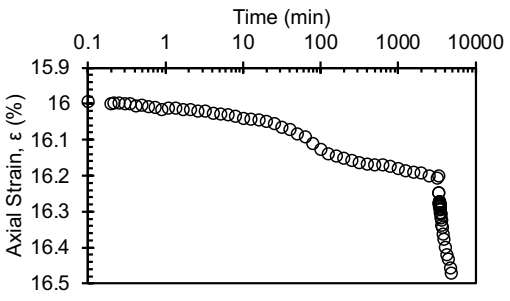

LIR = 0.385

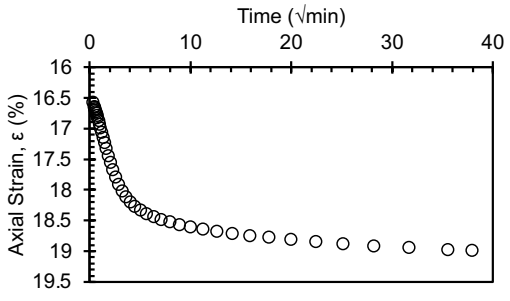

1000 kPa

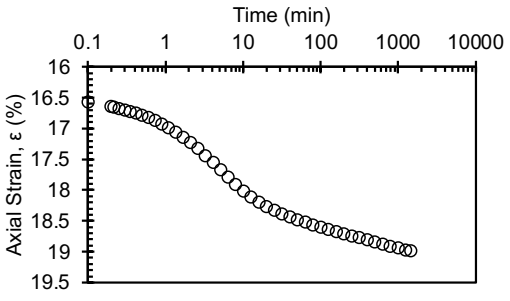

LIR = 0.111

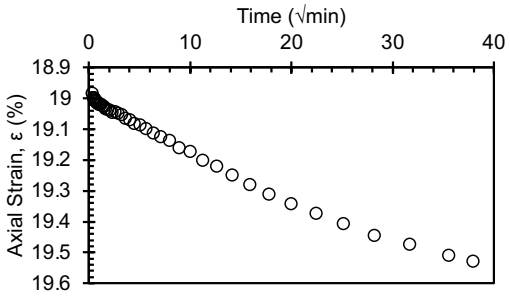

2500 kPa

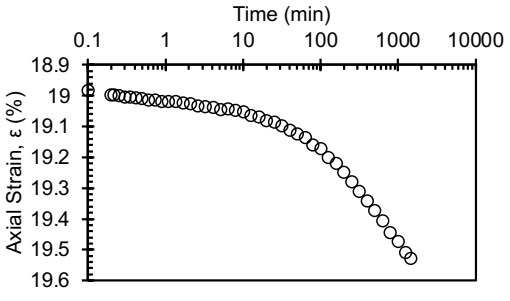

LIR = 1.5

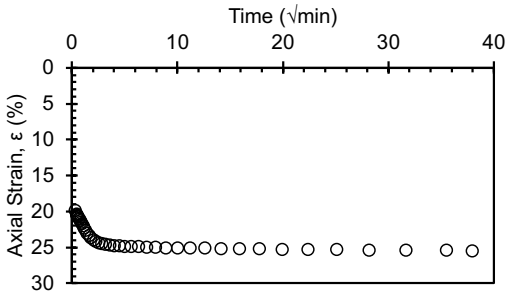

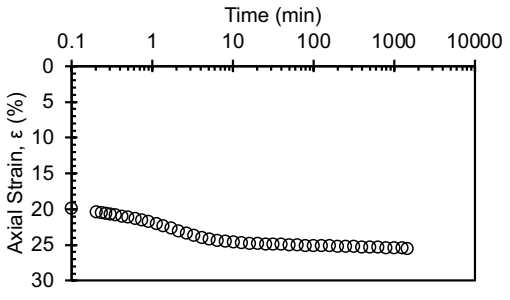

Final

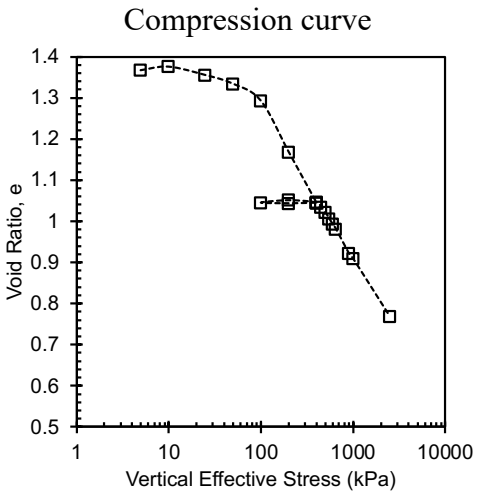
Compression curve
Void Ratio, e
1.4
1.3
1.2
1.1
1
0.9
0.8
0.7
0.6
0.5
1
10
100
1000
10000
Vertical Effective Stress (kPa)

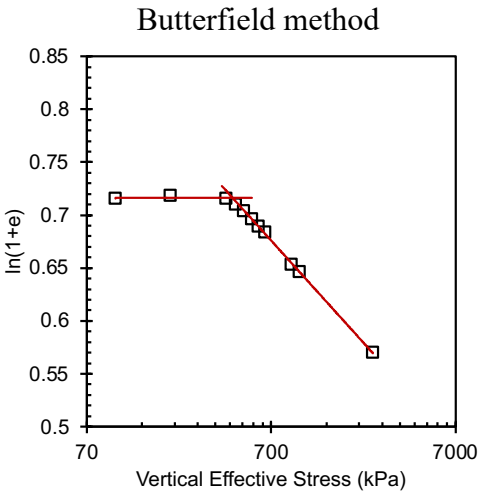
Butterfield method
ln(1+e)
0.85
0.8
0.75
0.7
0.65
0.6
0.55
0.5
70
700
7000
Vertical Effective Stress (kPa)

4 °C

Consolidation Test Data Sheet			
Test No.	4_NC_KAOL_EXT_3	Consolidometer No.	Sigma1_5k_10
Date started	11/2/24	Date ended	11/24/24
Test method	B	Condition of test	Inundated
Interpretation Method	Both 1 and 2	Classification	Remolded EPK (CH)
	Before Test - 20°C		After Test - 4°C
	Specimen	Trimmings	Specimen
Tare No.	Ring	T-03	dish
Tare plus wet soil (g)	353.26	250.55	137.42
Tare plus dry soil (g)	-	175.91	106.05
Tare (g)	215.72	17.83	13.54
Water (g)	44.11	74.64	31.37
Dry Soil (g)	93.43	158.08	92.51
Water content (%)	47.2	47.2	33.9
Area of specimen, A (cm^2)	31.67		
Specific Gravity of Solids, G_s	2.7		
Height of solids, H_s (cm)	1.093		
Initial - 20°C		Final - 4°C	
Height of specimen, H_0 (cm)	2.540	Height of specimen, H_f (cm)	2.085
Height of water, H_{w0} (cm)	1.393	Height of water, H_{wf} (cm)	0.991
Height of voids, H_{v0} (cm)	1.447	Height of voids, H_{vf} (cm)	0.992
Void ratio, e_0	1.32	Void ratio, e_f	0.91

Degree of saturation, S0 (%)	96.2	Degree of saturation, S_f (%)	99.8
Dry density, γ_0 (g/cm^2)	1.16	Dry density, γ_f (g/cm^2)	1.42
		Differential height, H_d (cm)	-0.036
		Preconsolidation pressure, σ_p'(kPa)	440
		Load increments (kPa) - seating loads held for 60 min, all other loads 1440 min	
Initial temperature, 20°C		5 (seating), 10, 25, 50, 100, 200, 400	
Temperature change(s)	20°C to 4°C	400	
Final temperature (°C)	4°C	400 (seating), 200, 100, 200, 400, 500, 550, 600, 650, 700, 800, 900, 1000, 2500	
Notes			
Note that the final height of the specimen H_f is the height recorded at the end of the test after the specimen was rebounded to 5 kPa until strain stabilized - it does not correspond to the final height at the maximum applied stress. The differential height is the difference between the final recorded height H_f and final height measured with a caliper following specimen extraction from ring at the end of the test.			

Initial Consolidation C1 (20 °C)

5 kPa

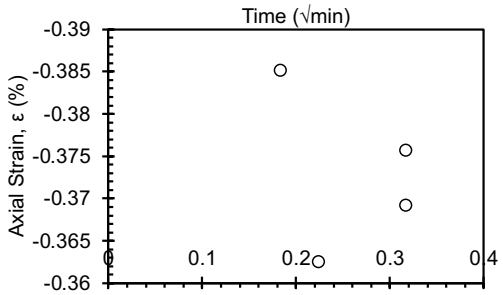

10 kPa

Seating Load

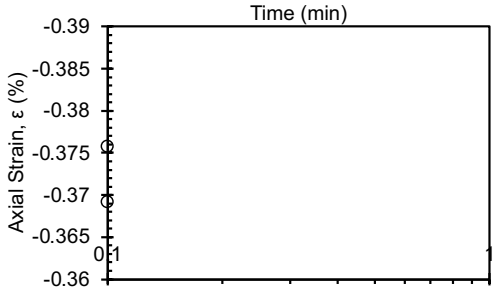

LIR = 1

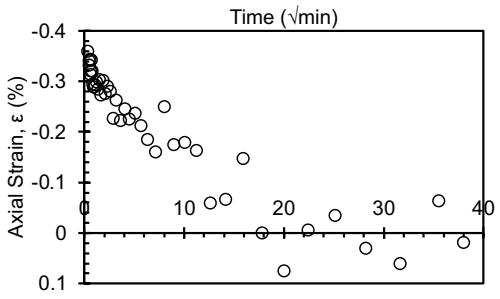

25 kPa

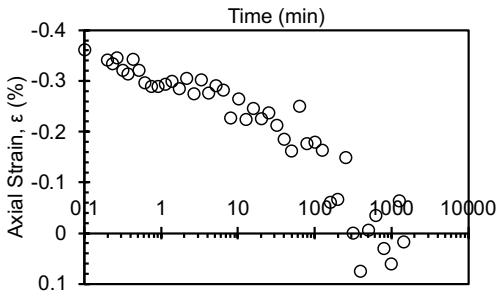

LIR = 1.5

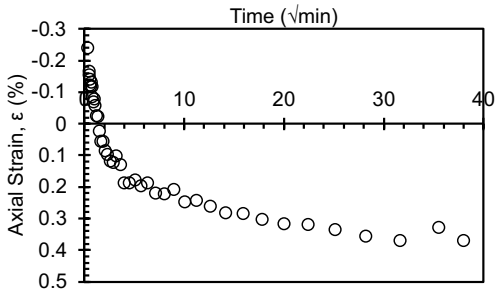

50 kPa

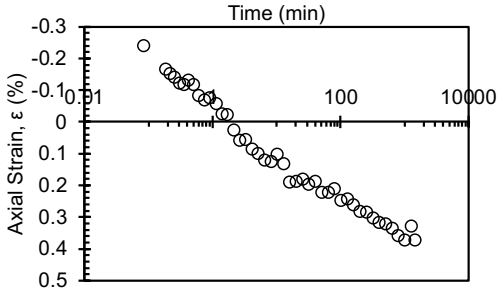

LIR = 1

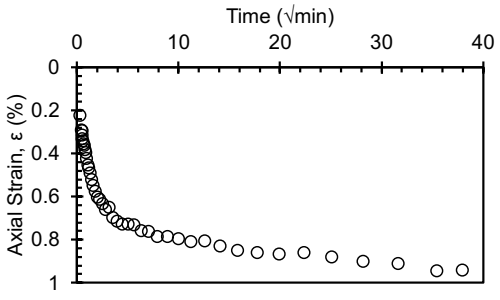

100 kPa

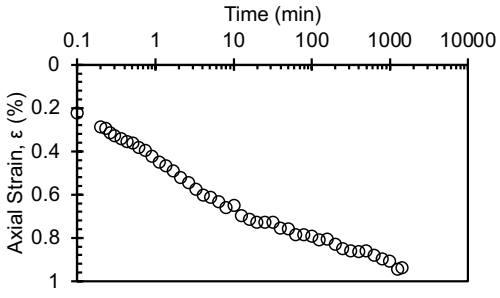

LIR = 1

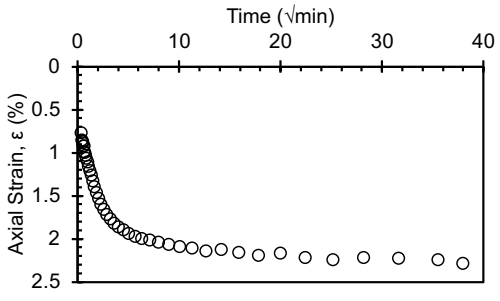

200 kPa

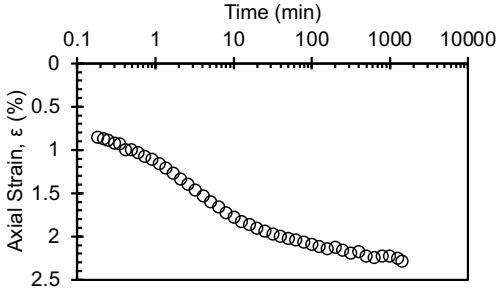

LIR = 1

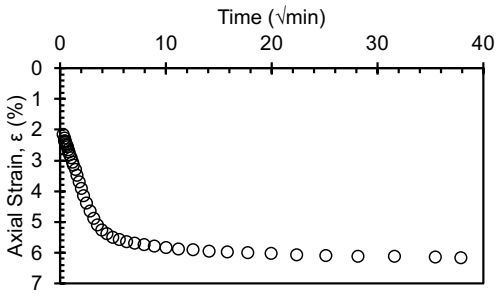

400 kPa

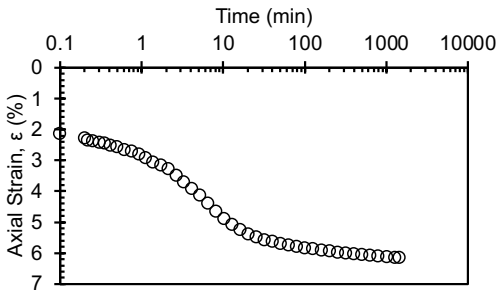

LIR = 1

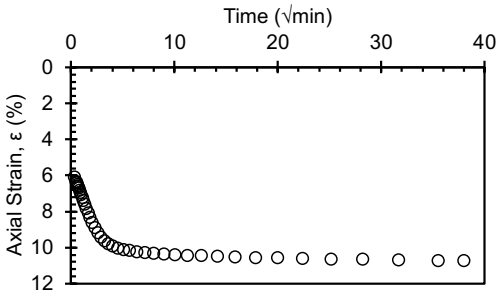

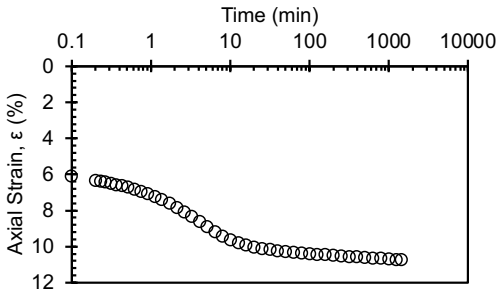

Temperature Change Stage: 20 °C>4 °C

400 kPa

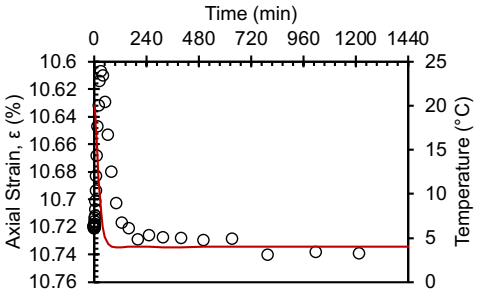

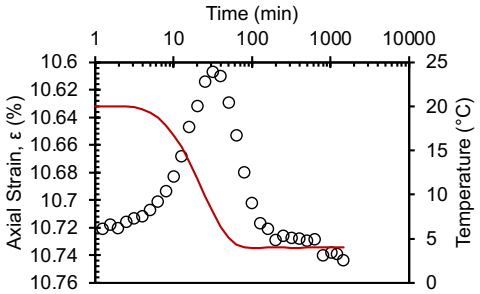

Second Consolidation C2 (4 °C)

200 kPa

LIR = -0.5

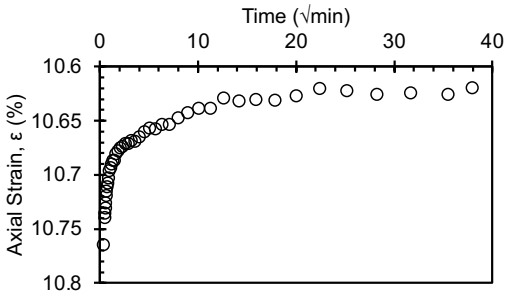

100 kPa

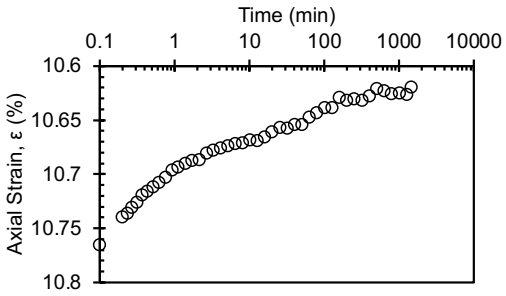

LIR =-0.5

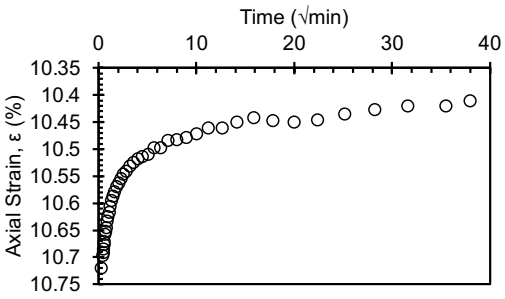

200 kPa

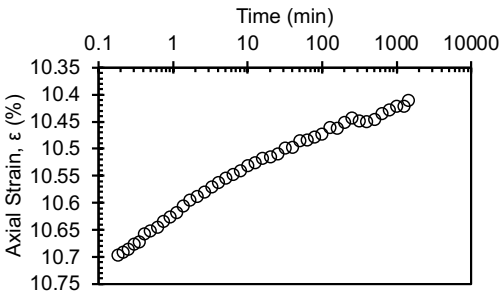

LIR = 1

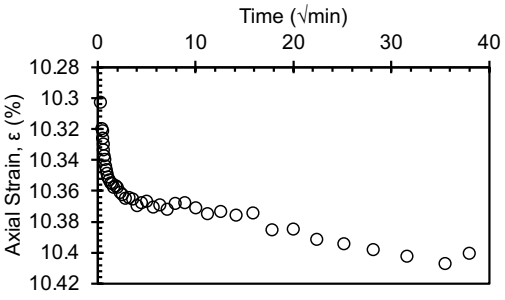

400 kPa

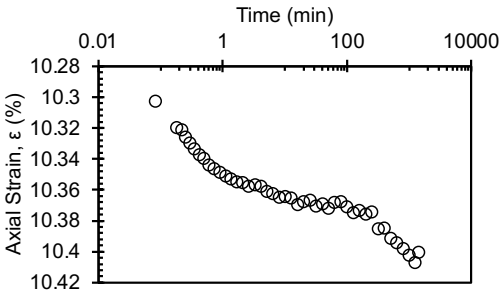

LIR = 1

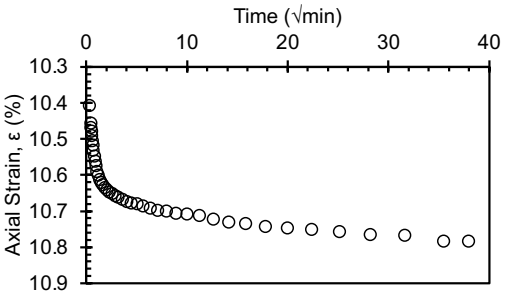

500 kPa

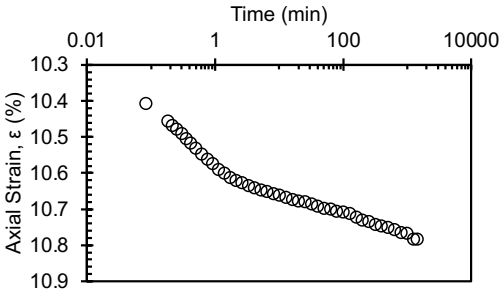

LIR = 0.25

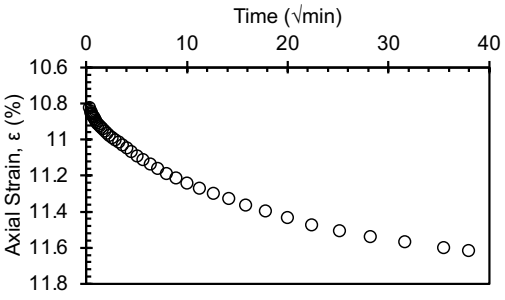

550 kPa

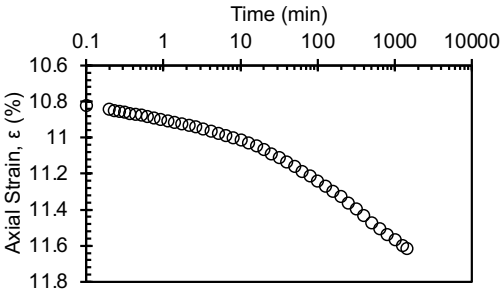

LIR = 0.1

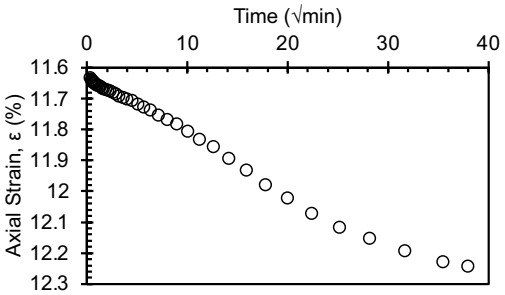

600 kPa

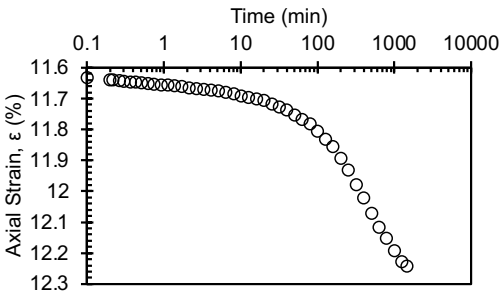

LIR = 0.091

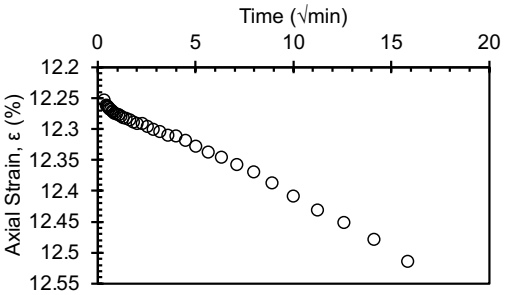

650 kPa

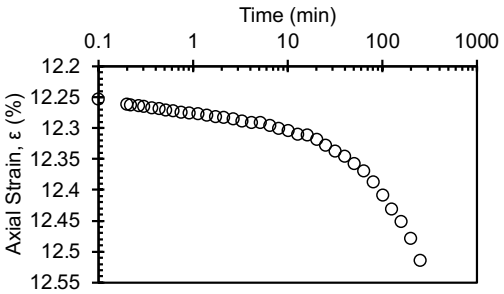

LIR = 0.083

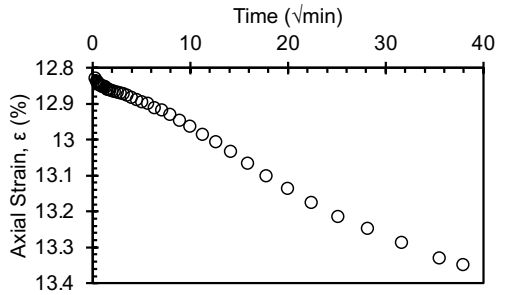

700 kPa

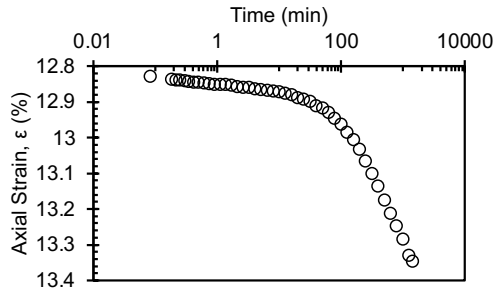

LIR = 0.077

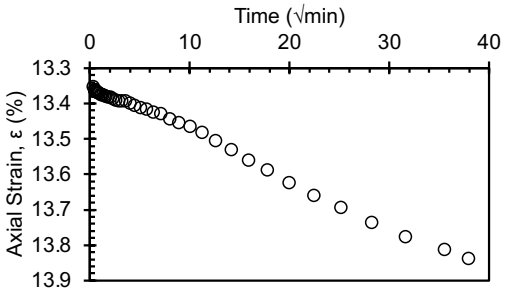

800 kPa

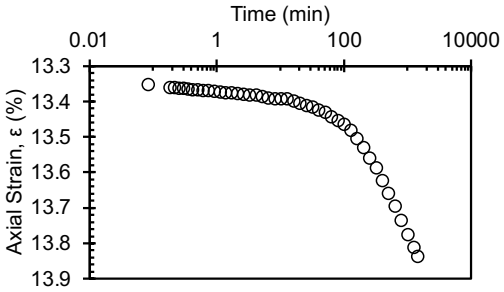

LIR = 0.143

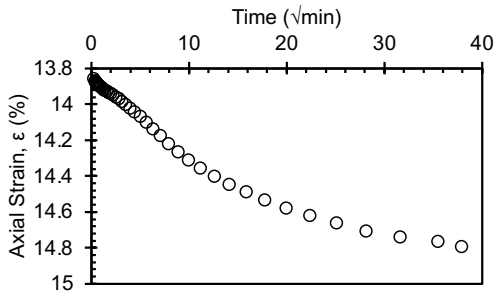

900 kPa

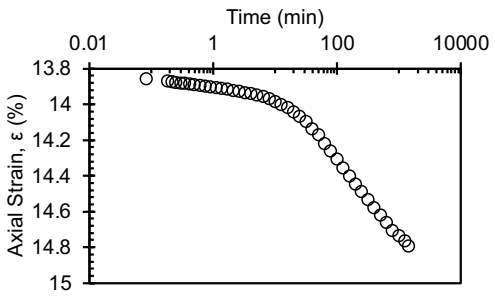

LIR = 0.125

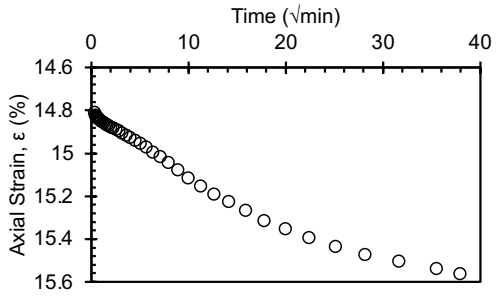

1000 kPa

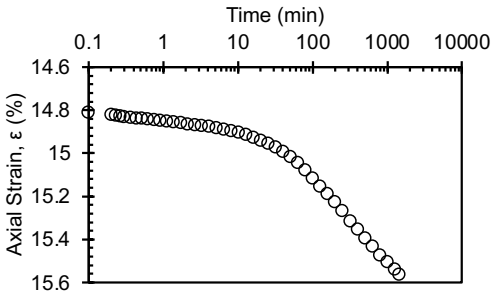

LIR = 0.111

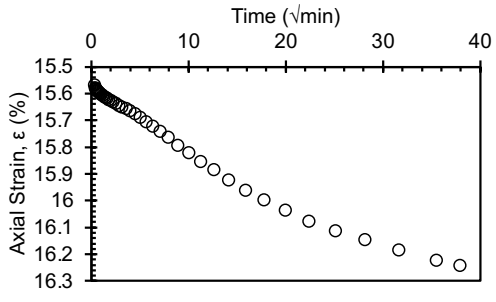

2500 kPa

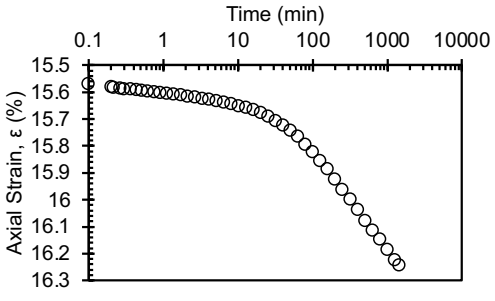

LIR = 1.5

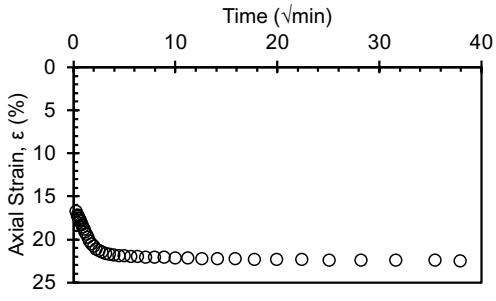

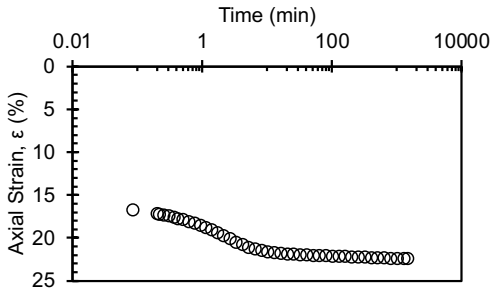

Final

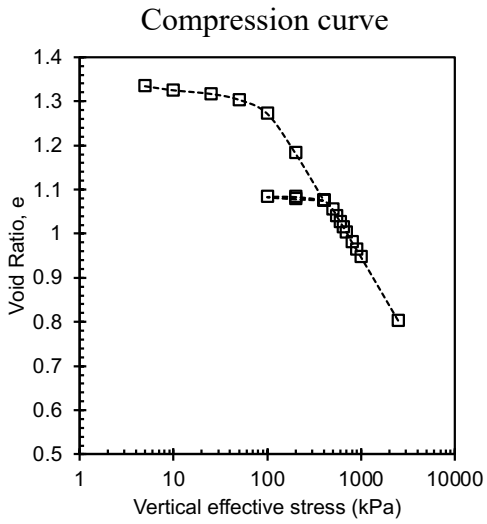
Compression curve
Void Ratio, e
1.4
1.3
1.2
1.1
1
0.9
0.8
0.7
0.6
0.5
1
10
100
1000
10000
Vertical effective stress (kPa)

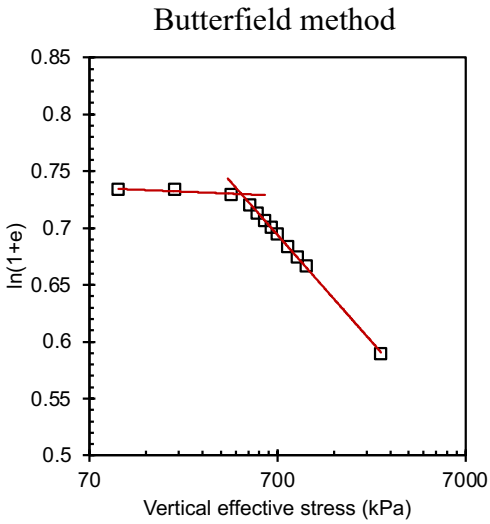
Butterfield method
ln(1+e)
0.85
0.8
0.75
0.7
0.65
0.6
0.55
0.5
70
700
7000
Vertical effective stress (kPa)

0 °C

Consolidation Test Data Sheet			
Test No.	0_NC_KAOL_EXT_2	Consolidometer No.	Sigma1_5k_10
Date started	10/13/24	Date ended	11/1/24
Test method	B	Condition of test	Inundated
Interpretation Method	Both 1 and 2	Classification	Remolded EPK (CH)
	Before Test - 20°C		After Test - 0°C
	Specimen	Trimmings	Specimen
Tare No.	Ring	LUIGI	MII
Tare plus wet soil (g)	352.92	256.24	158.17
Tare plus dry soil (g)	-	180.46	126.59
Tare (g)	215.72	21.92	34.35
Water (g)	44.37	75.78	31.58
Dry Soil (g)	92.83	158.54	92.24
Water content (%)	47.8	47.8	34.2
Area of specimen, A (cm^2)	31.67		
Specific Gravity of Solids, G_s	2.7		
Height of solids, H_s (cm)	1.086		
Initial - 20°C		Final - 0°C	
Height of specimen, H_0 (cm)	2.540	Height of specimen, H_f (cm)	2.080
Height of water, H_{w0} (cm)	1.401	Height of water, H_{wf} (cm)	0.997
Height of voids, H_{v0} (cm)	1.454	Height of voids, H_{vf} (cm)	0.994
Void ratio, e_0	1.34	Void ratio, e_f	0.92

Degree of saturation, S0 (%)	96.3	Degree of saturation, S_f (%)	100.3
Dry density, γ_0 (g/cm^2)	1.15	Dry density, γ_f (g/cm^2)	1.41
		Differential height, H_d (cm)	-0.037
		Preconsolidation pressure, σ_p'(kPa)	430
		Load increments (kPa) - seating loads held for 60 min, all other loads 1440 min	
Initial temperature, 20°C		5 (seating), 10, 25, 50, 100, 200, 400	
Temperature change(s)	20°C to 0°C	400	
Final temperature (°C)	0°C	400 (seating), 200, 100, 200, 400, 500, 600, 700, 800, 900, 1000, 2000, 2500	
Notes			
Note that the final height of the specimen H_f is the height recorded at the end of the test after the specimen was rebounded to 5 kPa until strain stabilized - it does not correspond to the final height at the maximum applied stress. The differential height is the difference between the final recorded height H_f and final height measured with a caliper following specimen extraction from ring at the end of the test.			

Initial Consolidation C1 (20 °C)

5 kPa

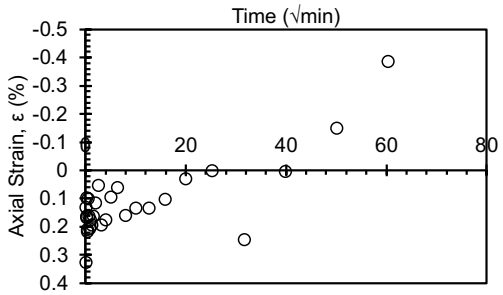

10 kPa

Seating Load

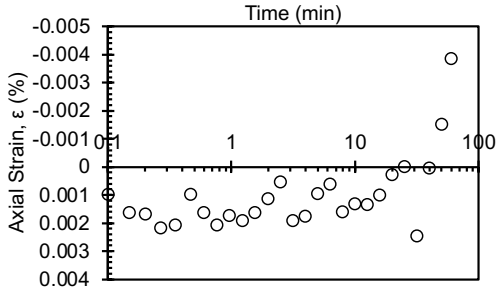

LIR = 1

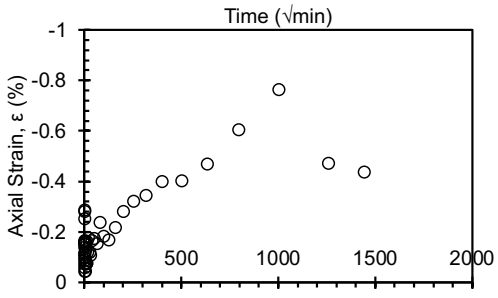

25 kPa

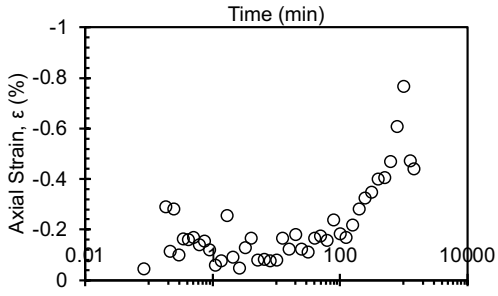

LIR = 1.5

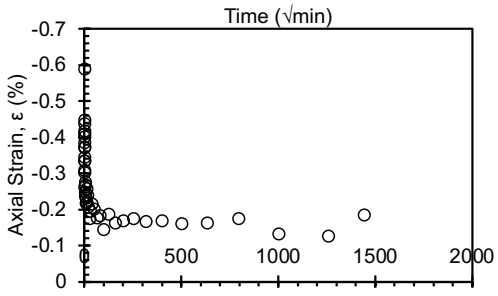

50 kPa

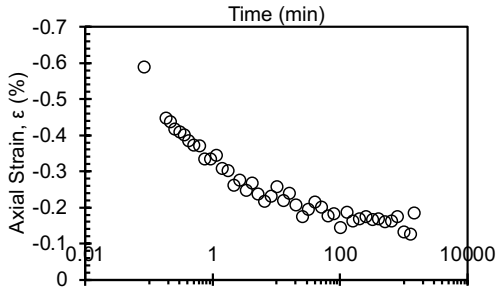

LIR = 1

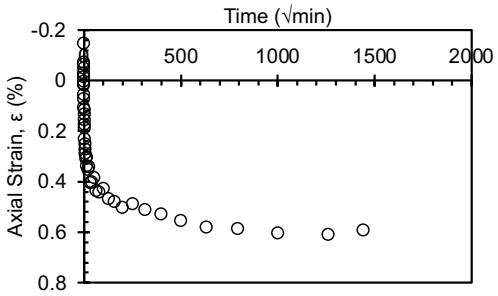

100 kPa

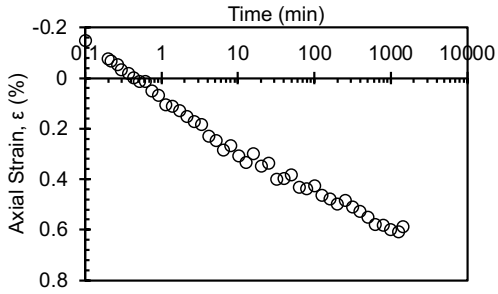

LIR = 1

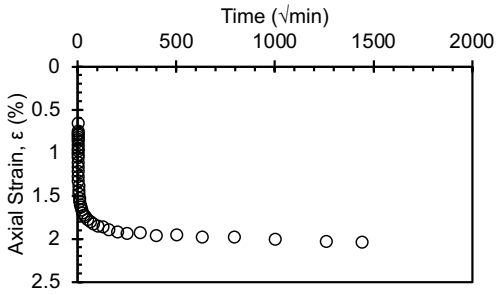

200 kPa

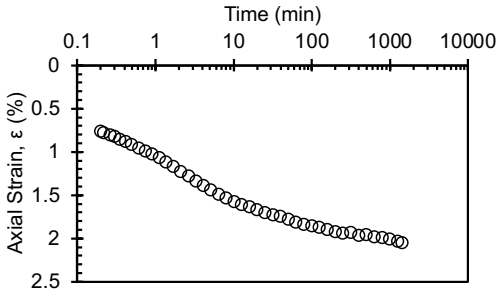

LIR = 1

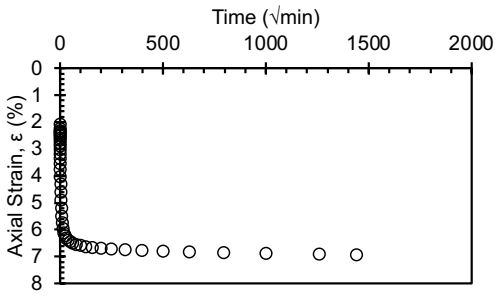

400 kPa

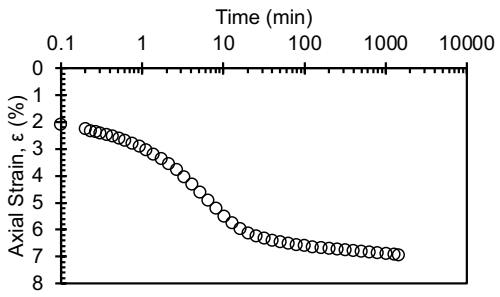

LIR = 1

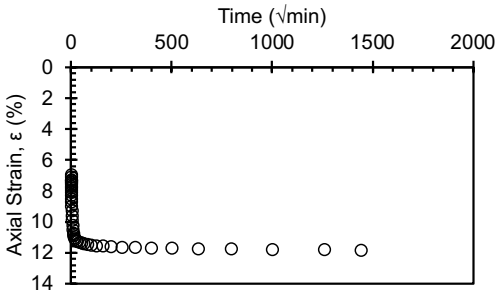

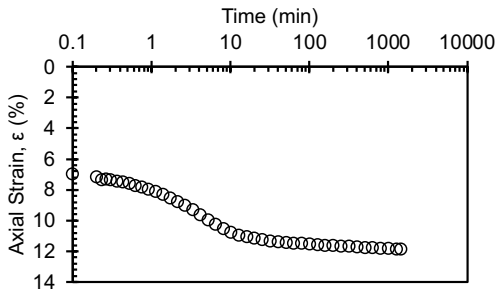

Temperature Change Stage: 20 °C>0 °C

400 kPa

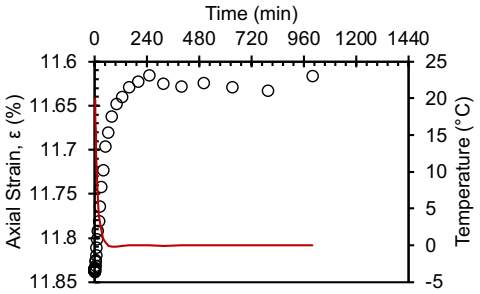

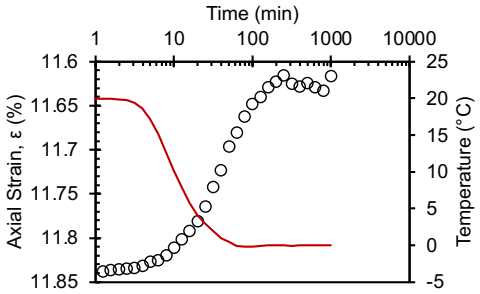

Second Consolidation C2 (0 °C)

400 kPa

Seating load

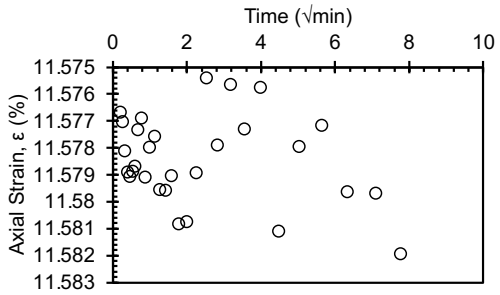

200 kPa

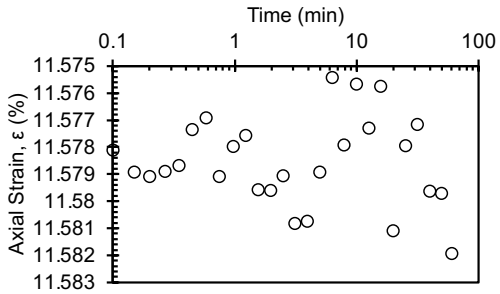

LIR = -0.5

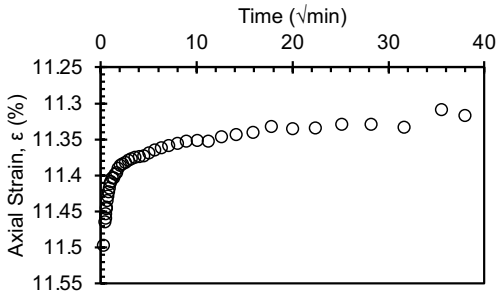

100 kPa

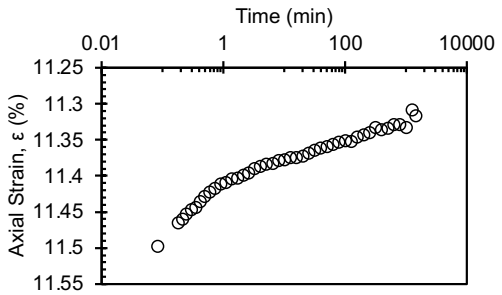

LIR =-0.5

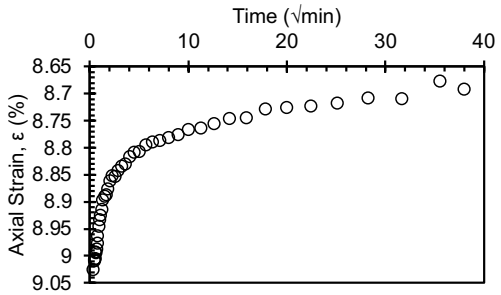

200 kPa

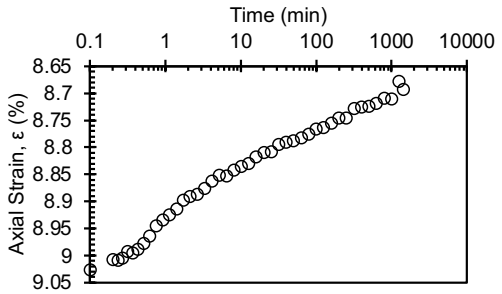

LIR = 1

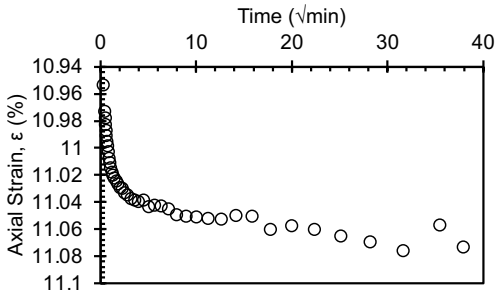

400 kPa

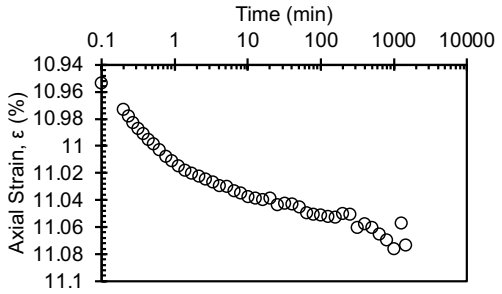

LIR = 1

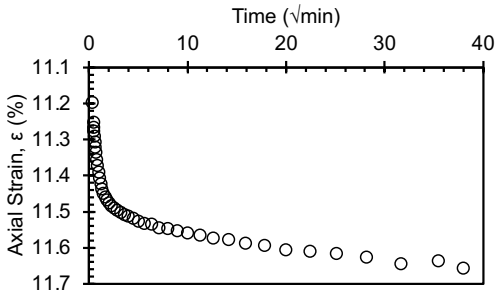

500 kPa

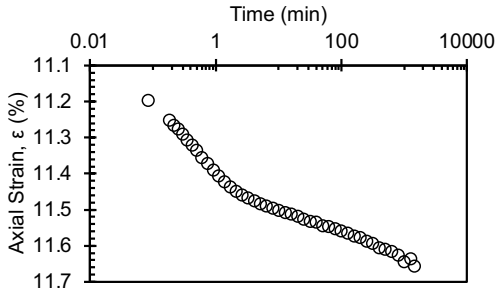

LIR = 0.25

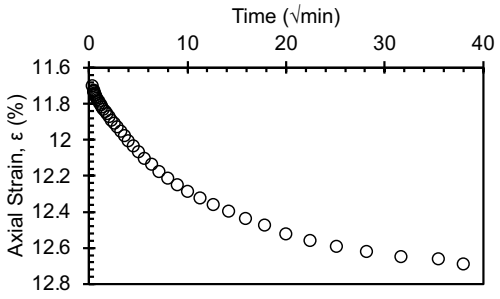

600 kPa

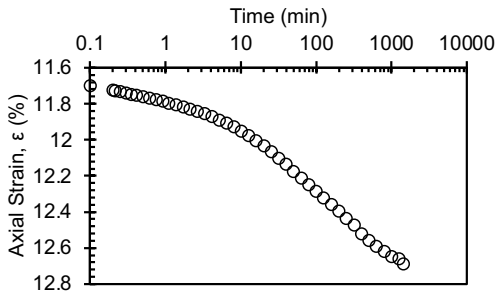

LIR = 0.2

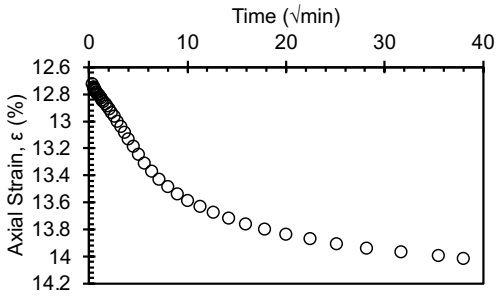

700 kPa

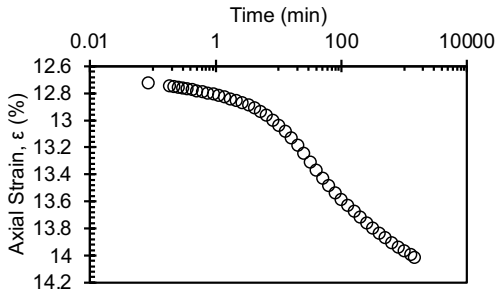

LIR = 0.167

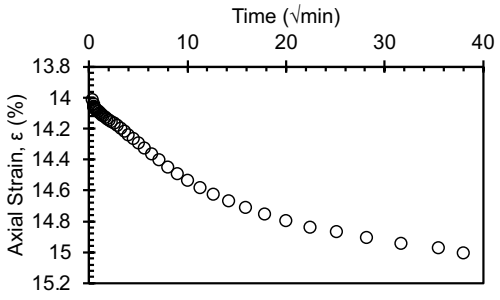

800 kPa

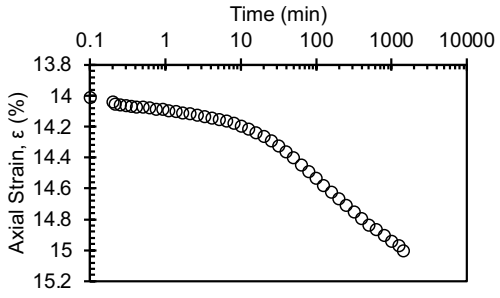

LIR = 0.143

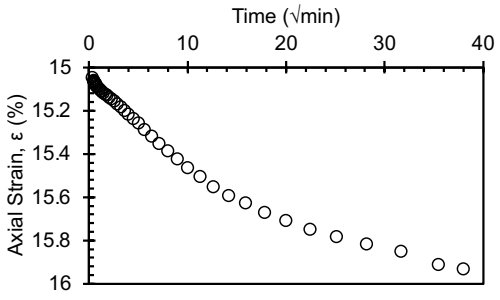

900 kPa

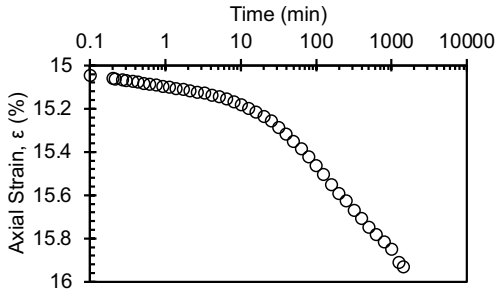

LIR = 0.125

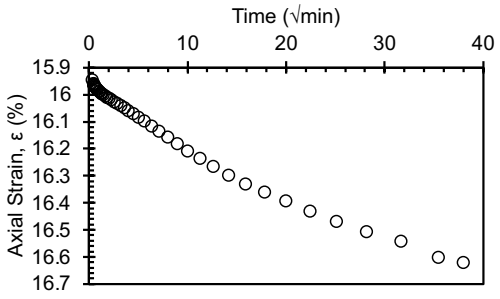

1000 kPa

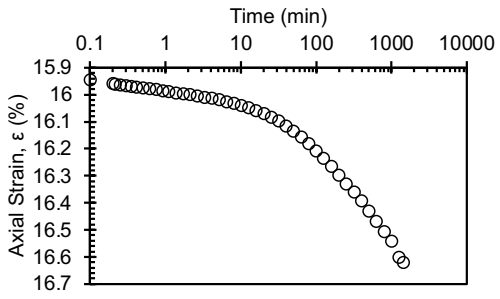

LIR = 0.111

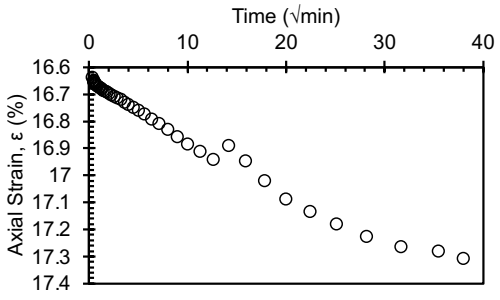

2000 kPa

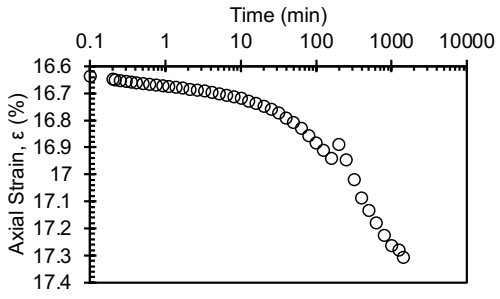

LIR = 0.5

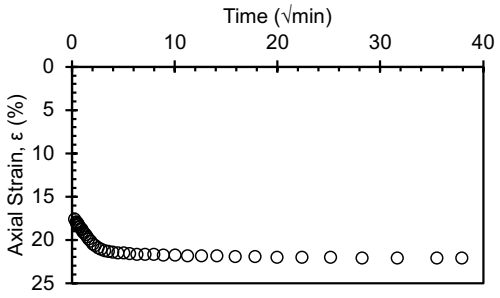

2500 kPa

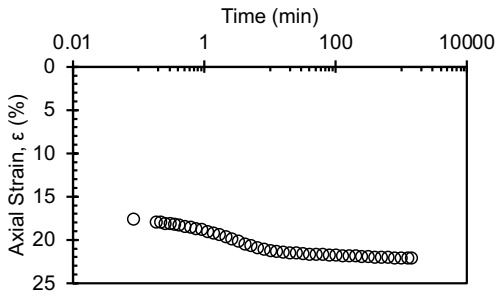

LIR = 0.25

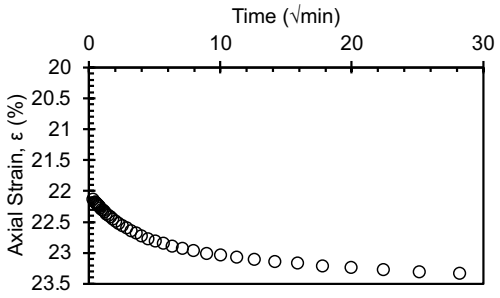

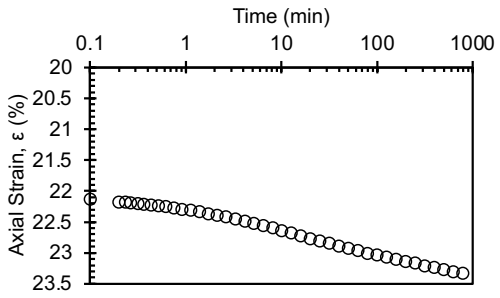

Final

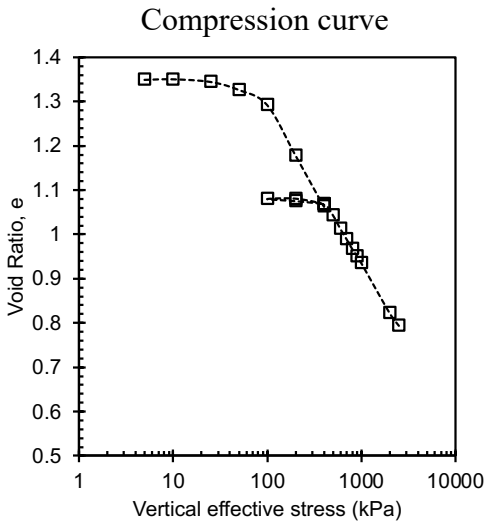
Compression curve
Void Ratio, e
1.4
1.3
1.2
1.1
1
0.9
0.8
0.7
0.6
0.5
1
10
100
1000
10000
Vertical effective stress (kPa)

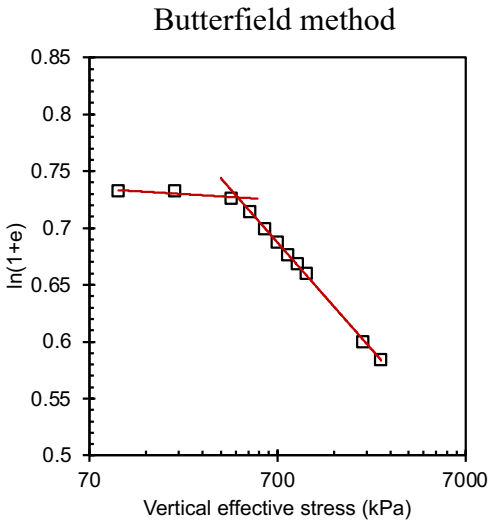
Butterfield method
ln(1+e)
0.85
0.8
0.75
0.7
0.65
0.6
0.55
0.5
70
700
7000
Vertical effective stress (kPa)

-2 °C

Consolidation Test Data Sheet			
Test No.	-2_NC_KAOL_EXT	Consolidometer No.	Sigma1_5k_10
Date started	9/21/24	Date ended	10/13/24
Test method	B	Condition of test	Inundated
Interpretation Method	Both 1 and 2	Classification	Remolded EPK (CH)
	Before Test - 20°C		After Test - (-2)°C
	Specimen	Trimmings	Specimen
Tare No.	Ring	5C	MARIO
Tare plus wet soil (g)	352.86	249.72	146.02
Tare plus dry soil (g)	-	179.88	115.07
Tare (g)	215.71	32.35	22.75
Water (g)	44.07	69.84	30.95
Dry Soil (g)	93.08	147.53	92.32
Water content (%)	47.3	47.3	33.5
Area of specimen, A (cm^2)	31.67		
Specific Gravity of Solids, G_s	2.7		
Height of solids, H_s (cm)	1.089		
Initial - 20°C		Final - (-2)°C	
Height of specimen, H_0 (cm)	2.540	Height of specimen, H_f (cm)	2.066
Height of water, H_{w0} (cm)	1.391	Height of water, H_{wf} (cm)	0.977
Height of voids, H_{v0} (cm)	1.451	Height of voids, H_{vf} (cm)	0.977

Void ratio, e_0	1.33	Void ratio, e_f	0.90
Degree of saturation, S0 (%)	95.9	Degree of saturation, S_f (%)	100.0
Dry density, γ_0 (g/cm^2)	1.16	Dry density, γ_f (g/cm^2)	1.42
		Differential height, H_d (cm)	-0.053
		Preconsolidation pressure, σ_p'(kPa)	440
		Load increments (kPa) - seating loads held for 60 min, all other loads 1440 min	
Initial temperature, 20°C		5 (seating), 10, 25, 50, 100, 200, 400	
Temperature change(s)	20°C to (-2)°C	400	
Final temperature (°C)	(-2)°C	400 (seating), 200, 100, 200, 300, 400, 500, 600, 700, 800, 900, 1000, 1500, 200, 2500	
Notes			
Note that the final height of the specimen H_f is the height recorded at the end of the test after the specimen was rebounded to 5 kPa until strain stabilized - it does not correspond to the final height at the maximum applied stress. The differential height is the difference between the final recorded height H_f and final height measured with a caliper following specimen extraction from ring at the end of the test.			

Initial Consolidation C1 (20 °C)

5 kPa

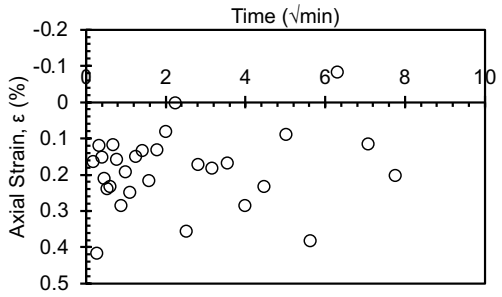

10 kPa

Seating Load

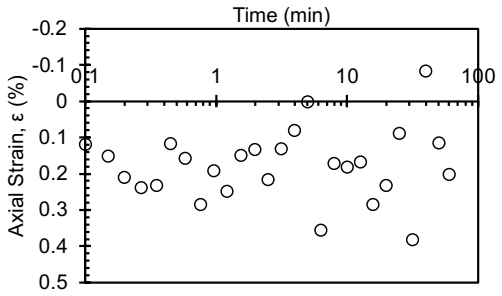

LIR = 1

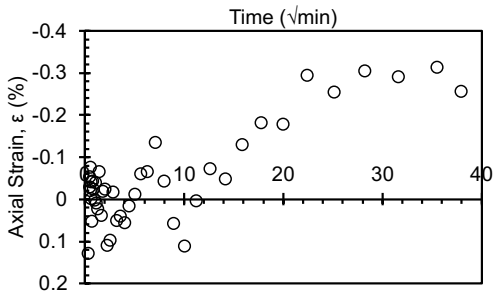

25 kPa

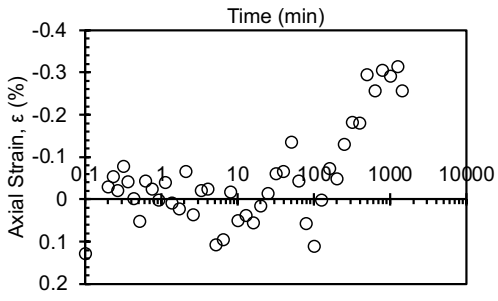

LIR = 1.5

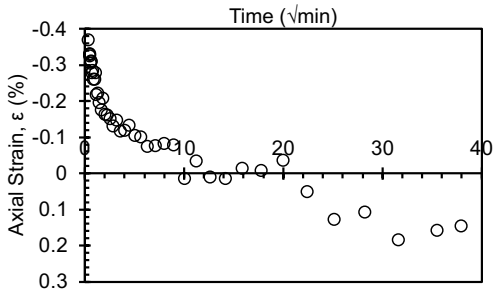

50 kPa

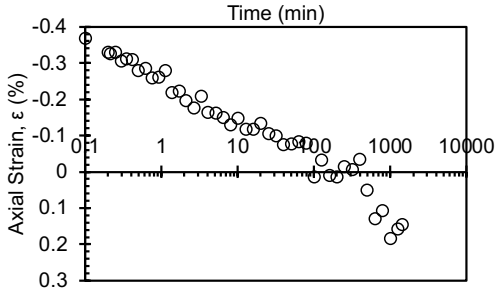

LIR = 1

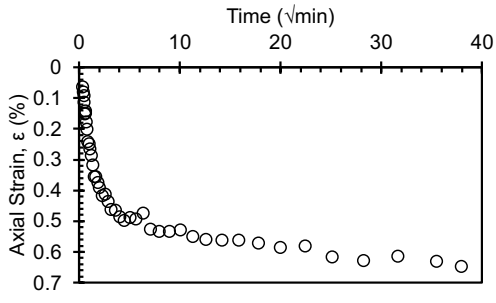

100 kPa

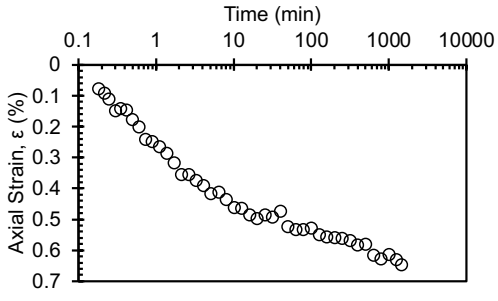

LIR = 1

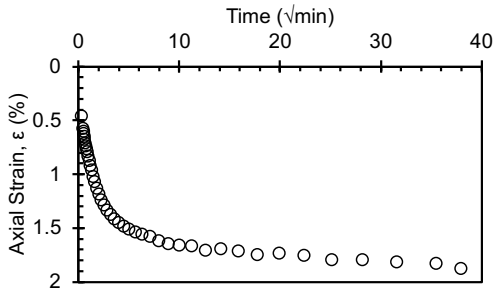

200 kPa

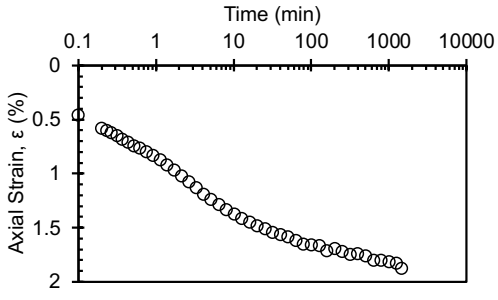

LIR = 1

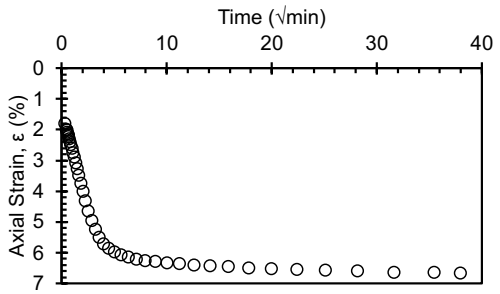

400 kPa

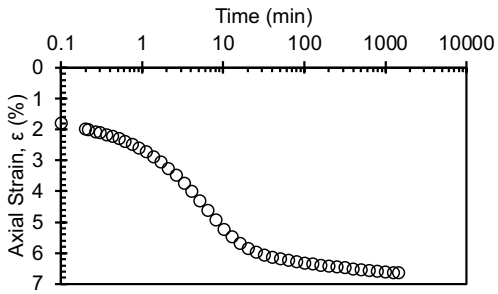

LIR = 1

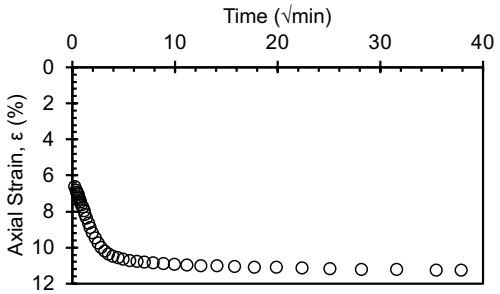

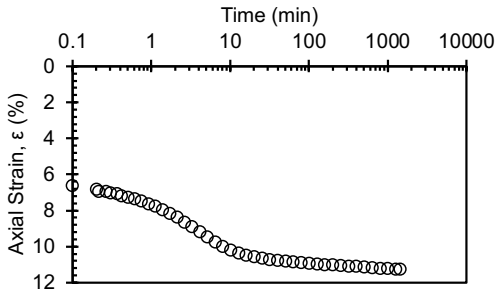

Temperature Change Stage: 20 °C>-2 °C

400 kPa

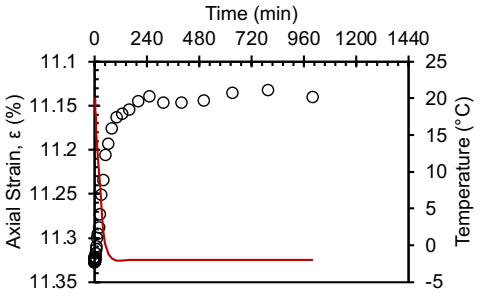

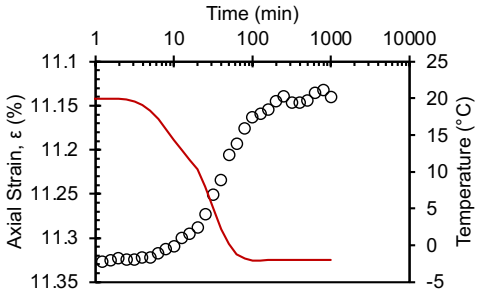

Second Consolidation C2 (-2 °C)

400 kPa

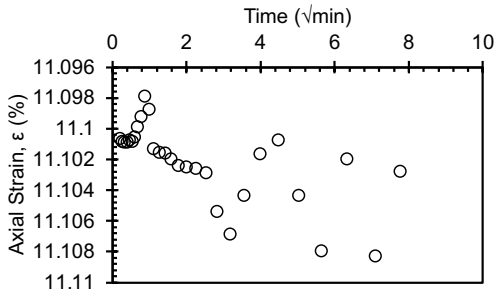

200 kPa

Seating load

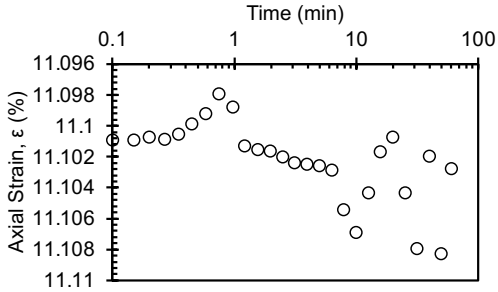

LIR = -0.5

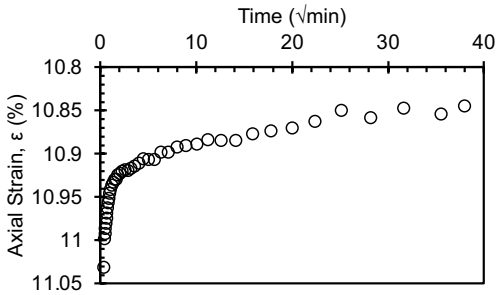

100 kPa

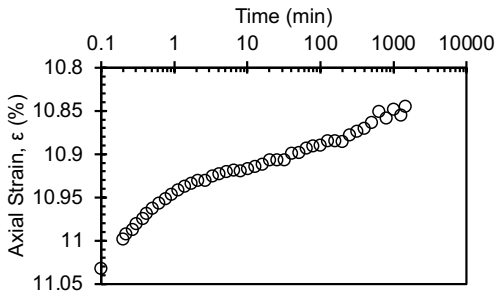

LIR =-0.5

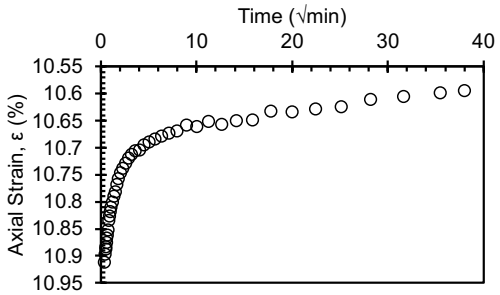

200 kPa

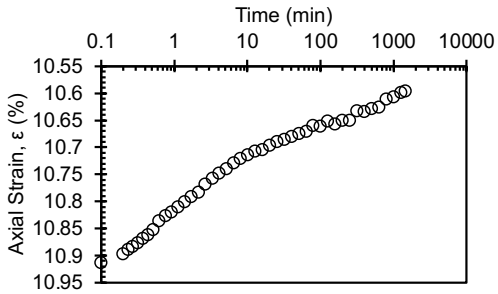

LIR = 1

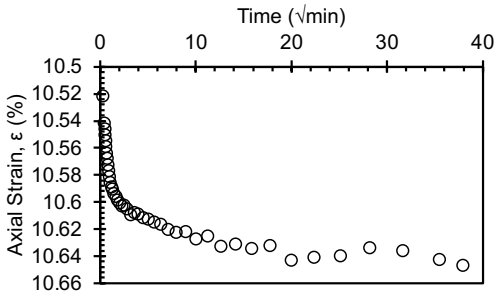

300 kPa

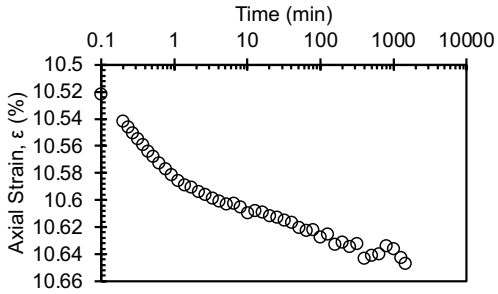

LIR=0.5

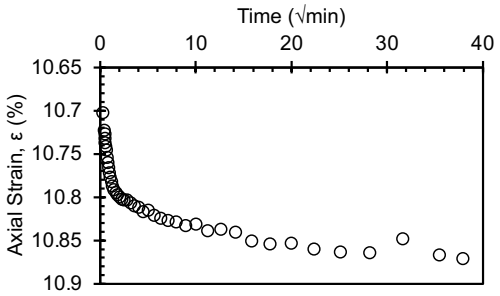

400 kPa

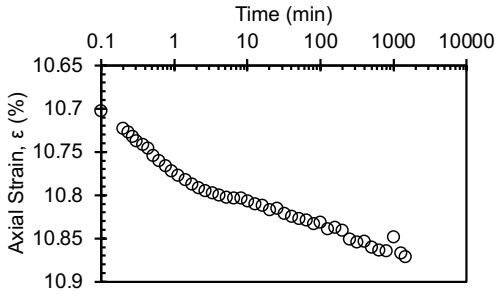

LIR = 0.333

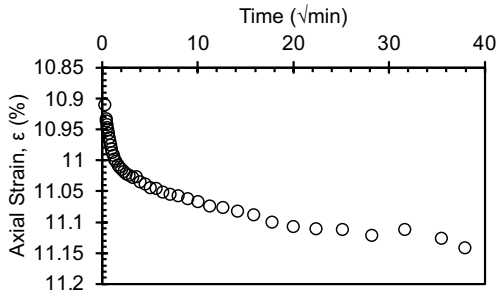

500 kPa

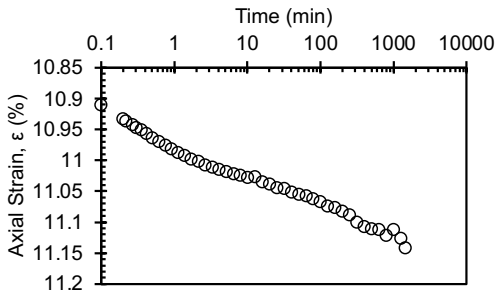

LIR = 0.25

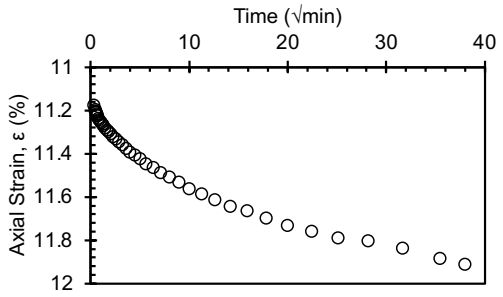

600 kPa

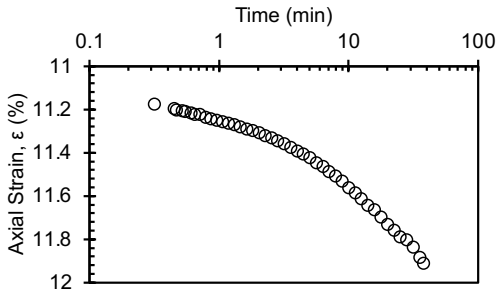

LIR = 0.2

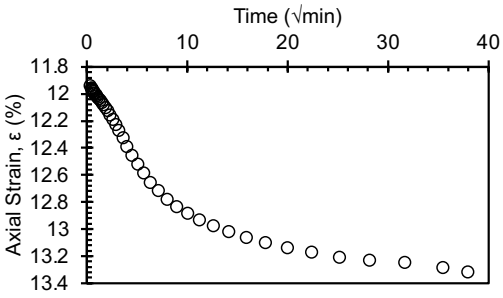

700 kPa

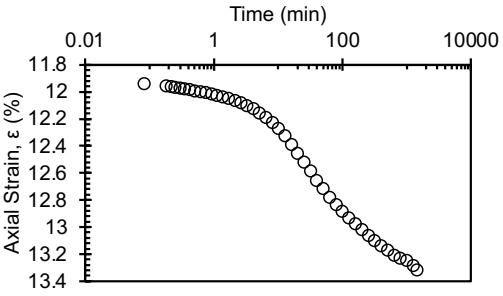

LIR = 0.167

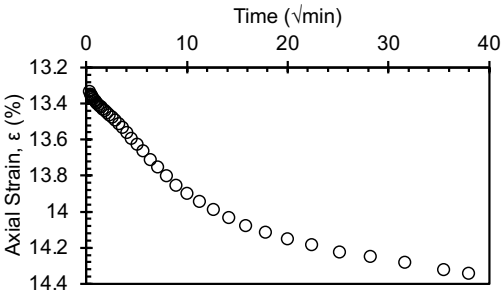

800 kPa

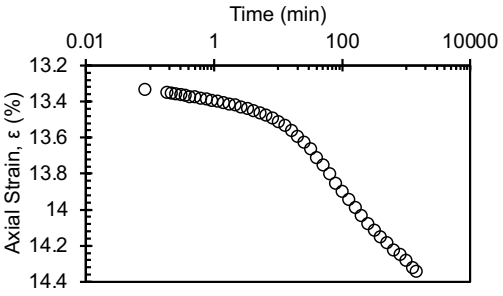

LIR = 0.143

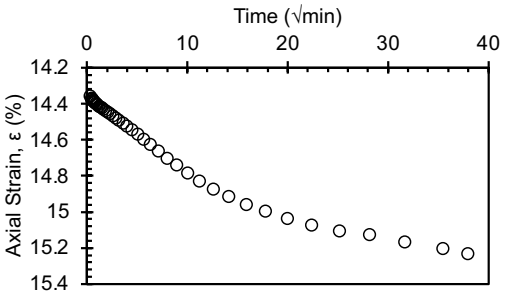

900 kPa

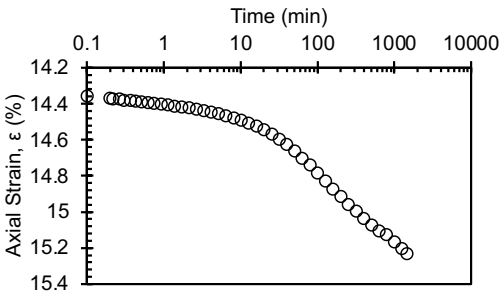

LIR = 0.125

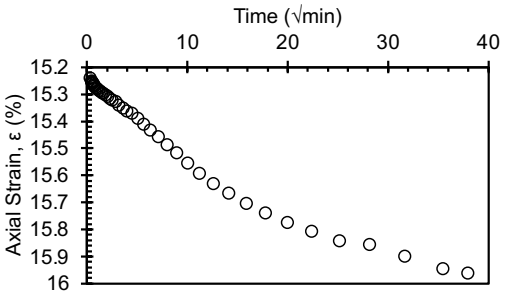

1000 kPa

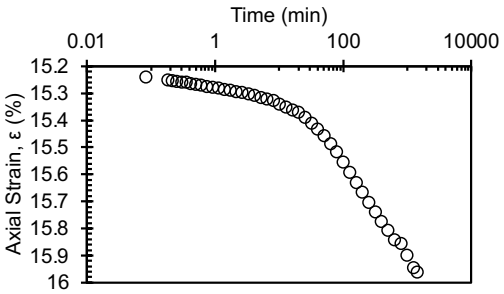

LIR = 0.111

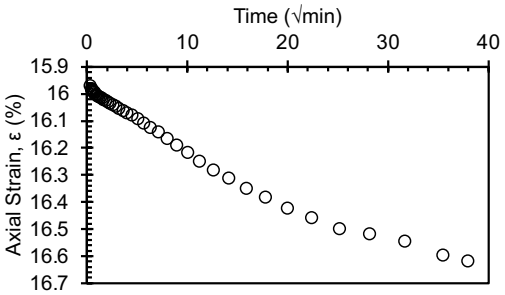

1500 kPa

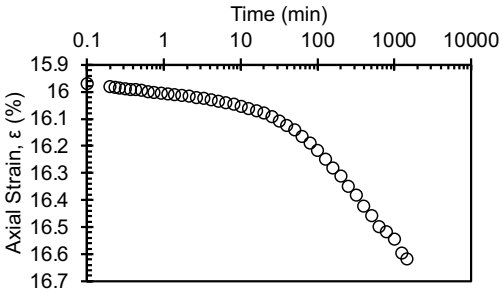

LIR = 0.5

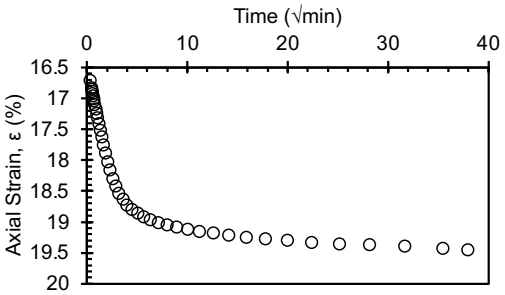

2000 kPa

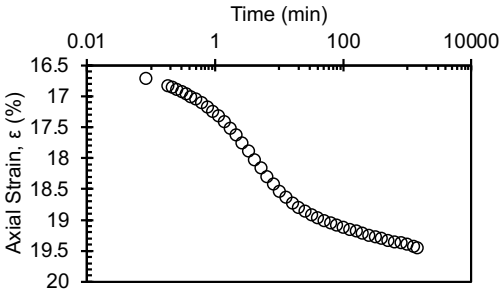

LIR = 0.333

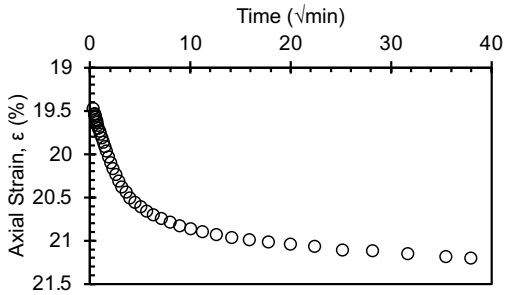

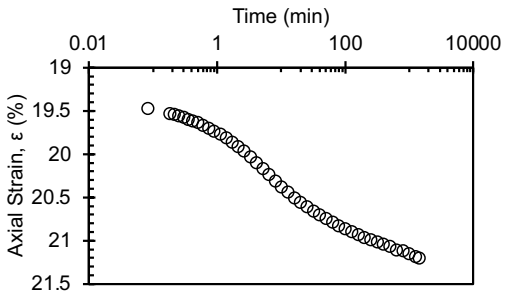

2500 kPa

LIR = 0.25

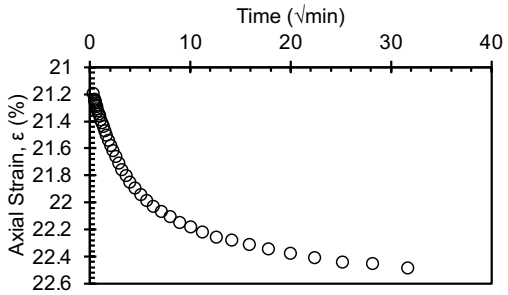

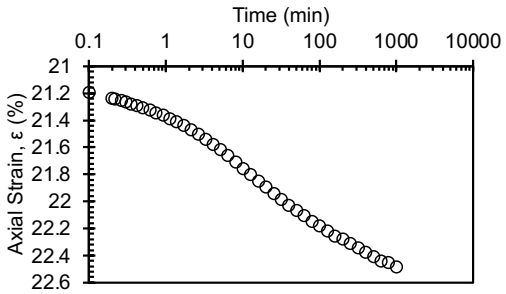

Final

Compression curve

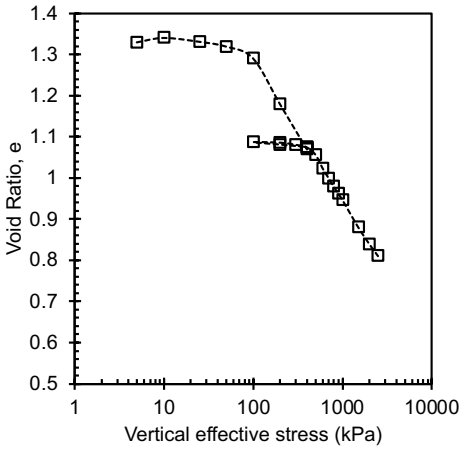

Butterfield method

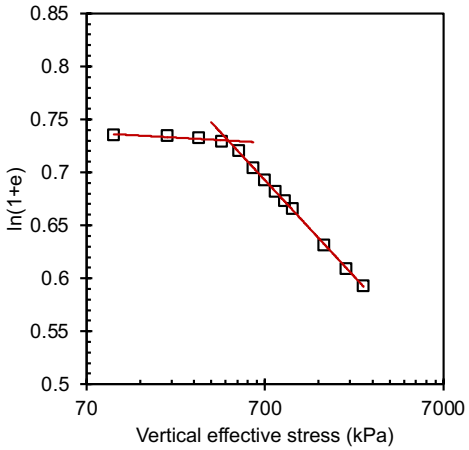

-4 °C

Consolidation Test Data Sheet			
Test No.	-4_NC_KAOL_EXT_3	Consolidometer No.	Sigma1_5k_10
Date started	6/2/24	Date ended	7/6/24
Test method	B	Condition of test	Inundated
Interpretation Method	Both 1 and 2	Classification	Remolded EPK (CH)
	Before Test - 20°C		After Test - (-4)°C
	Specimen	Trimmings	Specimen
Tare No.	Ring	5C	5C
Tare plus wet soil (g)	351.89	256.59	154.21
Tare plus dry soil (g)	-	184.17	123.30
Tare (g)	215.72	32.27	32.27
Water (g)	43.96	72.42	30.91
Dry Soil (g)	92.21	151.90	91.03
Water content (%)	47.7	47.7	34.0
Area of specimen, A (cm^2)	31.67		
Specific Gravity of Solids, G_s	2.7		
Height of solids, H_s (cm)	1.078		
Initial - 20°C		Final - (-4)°C	
Height of specimen, H_0 (cm)	2.540	Height of specimen, H_f (cm)	2.052
Height of water, H_{w0} (cm)	1.388	Height of water, H_{wf} (cm)	0.976
Height of voids, H_{v0} (cm)	1.462	Height of voids, H_{vf} (cm)	0.974

Void ratio, e_0	1.36	Void ratio, e_f	0.90
Degree of saturation, S0 (%)	95.0	Degree of saturation, S_f (%)	100.2
Dry density, γ_0 (g/cm^2)	1.15	Dry density, γ_f (g/cm^2)	1.42
		Differential height, H_d (cm)	0.185
		Preconsolidation pressure, σ_p'(kPa)	6000
		Load increments (kPa) - seating loads held for 60 min, all other loads 1440 min	
Initial temperature, 20°C		5 (seating), 10, 25, 50, 100, 200, 400	
Temperature change(s)	20°C to (-4)°C	400	
Final temperature (°C)	(-4)°C	400 (seating), 200, 100, 200, 300, 400, 500, 600, 700, 800, 900, 1000, 1500, 2000, 2500, 3000, 3500, 4000, 4500, 5000, 5500, 6000, 6500, 6800	
Notes			
Note that the final height of the specimen H_f is the height recorded at the end of the test after the specimen was rebounded to 5 kPa until strain stabilized - it does not correspond to the final height at the maximum applied stress. The differential height is the difference between the final recorded height H_f and final height measured with a caliper following specimen extraction from ring at the end of the test.			

Initial Consolidation C1 (20 °C)

5 kPa

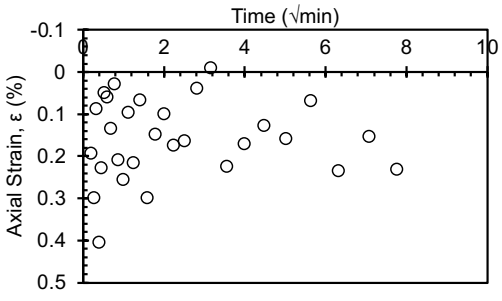

Seating Load

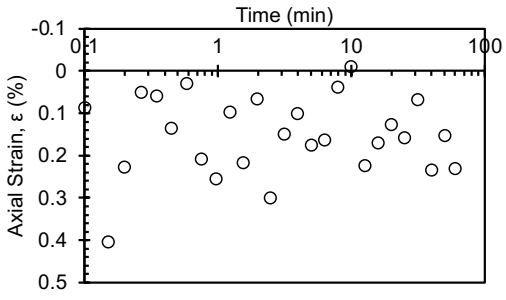

10 kPa

LIR = 1

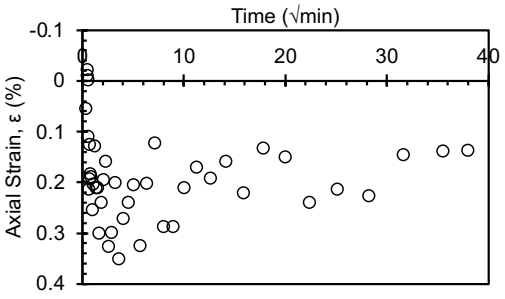

25 kPa

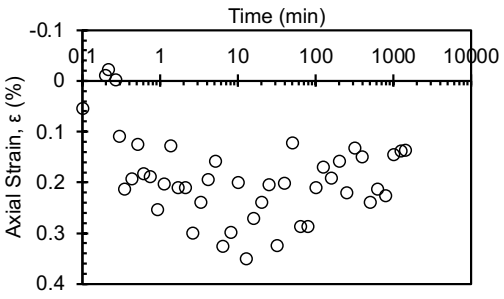

LIR = 1.5

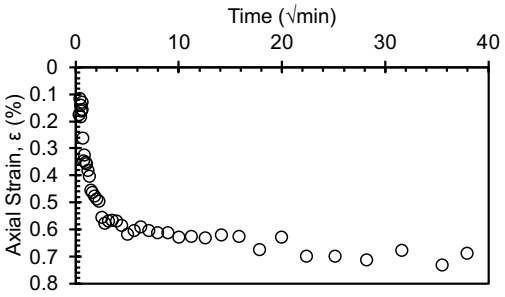

50 kPa

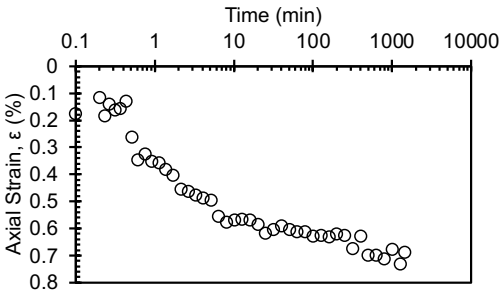

LIR = 1

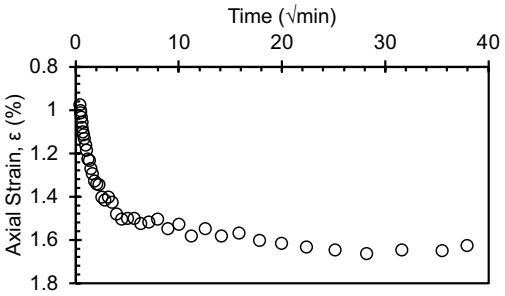

100 kPa

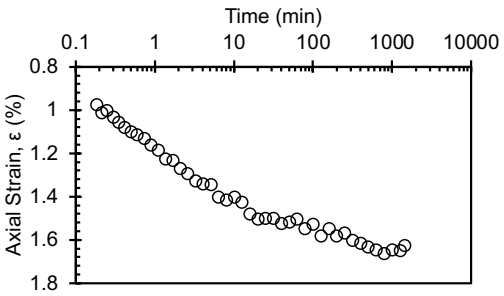

LIR = 1

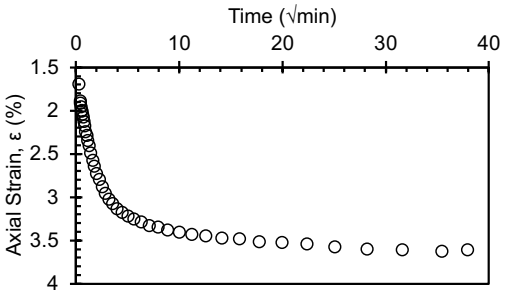

200 kPa

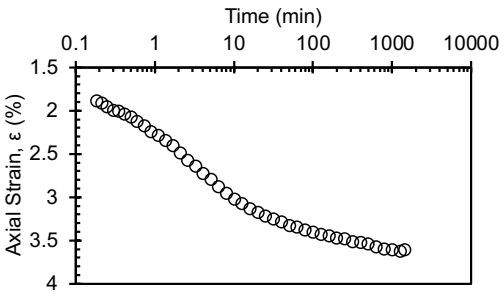

LIR = 1

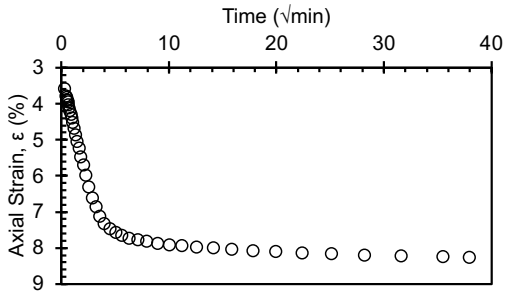

400 kPa

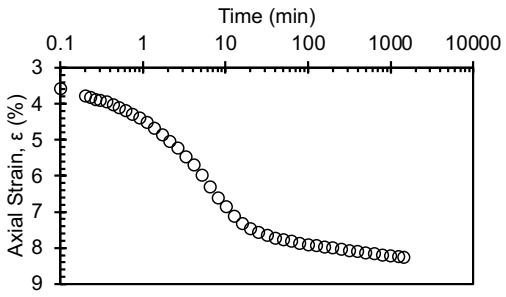

LIR = 1

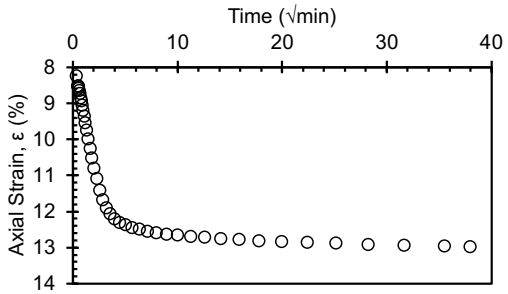

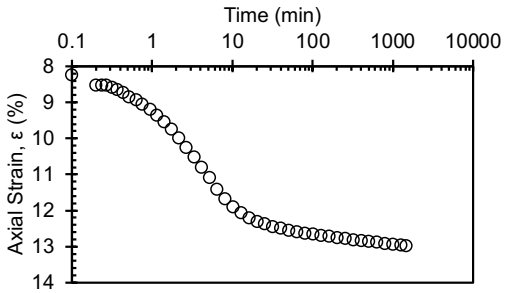

Temperature Change Stage: 20 °C>-4 °C

400 kPa

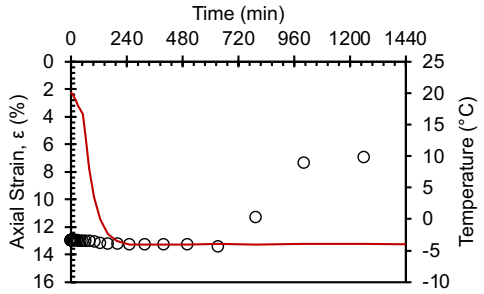

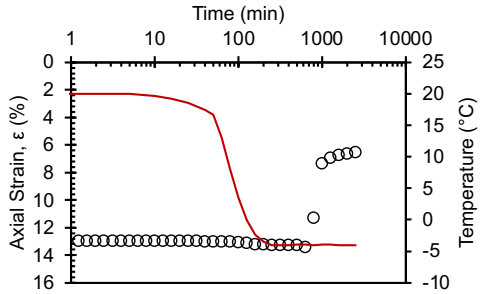

Second Consolidation C2 (-4 °C)

400 kPa

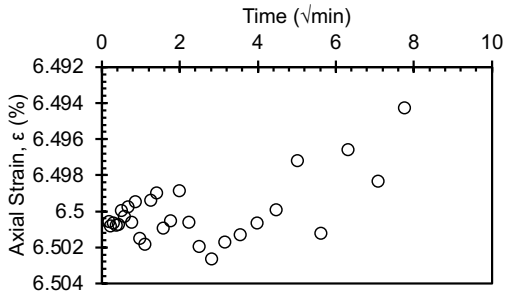

200 kPa

Seating load

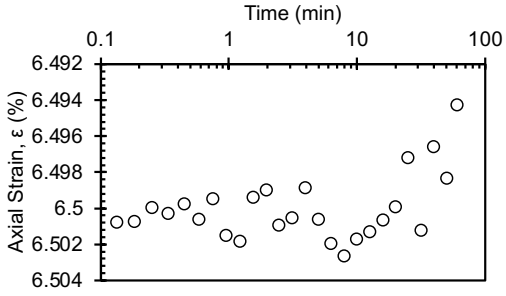

LIR = -0.5

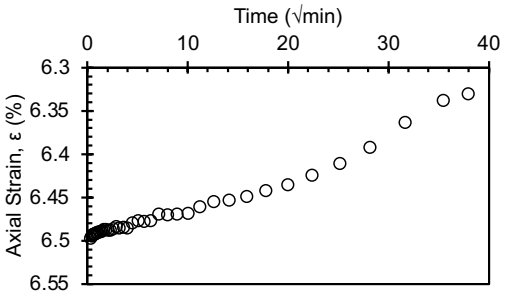

100 kPa

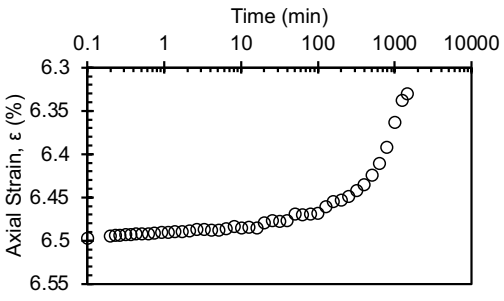

LIR =-0.5

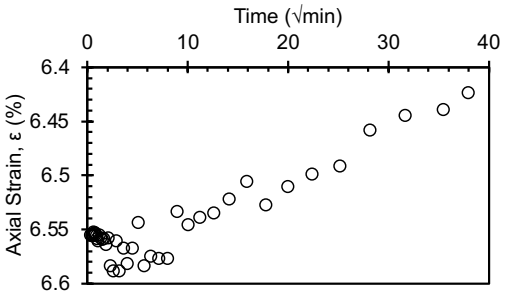

200 kPa

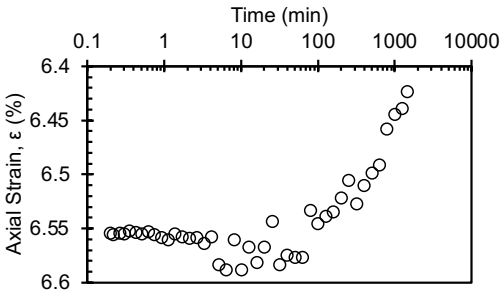

LIR = 1

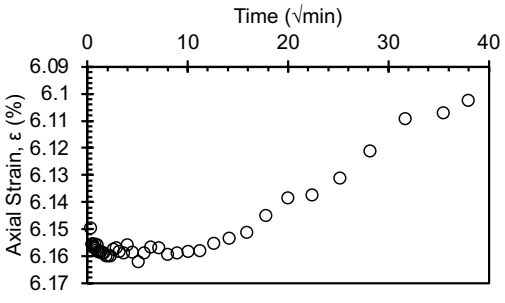

300 kPa

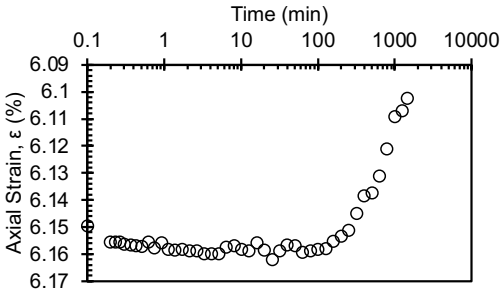

LIR = 0.5

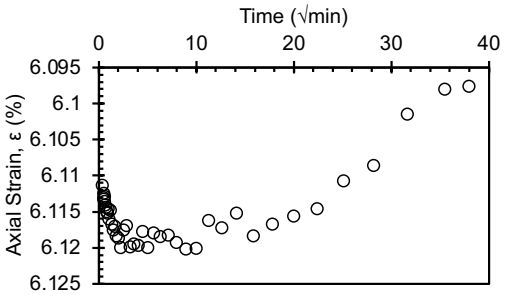

400 kPa

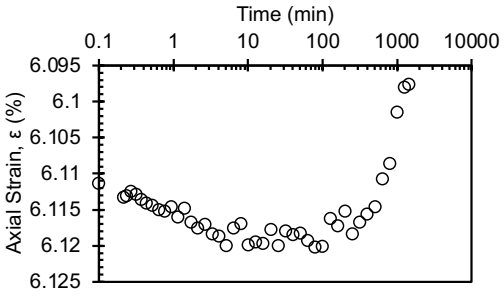

LIR = 0.333

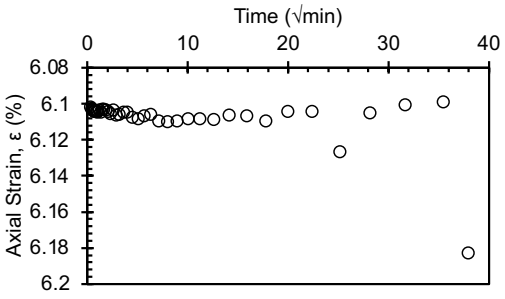

500 kPa

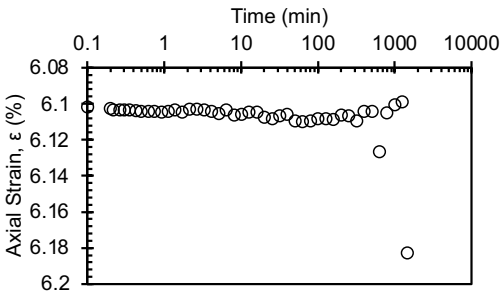

LIR = 0.25

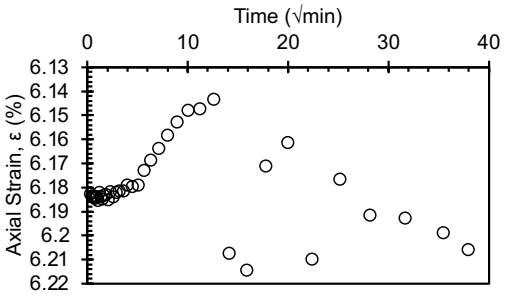

600 kPa

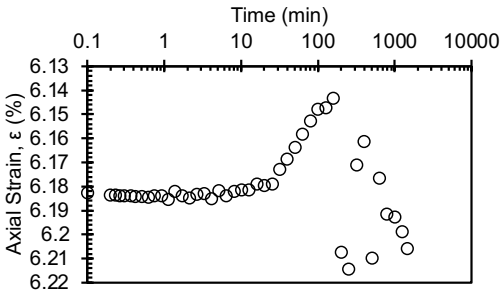

LIR = 0.2

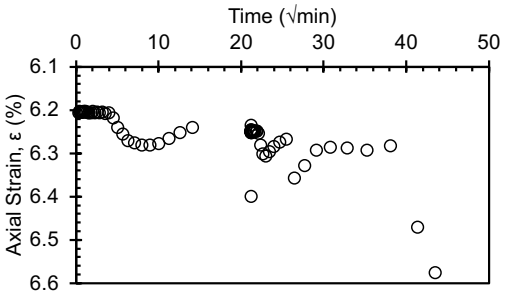

700 kPa

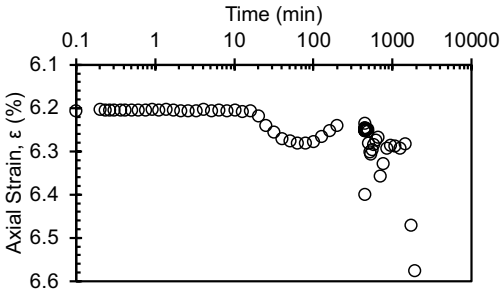

LIR = 0.167

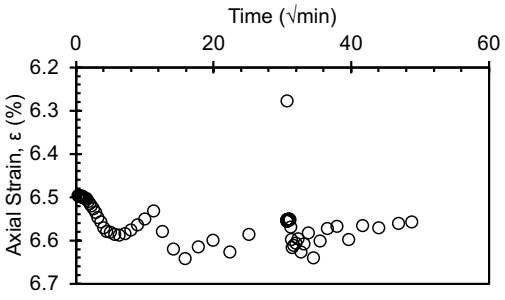

800 kPa

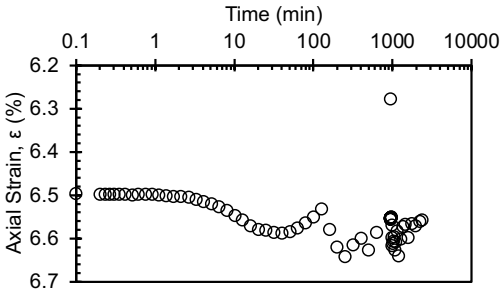

LIR = 0.143

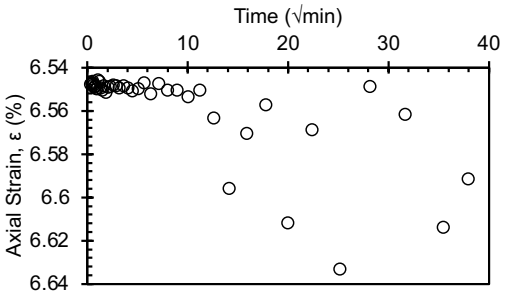

900 kPa

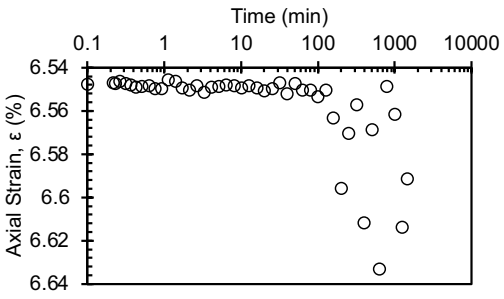

LIR = 0.125

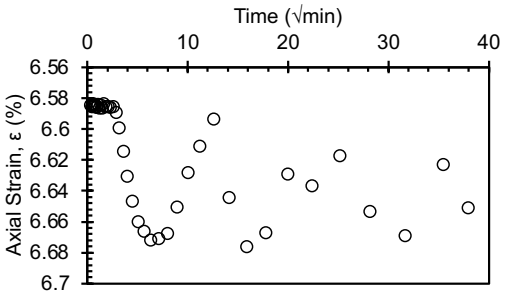

1000 kPa

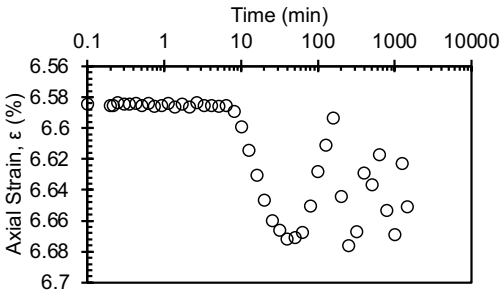

LIR = 0.111

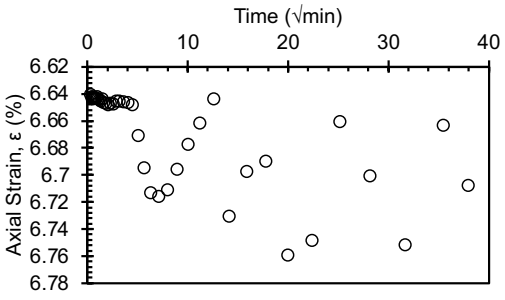

1500 kPa

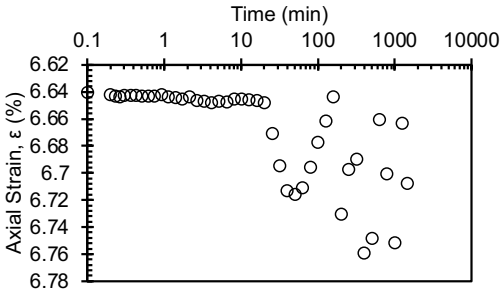

LIR = 0.5

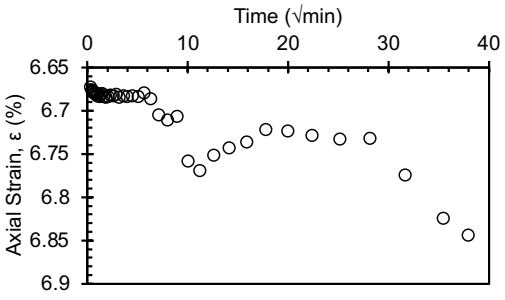

2000 kPa

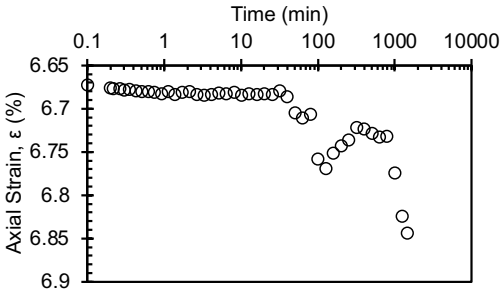

LIR = 0.333

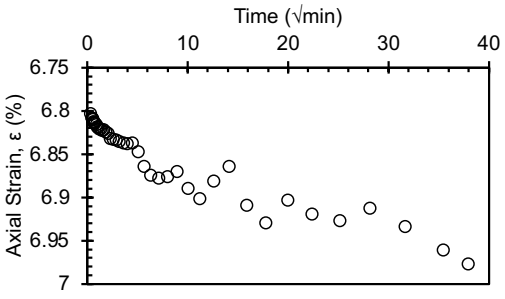

2500 kPa

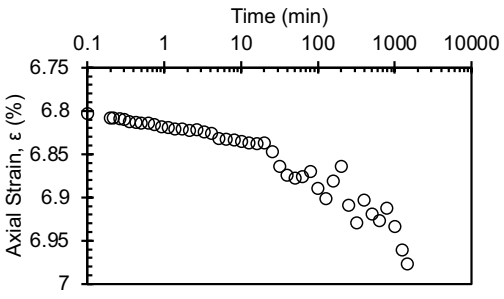

LIR = 0.25

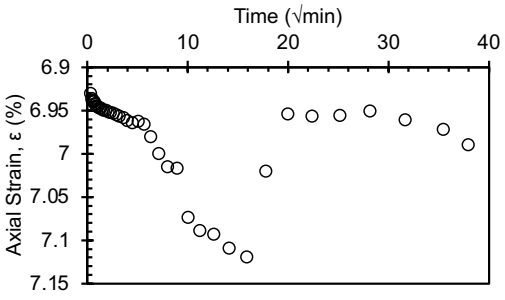

3000 kPa

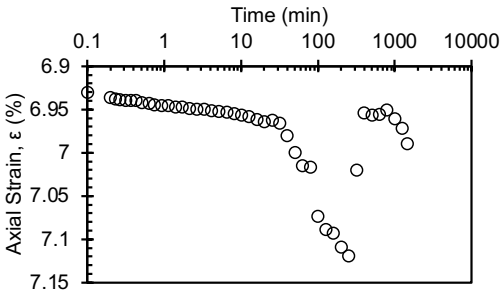

LIR = 0.2

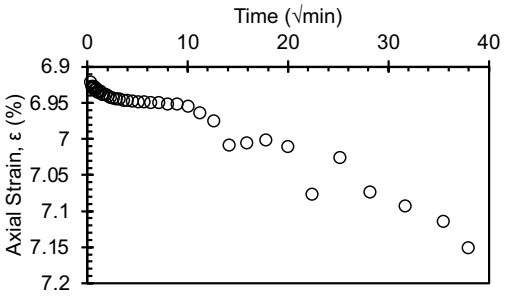

3500 kPa

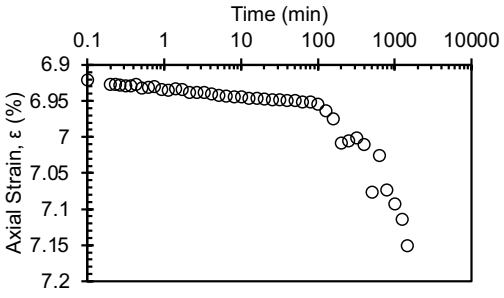

LIR = 0.167

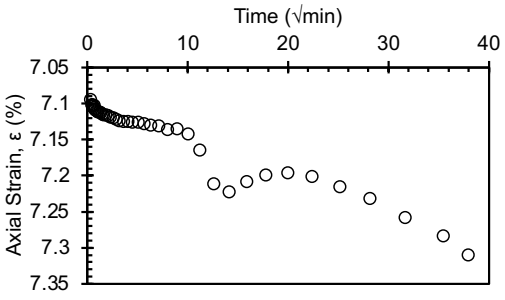

4000 kPa

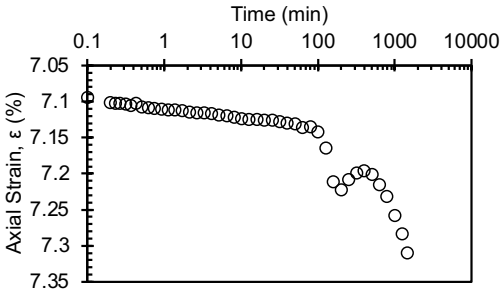

LIR = 0.143

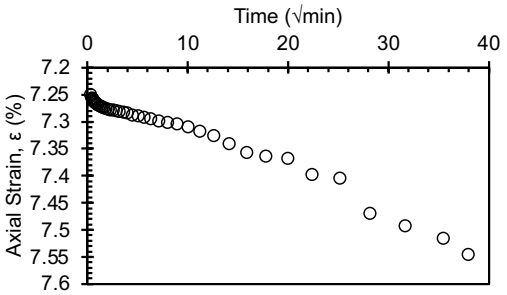

4500 kPa

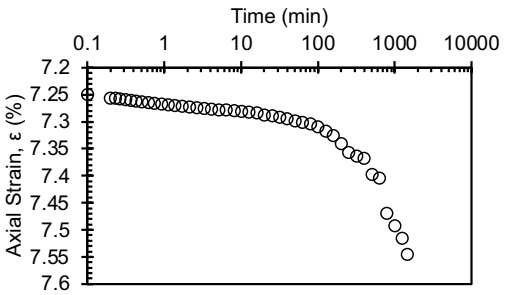

LIR = 0.125

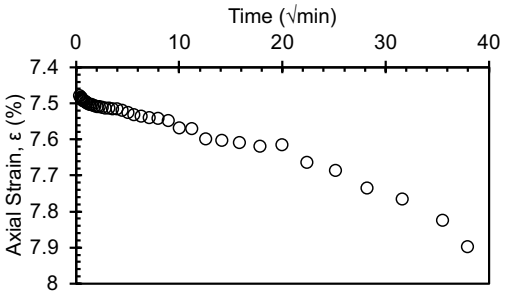

5000 kPa

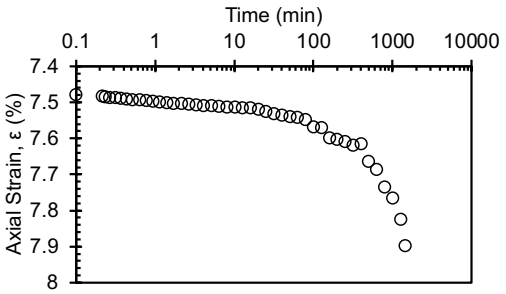

LIR = 0.111

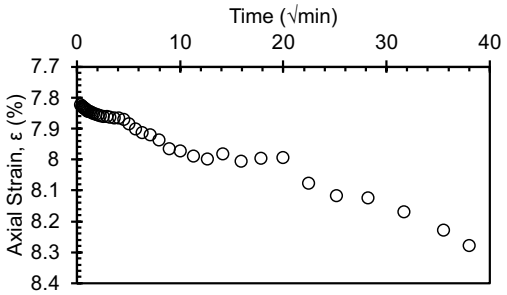

5500 kPa

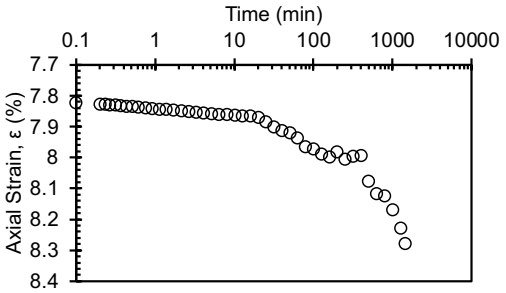

LIR = 0.1

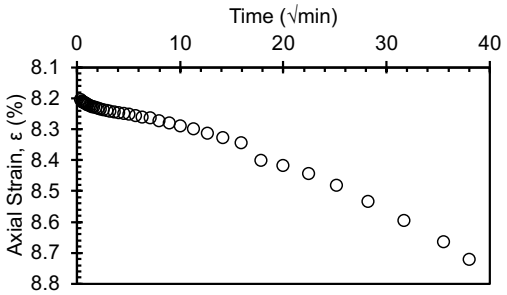

6000 kPa

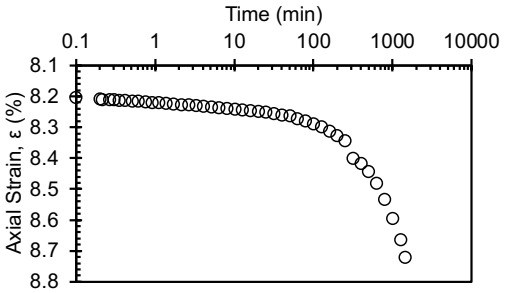

LIR = 0.091

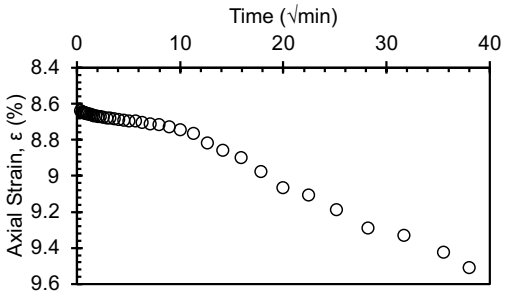

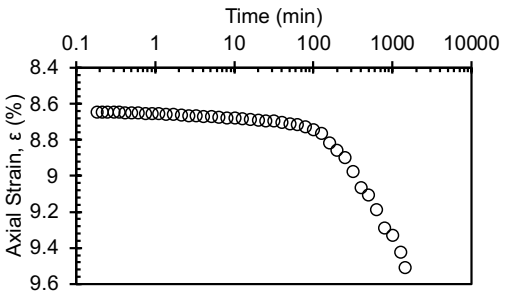

6500 kPa

LIR = 0.083

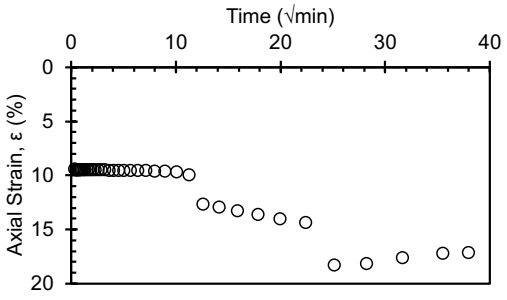

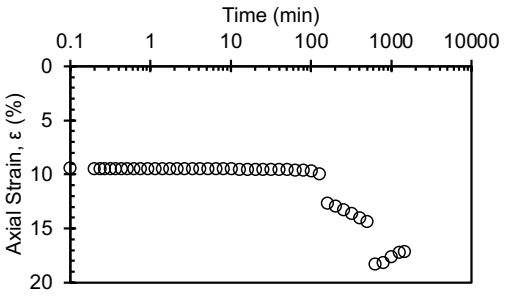

6800 kPa

LIR = 0.077

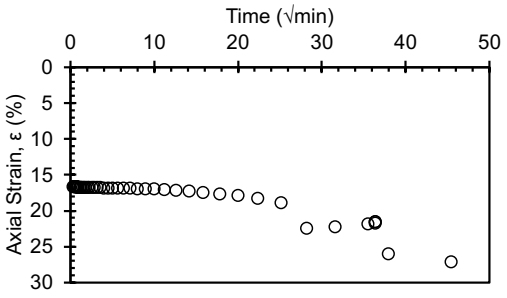

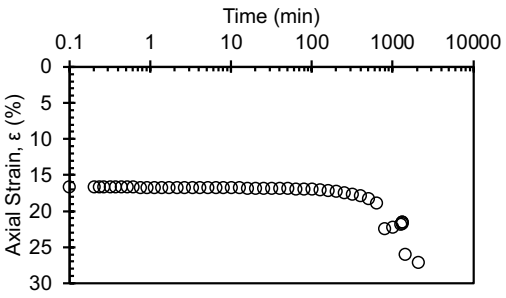

Final

Compression curve

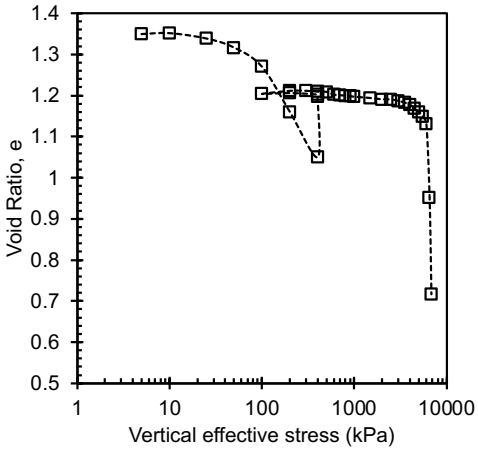

Butterfield method

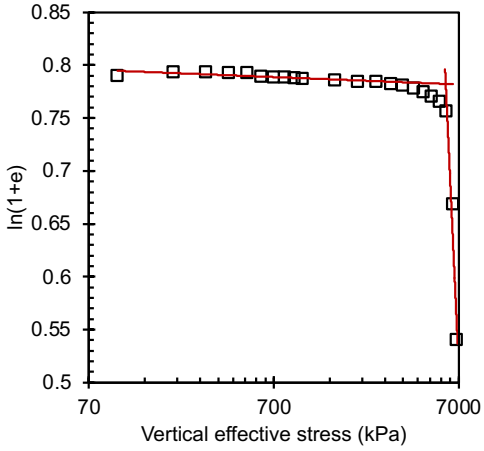

-5.5 °C

Consolidation Test Data Sheet			
Test No.	-5.5_NC_KAOL_EXT	Consolidometer No.	Sigma1_10k_10
Date started	11/2/24	Date ended	11/29/24
Test method	B	Condition of test	Inundated
Interpretation Method	Both 1 and 2	Classification	Remolded EPK (CH)
	Before Test - 20°C		After Test - (-5.5)°C
	Specimen	Trimmings	Specimen
Tare No.	Ring	LUIGI	5C
Tare plus wet soil (g)	354.08	268.37	150.97
Tare plus dry soil (g)	-	189.73	120.03
Tare (g)	216.96	21.94	32.27
Water (g)	43.8	78.64	30.94
Dry Soil (g)	93.4	167.79	87.76
Water content (%)	46.9	46.9	35.3
Area of specimen, A (cm^2)	31.67		
Specific Gravity of Solids, G_s	2.7		
Height of solids, H_s (cm)	1.092		
Initial - 20°C		Final - (-5.5)°C	
Height of specimen, H_0 (cm)	2.540	Height of specimen, H_f (cm)	2.070
Height of water, H_{w0} (cm)	1.382	Height of water, H_{wf} (cm)	0.977
Height of voids, H_{v0}	1.448	Height of voids, H_{vf} (cm)	0.978

(cm)			
Void ratio, e_0	1.33	Void ratio, e_f	0.90
Degree of saturation, S0 (%)	95.4	Degree of saturation, S_f (%)	99.9
Dry density, γ_0 (g/cm^2)	1.16	Dry density, γ_f (g/cm^2)	1.42
		Differential height, H_d (cm)	-0.015
		Preconsolidation pressure, σ_p'(kPa)	11000
		Load increments (kPa) - seating loads held for 60 min, all other loads 1440 min	
Initial temperature, 20°C		5 (seating), 10, 25, 50, 100, 200, 400	
Temperature change(s)	20°C to (-5.5)°C	400	
Final temperature (°C)	(-5.5)°C	400 (seating), 200, 100, 200, 400, 1000, 2000, 3000, 4000, 5000, 6000, 7000, 8000, 9000, 10000, 11000, 12000, 13000, 14000, 15000	
Notes			
Note that the final height of the specimen H_f is the height recorded at the end of the test after the specimen was rebounded to 5 kPa until strain stabilized - it does not correspond to the final height at the maximum applied stress. The differential height is the difference between the final recorded height H_f and final height measured with a caliper following specimen extraction from ring at the end of the test.			

Initial Consolidation C1 (20 °C)

5 kPa

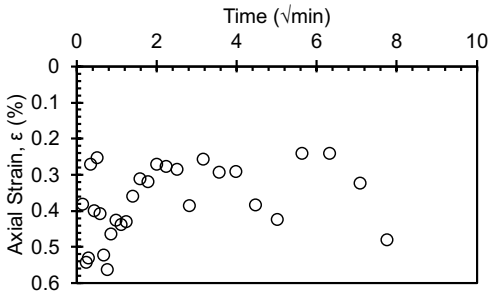

Seating Load

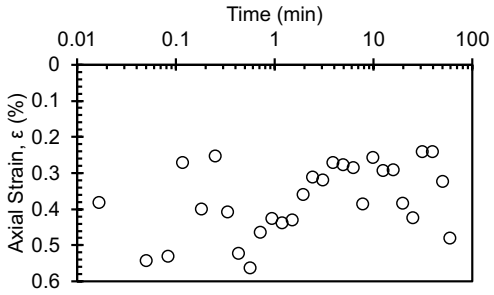

10 kPa

LIR = 1

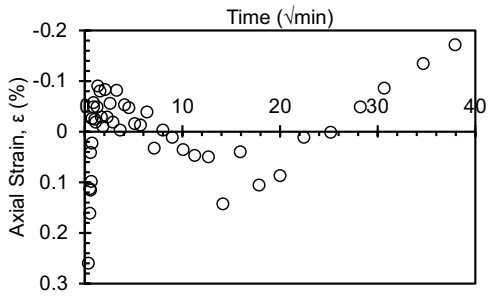

25 kPa

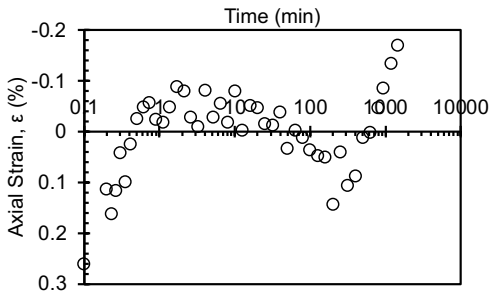

LIR = 1.5

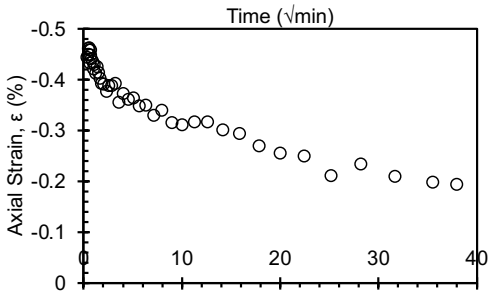

50 kPa

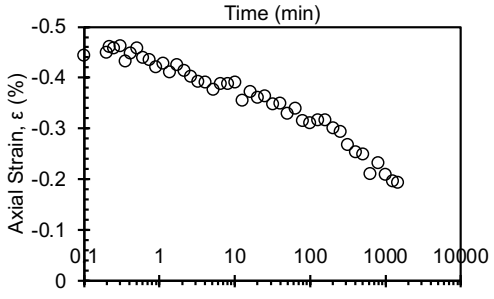

LIR = 1

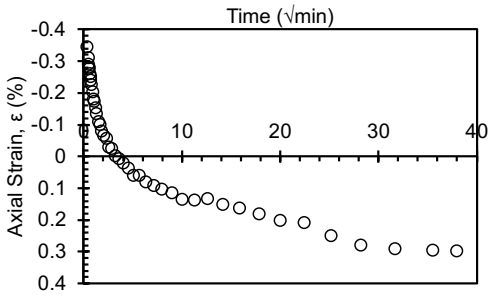

100 kPa

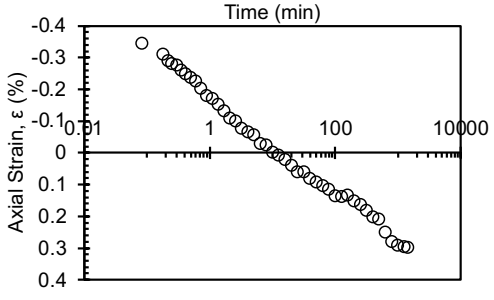

LIR = 1

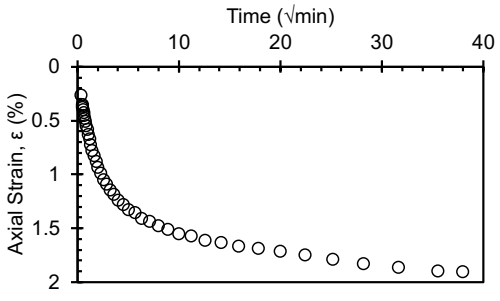

200 kPa

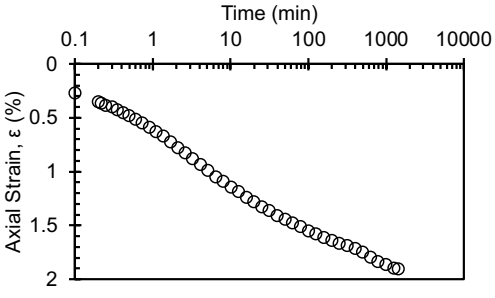

LIR = 1

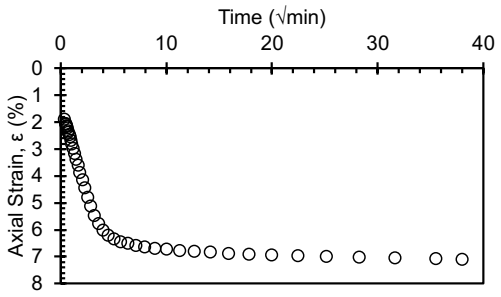

400 kPa

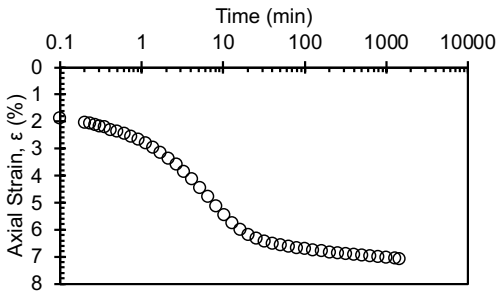

LIR = 1

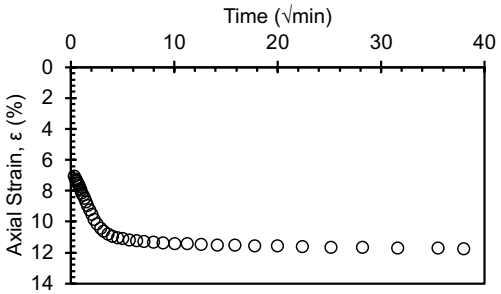

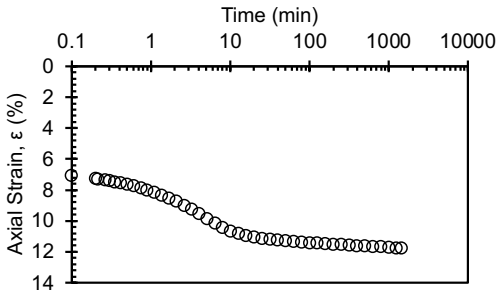

Temperature Change Stage: 20 °C>-5.5 °C

400 kPa

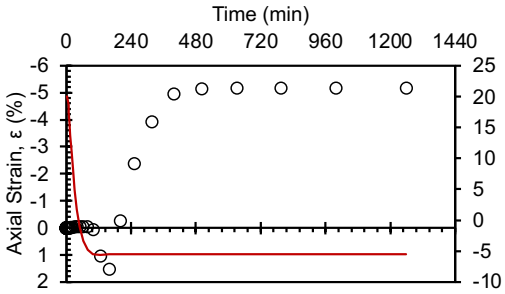

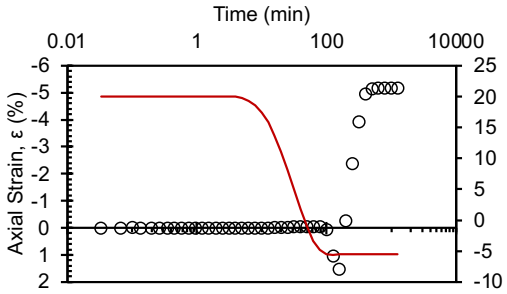

Second Consolidation C2 (-5.5 °C)

400 kPa

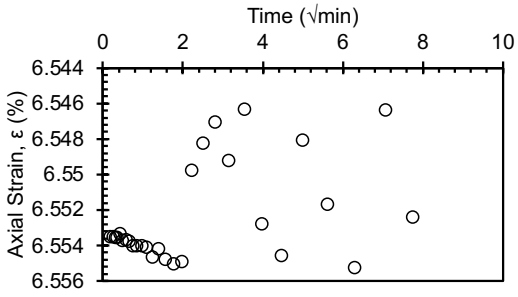

200 kPa

Seating load

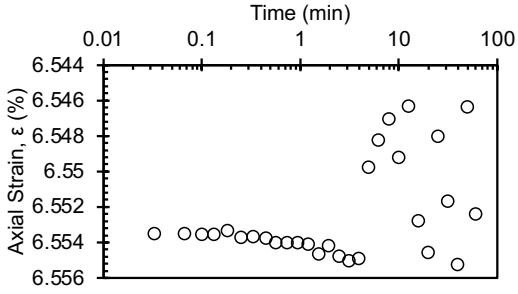

LIR = -0.5

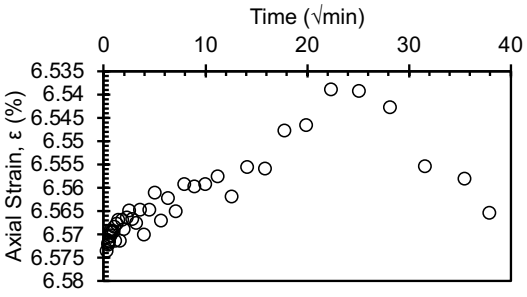

100 kPa

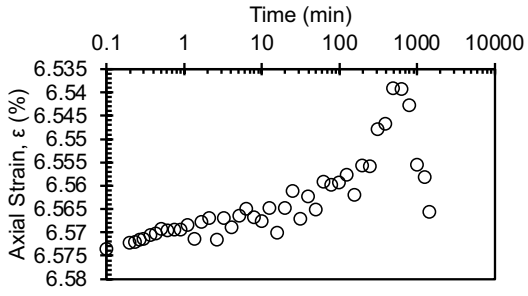

LIR =-0.5

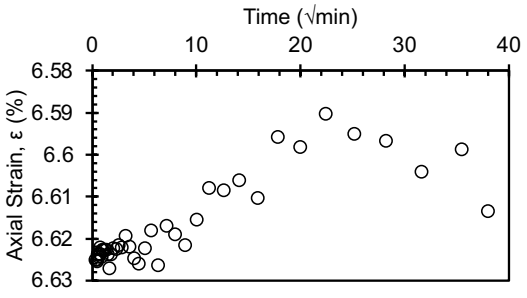

200 kPa

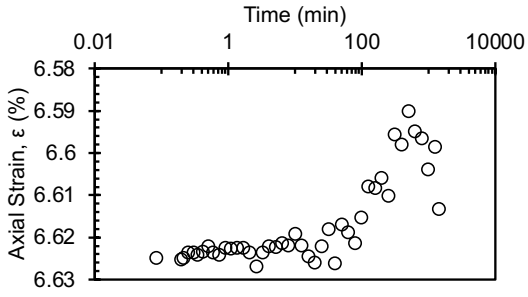

LIR = 1

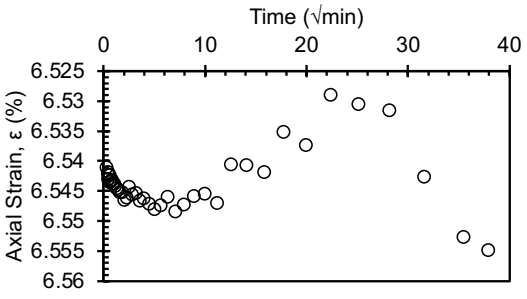

400 kPa

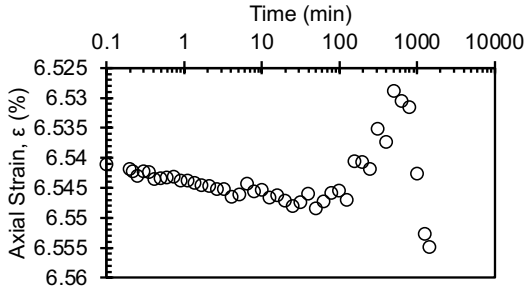

LIR = 1

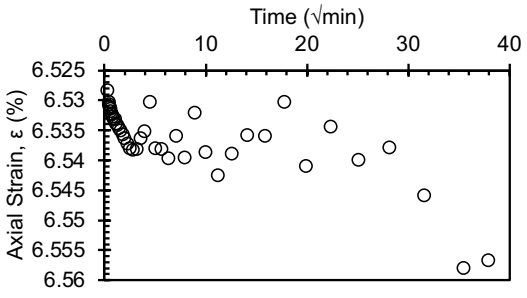

1000 kPa

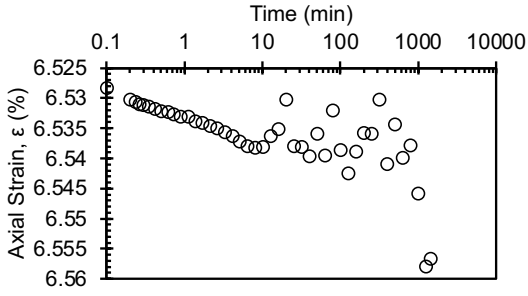

LIR = 1.5

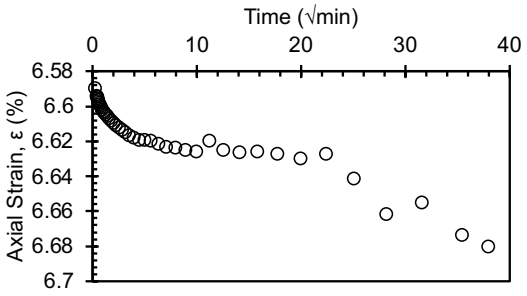

2000 kPa

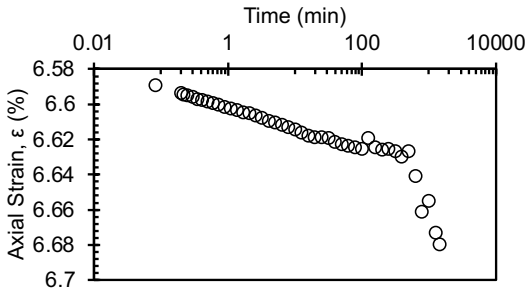

LIR = 1

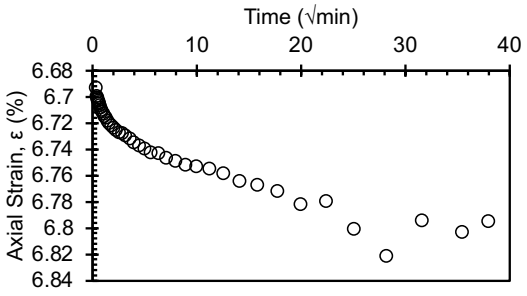

3000 kPa

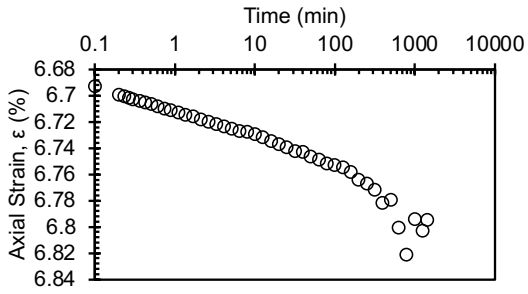

LIR = 0.5

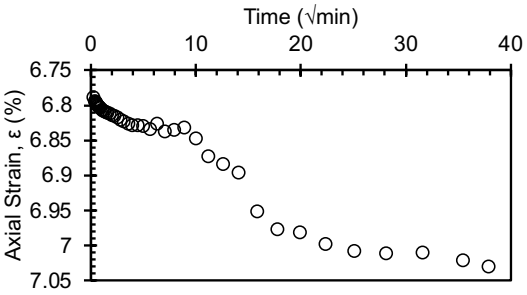

4000 kPa

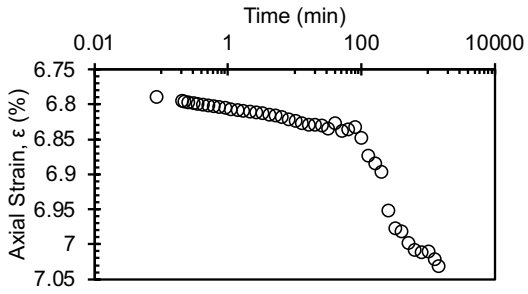

LIR = 0.3331

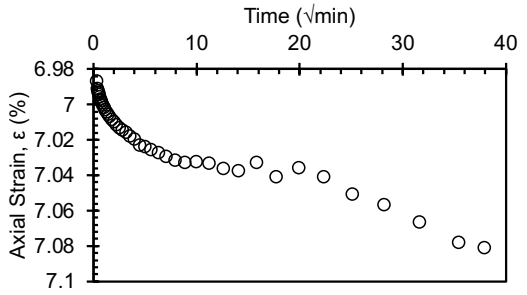

5000 kPa

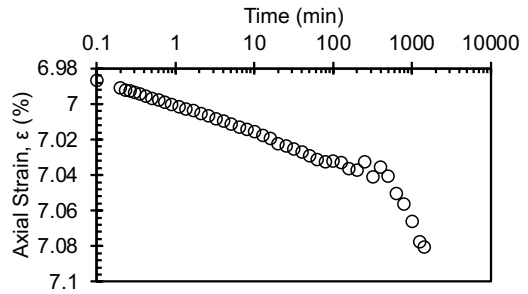

LIR = 0.25

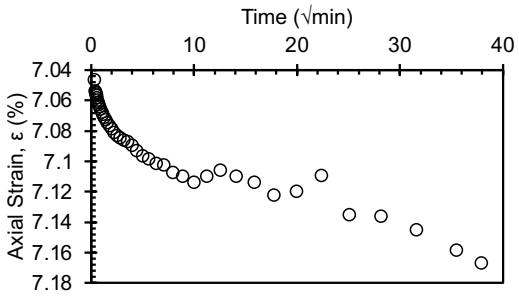

6000 kPa

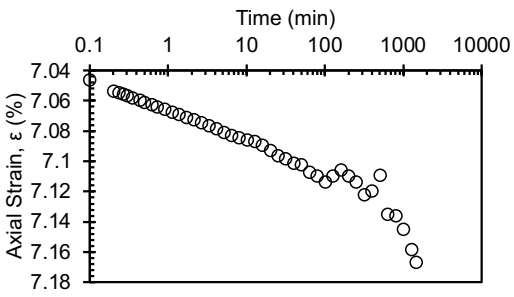

LIR = 0.2

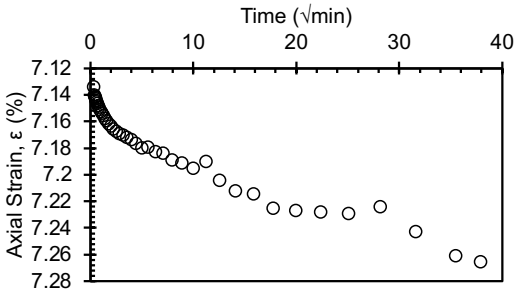

7000 kPa

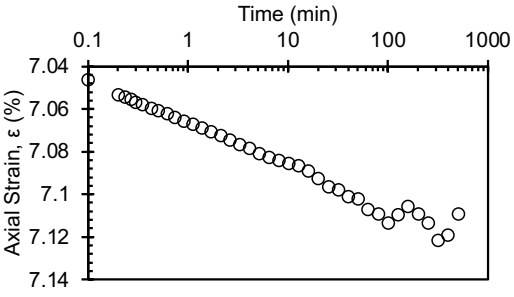

LIR = 0.167

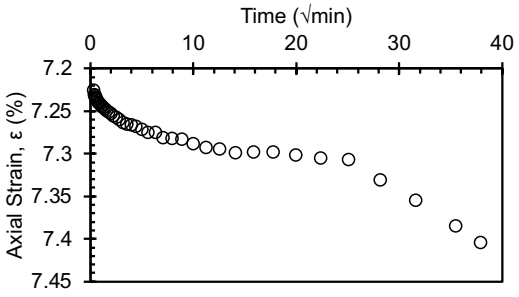

8000 kPa

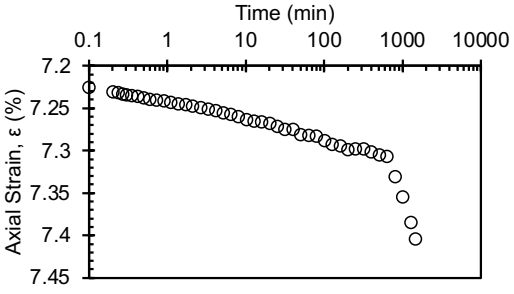

LIR = 0.143

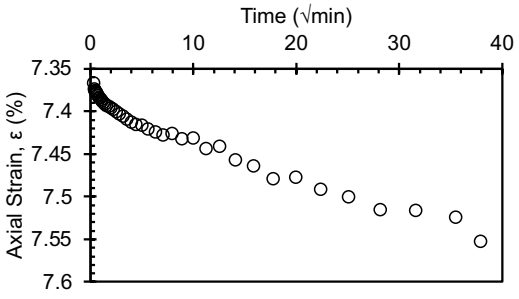

9000 kPa

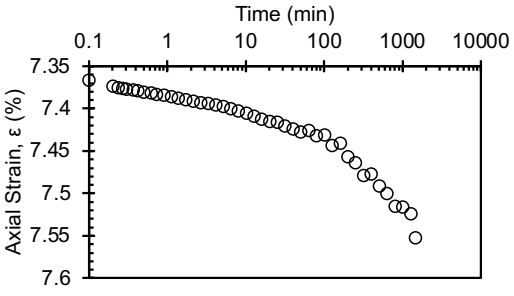

LIR = 0.125

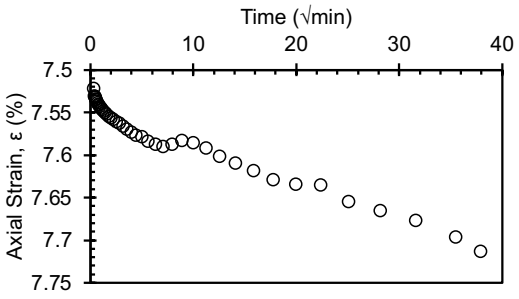

10000 kPa

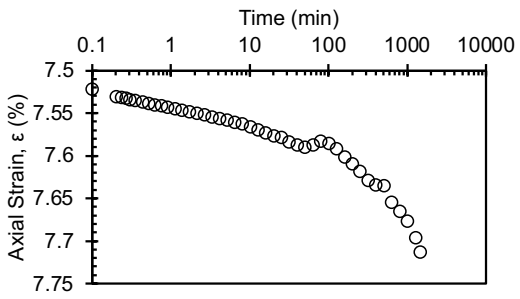

LIR = 0.111

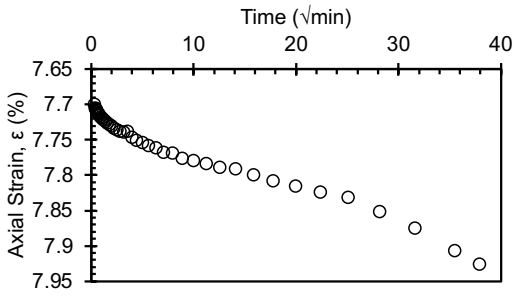

11000 kPa

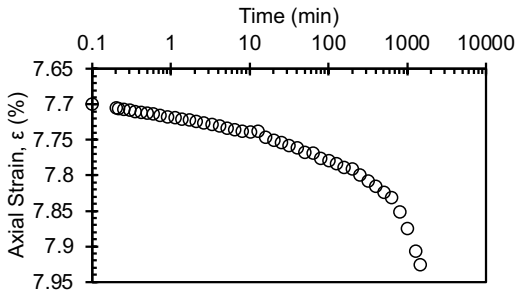

LIR = 0.1

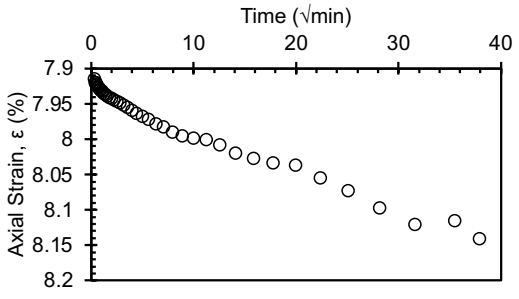

12000 kPa

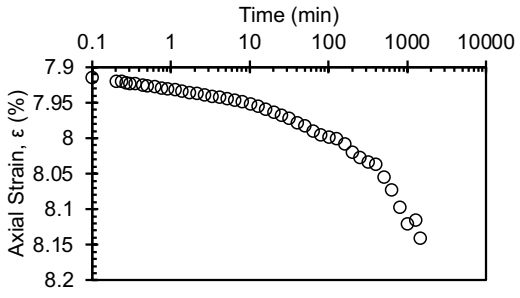

LIR = 0.091

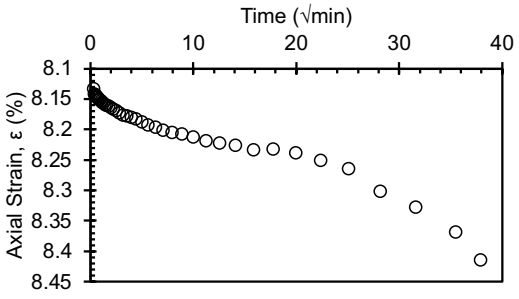

13000 kPa

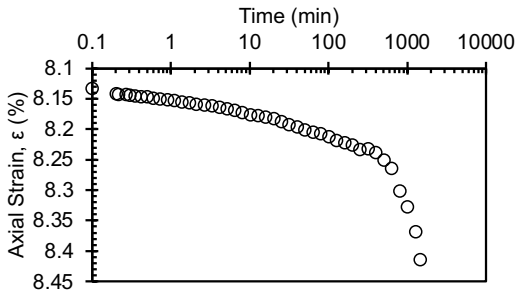

LIR = 0.084

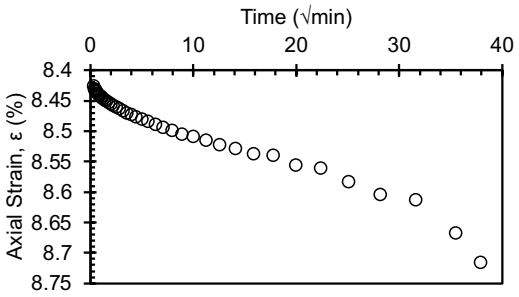

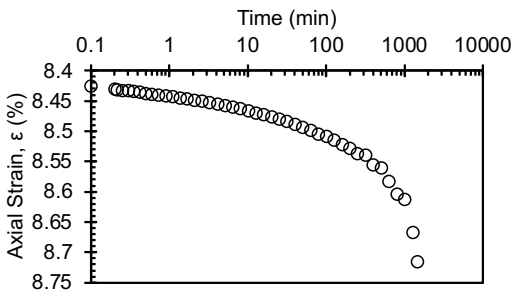

14000 kPa

LIR = 0.077

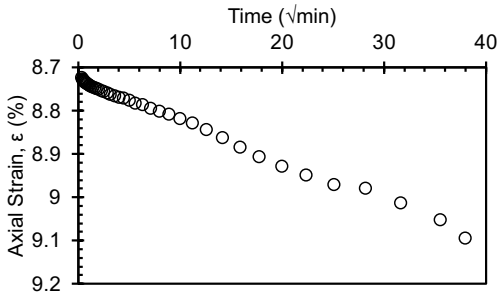

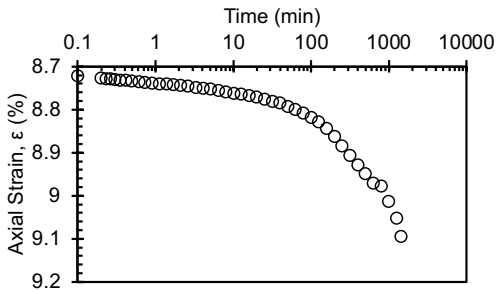

15000 kPa

LIR = 0.071

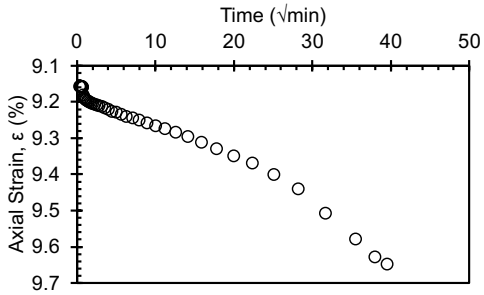

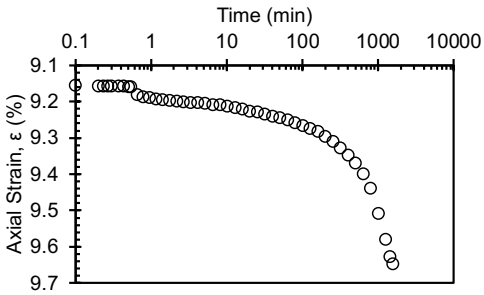

Final

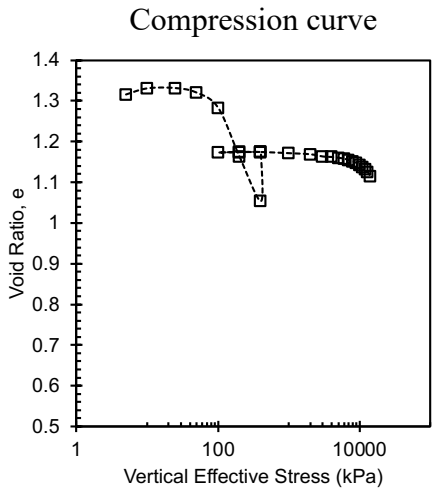
Compression curve
Void Ratio, e
1.4
1.3
1.2
1.1
1
0.9
0.8
0.7
0.6
0.5
1
100
10000
Vertical Effective Stress (kPa)

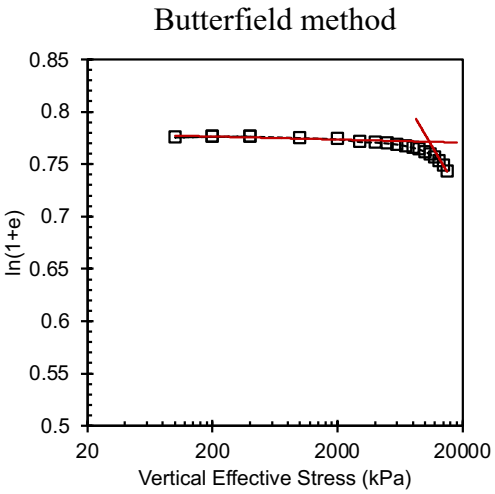
Butterfield method
ln(1+e)
0.85
0.8
0.75
0.7
0.65
0.6
0.55
0.5
20
200
2000
20000
Vertical Effective Stress (kPa)

-7 °C

Consolidation Test Data Sheet			
Test No.	-7_NC_KAOL_EXT_2	Consolidometer No.	Sigma1_10k_10
Date started	10/6/24	Date ended	11/1/24
Test method	B	Condition of test	Inundated
Interpretation Method	Both 1 and 2	Classification	Remolded EPK (CH)
	Before Test - 20°C		After Test - (-7)°C
	Specimen	Trimmings	Specimen
Tare No.	Ring	T81	MARIO
Tare plus wet soil (g)	354.13	269.89	142.61
Tare plus dry soil (g)	-	193.31	109.38
Tare (g)	216.98	32.13	22.76
Water (g)	44.17	76.58	33.23
Dry Soil (g)	92.98	161.18	86.62
Water content (%)	47.5	47.5	38.4
Area of specimen, A (cm^2)	31.67		
Specific Gravity of Solids, G_s	2.7		
Height of solids, H_s (cm)	1.087		
Initial - 20°C		Final - (-7)°C	
Height of specimen, H_0 (cm)	2.540	Height of specimen, H_f (cm)	2.140
Height of water, H_{w0} (cm)	1.395	Height of water, H_{wf} (cm)	1.049
Height of voids, H_{v0}	1.453	Height of voids, H_{vf} (cm)	1.053

(cm)			
Void ratio, e_0	1.34	Void ratio, e_f	0.97
Degree of saturation, S0 (%)	96.0	Degree of saturation, S_f (%)	99.7
Dry density, γ_0 (g/cm^2)	1.16	Dry density, γ_f (g/cm^2)	1.37
		Differential height, H_d (cm)	-0.190
		Preconsolidation pressure, σ_p'(kPa)	indeterminable
		Load increments (kPa) - seating loads held for 60 min, all other loads 1440 min	
Initial temperature, 20°C		5 (seating), 10, 25, 50, 100, 200, 400	
Temperature change(s)	20°C to (-7)°C	400	
Final temperature (°C)	(-7)°C	400 (seating), 200, 100, 200, 400, 1000, 2000, 3000, 4000, 5000, 6000, 7000, 8000, 9000, 10000, 11000, 12000, 13000, 14000	
Notes			
Note that the final height of the specimen H_f is the height recorded at the end of the test after the specimen was rebounded to 5 kPa until strain stabilized - it does not correspond to the final height at the maximum applied stress. The differential height is the difference between the final recorded height H_f and final height measured with a caliper following specimen extraction from ring at the end of the test.			

Initial Consolidation C1 (20 °C)

5 kPa

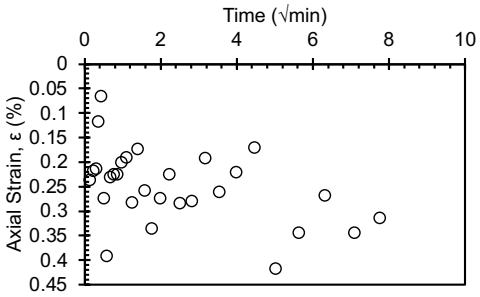

Seating Load

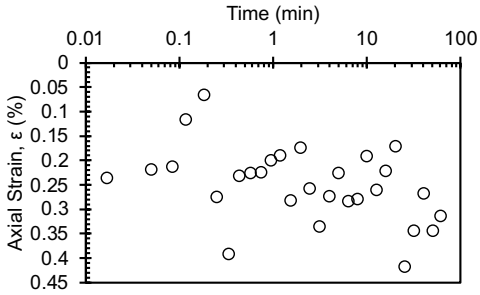

10 kPa

LIR = 1

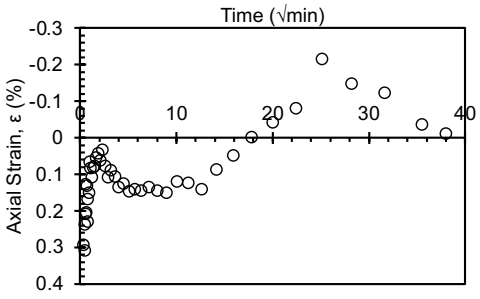

25 kPa

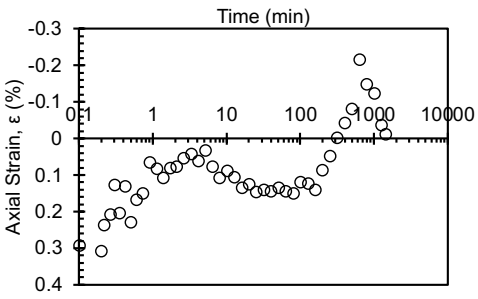

LIR = 1.5

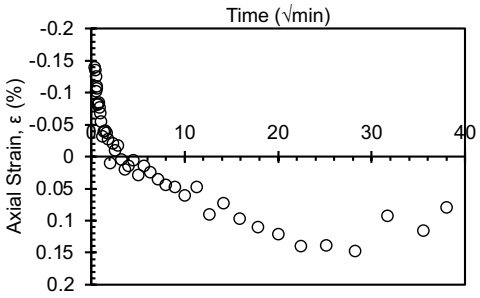

50 kPa

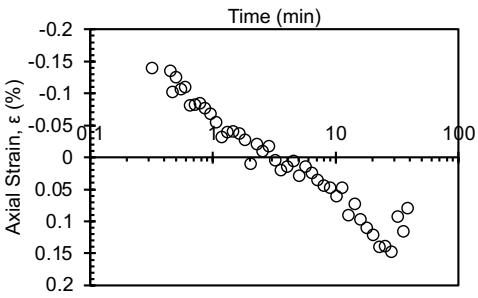

LIR = 1

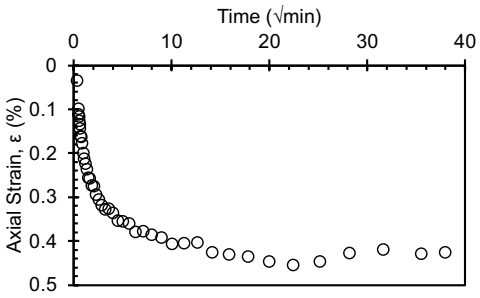

100 kPa

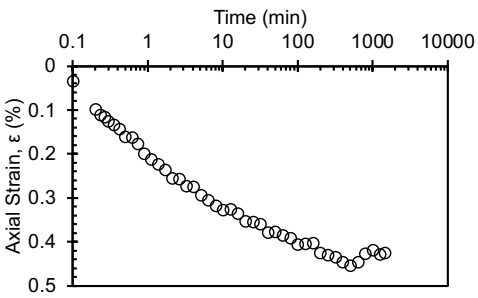

LIR = 1

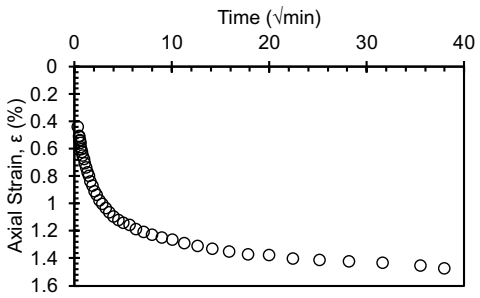

200 kPa

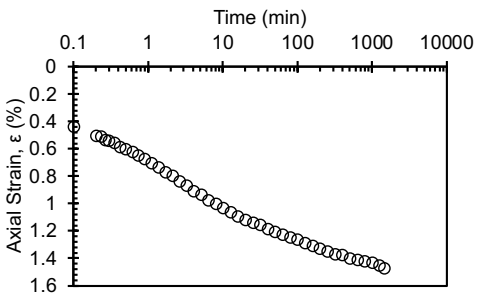

LIR = 1

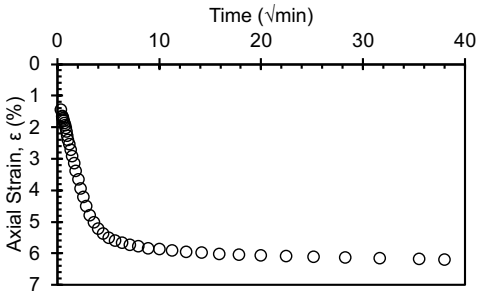

400 kPa

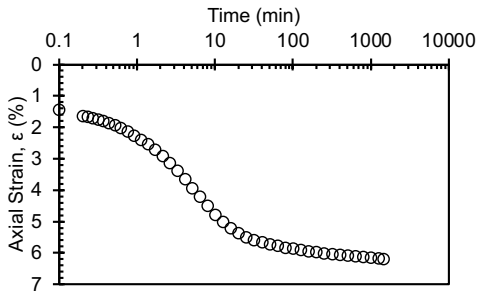

LIR = 1

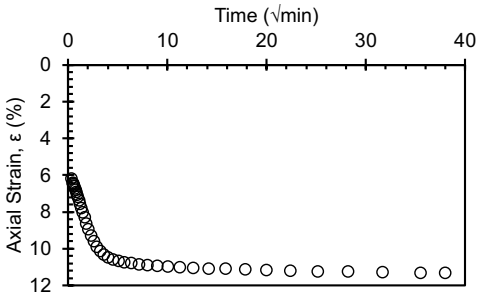

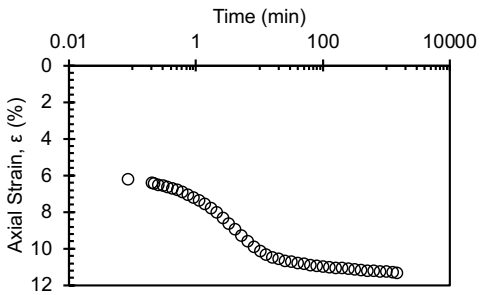

Temperature Change Stage: 20 °C>-7 °C

400 kPa

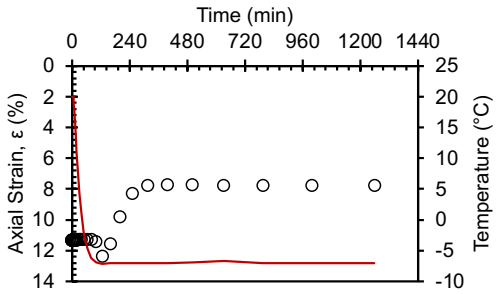

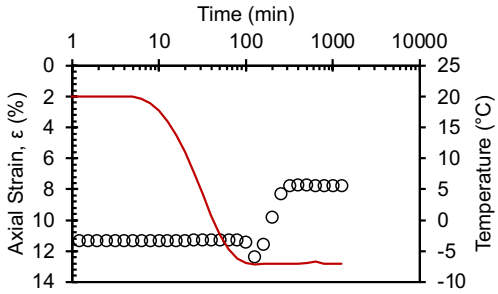

Second Consolidation C2 (-7 °C)

400 kPa

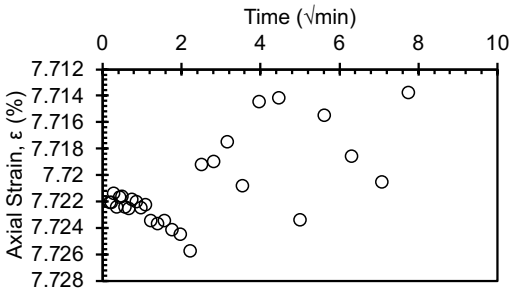

200 kPa

Seating load

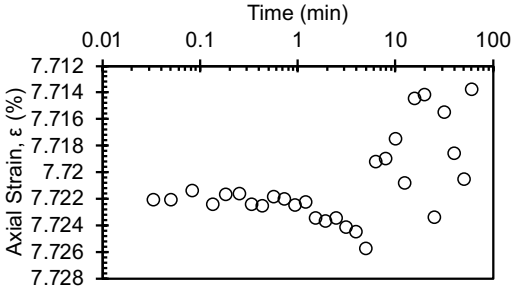

LIR = -0.5

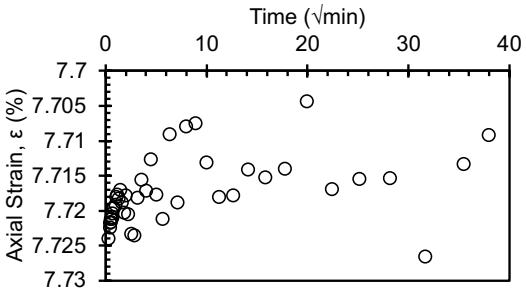

100 kPa

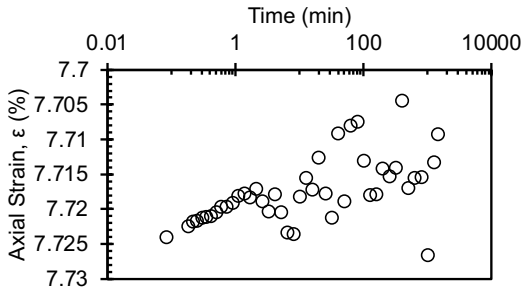

LIR =-0.5

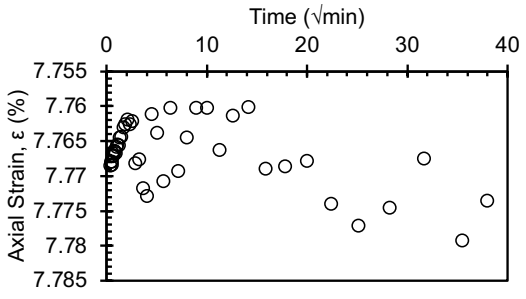

200 kPa

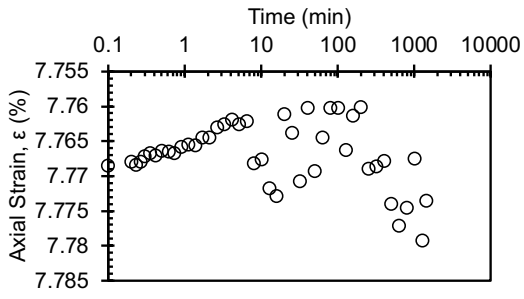

LIR = 1

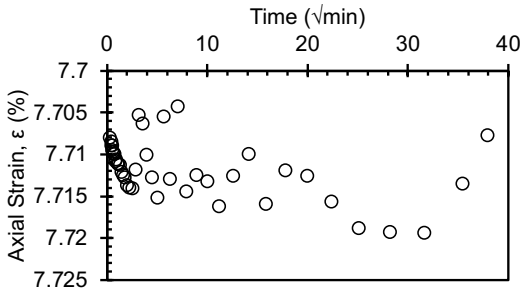

400 kPa

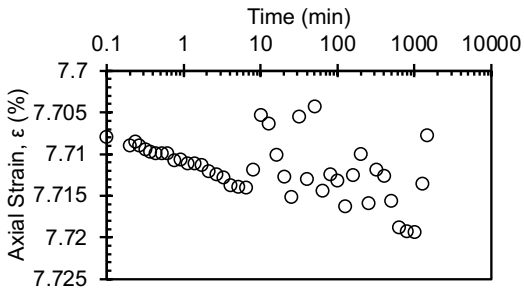

LIR = 1

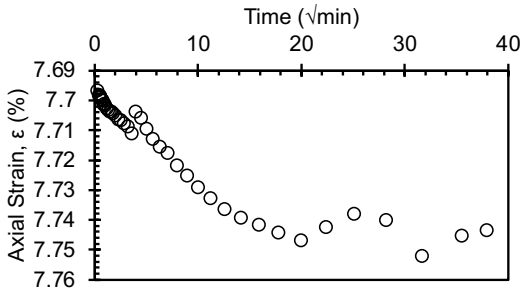

1000 kPa

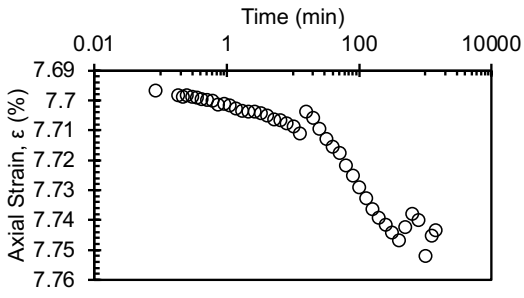

LIR = 1.5

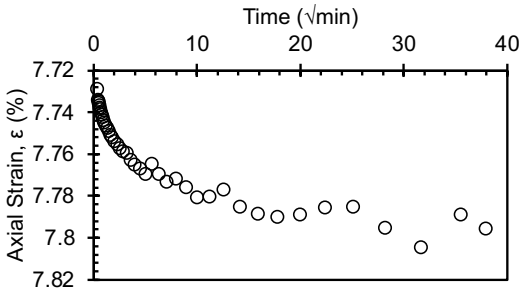

2000 kPa

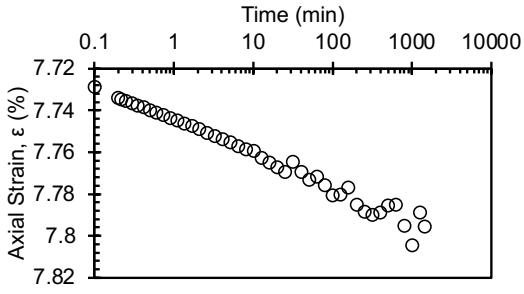

LIR = 1

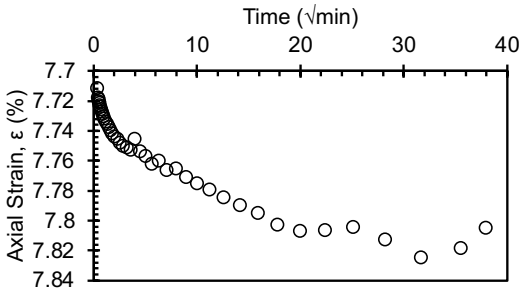

3000 kPa

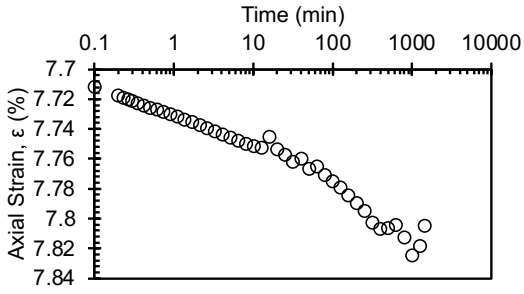

LIR = 0.5

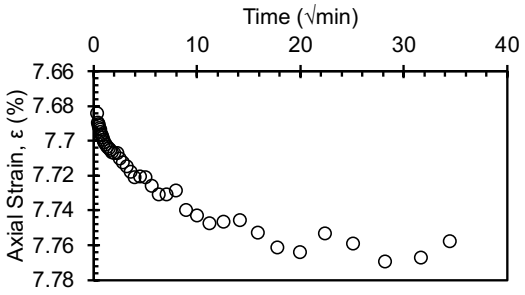

4000 kPa

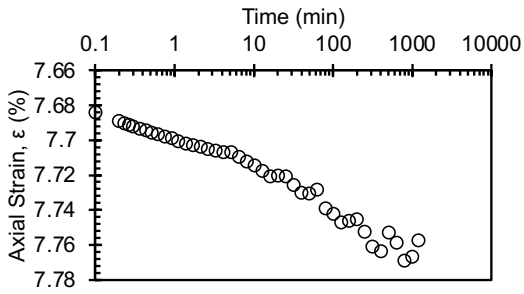

LIR = 0.3331

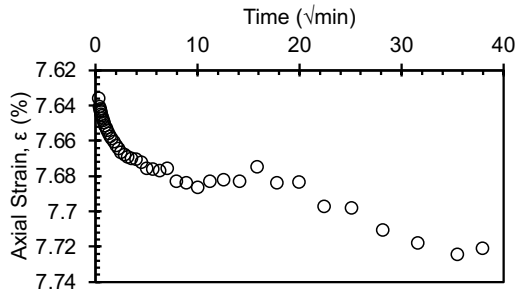

5000 kPa

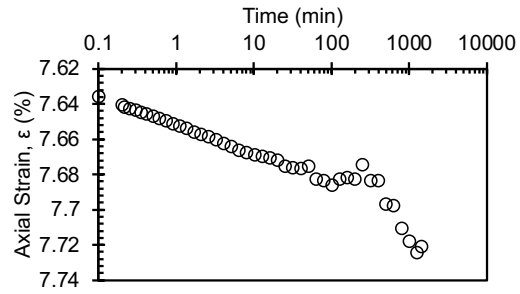

LIR = 0.25

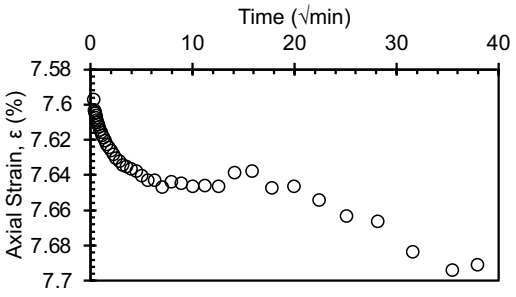

6000 kPa

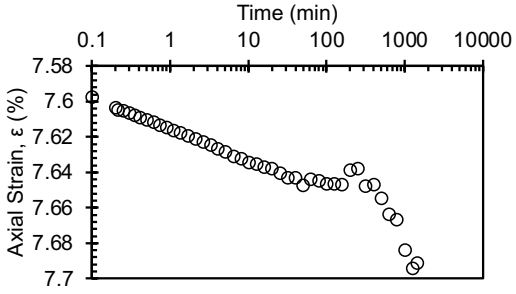

LIR = 0.2

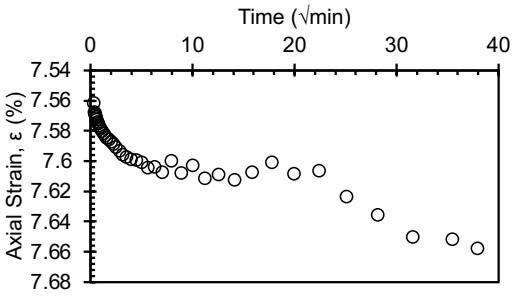

7000 kPa

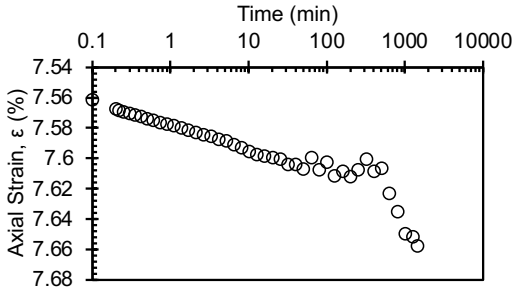

LIR = 0.167

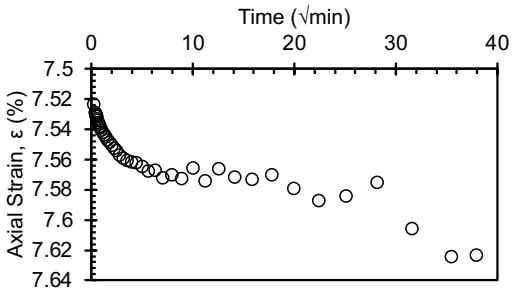

8000 kPa

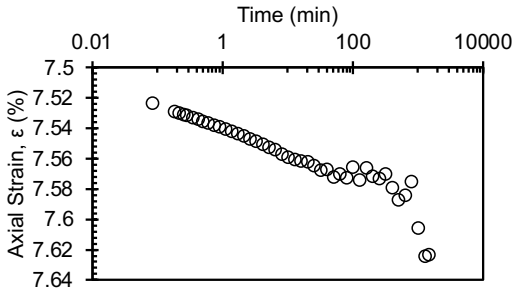

LIR = 0.143

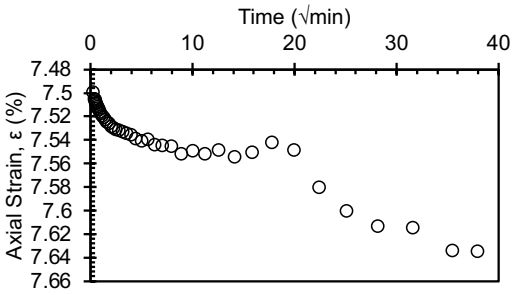

9000 kPa

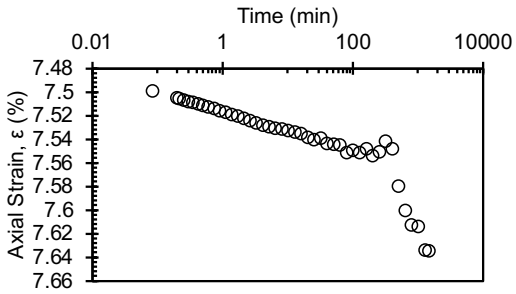

LIR = 0.125

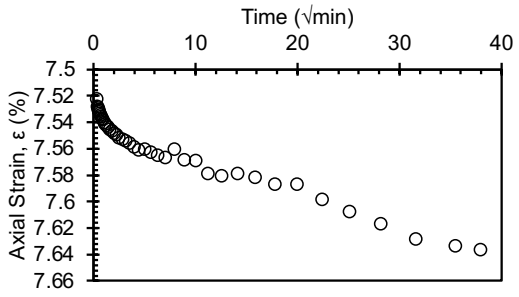

10000 kPa

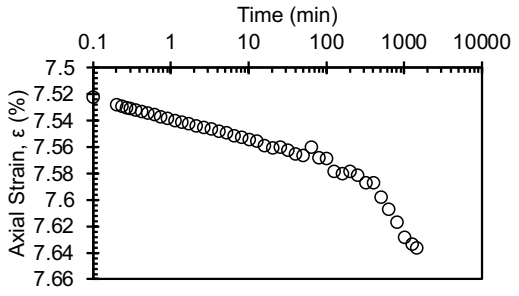

LIR = 0.111

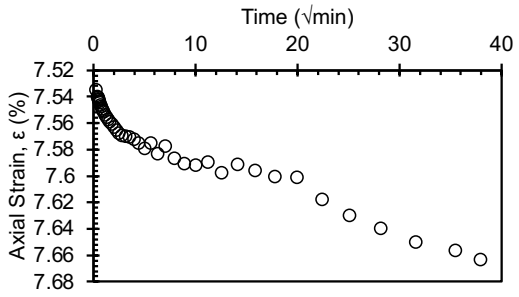

11000 kPa

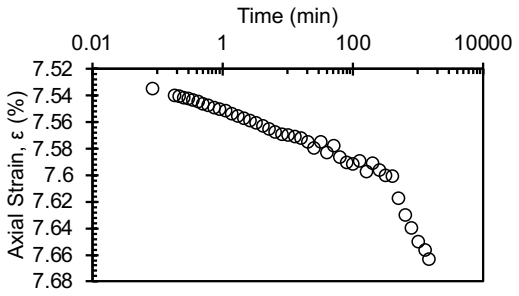

LIR = 0.1

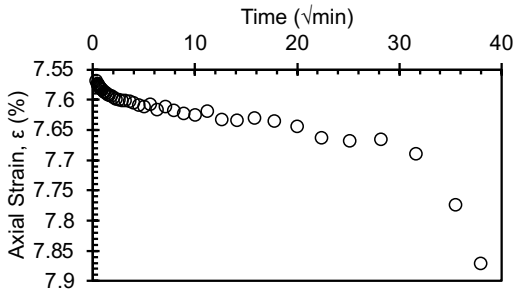

12000 kPa

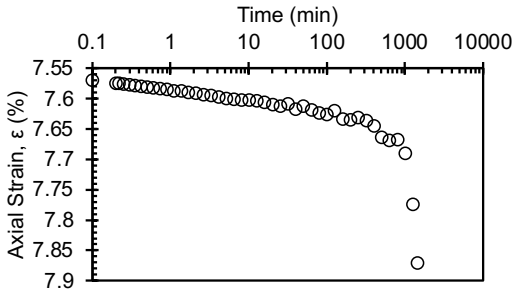

LIR = 0.091

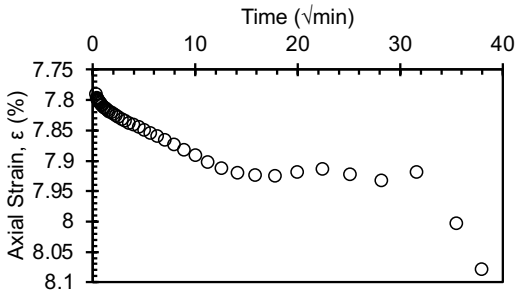

13000 kPa

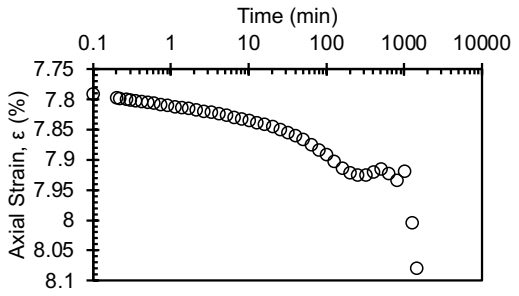

LIR = 0.084

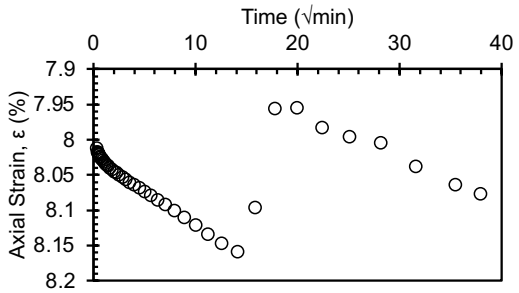

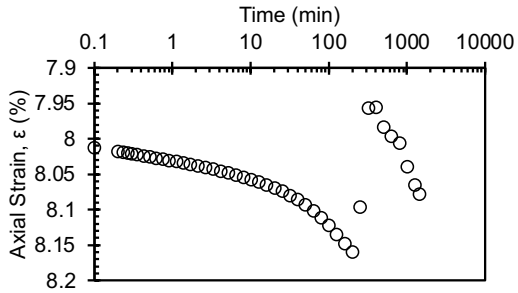

14000 kPa

LIR = 0.077

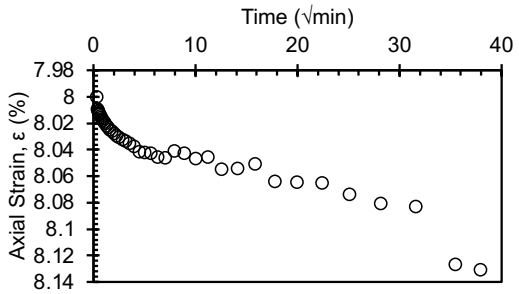

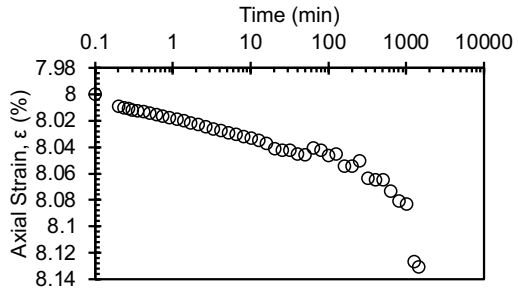

Final

Compression curve

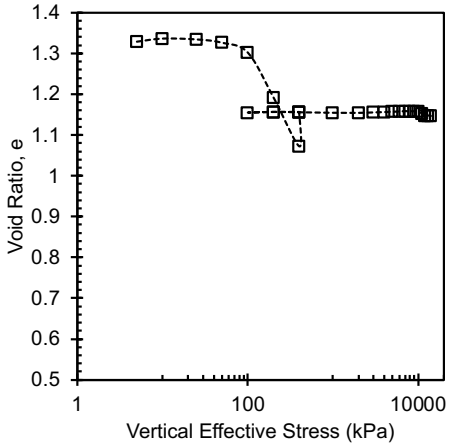

Butterfield method

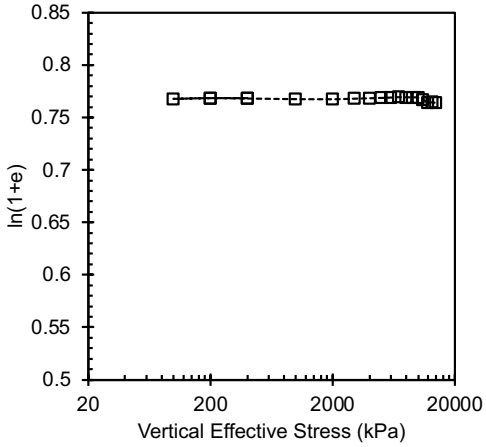

-15>50 °C

Consolidation Test Data Sheet			
Test No.	-15_50_NC_KAOL_EXT	Consolidometer No.	Geojac_2k_20
Date started	6/25/24	Date ended	7/25/24
Test method	B	Condition of test	Inundated
Interpretation Method	Both 1 and 2	Classification	Remolded EPK (CH)
	Before Test - 20°C		After Test - 50°C
	Specimen	Trimmings	Specimen
Tare No.	Ring	5C	LUIGI
Tare plus wet soil (g)	353.87	255.89	144.75
Tare plus dry soil (g)	-	184.38	114.72
Tare (g)	216.17	32.24	21.77
Water (g)	44.03	71.51	30.03
Dry Soil (g)	93.67	152.14	92.95
Water content (%)	47.0	47.0	32.3
Area of specimen, A (cm^2)	31.67		
Specific Gravity of Solids, G_s	2.7		
Height of solids, H_s (cm)	1.095		
Initial - 20°C		Final - 50°C	
Height of specimen, H_0 (cm)	2.540	Height of specimen, H_f (cm)	2.042
Height of water, H_{w0} (cm)	1.390	Height of water, H_{wf} (cm)	0.948
Height of voids, H_{v0} (cm)	1.445	Height of voids, H_{vf} (cm)	0.947

Void ratio, e_0	1.32	Void ratio, e_f	0.86
Degree of saturation, S0 (%)	96.2	Degree of saturation, S_f (%)	100.1
Dry density, γ_0 (g/cm^2)	1.16	Dry density, γ_f (g/cm^2)	1.45
		Differential height, H_d (cm)	-0.054
		Preconsolidation pressure, σ_p'(kPa)	610
		Load increments (kPa) - seating loads held for 60 min, all other loads 1440 min	
Initial temperature, 20°C		5 (seating), 10, 25, 50, 100, 200, 400	
Temperature change(s)	20°C to (-15)°C, (-15)°C to 50°C	400	
Final temperature (°C)	50°C	400 (seating), 200, 100, 200, 400, 1000, 2000, 3000, 4000, 5000, 6000, 7000, 8000, 9000, 10000, 11000, 12000, 13000, 14000	
Notes			
Note that the final height of the specimen H_f is the height recorded at the end of the test after the specimen was rebounded to 5 kPa until strain stabilized - it does not correspond to the final height at the maximum applied stress. The differential height is the difference between the final recorded height H_f and final height measured with a caliper following specimen extraction from ring at the end of the test.			

Initial Consolidation C1 (20 °C)

5 kPa

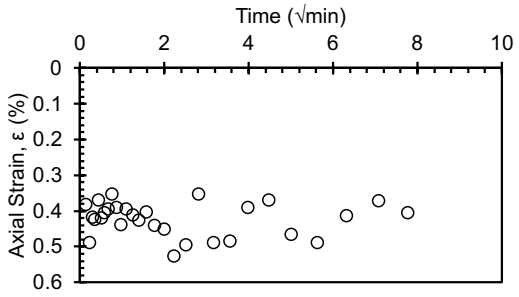

Seating load

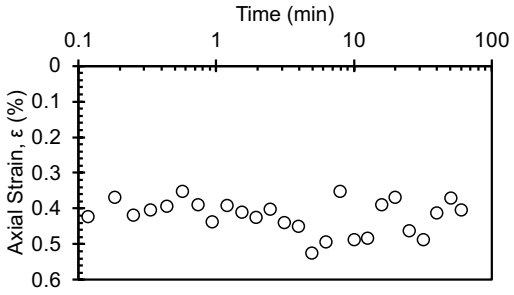

10 kPa

LIR = 1

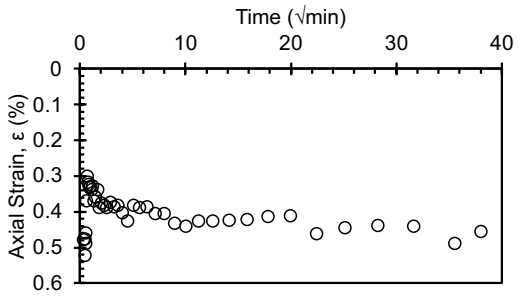

25 kPa

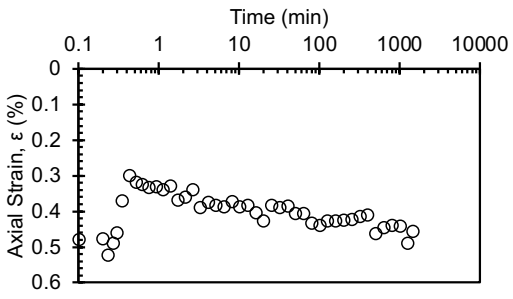

LIR = 1.5

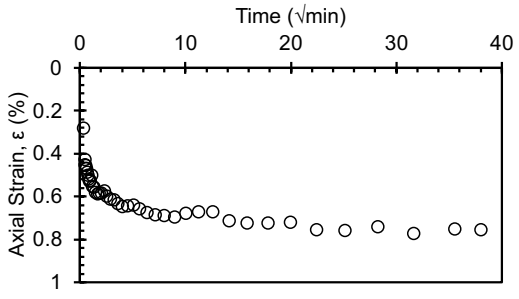

50 kPa

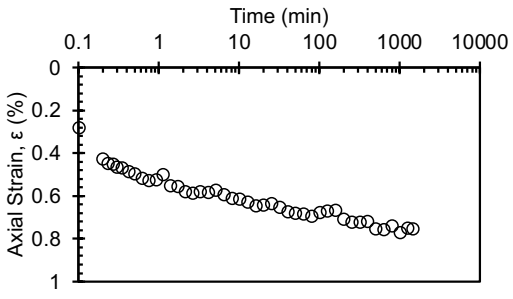

LIR = 1

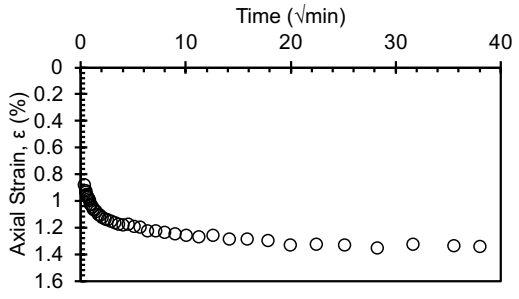

100 kPa

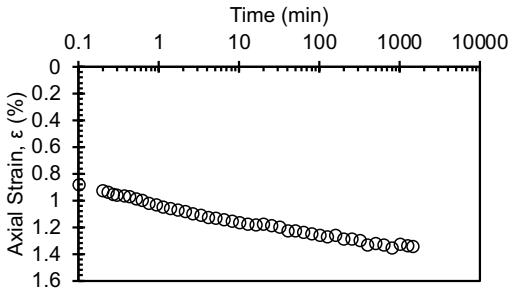

LIR = 1

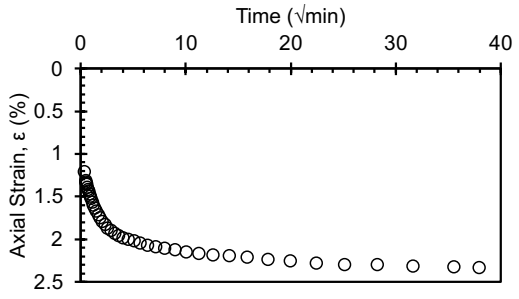

200 kPa

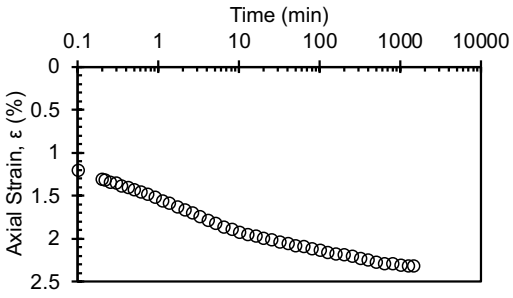

LIR = 1

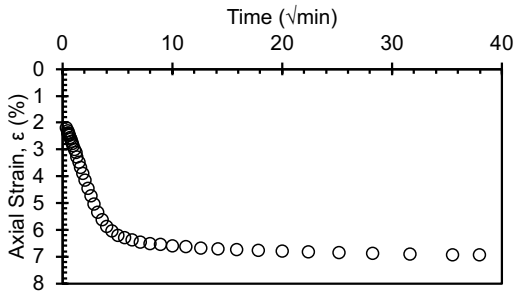

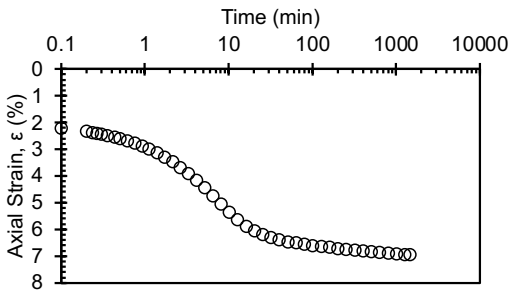

400 kPa

LIR = 1

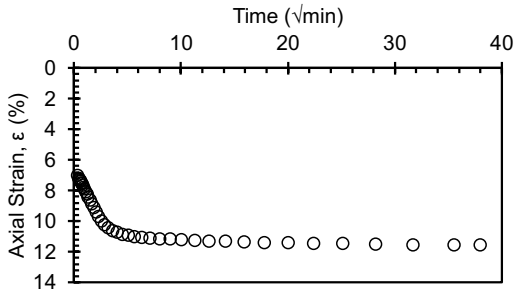

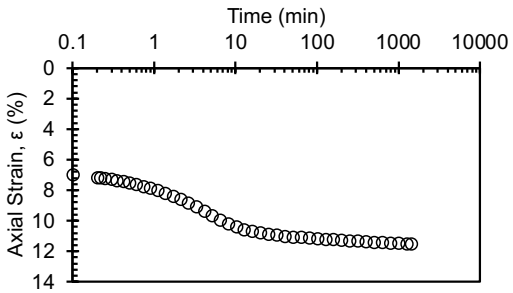

Temperature Change Stage: 20 °C>-15 °C

400 kPa

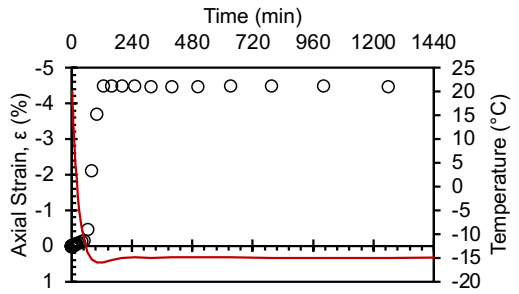

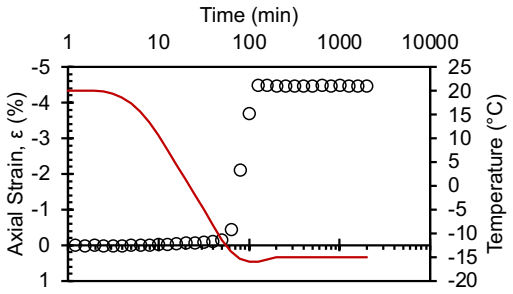

Temperature Change Stage: -15 °C>50 °C

400 kPa

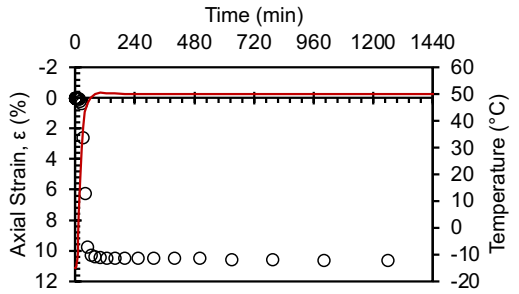

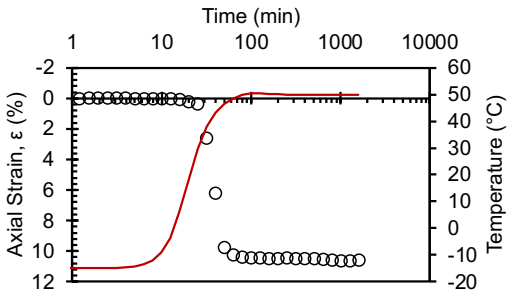

Second Consolidation C2 (50 °C)

400 kPa

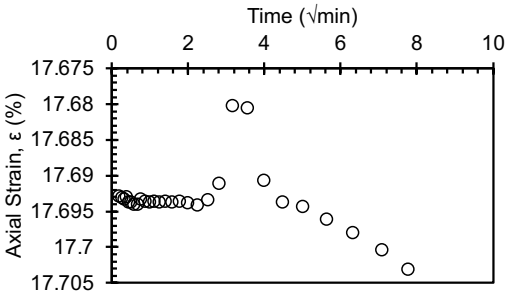

Seating load

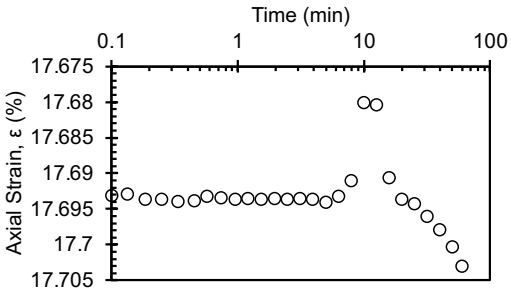

200 kPa

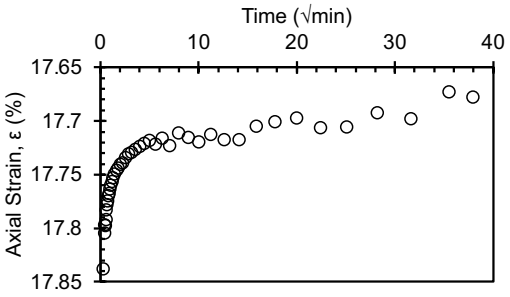

LIR = -0.5

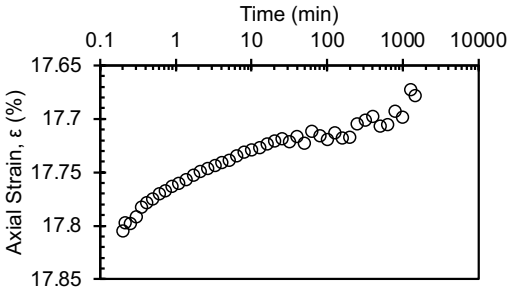

100 kPa

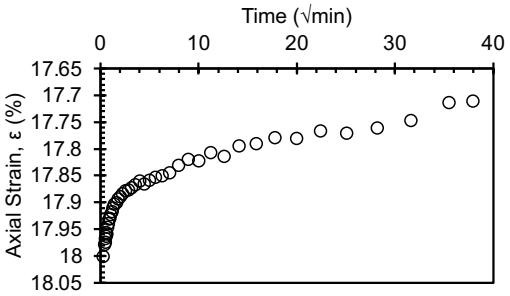

LIR =-0.5

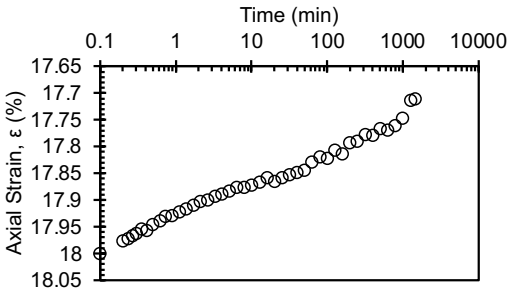

200 kPa

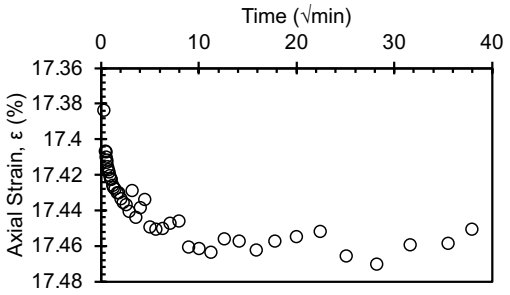

LIR = 1

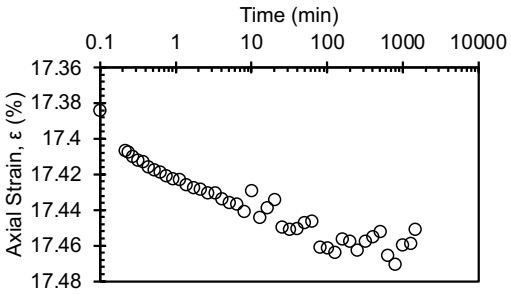

300 kPa

LIR = 0.5

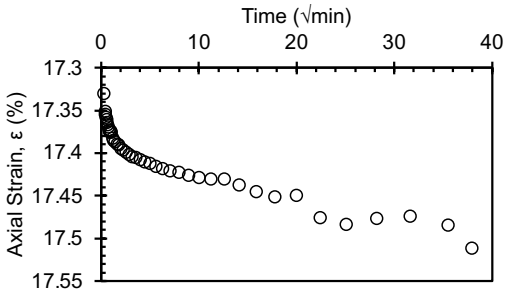

400 kPa

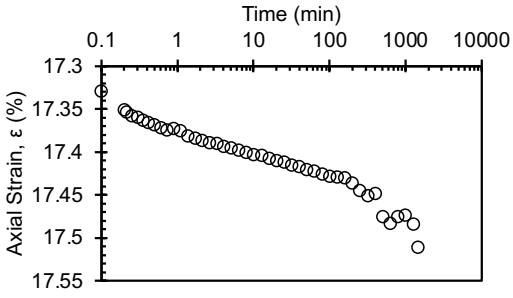

LIR = 0.333

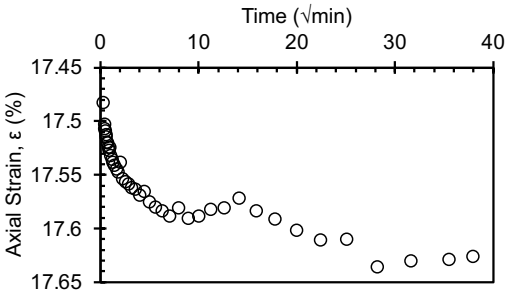

450 kPa

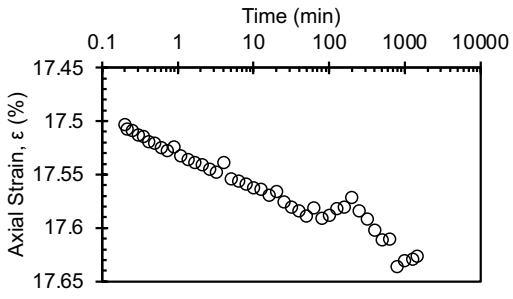

LIR = 0.125

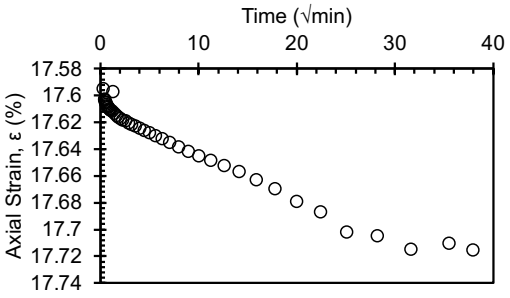

500 kPa

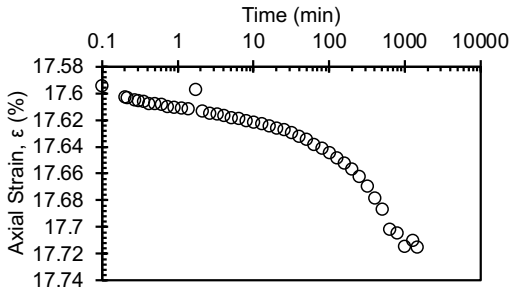

LIR = 0.11

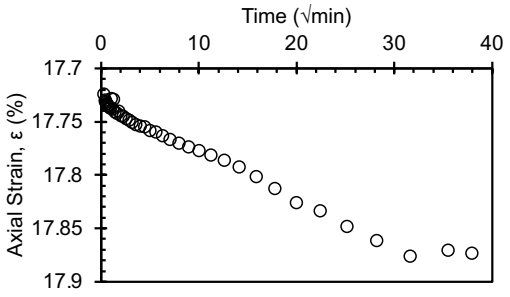

550 kPa

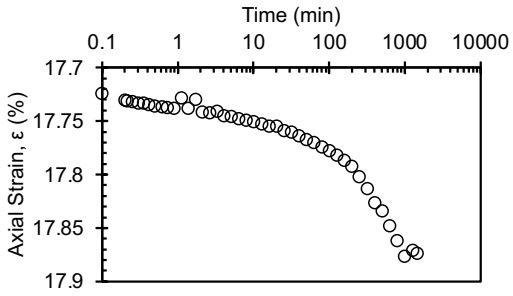

LIR = 0.1

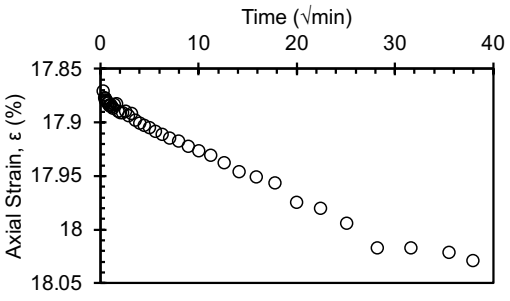

600 kPa

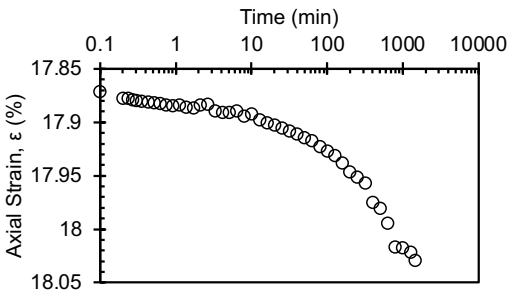

LIR = 0.091

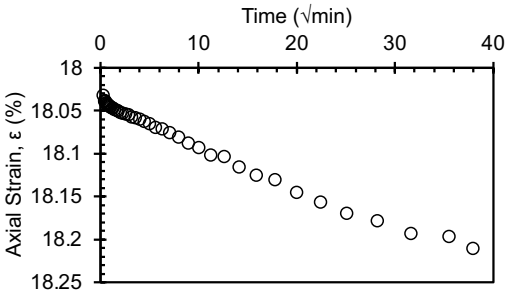

650 kPa

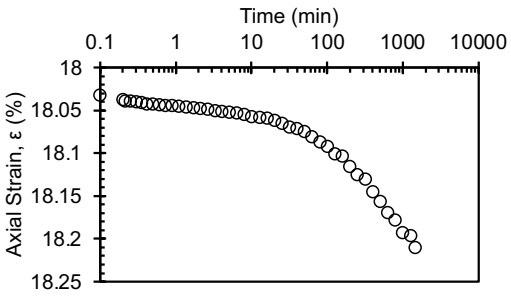

LIR = 0.83

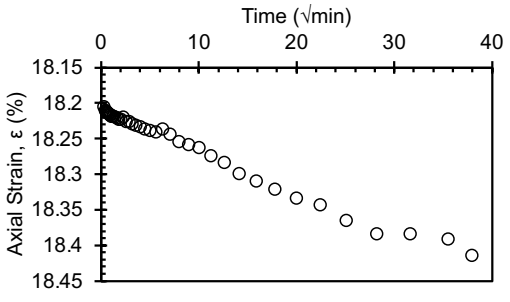

700 kPa

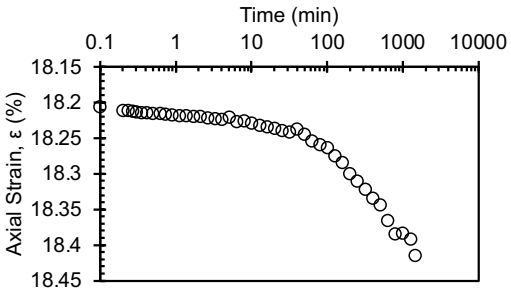

LIR = 0.077

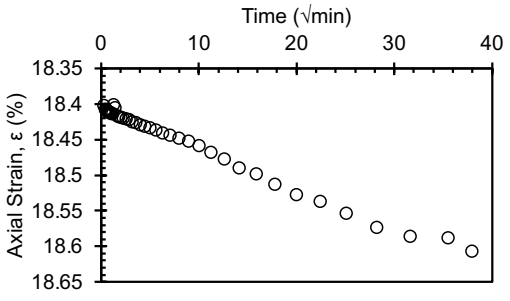

750 kPa

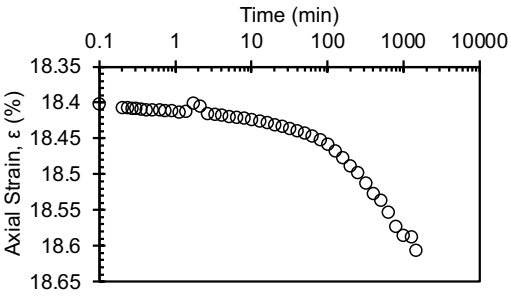

LIR = 0.071

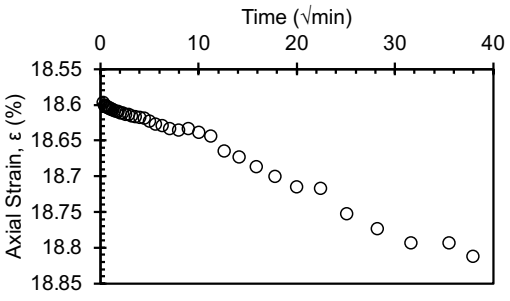

800 kPa

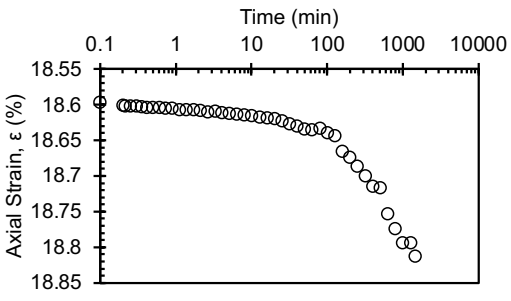

LIR = 0.067

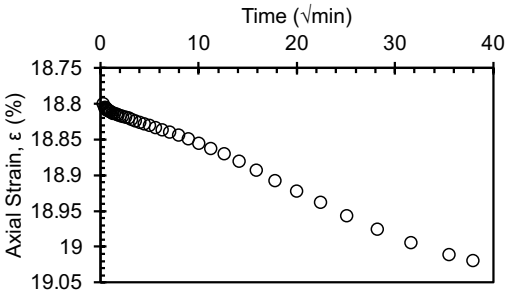

850 kPa

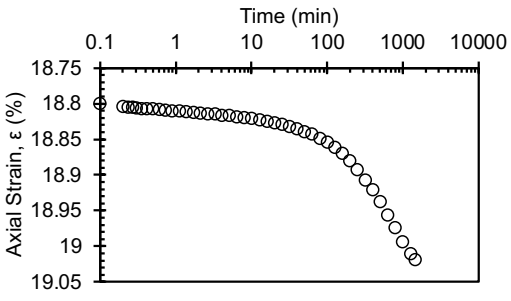

LIR = 0.063

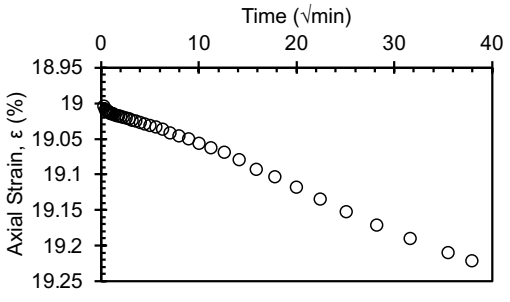

900 kPa

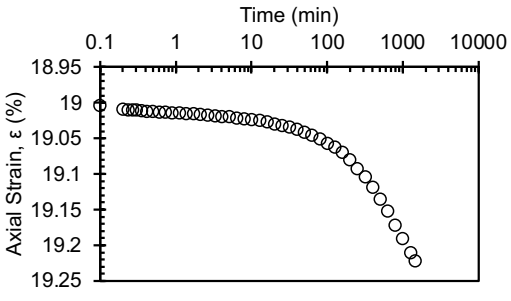

LIR = 0.059

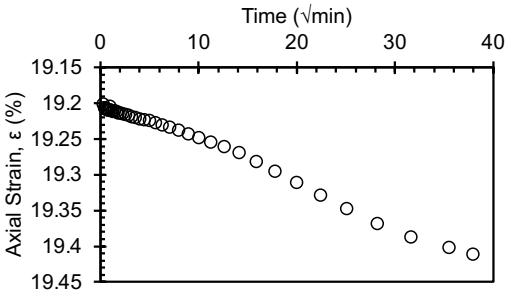

950 kPa

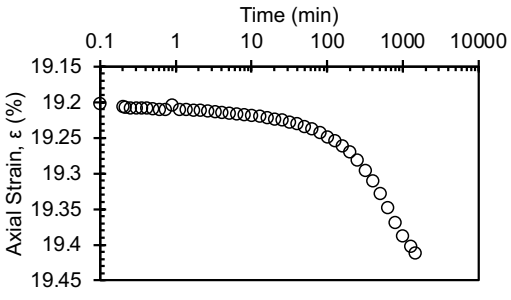

LIR = 0.056

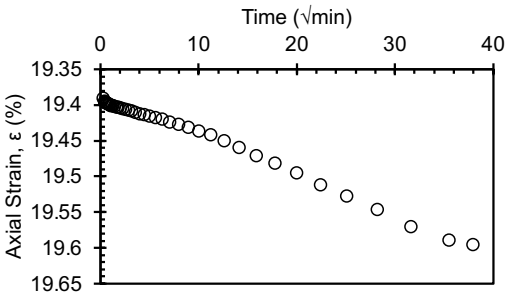

1000 kPa

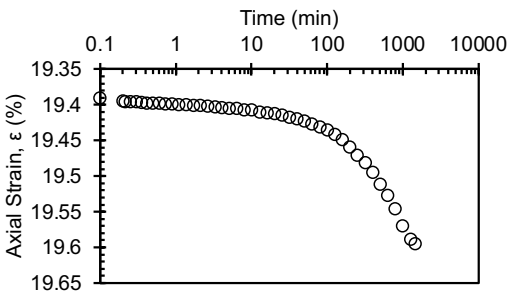

LIR = 0.053

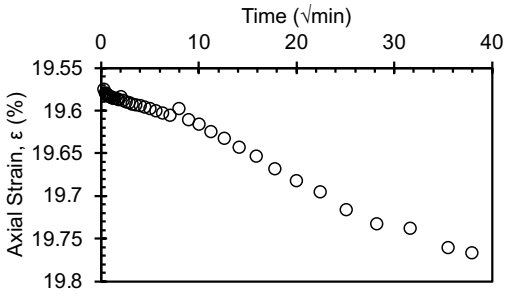

1500 kPa

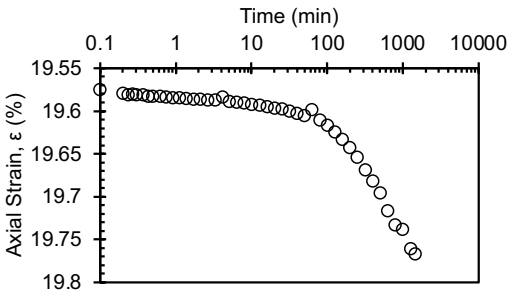

LIR = 0.5

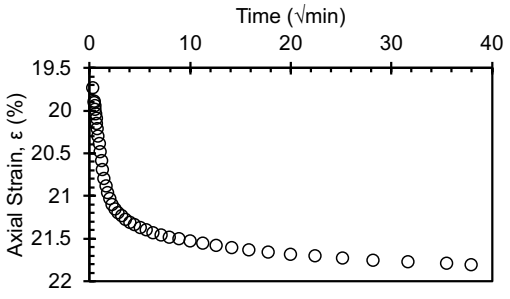

2000 kPa

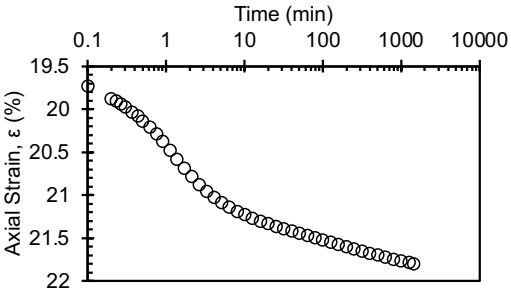

LIR = 0.333

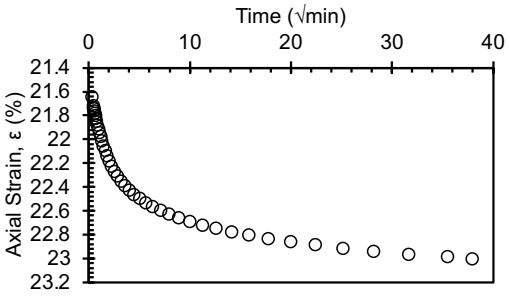

2500 kPa

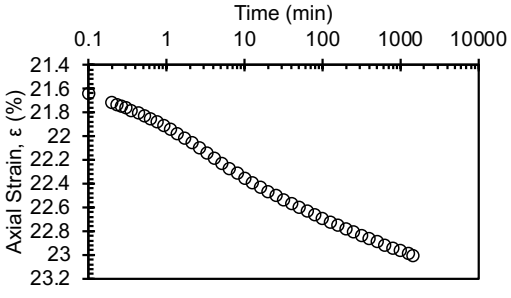

LIR = 0.25

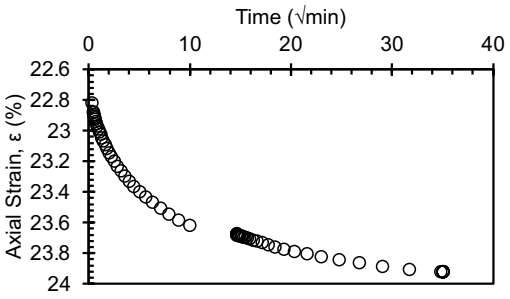

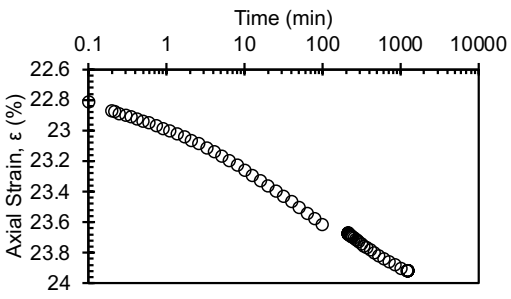

Final

Compression curve

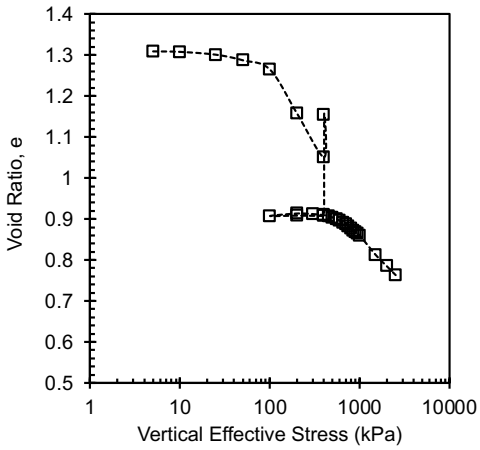

Butterfield method

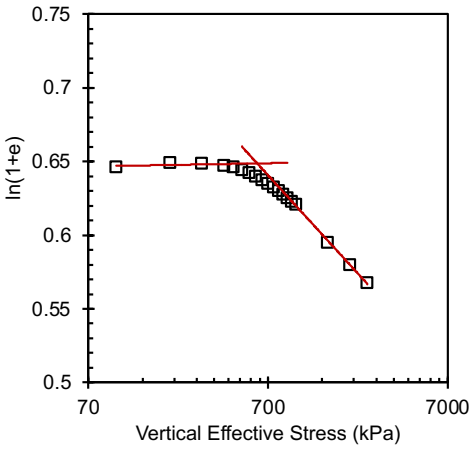

-15>30 °C

Consolidation Test Data Sheet			
Test No.	-15_30_NC_KAOL_EXT_2	Consolidometer No.	Sigma1_5k_10
Date started	11/24/24	Date ended	12/20/24
Test method	B	Condition of test	Inundated
Interpretation Method	Both 1 and 2	Classification	Remolded EPK (CH)
	Before Test - 20°C		After Test - 30°C
	Specimen	Trimmings	Specimen
Tare No.	Ring	T-03	T-01
Tare plus wet soil (g)	352.09	238.95	142.44
Tare plus dry soil (g)	-	168.21	110.96
Tare (g)	215.72	17.82	18.15
Water (g)	43.6	70.74	31.48
Dry Soil (g)	92.7	150.39	92.81
Water content (%)	47.0	47.0	33.9
Area of specimen, A (cm2)	31.67		
Specific Gravity of Solids, Gs	2.7		
Height of solids, Hs (cm)	1.085		
Initial - 20°C		Final - 30°C	
Height of specimen, H0 (cm)	2.540	Height of specimen, Hf (cm)	2.037
Height of water, Hw0 (cm)	1.378	Height of water, Hwf (cm)	0.994
Height of voids, Hv0	1.455	Height of voids, Hvf (cm)	0.952

(cm)			
Void ratio, e0	1.34	Void ratio, ef	0.88
Degree of saturation, S0 (%)	94.7	Degree of saturation, Sf (%)	100.4
Dry density, γ0 (g/cm2)	1.15	Dry density, γf (g/cm2)	1.44
		Differential height, Hd (cm)	0.005
		Preconsolidation pressure, σp'(kPa)	620
		Load increments (kPa) - seating loads held for 60 min, all other loads 1440 min	
Initial temperature, 20°C		5 (seating), 10, 25, 50, 100, 200, 400	
Temperature change(s)	20°C to (-15)°C, (-15)°C to 30°C	400	
Final temperature (°C)	30°C	400 (seating), 200, 100, 200, 400, 450, 500, 550, 600, 650, 700, 750, 800, 1000, 2000, 2500	
Notes			
Note that the final height of the specimen Hf is the height recorded at the end of the test after the specimen was rebounded to 5 kPa until strain stabilized - it does not correspond to the final height at the maximum applied stress. The differential height is the difference between the final recorded height Hf and final height measured with a caliper following specimen extraction from ring at the end of the test.			

Initial Consolidation C1 (20 °C)

5 kPa

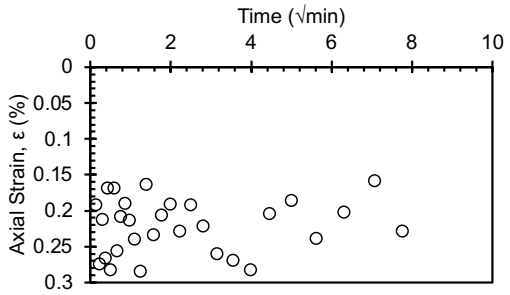

Seating load

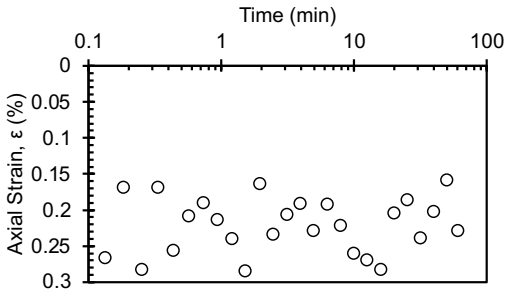

10 kPa

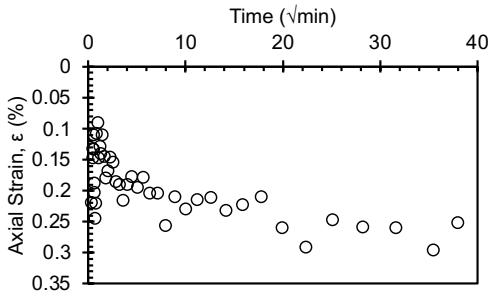

LIR = 1

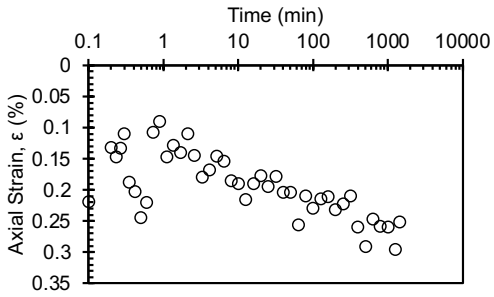

25 kPa

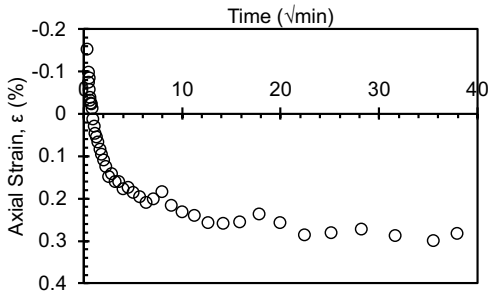

LIR = 1.5

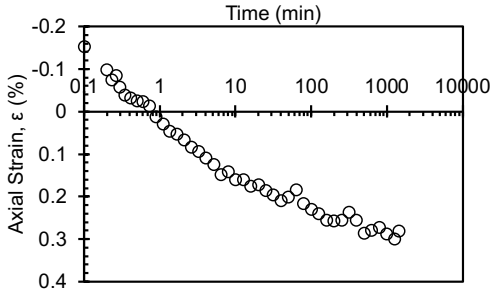

50 kPa

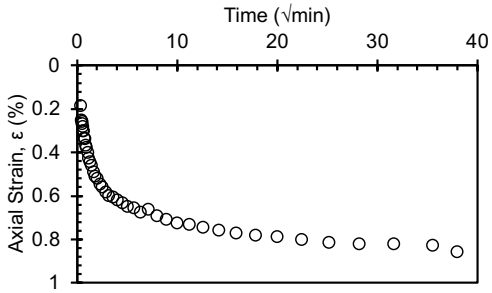

LIR = 1

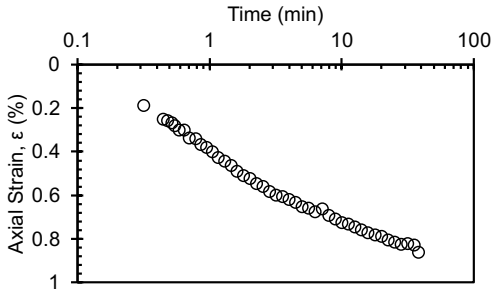

100 kPa

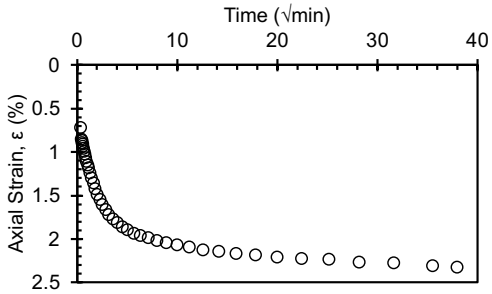

LIR = 1

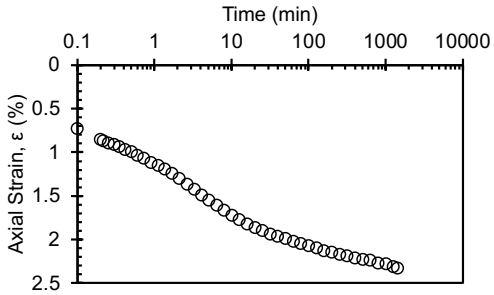

200 kPa

LIR = 1

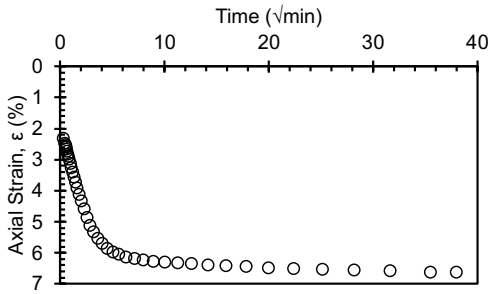

400 kPa

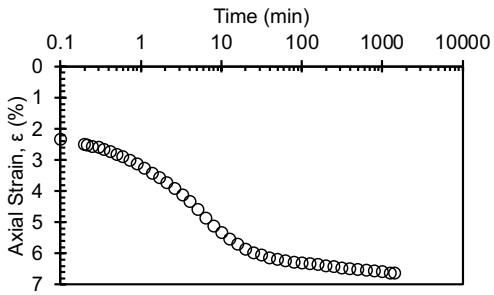

LIR = 1

Temperature Change Stage: 20 °C>-15 °C

400 kPa

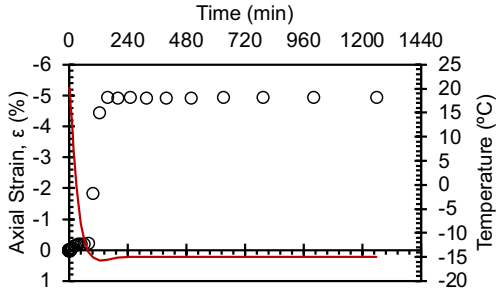

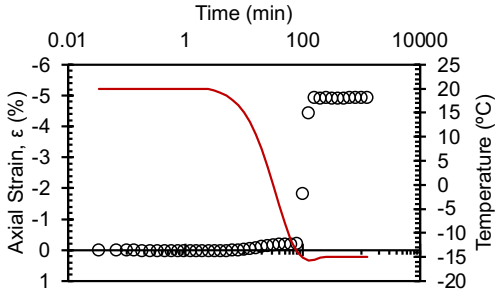

Temperature Change Stage: -15 °C>30 °C

400 kPa

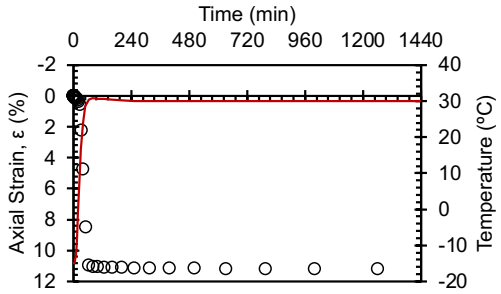

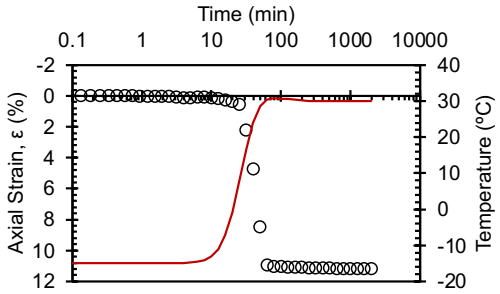

Second Consolidation C2 (30 °C)

400 kPa

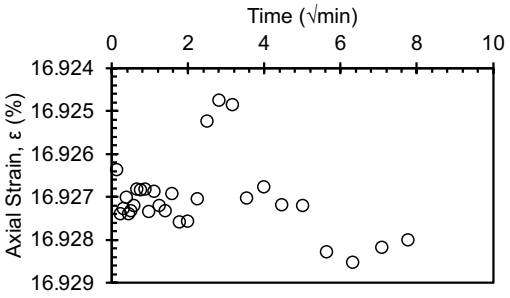

Seating load

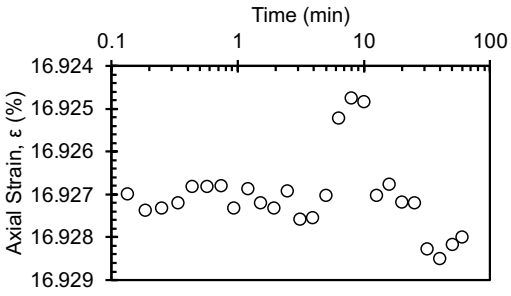

200 kPa

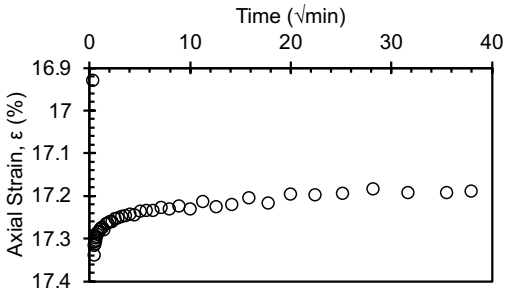

LIR = -0.5

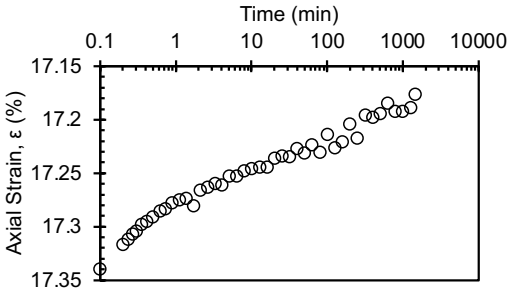

100 kPa

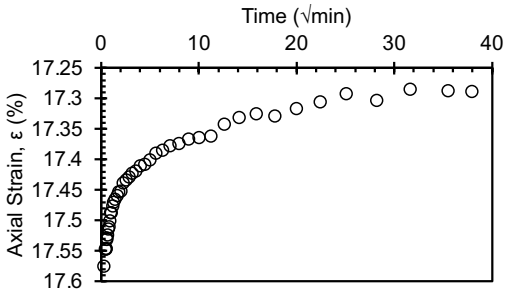

LIR =-0.5

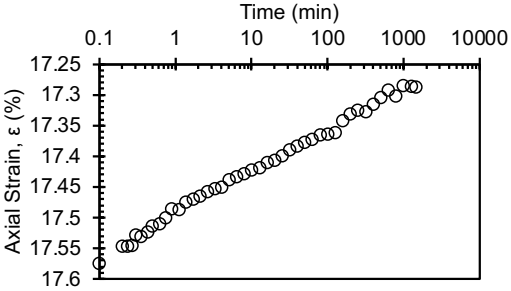

200 kPa

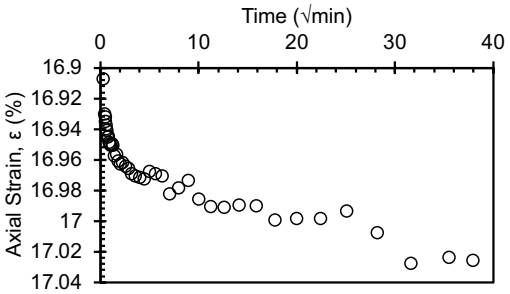

LIR = 1

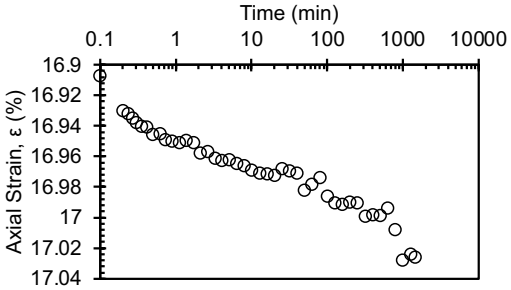

400 kPa

LIR = 1

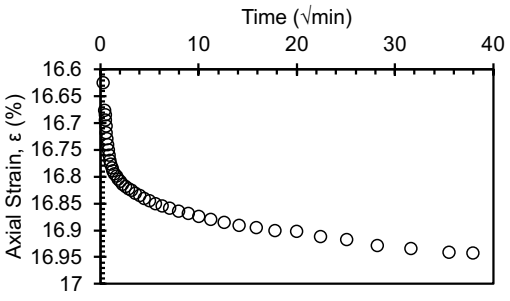

450 kPa

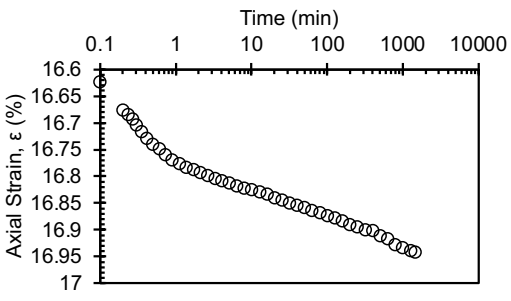

LIR = 0.125

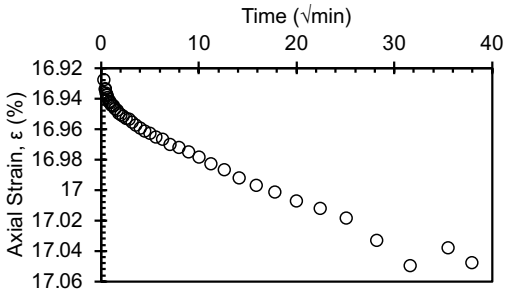

500 kPa

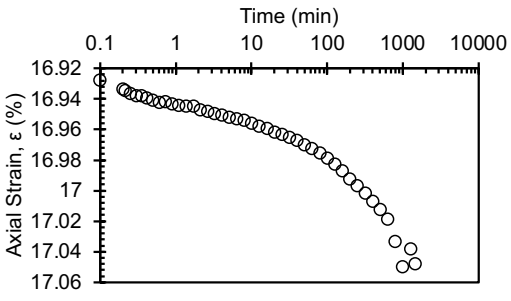

LIR = 0.11

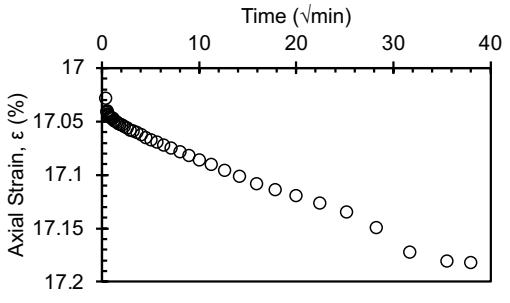

550 kPa

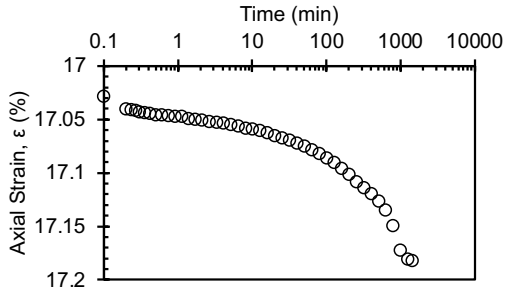

LIR = 0.1

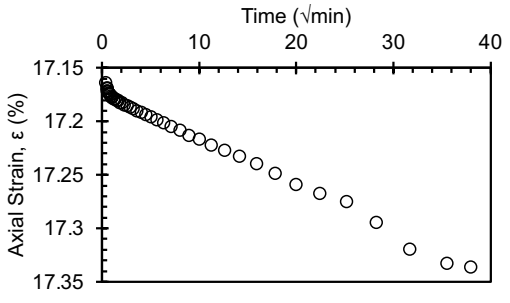

600 kPa

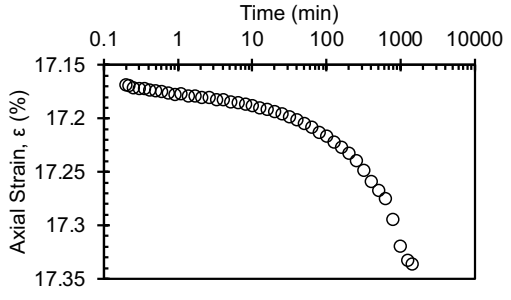

LIR = 0.091

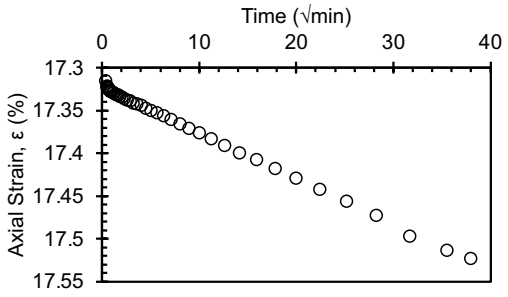

650 kPa

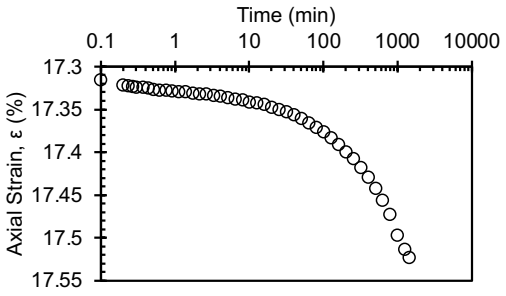

LIR = 0.83

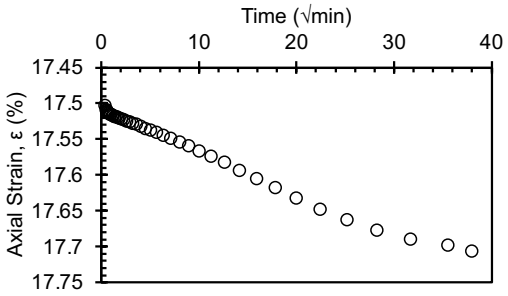

700 kPa

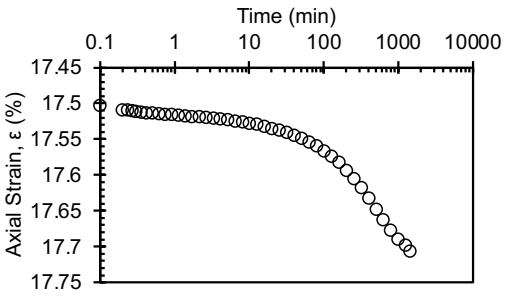

LIR = 0.077

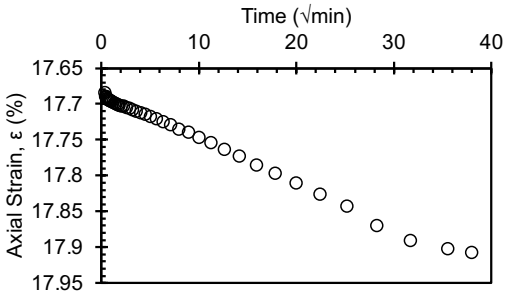

750 kPa

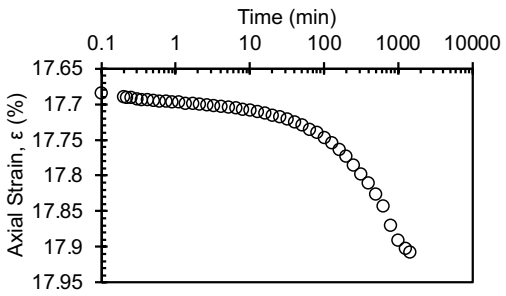

LIR = 0.071

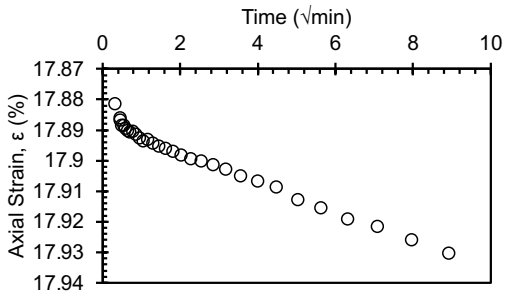

800 kPa

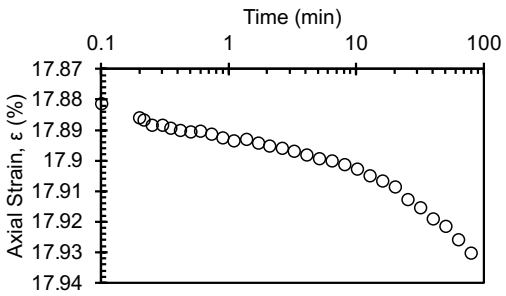

LIR = 0.067

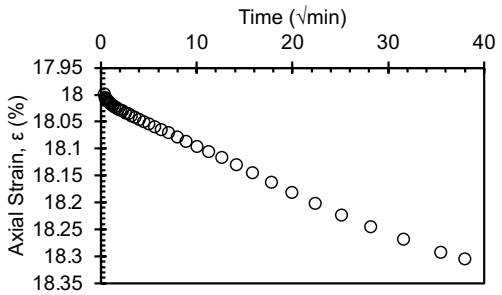

1000 kPa

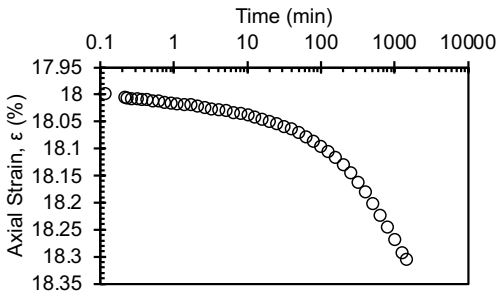

LIR = 0.25

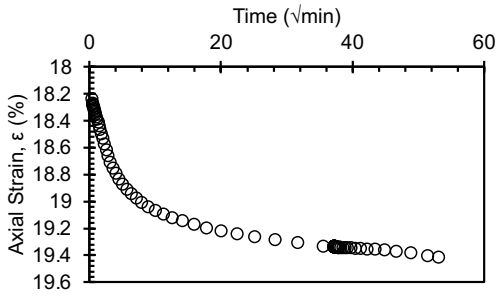

2000 kPa

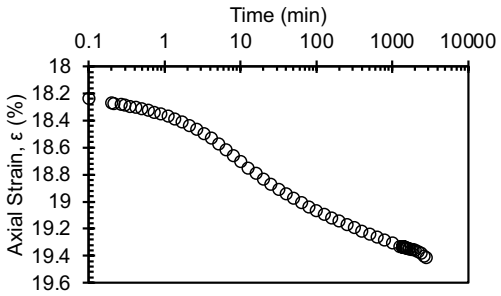

LIR = 1

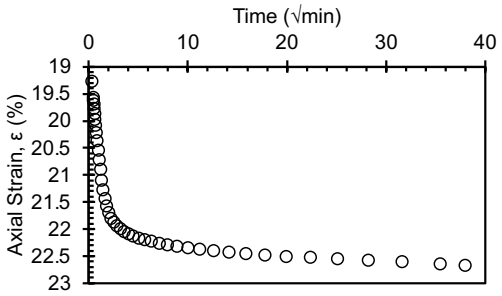

2500 kPa

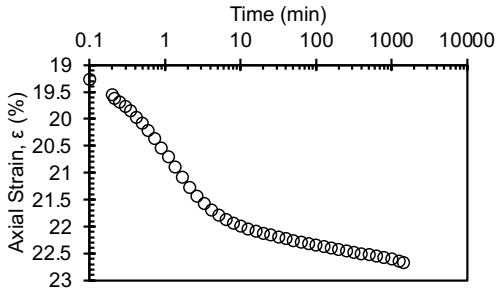

LIR = 0.25

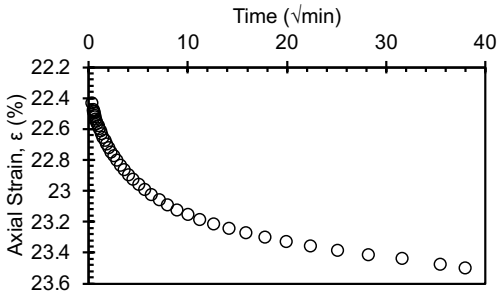

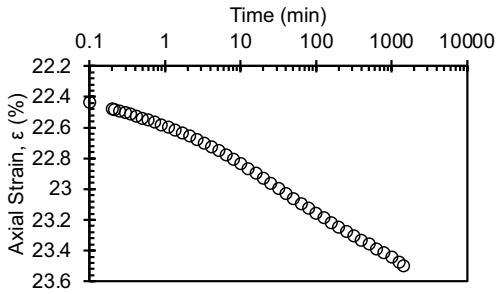

Final

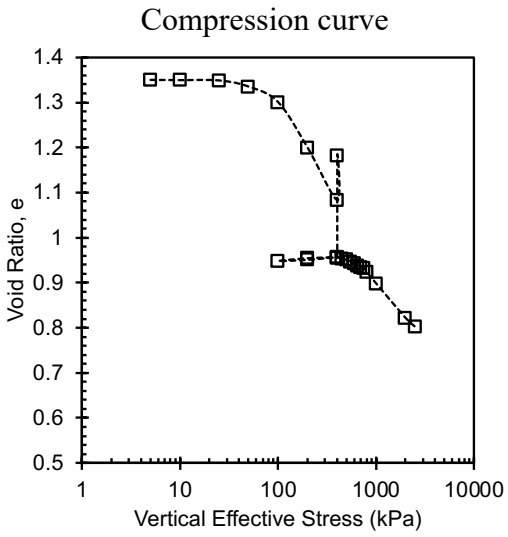
Compression curve
Void Ratio, e
1.4
1.3
1.2
1.1
1
0.9
0.8
0.7
0.6
0.5
1
10
100
1000
10000
Vertical Effective Stress (kPa)

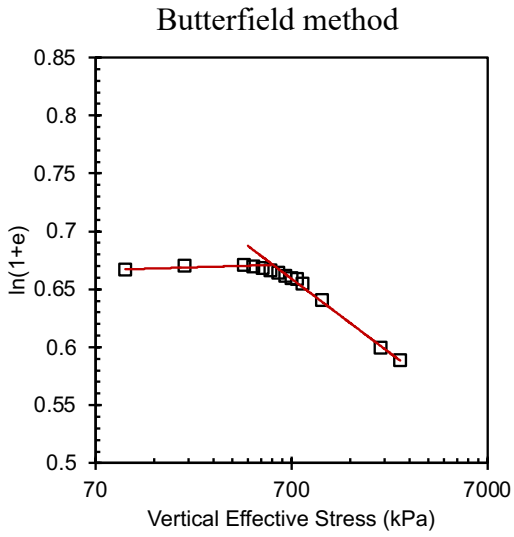
Butterfield method
ln(1+e)
0.85
0.8
0.75
0.7
0.65
0.6
0.55
0.5
70
700
7000
Vertical Effective Stress (kPa)

-15>20 °C

Consolidation Test Data Sheet			
Test No.	-15_20_NC_KAOL_EXT_2	Consolidometer No.	Geojac_2k_20
Date started	7/25/24	Date ended	8/24/24
Test method	B	Condition of test	Inundated
Interpretation Method	Both 1 and 2	Classification	Remolded EPK (CH)
	Before Test - 20°C		After Test - 20°C
	Specimen	Trimmings	Specimen
Tare No.	Ring	TRIAL3	MII
Tare plus wet soil (g)	350.54	269.03	154.65
Tare plus dry soil (g)	-	189.50	124.58
Tare (g)	215.09	21.67	34.35
Water (g)	43.55	79.53	30.07
Dry Soil (g)	91.90	167.83	90.23
Water content (%)	47.4	47.4	33.3
Area of specimen, A (cm^2)	31.67		
Specific Gravity of Solids, G_s	2.7		
Height of solids, H_s (cm)	1.075		
Initial - 20°C		Final - 20°C	
Height of specimen, H_0 (cm)	2.540	Height of specimen, H_f (cm)	2.020
Height of water, H_{w0} (cm)	1.375	Height of water, H_{wf} (cm)	0.950
Height of voids, H_{v0}	1.465	Height of voids, H_{vf} (cm)	0.945

(cm)			
Void ratio, e_0	1.36	Void ratio, e_f	0.88
Degree of saturation, S0 (%)	93.9	Degree of saturation, S_f (%)	100.5
Dry density, γ_0 (g/cm^2)	1.14	Dry density, γ_f (g/cm^2)	1.44
		Differential height, H_d (cm)	-0.028
		Preconsolidation pressure, σ_p'(kPa)	610
		Load increments (kPa) - seating loads held for 60 min, all other loads 1440 min	
Initial temperature, 20°C		5 (seating), 10, 25, 50, 100, 200, 400	
Temperature change(s)	20°C to (-15)°C, (-15)°C to 20°C	400	
Final temperature (°C)	20°C	400 (seating), 200, 100, 200, 400, 1000, 2000, 3000, 4000, 5000, 6000, 7000, 8000, 9000, 10000, 11000, 12000, 13000, 14000	
Notes			
Note that the final height of the specimen H_f is the height recorded at the end of the test after the specimen was rebounded to 5 kPa until strain stabilized - it does not correspond to the final height at the maximum applied stress. The differential height is the difference between the final recorded height H_f and final height measured with a caliper following specimen extraction from ring at the end of the test.			

Initial Consolidation C1 (20 °C)

5 kPa

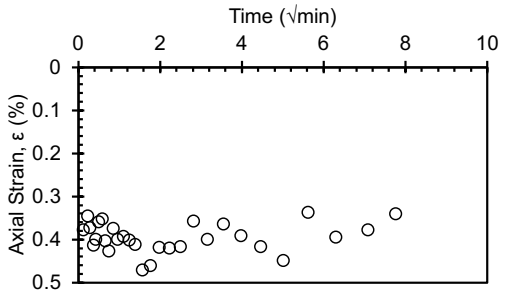

10 kPa

Seating load

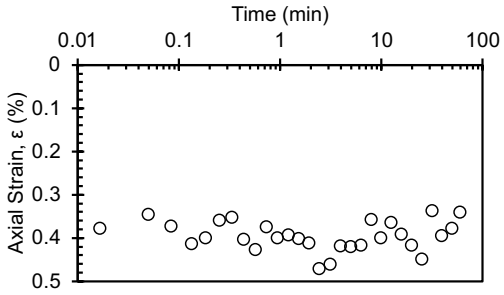

LIR = 1

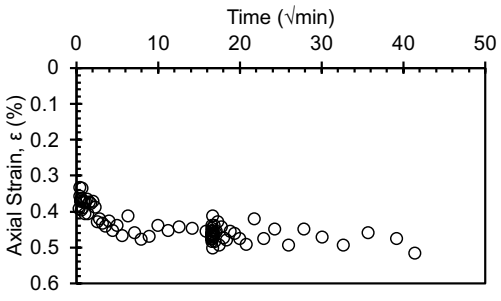

25 kPa

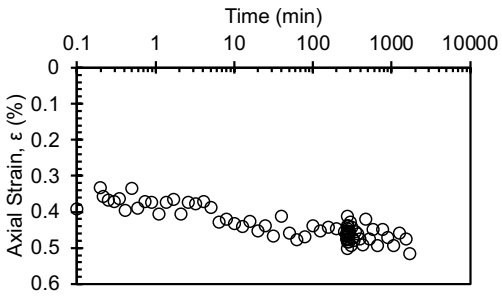

LIR = 1.5

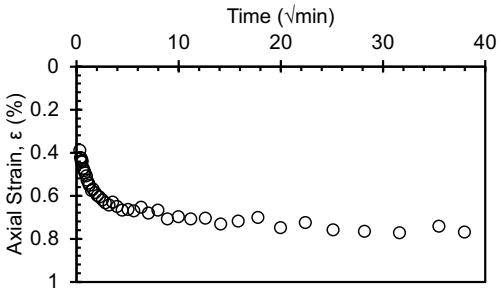

50 kPa

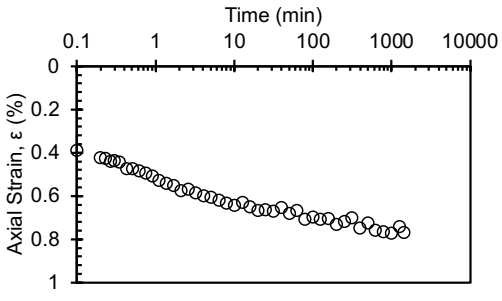

LIR = 1

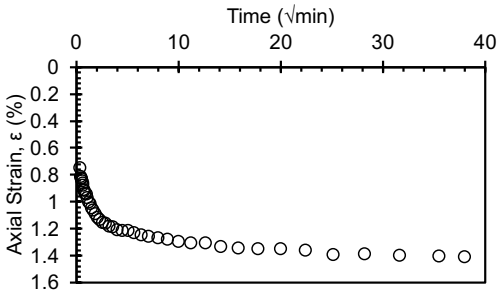

75 kPa

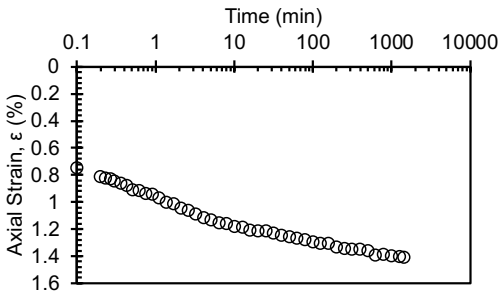

LIR = 0.5

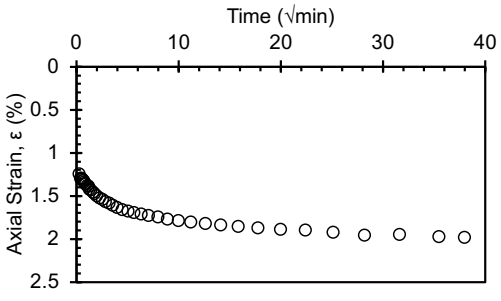

100 kPa

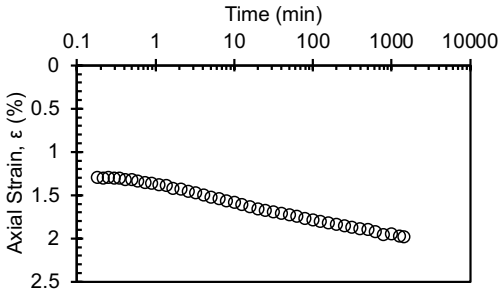

LIR = 0.333

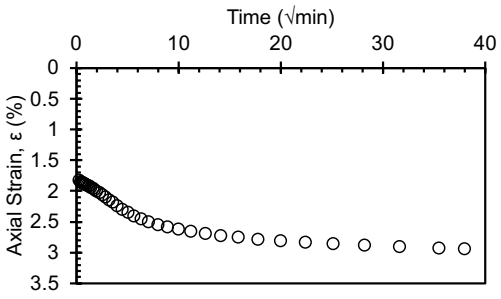

200 kPa

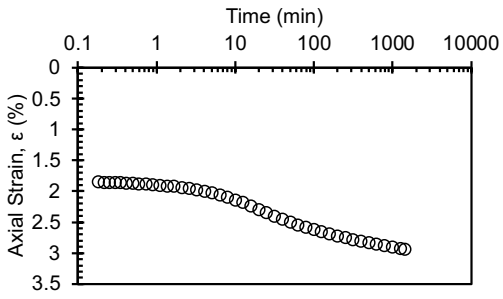

LIR = 1

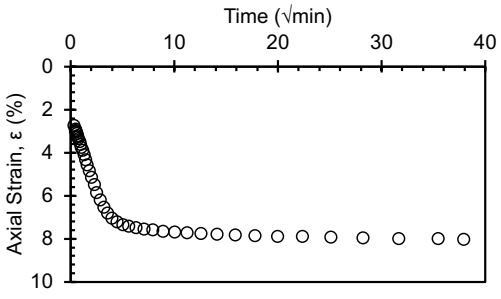

400 kPa

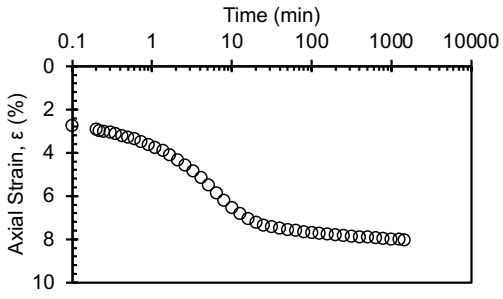

LIR = 1

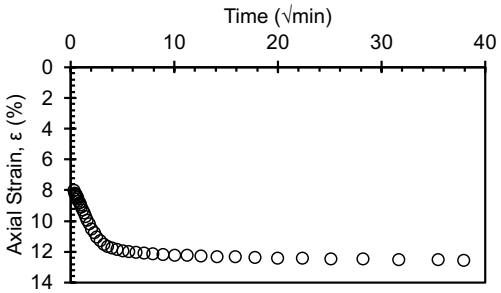

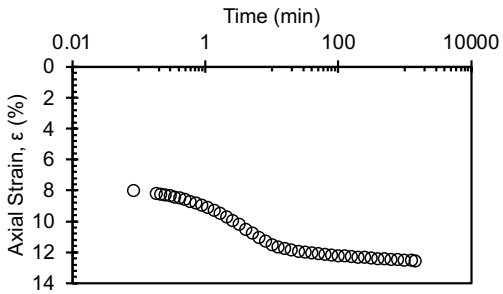

Temperature Change Stage: 20 °C>-15 °C

400 kPa

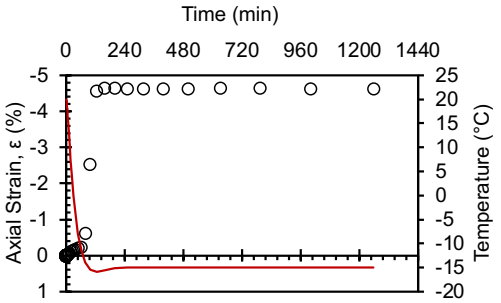

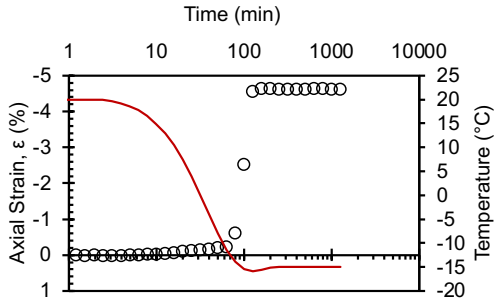

Temperature Change Stage: -15 °C>20 °C

400 kPa

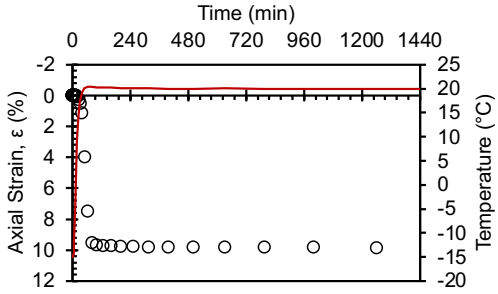

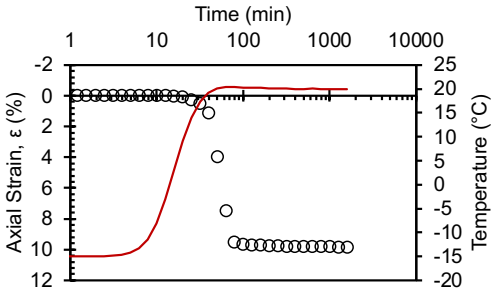

Second Consolidation C2 (20 °C)

400 kPa

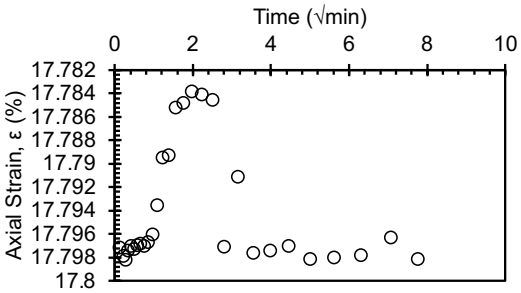

Seating load

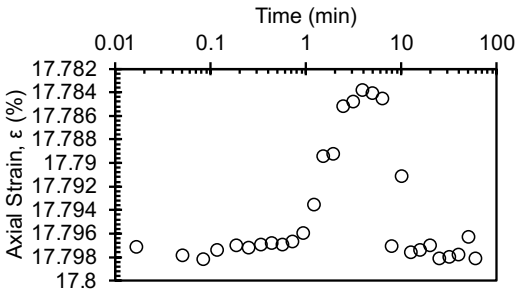

200 kPa

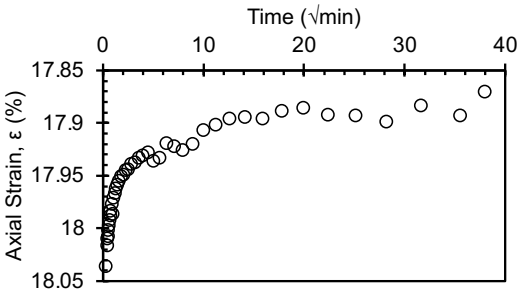

LIR = -0.5

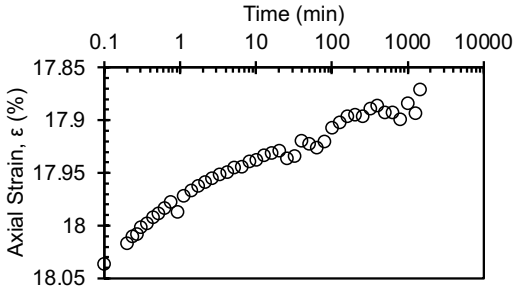

100 kPa

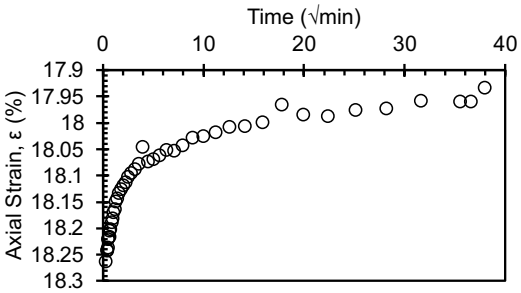

LIR =-0.5

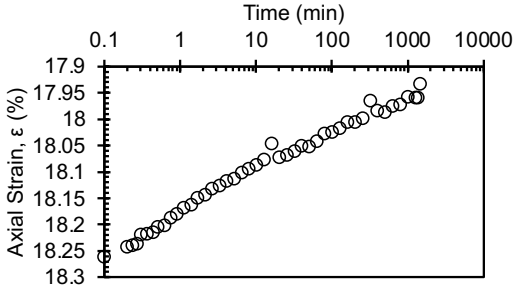

200 kPa

LIR = 1

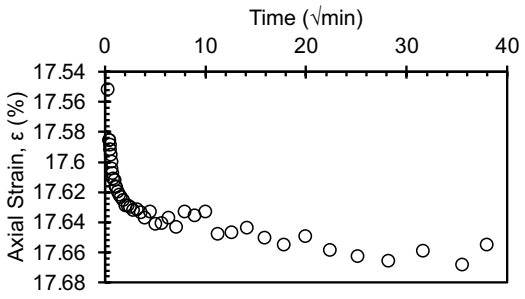

300 kPa

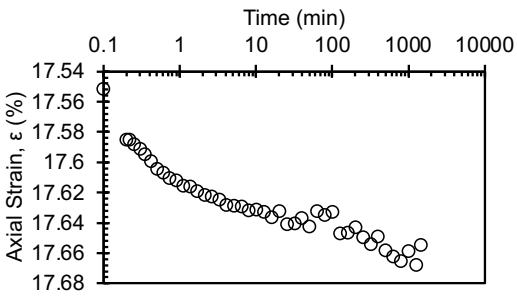

LIR = 0.5

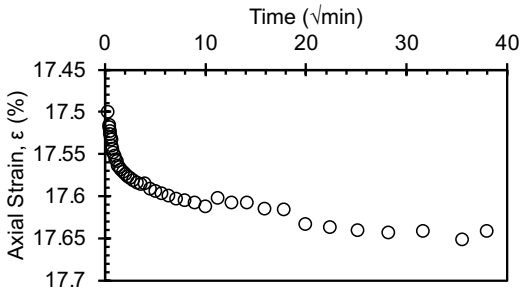

400 kPa

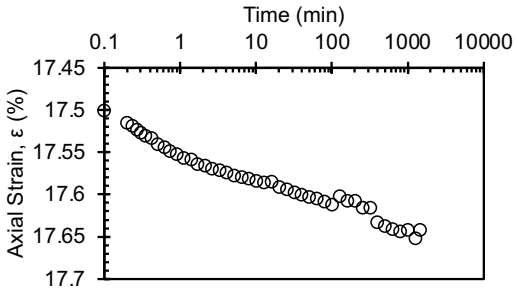

LIR = 0.333

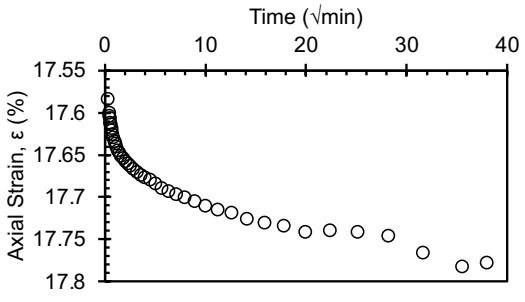

450 kPa

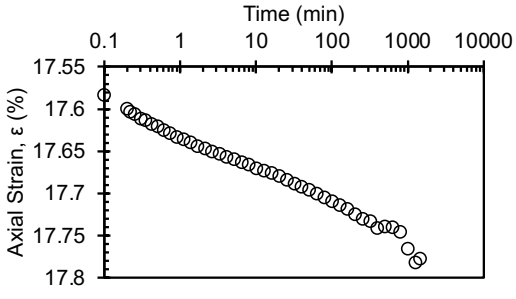

LIR = 0.125

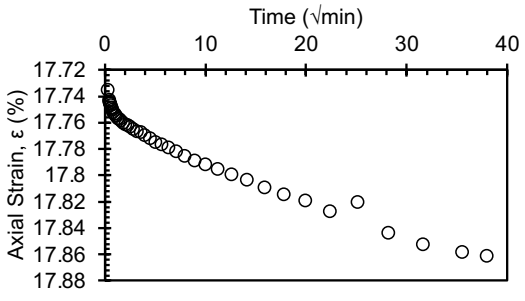

500 kPa

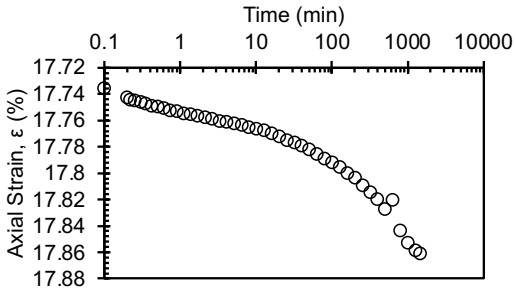

LIR = 0.11

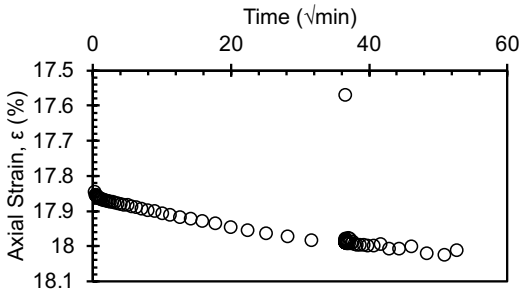

550 kPa

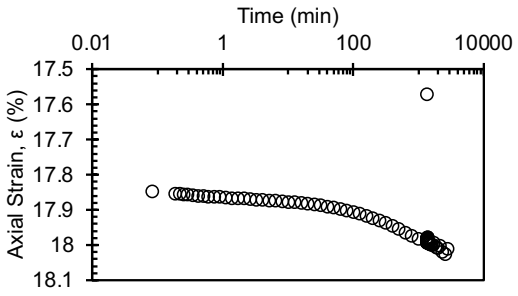

LIR = 0.1

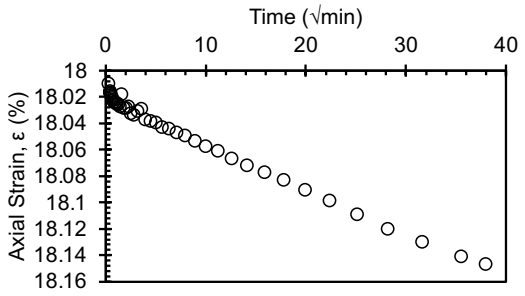

600 kPa

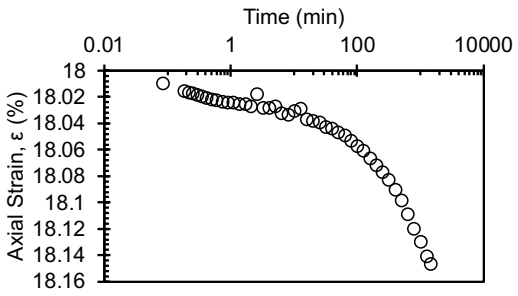

LIR = 0.091

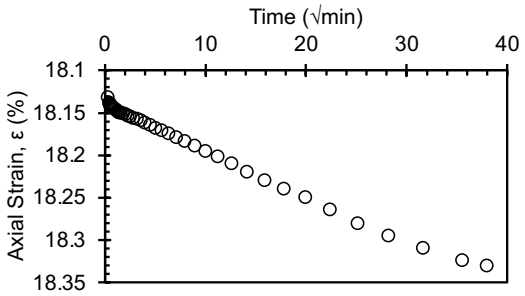

650 kPa

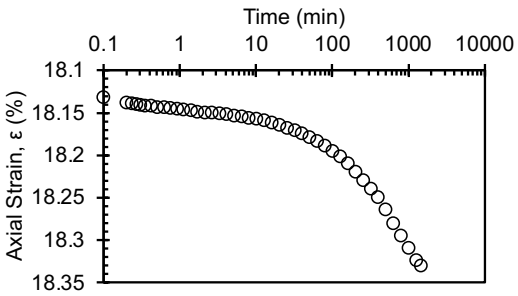

LIR = 0.83

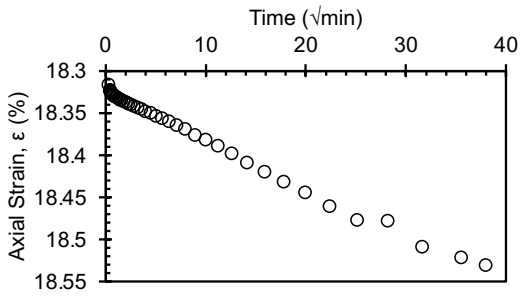

700 kPa

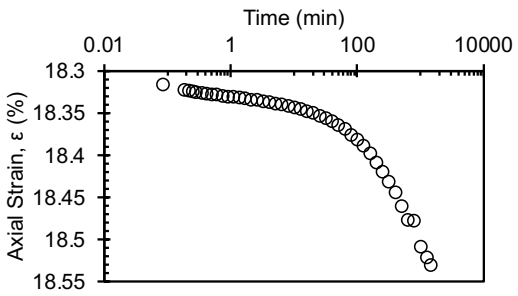

LIR = 0.077

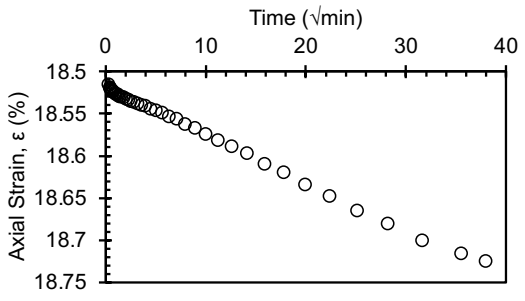

750 kPa

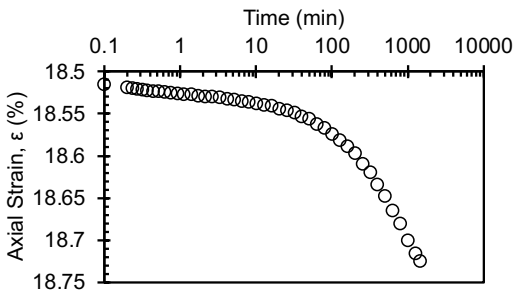

LIR = 0.071

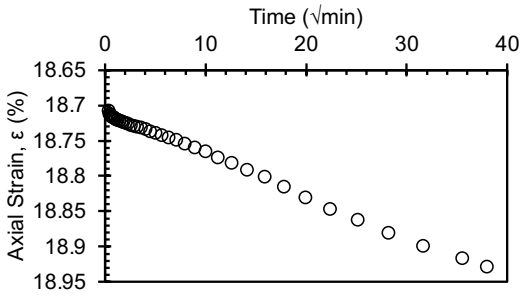

800 kPa

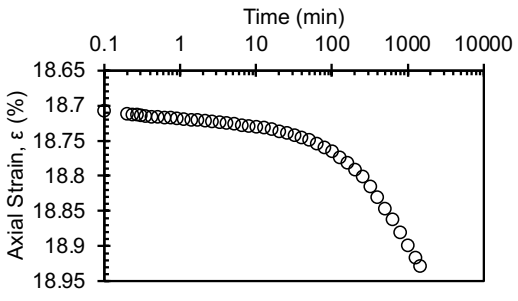

LIR = 0.067

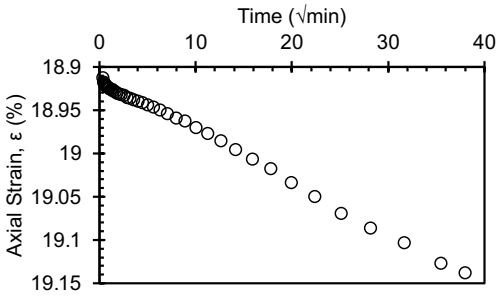

850 kPa

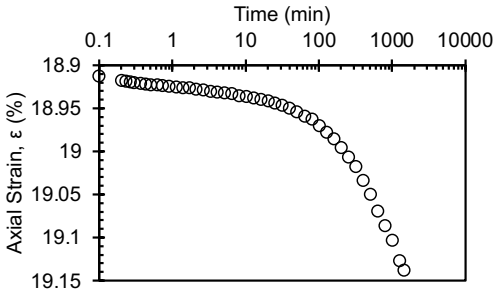

LIR = 0.063

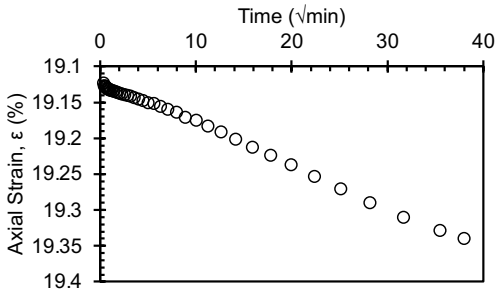

900 kPa

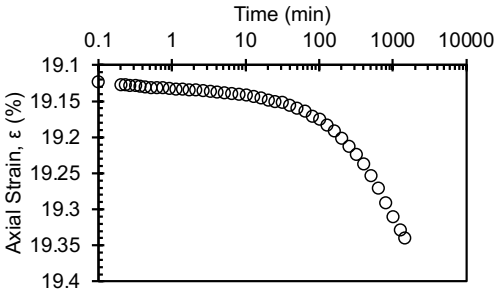

LIR = 0.059

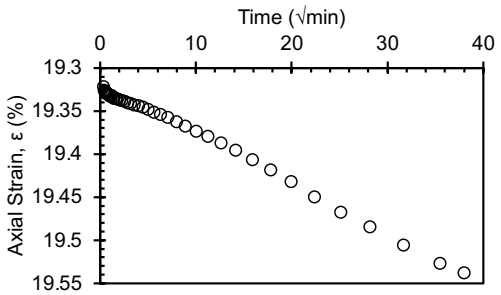

950 kPa

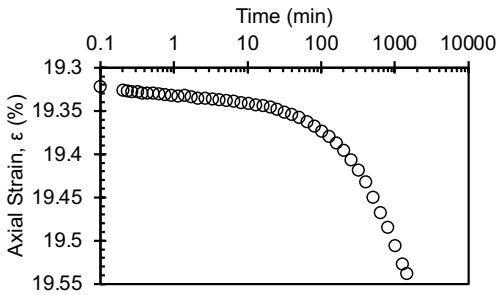

LIR = 0.056

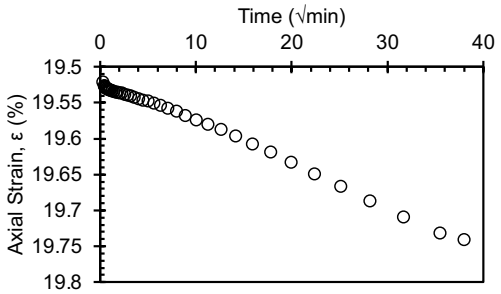

1000 kPa

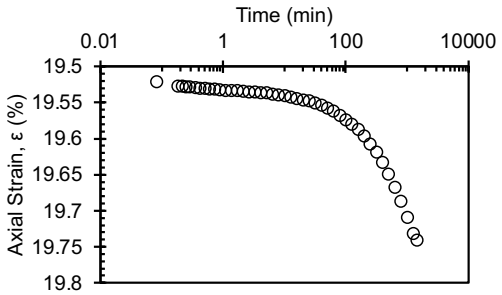

LIR = 0.053

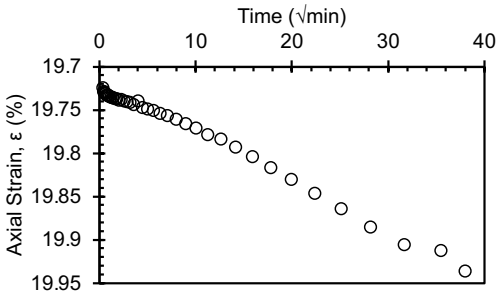

1500 kPa

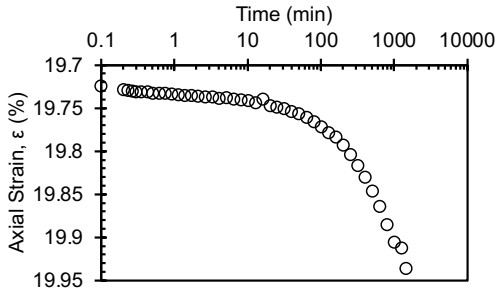

LIR = 0.5

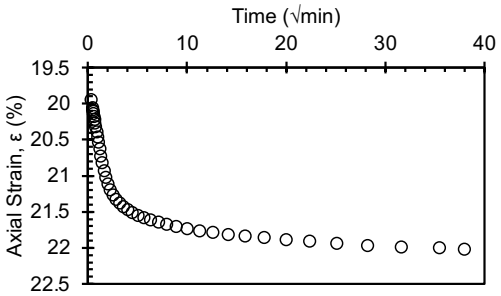

2000 kPa

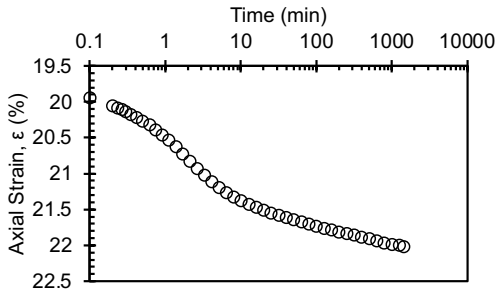

LIR = 0.333

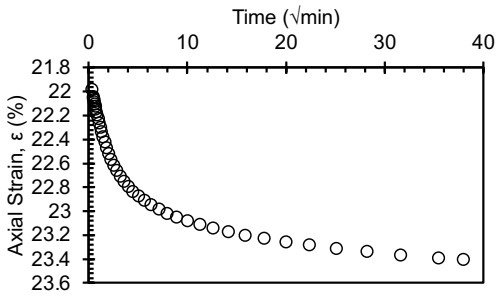
Time (√min)
0
10
20
30
40
Axial Strain, ε (%)
21.8
22
22.2
22.4
22.6
22.8
23
23.2
23.4
23.6

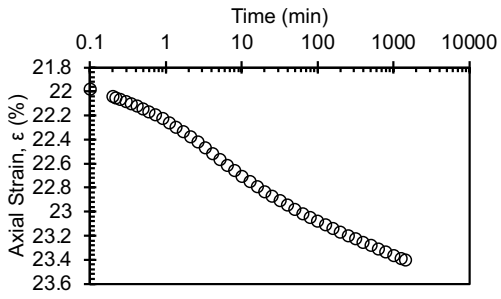
Time (min)
0.1
1
10
100
1000
10000
Axial Strain, ε (%)
21.8
22
22.2
22.4
22.6
22.8
23
23.2
23.4
23.6

Final

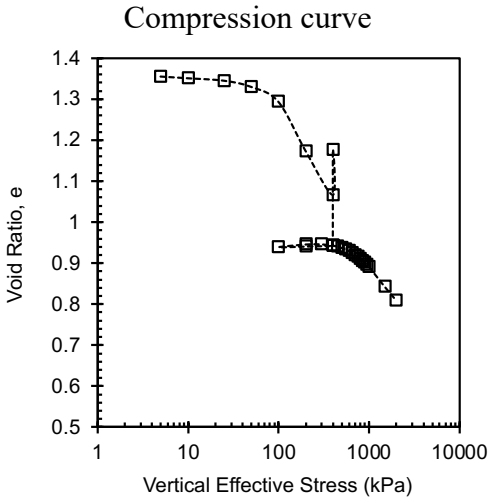
Compression curve
Void Ratio, e
1.4
1.3
1.2
1.1
1
0.9
0.8
0.7
0.6
0.5
1
10
100
1000
10000
Vertical Effective Stress (kPa)

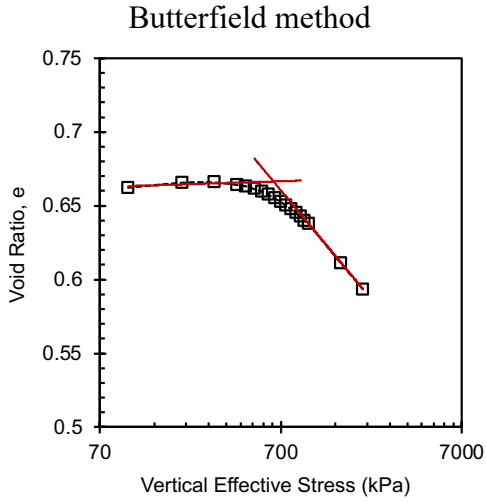
Butterfield method
Void Ratio, e
0.75
0.7
0.65
0.6
0.55
0.5
70
700
7000
Vertical Effective Stress (kPa)